GENERATION AND CHARACTERIZATION OF HUMAN EMBRYONIC STEM CELLS-DERIVED SKELETAL MUSCLE PROGENITORS

Michael L. Shelton

Thesis submitted to:

The Faculty of Graduate and Postdoctoral Studies

In partial fulfilment of the requirements for the degree of:

Doctor of Philosophy

Department of Biochemistry, Microbiology, and Immunology

University of Ottawa

Ottawa, ON, Canada

Abstract

The long-term treatment of injured, aging, or pathological skeletal muscle using stem cell therapy requires an abundant source of skeletal muscle progenitors (SMP) that are capable of self-replenishment. While adult SMPs—known as satellite cells and marked by PAX7 expression—can be collected from healthy donors, these satellite cells have limited replication potential once extracted, and may have difficulties providing sufficient numbers for therapy. Therefore, we sought to utilize the near-unlimited replication potential of human embryonic stem cells (hESC) to generate large quantities of SMPs *in vitro*. We developed a 50-day directed hESC differentiation that produced cultures with up to 90% myogenic identity; roughly 43 ± 4% become $PAX7^+$ SMPs, and 47 ± 3% of cells become skeletal myocytes. We also performed gene expression profiling on our differentiating cultures to better understand *in vitro* skeletal myogenesis, and to better characterize *in vitro* hESC-derived SMPs, which remain poorly understood relative to adult satellite cells. 50-day cultures shared gene expression profiles more similar to quiescent rather than activated satellite cells, featuring a number of genes related to FOS/JUN, NOTCH, and TGFB-signaling. Day 50 cultures also expressed surface proteins known to mark adult or embryonic SMPs: CD82, CXCR4, ERBB3, NGFR, and PDGFRA. Transplanting 50-day cultures into cardiotoxin or $BaCl_2$ injured immunodeficient murine muscle showed donor human cells persisted within the host muscle for 1 – 2 months post-injection; however, donor cells were confined to the interstitial space and did not contribute to host myofibers or the satellite cell niche. Together, these studies provide a tool for generating large quantities of embryonic skeletal muscle, and a gene expression resource that can provide insight into signaling factors that might improve or accelerate SMP development, or provide putative new surface receptors that may isolate embryonic SMPs better suited for *in vivo* transplantation.

Acknowledgments

First and foremost I would like to thank my supervisor Dr. Ilona Skerjanc for seeing potential in me and guiding me through my graduate studies. Your experience has greatly honed my scientific curiosity into what it is today. I would also like to extend my thanks to my thesis advisory committee members Dr. Jeffrey Dilworth, Dr. Lisheng Wang, and Dr. Nadine Wiper-Bergeron for helping improve and focus the direction of my work, especially during Ilona's leave. My research could not have happened without Dr. William "Bill" Stanford and Jun Liu ensuring the cells must flow. To all of my fellow lab mates—from past to present—our comradery made graduate studies more than just a degree and kept me going over the years: together we survived the Mycoplasma War. Finally, I must extend my sincerest gratitude to Dr. Alexandre Blais for assuming the mantle of co-supervisor and seeing my work through to the bitter (sweet) end.

Table of Contents

List of Abbreviations

AAV	Adeno associated virus
ADP	Adenosine diphosphate
ALS	Amyotrophic lateral sclerosis
AMD	Age-related macular degeneration
ATP	Adenosine triphosphate
$BaCl_2$	Barium chloride
BIO	6-bromoindirubin-3′-oxime
BMP	Bone morphogenic protein
cDNA	Complementary deoxyribonucleic acid
CHRN	Cholinergic receptor nicotinic
cRNA	Complementary ribonucleic acid
EB	Embryoid body
ECM	Extracellular matrix
DGC	Dystroglycan complex
DMD	Duchenne muscular dystrophy / Dystrophin
DPBS	Dulbecco's phosphate buffered saline
DPI	Day post injection
EDL	Extensor digitorum longus
EdU	5-Ethynyl-2′-deoxyuridine
EMT	Epithelial to mesenchymal transition
ERBB	Erythroblastosis oncogene B
ESC	Embryonic stem cell
EXPANDER	Expression analyzer and displayer
FACS	Fluorescence activated cell sort
FBS	Fetal bovine serum
FSHD	Facioscapulohumeral dystrophy
GO	Gene ontology
hESC	Human embryonic stem cell
HGNC	HUGO gene nomenclature committee
hiPSC	Human induced pluripotent stem cell
HOX	Homeobox
HUGO	Human genome organization
FGF	Fibroblast growth factor
IF	Immunofluorescence
iPSC	Induced pluripotent stem cell
kB	Kilobase
LEF	Lymphoid enhancer-binding factor
LMNA	Lamin A/C
MACS	Magnetic activated cell sort

MADS	MCM1 Agamous Deficiens SRF
MAPK	Mitogen activated protein kinase
MB	Megabase
MEF	Myocyte enhancer factor
mESC	Mouse embryonic stem cell
MYH	Myosin heavy chain
NSG	NOD.Cg-Prkdc^{scid} Il2rg^{tm1Wjl}/SzJ
PANTHER	Protein analysis through evolutionary relationships
PAX	Paired box
PBS	Phosphate buffered saline
PCBC	Progenitor cell biology consortium
PCR	Polymerase chain reaction
P_i	Inorganic phosphate
qPCR	Quantitative
RA	Retinoic acid
RPE	Retinal pigment epithelium
SCID	Severe combined immunodeficiency
SERCA	Sarcoendoplasmic reticulum calcium ATPase
SMD	Stargardt macular degeneration
SMP	Skeletal muscle progenitor
sPBS	Stockholm's phosphate buffered saline
SRF	Serum response factor
TA	Tibialis anterior
TCF	T cell factor
TFBS	Transcription factor binding site
TGFB	Transforming growth factor beta
TTN	Titin
WNT	Wingless-related integration site

List of Figures

List of Tables

Chapter 1: General Introduction: Embryonic skeletal myogenesis *in vitro* and its potential therapeutic applications

1.1 Rationale & Statement of Objectives

Collectively, skeletal muscle makes up the largest organ system of the healthy human body at approximately 35 – 45% of lean body mass (1). Therefore, treating dysfunctional muscle via cell therapy poses a formidable challenge of scale. Myoblasts and satellite cells derived from adult donor muscle biopsies may not provide the cell quantities necessary for effective system-wide administration (2), and become less functional with *in vitro* expansion (3, 4). The near-limitless replication potential of human embryonic stem cells (hESC) may overcome this limitation; however, their differentiation must proceed efficiently into the skeletal muscle lineage. Conventional serum-dependent *in vitro* differentiation protocols are inefficient, driving fewer than 5% of the total culture into the skeletal muscle lineage (5–7). The low frequency of cells in the desired myogenic lineage, and heterogeneity of off-target cell types, makes the use or study of hESC-derived myogenic cultures confoundingly difficult. Therefore future study of myogenesis should strive to reach the following goals:

1) A directed *in vitro* skeletal muscle differentiation—guided by the signaling events during normal *in vivo* muscle development—should be designed to drive the majority of hESCs in culture through the myogenic lineage.
2) The hESC-derived myogenic cultures should contain skeletal muscle progenitors (SMP) characteristically similar to quiescent satellite cells—according to gene expression profiling—to provide the greatest *in vivo* therapeutic potential (8).
3) SMPs should replenish the satellite cell niche and contribute to host muscle fibers after the cells' injection into the injured hind limbs of immunodeficient mice.

The works presented in this thesis have attempted to address all three fronts.

1.2 Skeletal Muscle Structure & Function

1.2.1 Muscle cell structure

A single multinucleated muscle cell (myofiber) contains highly organized contractile protein bundles (myofibrils) that are themselves composed of alternating strands of structural proteins (myofilaments): actin (thin filaments) and myosin (thick filaments), as reviewed in (9, 10). The myofilaments are organized into basic contractile units (sarcomeres) that repeat along the length of the myofibrils. Either end of the sarcomere is defined by the Z line: a dense bundle of structural proteins that serves to directly anchor the thin filament actin, and indirectly anchor the thick filament myosin through titin (TTN). The Z line also connects the sarcomere to the dystroglycan complex (DGC) on the myofiber cell membrane (sarcolemma) via gamma actin and desmin intermediate filaments. Dystrophin (DMD) also helps anchor the sarcomere to the DGC via binding with the filamentous actin. At the center of each sarcomere is the M line: a bundle of myomesin and obscurin proteins that bind to and provide support for myosin and TTN of the thick filaments.

The myofibrils are surrounded by the sarcoplasmic reticulum and mitochondria. The sarcoplasmic reticulum serves as a calcium store in myofibers. The mitochondria generate ATP required to prime myosin for contraction, and are more numerous in aerobic slow twitch (Type I-MYH7^{+}) myofibers. Aerobic myofibers appear histologically red due to the relative abundance of iron-rich myoglobin relative to pale-white anaerobic fast twitch myofibers. Fast twitch (Type IIA-MYH2^{+} and IIX-MYH1^{+}) myofibers, meanwhile, are more dependent on glycolytic than mitochondrial ATP generation. Type IIB-MYH4^{+} myofibers are not present in human muscle despite the presence of MYH4 in the human genome (11).

1.2.2 Muscle repair

New muscle tissue is formed via regeneration—triggered by exercise- or injury-induced repair—from a dormant population of myoblasts known as satellite cells. Satellite cells remain mitotically quiescent in their resting state, and are characterized by the expression of PAX7 (12), and by the absence of the myogenic regulatory factors (MRF) MYOD1, MYF6 (MRF4), and MYOG. Resting satellite cells may or may not express mRNA of the MRF MYF5 (13); however, post-transcriptional sequestration of its transcript in mRNP granules may prevent the translation of functional MYF5 protein (14). Similarly, ZFP36 (TTP) promotes the post-transcriptional decay of MYOD1 mRNA to help maintain satellite cell quiescence (15).

Upon activation, MYF5 mRNA is released from regulatory mRNP granules (14), and elevated MAPK (p38) signaling helps induce MYOD1 protein expression (16). Post-translational inactivation of PAX7 in activated satellite cells is also required for the differentiation program to proceed. Recent studies indicate that NEDD4 can bind and ubiquitinate PAX7 (17), marking the protein for degradation; also, CASP3 can cleave and inactivate PAX7 directly (18).

Activated $MYF5^{+}$/$MYOD1^{+}$ satellite cells are highly proliferative. After several days of cell division, the upregulation of MYF6 and MYOG help remove myoblasts from the cell cycle and encourage their differentiation into MYH-expressing myocytes (19–21). These terminally differentiated myocytes align and fuse with each other or the adjacent myofibers, adding structural bulk to new or growing myofibers. Other side populations of cells also contribute to muscle function and repair (22), including fibro-adipogenic progenitors (FAP)(23, 24), $PEG3^{+}$ interstitial cells (25), $TWIST2^{+}$ progenitors (26), as well as blood vessel-associated mesoangioblasts (27, 28), pericytes (29), and macrophages (30).

Another important function of satellite cells is their self-replenishment; a subset of activated satellite cells reverts back into a quiescent state. This is achieved partly by the manner in which $PAX7^{+}/MYF5^{-}$ satellite cells divide. These cells can undergo asymmetric division, wherein one daughter cell maintains its $PAX7^{+}/MYF5^{-}$ progenitor state while the other cell becomes a $PAX7^{+}/MYF5^{+}$ myoblast (13). This polarity is achieved—in part—by the selective segregation of pro-differentiation intracellular components towards the $PAX7^{+}/MYF5^{+}$ fated daughter cell (16, 31). This provides a source of proliferative $PAX7^{+}/MYF5^{+}$ myoblasts for differentiation and repair while simultaneously replenishing and maintaining the $PAX7^{+/}MYF5^{-}$ satellite cell pool. Thus, the muscle is capable of maintaining its integrity under the frequent or heavy use throughout life. Pathological conditions such as advanced age or genetic diseases, however, can prevent skeletal muscle from functioning properly, or result in satellite cells being unable to keep pace with repairing the abnormal levels of damage. Mouse studies suggest that aged satellite cells may be functionally competent; rather, the aged muscle environment or systemic factors may be responsible for impaired muscle regeneration in elderly animals (32–34). More recent human studies on the subject of ageing skeletal muscle have proven less conclusive (35, 36).

1.3 Muscular Dystrophy

1.3.1 History of muscular dystrophy and the dystrophin gene

Sir Charles Bell is credited with first describing muscular dystrophy in his 1824 "An Exposition of the Natural System of Nerves of the Human Body" (37). However, the leading form of the disease is named after Guillaume Duchenne de Boulogne (38): mentor to the "father of neurology" Jean-Martin Charcot, and a credited influence on the works of Charles Darwin (39). Since de Boulogne's characterization of Duchenne Muscular Dystrophy

(DMD) in 1868, several other types of muscular dystrophy have been identified, the more prominent of which include: Becker, Emery-Dreifuss, Facioscapulohumeral (FSHD), Limb-Girdle, Myotonic, Oculopharyngeal, and broad-category Congenital Muscular Dystrophies.

The genetic causes of most but not all muscular dystrophies are mutation in the genes of—or related to—the dystroglycan complex (Section 1.2.1). Briefly, the DGC is a membrane associated complex responsible for linking the myofibers' contractile cytoskeleton with the extracellular matrix, thereby providing structural integrity to the myofiber membrane. Without a fully functional DGC, myofiber cell membrane integrity is compromised and can tear with contraction. This chronic stress can lead to ion leakage and imbalance, inflammation, and myofiber necrosis. Furthermore, dystrophin of the DGC plays a role in establishing satellite cell polarity during asymmetric division (31); the lack of satellite cell polarity may also be an aggregating factor in muscular dystrophy pathology as the satellite cell progenitor pool becomes dysfunctional or exhausted.

The labs of Ronald G. Worton and Louis M. Kunkel succeeded in identifying the underlying cause of DMD over 1986 and 1867 with the characterization of the dystrophin gene, also named DMD (40–42). The gene is located on the Xp21 chromosome region at 2.3 MBs long. Its 14 kB mature mRNA takes 16 hours to transcribe and contains 79 exons encoding a 3 685 amino acid protein (43).

Almost half of all muscular dystrophy patients fall under Duchenne and Becker categories, meaning they harbor mutations in the DMD gene (44). Duchenne manifests as the more severe form of the two, owing to more deleterious mutations in the DMD gene such as deletions that alter the reading frame and introduce premature stop codons. Truncated DMD proteins are unstable and degrade rapidly, leading to no detectable dystrophin in patients with the Duchenne form of muscular dystrophy. The Becker form consists of milder types of

DMD mutations—such as in-frame deletions within the central rod domain—leading to a shortened but stable and functional protein product. The muscle weakness associated with the Duchenne form manifests itself in early childhood, with affected individuals confined to a wheelchair by their teen years. The disease becomes fatal from the late teens to early twenties primary due to cardiac and pulmonary failure, as heart and diaphragm function are progressively compromised (45–47). Becker muscular dystrophy presents closer to the pre-teen years, with life expectancy reaching into the patients' thirties and forties. As cardiac dysfunction also presents in muscular dystrophy, supplemental cardiac intervention will be important to consider in conjunction with treatment of the diaphragm and skeletal muscles.

1.3.2 Contemporary and novel interventions

Conventional intervention in DMD may include pharmacological treatment—especially with corticosteroids—to slow disease progression (48). Physiotherapy is also often used to mitigate the effects of muscle weakness and help improve patient breathing (49).

The more experimental interventions include gene therapies, which have shown promising results with *in vivo* models of muscular dystrophies. While the full length DMD cDNA is 14 kb long, various microdystrophin cDNA have been engineered under 4.9 kb by eliminating most of the spectrin-like repeats in DMD's central rod domain. Golden retriever animal models of muscular dystrophy show efficient (> 50%) and long term (> 2 years) expression of Adeno-associated virus (AAV) mediated-delivery of microdystrophin, imparting significant improvements in force generation in the virus-injected muscles (50, 51). Other animal studies show systemic AVV-mediated gene therapy can target and improve *mdx* mouse hearts, and can be directed to the diaphragm in human patients (52, 53). AAV-mediated gene therapy is applicable to myopathies and neuropathies involving other

components of the contractile apparatus as well; clinical trials have been undertaken to replace SMN1 in spinal muscular atrophy (SMA), and to replace dysfunctional sarcoglycans of the DGC (54). Clinical trials with AVV-delivered microdystrophin, however, have not shown long-term dystrophin expression, and may even lead to dystrophin-immunity (55). Other research has focused on the regulation of the UTRN gene (56). Utrophin is a homolog of dystrophin normally found at the neuromuscular junction, but its over-expression may help compensate for the lack of dystrophin across diseased muscle fibers.

Technological advances are not to be discounted in addressing different facets of muscle wasting disorders, including the weakening heart, loss of diaphragm function, and loss of mobility.

Human trials have shown patients living weeks with artificial hearts until suitable biological donor hearts could be obtained. Pump systems—similar to ventricular assist devices already used by hundreds of thousands of patients—can completely take over cardiac function in bovine and human subjects for months, letting subjects live with no discernable heartbeat (57–59). Several artificial lung prototypes are in development, and in animal models, can sustain breathing function for hours to weeks depending on whether the devices operate with either ambient air or portable oxygen tanks (60–62).

Though less imperative than the internal organs, prosthetic limbs and exoskeletons have advanced rapidly. Prosthetics from BionX (63), Mobius Bionics (64), and Open Bionics allow a person's own nerves to be remapped onto wireless controls, offering fairly natural movement of the prosthetic limbs and even gross motor control over individual fingers. Lower and upper body exoskeletons by HAL sense intended muscle contractions through the skin to aid movement, and are in testing with para- and quadriplegic patients (65, 66). Also, 3D-printable soft synthetic materials are being developed that may provide a more natural

look and feel to prosthetics. These materials—at a cost of 3 cents/gram—are capable of contraction through simple electrical stimulation, lifting over 1 000× its own weight (67).

1.4 Stem Cells

1.4.1 Discovery of the stem cell

Conceptualization of the "stem cell" was undertaken by several minds of the late 1800's to explain the origins of an entire organism, including Charles Darwin's gemmules (68), Ernst Haeckel's stammzelle (69), and August Weismann's germ-plasm (70). Much of the earliest work to experimentally demonstrate stem cells, however, revolved around the adult hematopoietic system. Artur Pappenheim and Alexander Maximow describe their observations of the hematopoietic stem cell and its progeny at the turn of the 20th century (71), but it was not until seminal work by Dr. Florence Sabin the 1930's that the hematopoietic stem cell was experimentally supported (72, 73). Sabin suggested that the hematopoietic stem cell resided in bone marrow and that radiation inhibited the cells' differentiation. Similar findings were reported by Jacobson *et al*. in the 1940's regarding irradiation experiments of the spleen (74), wherein non-marrow hematopoietic progenitors also reside. In the mid 1950's, Ford and colleagues would go on to show that spleen transplant (75)—and Dr. Edward Thomas that bone marrow transplant (76)—could restore lethal irradiation-ablated hematopoiesis, building further support of the hematopoietic stem cell. Shortly thereafter in the early 1960's, McCulloch and Till developed a method to clonally demonstrate that many cells of the hematopoietic lineage definitely originate from a common progenitor (77, 78).

It was around this time—in 1961—that Alexander Mauro first described the existence of muscle satellite cells in adult frog muscle (79). Here, Mauro observes cells with little to no

cytoplasm residing adjacent to the muscle cell membrane, but beneath the basal lamina that encapsulates each muscle fiber. It was postulated at the time that these satellite cells may be the stem cell of muscle regeneration; this turned out to be the case (Section 1.2.2).

1.4.2 Cell therapy

Donor myoblasts or satellite cells—being the muscles' resident stem cell—would intuitively be a source of donor material for the stem cell therapy of Duchenne muscular dystrophy. In fact, clinical trials of myoblast cell therapy have been underway since the turn of the 1990's yet myoblast cell therapies have not progressed beyond the trial stage (reviewed in (80)). Research has importantly, however, made progress into revealing what does not work.

Broadly speaking, these trials have collectively demonstrated that donor cell engraftment is primarily limited to the injection trajectory of the needle used to deliver the cells, and that immune-rejection of donor cells likely prevents meaningful SMP proliferation and long-term engraftment (2, 81). Cell therapies using other types of myogenic progenitors—including bone barrow or mesoangioblast cells—also show limited viability with low engraftment and retention rates (82, 83).

Direct intramuscular injections often require tens to hundreds of millions of myoblasts, and even then the area of muscle that can be treated is limited.

Some clinical studies suggest that high density injection of tens of millions of myoblasts over just 1 cm^2 may be required to obtain notable engraftment (2). In line with this observation, the treatment of smaller dystrophic muscles with myoblast cell therapy has been more fruitful: one clinical study showed that treatment of the pharyngeal muscles significantly improved swallowing time in patients with Oculopharyngeal muscular

dystrophy (84). However, most clinical studies in treating muscular dystrophy with cell therapy show non-viable levels of engraftment, and especially poor long-term donor cell retention (80).

The magnitude of cell requirements in muscle stem cell therapy is such that one adult donor can often supply the cells required for just one patient (2, 83). And while satellite cells can be proliferated *in vitro*, their culture is associated with differentiation and a decrease in engraftment potential (3, 4); animal models demonstrate that freshly isolated or more quiescent satellite cells are associated with better engraftment rates than their activated counterparts. Some studies have made progress in suppressing differentiation of activated satellite cells *in vitro* while still allowing for their proliferation (8, 85, 86). Also concerning the *in vitro* expansion of therapeutic populations, the adult cell may proliferate notably slower than its embryonic counterpart (27, 83).

Embryonic stem cells, however, are capable of nearly unlimited proliferation, and can differentiate into cells of the skeletal muscle lineage (87, 88). Various pluripotent stem cell-derived tissues have undergone or are undergoing clinical trials, lending credence to their safety in patients (Table 1.1). Therefore, the *in vitro* skeletal myogenesis of embryonic stem cells offers an enticing avenue to generate a nearly unlimited supply of skeletal muscle progenitors that may be functionally analogous to adult-derived satellite cells.

1.4.3 Embryonic stem cells

The existence of pluripotent cells within the inner cell mass of the mouse blastocyst was experimentally demonstrated in 1970 (89), and an *in vitro* culture system was developed for mouse embryonic stem cells (mESCS) in 1981 (90). Reliably generating skeletal muscle from mESCs *in vitro* was demonstrated as a proof of concept in 1994 (87).

Principal Investigator	Trial Posted	Disease	Cell Type	Trial Status
Lanza, R. (91, 92)	2011	AMD / SMD	Retinal Pigment Epithelium	Complete
Coffey, P. J. (93)	2012	AMD	Retinal Pigment Epithelium	Complete
Menasché, P. (94, 95)	2014	Ischemic Heart Disease	Cardiac Progenitors	Active
Zhou, Q. (96)	2017	AMD	Retinal Pigment Epithelium	Recruiting
Lebkowski, J. S. (97)	2017	AMD	Retinal Pigment Epithelium	Recruiting
Zhou, Q. (96)	2017	Parkinson's	Neural Precursors	Recruiting
Gotkine, M. (98)	2018	ALS	Astrocyte Precursors	Recruiting
Lebkowski, J. S. (99, 100)		Spinal Cord Injury	Oligodendrocyte Progenitors	Pre-clinical
Perlingeiro R. C. R. (101)		DMD	iPAX7-Progenitors	Pre-clinical
Tabar, V. S. (102)		Parkinson's	Dopamine Neurons	Pre-clinical

Table 1.1

Table 1.1. Clinical trials of stem cell therapy using human embryonic stem cell-derived donor cells. Some of the earliest studies of Age-related macular degeneration (AMD) Stargardt macular degeneration (SMD) have shown improved patient vision out to one year after the transplantation of hESC-derived retinal pigment epithelium (RPE).

This method of differentiation made use of aggregating the cells in suspended clumps—known as embryoid bodies (EB)—prior to adhering them onto tissue culture plates. The EB aggregation and plating process was thought to recapitulate the cell to cell contacts necessary for development of the pre-implantation blastocyst and subsequent implanted stage of the embryo. In addition to the physical parameters driving differentiation, the culture media were also supplemented with fetal bovine serum (FBS)(87).

Human embryonic stem cell lines were derived in 1998 from the inner cell mass of blastocyst stage embryos—donated from *in vitro* fertilization clinics—and were shown to form striated muscle as part of an 8 week teratoma assay in SCID/Beige ($Prkdc^{scid}$ $Lyst^{bg}$) mice (88). The hESCs' potential for *in vitro* skeletal myogenesis was not demonstrated until 2005 (5). The *in vitro* hESC differentiation proceeded for approximately 6 weeks in monolayers, after which 5% of cells could be fluorescence-activated cell sorted (FACS) for CD73. A subset of these $CD73^{+}$ cells was found to express MYOD1 and form myotubes after an additional 2 to 3 weeks in culture. Like *in vitro* mESC skeletal myogenesis, FBS-supplemented media was utilized to help drive the differentiation of hESCs.

1.4.4 Induced pluripotent stem cells

Induced pluripotent stem cells (iPSC) are another source of pluripotent cells that does not require a human blastocyst. Somatic cells can be reprogrammed into an embryonic-like state by exposing the cells to the combination of KLF4, MYC, POU5F1 (OCT4), and SOX2 transcription factors (103). This reprogramming was traditionally achieved by retroviral transduction, however, other technologies are available today that do not permanently alter the cell genome (104): cells can be reprogrammed by non-integrating viruses or by direct transduction of recombinant mRNA molecules for each pluripotency-inducing gene (105).

iPSCs provide a unique avenue whereby gene therapy and cell therapy converge. A patient's own somatic cells can be harvested and reprogrammed into iPSCs, followed by the correction of their genetic mutation using any of an array of DNA editing technologies, such as TALEN and CRISPR (106–109). The genetically corrected iPSCs can then be proliferated to appreciable quantities and differentiated into the affected tissue type required for therapy (106, 110). The epigenetic patterns of iPSC genomes can be influenced by their tissue of origin or method of culture, however, which raises concerns that iPSCs may behave dissimilar to true pluripotent cells and show tissue-linage bias when differentiated (111–113).

Lineage bias and other precocious differentiation is concerning, as pluripotent cell-based therapy would be limited by the efficiency of *in vitro* differentiation into the desired tissue type. Serum-induced *in vitro* skeletal myogenesis was evidently inefficient, would indiscriminately produce off-target tissue lineages, and different serum lots would yield variable results (87). There is also the issue of introducing non-human biological material into patients.

This was especially concerning, as contemporary clinical trials of muscle stem cell therapy required as many as 300 million donor myoblasts (Section 1.4.2)(81). Clearly, the efficiency of *in vitro* hESC skeletal myogenesis needed to improve beyond a mere subset of 5% of total cells to meet the cell numbers required for stem cell therapy. Therefore, the undefined milieu of growth factors and signaling molecules native to FBS needed to be replaced with defined concentrations of specific compounds in order to direct *in vitro* differentiation towards only the skeletal muscle lineage. The types of compounds required, and the timing of their use, could be gleaned from knowledge of skeletal myogenesis in the embryo.

1.5 Embryonic Muscle Development

1.5.1.1 Mesoderm induction

Understanding *in vivo* embryonic development is pivotal in developing protocols to direct the *in vitro* differentiation of hESCs into specific tissue lineages. Development of the human embryo is temporally described by gestational age or embryonic age. These two systems differ in that gestational age—most commonly used clinically—begins from the last menstrual period, whereas embryonic age—as used in this thesis—begins from fertilization. Special attention must be given to the timing, transcription factors, and signaling molecules responsible for transforming one embryonic structure into its derivative structures (reviewed in (114–116)).

Fertilization marks embryonic day 1. The *in vitro* fertilized eggs used for deriving hESC lines are typically developed until the blastocyst stage around days 4 – 5 (117). The blastocyst contains an inner cell mass of pluripotent cells surrounded by a trophoblast cell layer and zona pellucida glycoprotein layer; the inner cell mass is extracted for generating *in vitro* pluripotent cell lines (Fig. 1.1)(88). Expression of the transcription factors NANOG (118), POU5F1 (119), and SOX2 (120), can be used to identify pluripotency at this stage.

The blastocyst attaches and implants into the uterine endometrium by the end of the first week (121). At this stage, the inner cell mass will develop into a bilaminar embryonic disc comprised of the dorsal epiblast and ventral hypoblast layer (Fig. 1.2). Structurally, the hypoblast layer only forms extraembryonic endoderm (122). The hypoblast layer does, however, provide signaling factors critical for embryo patterning (123, 124).

The epiblast will form all three germ layers of the embryo—ectoderm, endoderm, and mesoderm—through a process known as gastrulation (reviewed in (125)). Gastrulation begins around the end of the second week marked by the onset of the primitive streak: an

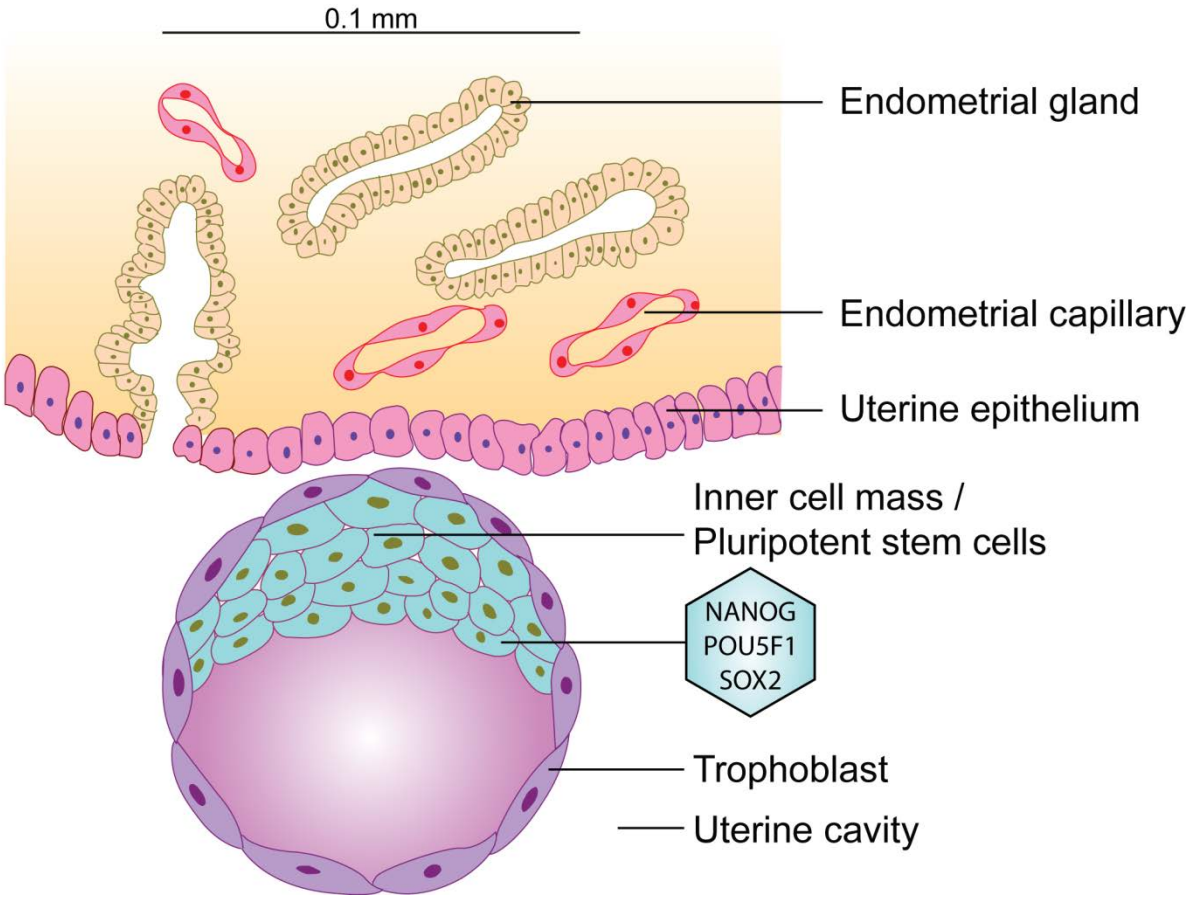
0.1 mm
Endometrial gland
Endometrial capillary
Uterine epithelium
Inner cell mass /
Pluripotent stem cells
NANOG
POU5F1
SOX2
Trophoblast
Uterine cavity

Figure 1.1

Figure 1.1. The inner cell mass from which pluripotent embryonic stem cells are derived is present in roughly day 5 pre-implantation human blastocysts. Transcription factors commonly used to denote pluripotency are indicated in the blue hexagon. Image adapted from Motifolio Inc.

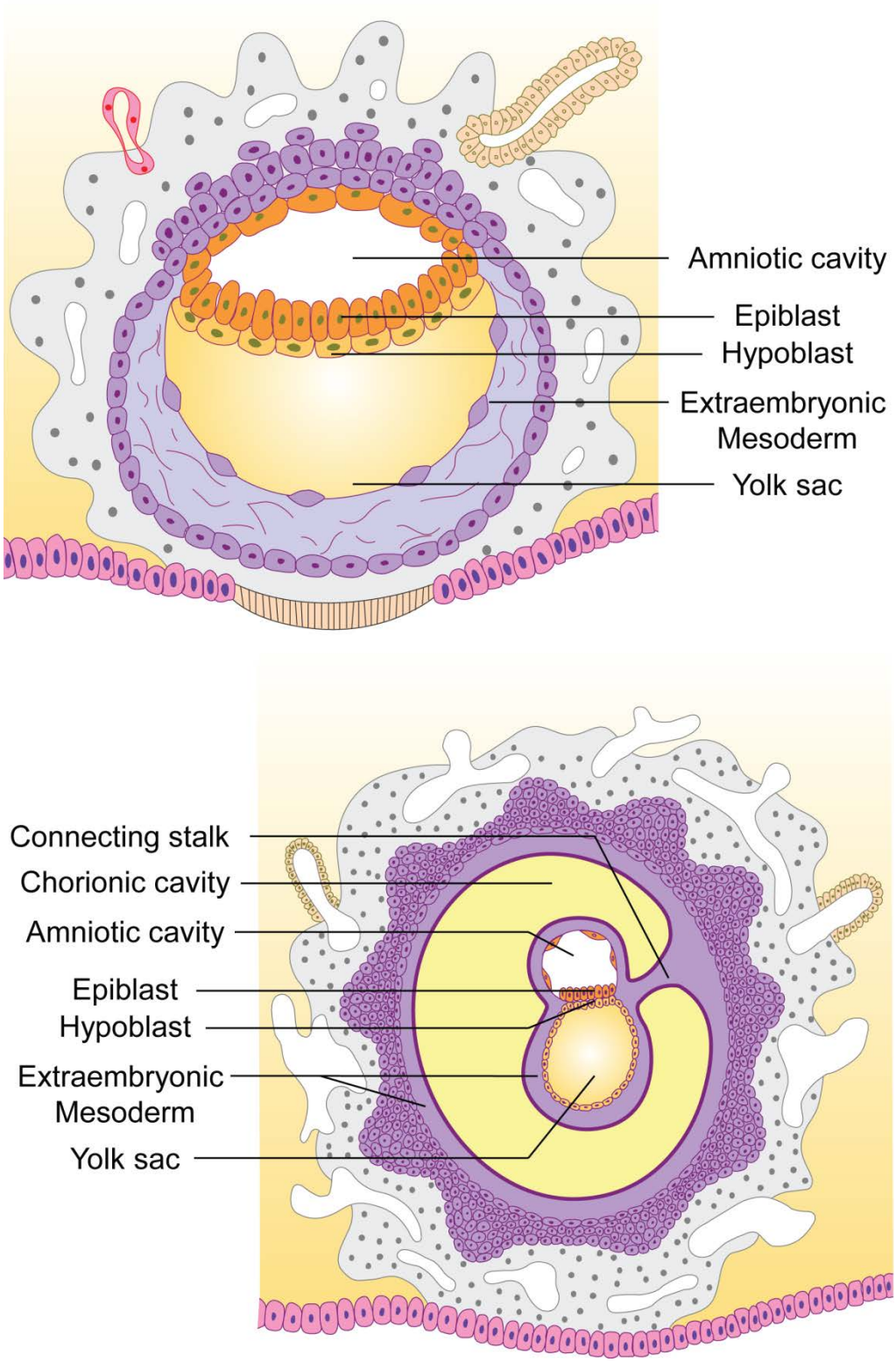
Amniotic cavity
Epiblast
Hypoblast
Extraembryonic Mesoderm
Yolk sac
Connecting stalk
Chorionic cavity
Amniotic cavity
Epiblast
Hypoblast
Extraembryonic Mesoderm
Yolk sac

Figure 1.2

Figure 1.2. The bilaminar embryonic disc is evident during the second week of development. Approximately day 9 (top) and day 13 (bottom) are represented. Notable development includes the establishment of amniotic and yolk cavities. Hollowing of the extraembryonic mesoderm (purple) adjacent to the yolk sac will form the chorionic cavity, which eventually surrounds and cushions the entire embryo. Image adapted from Motifolio Inc.

inward fold at the dorsal surface of the epiblast midline that runs along the anterior-posterior axis. Epiblast cells surrounding the primitive streak site undergo endothelial to mesenchymal transition (EMT) and migrate ventrolaterally through the fold, replacing the hypoblast with definitive endoderm, followed by formation of the mesoderm germ layer.

1.5.1.2 Mesoderm signaling events

Understanding the signaling molecules involved during generation of the mesoderm germ layer is critical for the directed differentiation of skeletal muscle *in vitro*, as all skeletal muscle is derived from this mesoderm. Some of the more well studied signaling systems during gastrulation include WNT (126, 127), NODAL, FGF (128, 129), and BMP (Fig. 1.3)(reviewed in (130)).

High levels of WNT signaling from the posterior epiblast activate NODAL signaling anteriorly, at the site that will become the primitive node (131–133): an organizing center for gastrulation and notochord development. While the hypoblast does not structurally contribute to the embryo, it secretes the TGFB-superfamily inhibitor CER1 to antagonize NODAL signaling from the anterior end of the embryo (123, 124), thus helping establishing the anterior boundary of the primitive streak. FGF signaling from the posterior end of the embryo coordinates with WNT and NODAL to initiate primitive streak formation, and will play a continued role in patterning the resulting mesoderm (134, 135). As the hypoblast is displaced with definitive endoderm, CER1 repression at the anterior end of the primitive node is damped and allows for the anterior extension of the primitive streak, after which predominantly posterior extension occurs (136).

The primitive node also secretes BMP inhibitors CHRD (137), and NOG (138), that play an important role in patterning mesoderm created from the primitive streak. BMP is

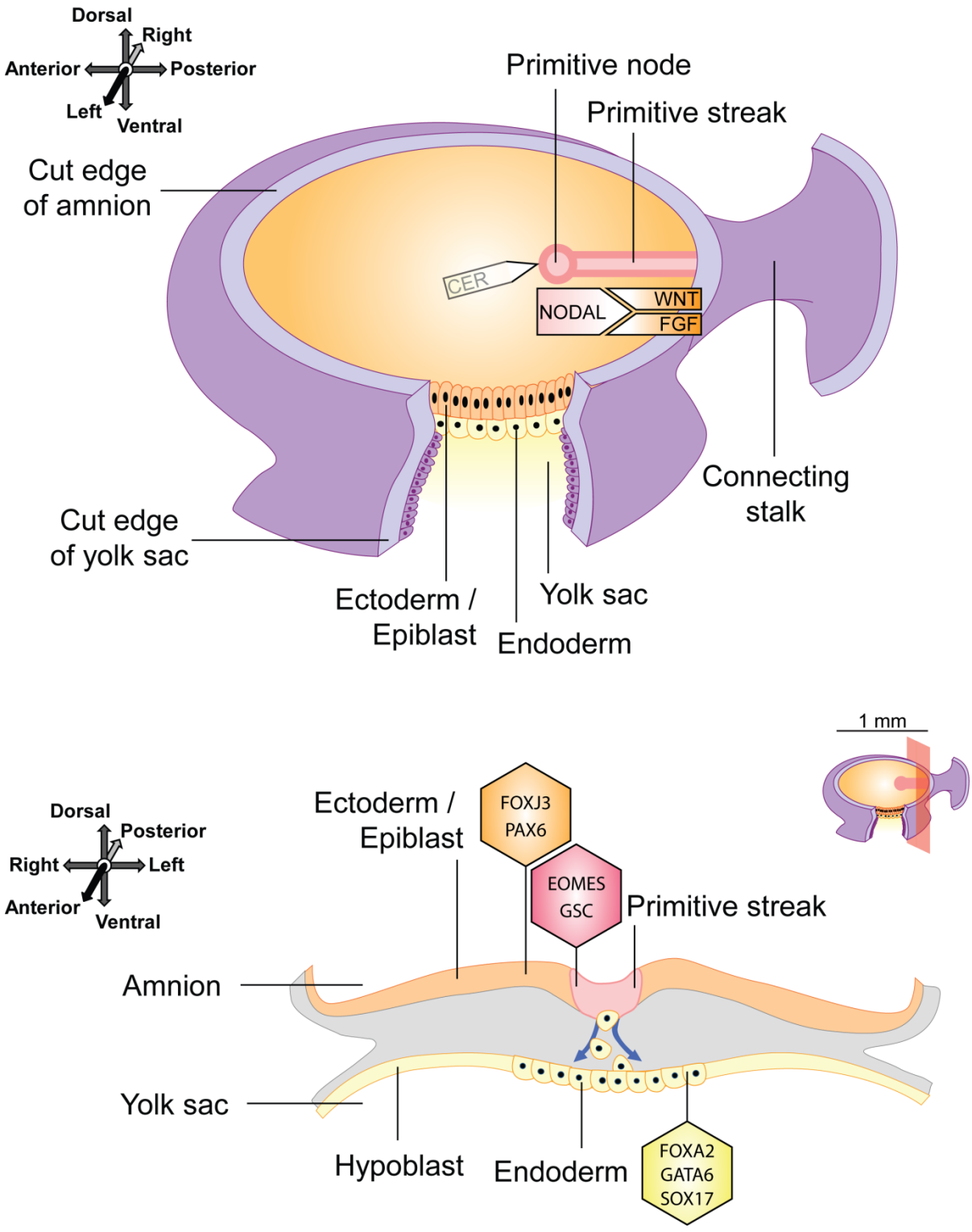
Dorsal
Right
Anterior
Posterior
Left
Ventral
Primitive node
Primitive streak
Cut edge of amnion
CER
NODAL
WNT
FGF
Connecting stalk
Cut edge of yolk sac
Ectoderm / Epiblast
Endoderm
Yolk sac
1 mm
Dorsal
Posterior
Right
Left
Anterior
Ventral
Ectoderm / Epiblast
FOXJ3
PAX6
EOMES
GSC
Primitive streak
Amnion
Yolk sac
Hypoblast
Endoderm
FOXA2
GATA6
SOX17

Figure 1.3

Figure 1.3. Primitive streak progression around day 15 marks the onset of formally specified endoderm, ectoderm, and mesoderm germ layers. A wide-view of the day 15 embryo (top) and transverse cross-section (bottom) are represented. Transcription factors that may identify the three early-stage germ layers are indicated in their respectively colored hexagons (139). The first cells to pass through the primitive streak displace the hypoblast and form definitive endoderm. An anatomical plane compass is located immediately top-left of both the wide-view and cross-section images. A positioning guide is located immediately top-right of the cross-section to indicate where the slice was taken from the wide-view embryo (red rectangle). Image adapted from Motifolio Inc.

secreted from the extraembryonic ectoderm, leading to high BMP signaling levels throughout the lateral epiblast (140). Therefore, CHRD and NOG establishes a unique zone of local BMP repression proximal to the primitive node (Fig. 1.4).

Mesoderm cells that migrate through the posterior end of the primitive streak—distant from the primitive node—are exposed to high levels of BMP signaling, and migrate anteriorly most distal to the midline to form the lateral plate mesoderm (141). The dorsal lateral plate mesoderm (somatic) will form the limb bud and ventral dermis mesoderm, while the ventral lateral plate mesoderm (splanchnic) derivatives include cardiac and smooth muscle, hematopoietic cells, and trunk mesoderm (142). Cells migrating through the middle of the primitive streak along its anterior-posterior axis become intermediate mesoderm, which is responsible for developing the urogenital system.

The anterior end of the primitive streak experiences repressed BMP signaling due to its proximity to CHRD and NOG secreted from the primitive node. These cells become fated towards paraxial mesoderm and migrate anteriorly more proximal to the midline on either side of the neural tube (141); its somite derivatives include the target tissue—skeletal muscle—as well as the trunk bones and dorsal dermis (142).

1.5.2 Somite development

Somites are roughly spherical structures that arise from segmentation of paraxial mesoderm. Segmentation begins at the anterior end of the paraxial mesoderm just before week 4, and progresses posteriorly at a rate of 3 to 4 somite pairs per day through week 5 (142, 143). The timing of segmentation and the size of each somite pair is a complex and tightly controlled process.

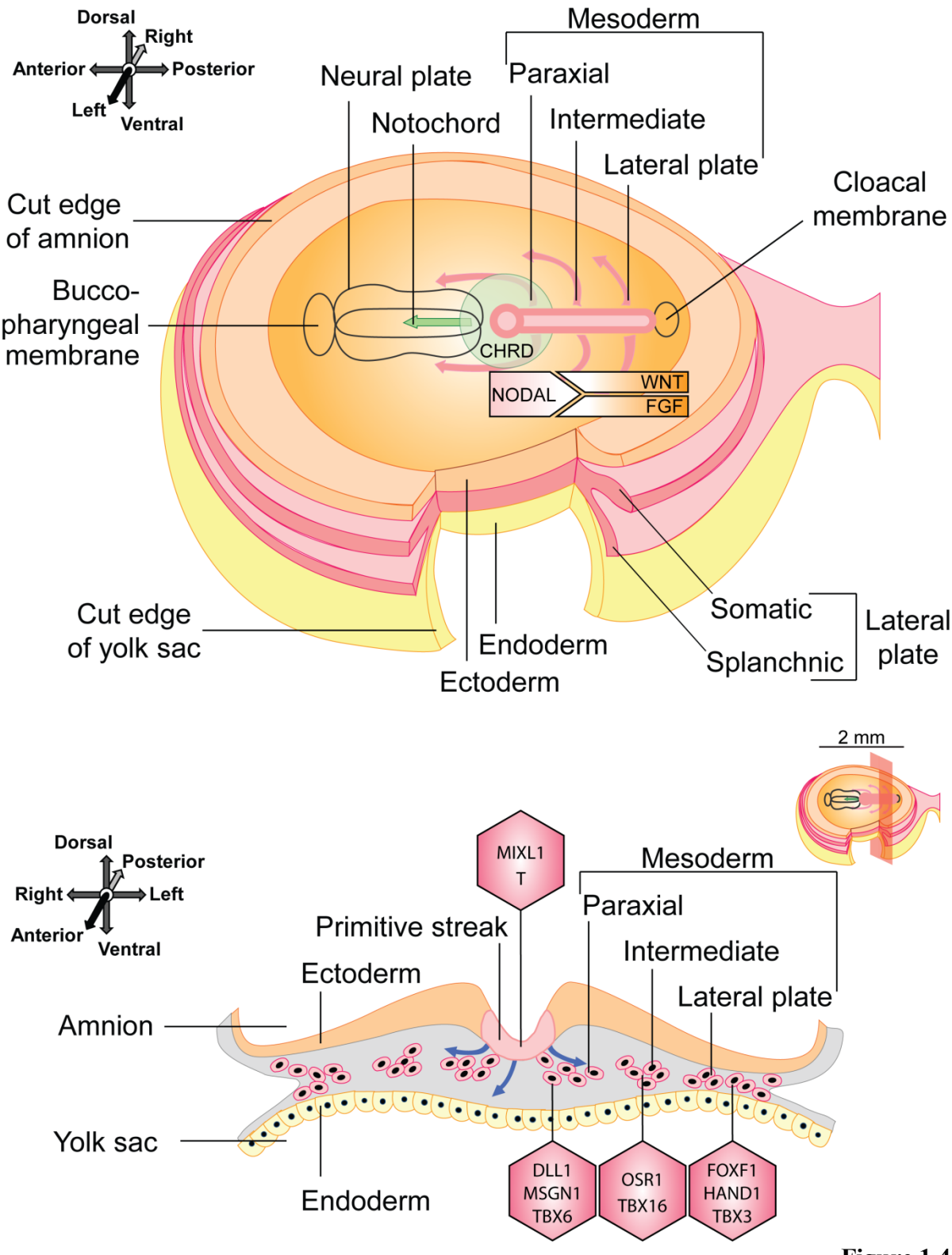
Dorsal
Right
Anterior
Posterior
Left
Ventral
Mesoderm
Neural plate
Paraxial
Notochord
Intermediate
Lateral plate
Cut edge of amnion
Cloacal membrane
Bucco-pharyngeal membrane
CHRD
NODAL
WNT
FGF
Cut edge of yolk sac
Endoderm
Ectoderm
Somatic
Splanchnic
Lateral plate
2 mm
Dorsal
Posterior
Right
Left
Anterior
Ventral
MIXL1
T
Mesoderm
Paraxial
Primitive streak
Intermediate
Ectoderm
Lateral plate
Amnion
Yolk sac
Endoderm
DLL1
MSGN1
TBX6
OSR1
TBX16
FOXF1
HAND1
TBX3

Figure 1.4

Figure 1.4. The three major sub-compartments of mesoderm are specified during the third week depending on the cells' migration position along the primitive streak and their local signaling environment. A wide-view of the day 19 embryo (top) and transverse cross-section (bottom) are represented. Transcription factors that can identify the various early-stage mesoderm sub-compartments are indicated in pink hexagons (139). An anatomical plane compass is located immediately top-left of both the wide-view and cross-section images. A positioning guide is located immediately top-right of the cross-section to indicate where the slice was taken from the wide-view embryo (red rectangle). Image adapted from Motifolio Inc.

Hester *et al.* formulated one of the most robust computational models of somitogenesis (135), integrating various earlier "clock and wavefront" models into a loop of FGF, WNT, and NOTCH signaling pathways (134). In the Hester *et al.* model of the clock and wavefront, briefly, high levels of FGF and WNT signaling at the posterior end of the paraxial mesoderm feed forward to activate NOTCH signaling. Each pathway also triggers its own negative feedback loop, which resets and primes FGF and WNT signaling pathways to trigger another cycle of NOTCH signaling. A gradient of retinoic acid (RA) signaling from the anterior end of the embryo directly antagonizes FGF signaling, helping to define the "determination front" where somites boundaries are formally established and ultimately segregated (134).

Fortunately for *in vitro* skeletal myogenesis, recent work has demonstrated that myogenic derivatives of the somite develop normally from ectopically transplanted paraxial mesoderm, absent of the tightly regulated spatiotemporal clock and wavefront (144). Only the anterior-posterior patterning of the sclerotome appears to be affected in ectopically-derived somites. Therefore, attempting to recapitulate isosynchronous waves of FGF, WNT, and NOTCH *in vitro* may be wholly unnecessary to mature paraxial mesoderm-like cells into a somite-like stage for skeletal myogenesis.

1.5.3.1 Primary myogenesis: trunk

Somites continue to mature *in vivo*, in part, through the signaling activity emanating from surrounding developmental tissues (Fig. 1.5)(reviewed in (145)). The dorsal neural tube and ectoderm secrete dorsalizing WNT signaling molecules to specify the dermomyotome (146). BMP and NOTCH signaling from the neural tube and neural crest will play a later role in repressing differentiation directly at the dorsomedial lip domain, presumably to maintain a

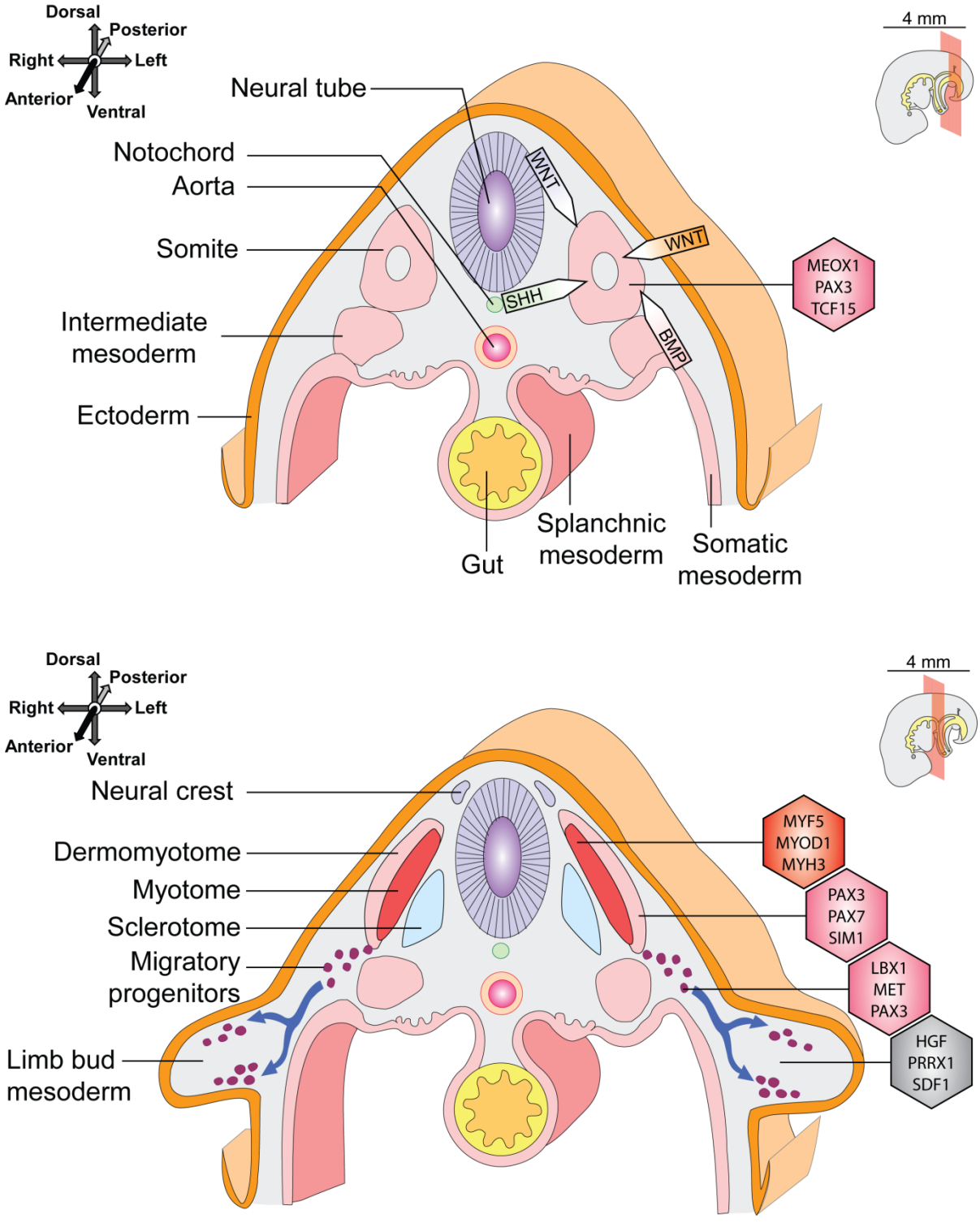
Dorsal
Posterior
Right
Left
Anterior
Ventral
4 mm
Neural tube
Notochord
Aorta
Somite
Intermediate mesoderm
Ectoderm
WNT
WNT
SHH
BMP
MEOX1
PAX3
TCF15
Gut
Splanchnic mesoderm
Somatic mesoderm
Dorsal
Posterior
Right
Left
Anterior
Ventral
4 mm
Neural crest
Dermomyotome
Myotome
Sclerotome
Migratory progenitors
Limb bud mesoderm
MYF5
MYOD1
MYH3
PAX3
PAX7
SIM1
LBX1
MET
PAX3
HGF
PRRX1
SDF1

Figure 1.5

Figure 1.5. The $PAX3^+/PAX7^+$ dermomyotome and migratory $PAX3^+$ cells mark the emergence of potential SMP populations. Two transverse cross-sections of the week 5 embryo showing relatively more immature posterior somites (top) and mature anterior dermomyotome (bottom) are represented. Transcription factors used to identify the mononuclear myotomal muscle are indicated in the red hexagon. Markers of the somite, dermomyotome, and its derivative migratory population are indicated in pink hexagons, while markers of the lateral plate-derived limb bud mesoderm are shown in grey. An anatomical plane compass is located immediately top-left of both the cross-section images. A positioning guide is located immediately top-right of the cross-sections to indicate where the slice was taken from a wide-view embryo (red rectangle). Image adapted from Motifolio Inc.

population of progenitor cells (146–148). Concomitantly, the ventral neural tube and notochord secretes ventralizing SHH molecules that specifies the sclerotome and aids in patterning the ventral myotome (146, 149). BMP signaling molecules from the lateral plate mesoderm also serve to pattern nascent somites (150), thus distinguishing the ventral lateral (hypaxial) region of the dermomyotome from the dorsal medial (epaxial) region.

At the transcription factor level, EYA1, EYA 2, SIX1 (151), and SIX4 (152), orchestrate the myogenic program in concert with the paired box (PAX) gene PAX3 throughout the dermomyotome, with especially high PAX3 expression observed at the dermomyotomal edges or lips (153, 154). $PAX3^+$ cells at the dorsomedial lip migrate under the dermomyotome (155), where PAX3 target genes MYF5 and MYOD1 are rapidly upregulated along with the concurrent downregulation of PAX3 as the cells become committed myoblasts (153). The myoblasts terminally differentiate into mononuclear myocytes as they align and elongate in the anterior-posterior direction (155), formally creating the first myotomal muscle around week 5 of development (156). $PAX3^+$ cells from the remaining dermomyotomal lips then migrate underneath and fuse with the mononuclear myotomal cells (157, 158), forming thin multinucleated myotubes that begin to express genes of the contractile apparatus (Section 1.2.1). The process of $PAX3^+$ cells migrating under the dermomyotomal lips to lay down myocytes—thus pioneering the first embryonic myotubes—is known as primary (embryonic) myogenesis of the trunk.

A version of this chapter has been published in Stem Cell Reports:

(1) Shelton, M., Metz, J., Liu, J., Carpenedo, R. L., Demers, S. P., Stanford, W. L., and Skerjanc, I. S. (2014) Derivation and expansion of PAX7-positive muscle progenitors from human and mouse embryonic stem cells. *Stem Cell Reports*. **3**, 516–529

1.5.3.2 Primary myogenesis: limb

Primary myogenesis in the limbs likewise revolves around migratory $PAX3^+$ progenitors, albeit with a more sophisticated network of migratory proteins (Fig. 1.5) (reviewed in (159, 160)). The anterior forelimb and posterior hindlimb bud—which arise at week 4 and 5, respectively (143)—are primarily composed of somatic lateral plate mesoderm until somite-derived myogenic progenitors migrate into the bud (161, 162). $PAX3^+$ limb muscle progenitors originate from the hypaxial dermomyotome of the cervical (C4 - C8, T1) and lumbar (L3 – L5) somites, respectively (163).

The ectodermal WNT and lateral plate BMP signaling factors unique to the hypaxial dermomyotome environment function with PAX3 to initiate the migratory program. Instead of activating the MRFs for myoblast commitment, some PAX3-expressing cells at the ventral lateral lip activate key migratory genes LBX1 and MET (164, 165), which in turn activates CXCR4 (166). MET and CXCR4 receptors initiate the EMT of hypaxial PAX3-expressing cells as they undergo chemoattraction towards the respective MET and CXCR4 ligands—HGF and SDF1—that are highly expressed in nascent limb bud mesoderm (166, 167). $PAX3^+$ migratory cells seed proliferative dorsal and ventral cell masses in the limb buds before undergoing myoblast commitment and terminal differentiation into skeletal myocytes, followed by fusion into thin multinucleated myotubes, thus achieving primary myogenesis in the limb (168).

1.5.4 Secondary myogenesis

The bulk of muscle mass forms during the subsequent phase of secondary (fetal) myogenesis from approximately week 8 (169). In the limb, secondary myogenesis occurs from populations of $PAX3^+/PAX7^+$ and $PAX3^-/PAX7^+$ cells that trace their origins to the

$PAX3^+$ migrating progenitors of the hypaxial dermomyotomal lip (170, 171)(reviewed in (172)). Recent evidence suggests that some $PAX7^+$ limb muscle progenitors may come from a linage distinct from the migratory $PAX3^+$ cells, and are rather associated with motor neuron outgrowths into the limb, though little is known about their significance (168).

$PAX7^+$ cells undergo a similar differentiation process as $PAX3^+$ myogenic progenitors, wherein MRF expression becomes elevated while PAX expression is downregulated. MRF-expressing myoblasts will seed new secondary fibers among the primary myotubes, and hypertrophy the myofibers through more robust myoblast fusion than that seen during primary myogenesis.

Secondary myogenesis in the trunk occurs from a population of $PAX7^+$ cells in the central region of the dermomyotome; these $PAX7^+$ cells migrate directly ventral into the myotome where they proliferate, differentiate, and fuse with primary myotubes of the trunk (170, 173). A subset of these diving $PAX7^+$ cells, however, maintain themselves in the undifferentiated state as they proliferate and take up residence immediately adjacent to the secondary myotubes (170). These self-replenishing progenitor cells—known as satellite cells for their "satellite" position adjacent to muscle fibers (79)—are essential for the continued muscle hypertrophy required as the fetus grows (Section 1.2.2)(12, 171). Evidence suggests that true satellite cells appear by E16.5 in the mouse (170), which corresponds to roughly week 12 or mid-secondary myogenesis of human fetal development (143, 174, 175).

Whereas PAX7 is dispensable for primary myogenesis (12, 171), PAX7 becomes the predominant PAX factor required for the maintenance of myogenic progenitors throughout adulthood (176), although PAX3 can be detected in the satellite cells of certain adult muscles (177, 178). Therefore, $PAX7^{\pm}$ SMPs showing myogenic potential represent a crucial

population for cell therapy. As such, novel protocols for the *in vitro* skeletal myogenesis of hESCs should strive to generate a robust population of PAX7$^{\pm}$ cells.

1.5.5 Craniofacial muscle development

Laryngeal and tongue muscle are largely derived from the occipital somites in a similar manner to the development of trunk and limb muscle, while the derivation of pharyngeal, facial expression, mastication, and extraocular muscles occurs via less well-understood mechanisms (reviewed in (179, 180)).

After gastrulation, the most anterior paraxial mesoderm settles at the cranial region and remains unsegmented. As development progresses, myogenic progenitors migrate from this cranial paraxial mesoderm towards the site of extraocular muscles, and into the pharyngeal arches from which the branchiomeric muscles—mastication, facial expression, and neck muscles—stem from. The pharyngeal arches are also seeded by splanchnic lateral plate mesoderm, and interestingly, give rise to the secondary heart field in addition to the various branchiomeric skeletal muscles. Thus, craniofacial skeletal muscles share developmental overlap and transcriptional regulators with certain cardiac muscles, including the expression of "canonically" cardiac genes such as ISL1, NKX2-5, and TBX1 (181–184). Further confounding the origins of craniofacial skeletal muscle are the observations that PAX3 expression in not detected in craniofacial progenitors while PAX7 is, but that craniofacial muscles can still migrate and develop normally in the absence of PAX7 (154).

1.6 Contemporary *in vitro* Myogenic Differentiation

1.6.1 Directed hESC myogenesis

The decade following the first demonstration of *in vitro* hESC skeletal myogenesis in 2005 has seen marked improvements to differentiation efficiency. Some of the most efficient differentiation protocols depend on the inducible overexpression of transgenic PAX3, PAX7, or MYOD1 constructs that commit over 90% of cells to the myogenic lineage (101, 185–187). However, virally-transduced cells may present a risk to patients, as genomic integration of the viral vector can be oncogenic, or trigger an inflammatory or immune response in the patient receiving altered cells (188–190). Inducing differentiation with transgenic constructs like MYOD1 also generates muscle from hESCs in scarcely over a week of culture, thus taking an overly artificial path of differentiation that may preclude the *in vitro* study or modelling of normal embryonic muscle development. Creating a directed *in vitro* skeletal myogenesis protocol for hESCs or patient-derived iPSCs may be especially useful in more closely modeling the natural pathology of congenital muscular dystrophies.

In order to have efficient skeletal myogenesis, pluripotent hESCs must first have efficient mesoderm induction. Since the serum-based approaches of Barberi *et al*. and Ryan *et al*., different strategies to induce pan- and cardiac-mesoderm from hESCs began to emerge that made use of recombinant proteins or small molecules to mimic the signaling activity during gastrulation (Section 1.5.1.2)(191–198). These mesoderm differentiation protocols provide insight into the effects of modulating WNT, BMP, and Activin/NODAL signaling at the onset of *in vitro* hESC differentiation. As might be expected from gastrulation in the embryo, active WNT and BMP signaling were paramount in generating lateral plate-like mesoderm for downstream cardiac myogenesis (191, 193, 196, 197). However, *in vivo* paraxial mesoderm is derived adjacent to the primitive node where BMP signaling is

repressed by CER1 and NOG: two proteins that are upregulated via coordinated WNT3A and NODAL function (132, 141).

In contrast with *in vitro*-derived WNT- and BMP-induced lateral plate mesoderm, therefore, we hypothesize that generating paraxial mesoderm from hESCs for downstream skeletal myogenesis should proceed with high WNT signaling absent of BMP induction.

1.6.2 WNT-mediated mesoderm induction

The small molecule CHIR99021 had proven effective at deriving various mesoderm subtypes from hESCs under serum-free conditions. CHIR99021 is an ATP-competitive inhibitor of GSK3B (reviewed in (199)). In addition regulating glycogen levels, the GSK3B kinase also phosphorylates and targets CTNNB1 (Beta-catenin) for degradation. CHIR99021-mediated inhibition of GSK3B allows CTNNB1 to accumulate in the cytoplasm where it can translocate to the nucleus to activate targets of canonical WNT signaling—as reviewed in (200, 201)—and initiate streak-like differentiation *in vitro* (133, 202).

The year 2013 saw several groups independently develop directed skeletal myogenesis protocols beginning with mesoderm induction—in part—via the small molecule GSK3B inhibitors CHIR99021 or 6-bromoindirubin-3′-oxime (BIO)(203–205). The duration of exposure to and concentration of the inhibitors varied, however, as did the apparent downstream efficiency of differentiation. Overall, these protocols using CHIR99021- or BIO-induced mesoderm for downstream skeletal myogenesis saw marked improvements in the proportion of cells that adopted a myogenic identity relative to previous serum-based differentiations, in which less than 5% of cultures were identifiably myoblasts or myocytes (Section 1.4.3)(5–7).

1.6.3 Characterizing in vitro-derived SMPs

Lower concentrations of CHIR99021 are sometimes used to differentiate mesoderm from hESCs for downstream skeletal myogenesis (203, 204). However, our own preliminary studies showed that initiating hESC differentiation with high concentrations of CHIR99021 led to greater expression of paraxial mesoderm-associated genes than with low concentrations of CHIR99021 (205). Therefore, we sought to perform gene expression profiling on high- and low-concentration CHIR99021-differentaited cultures to characterize and compare the potential cell populations being generated. Gene expression profiling after CHIR99021-treatment should reveal the presence of WNT target mesoderm-tissue genetic markers—such as T (206), MSGN1 (207), TBX6 (208), and TCF15 (Paraxis)(209)—and also markers of unwanted lineages such as ectoderm or endoderm, which WNT also plays a role in deriving (210, 211). Expression profiling of differentiating cultures would allow us to improve CHIR99021-based mesoderm induction by including additional signaling pathway inhibitors or activators known to repress the development of potential unwanted lineages; for example, NODAL or TGFB inhibition may suppress unwanted endoderm-like differentiation (195, 211).

Gene expression profiling of terminally differentiated hESC-derived skeletal muscle would also help to characterize the SMPs and myotubes being generated *in vitro*. Comparing *in vitro* hESC-derived myogenic cultures to the gene expression profiling of fetal muscle (212), or quiescent and activated satellite cells (213, 214), may aid in the characterization of, and in supporting the therapeutic *in viv*o potential of hESC-derived myogenic cultures.

1.7 Hypothesis

Therefore, we hypothesize that *in vitro* hESC-derived SMPs—PAX7-expressing cells showing myogenic potential—will share characteristics with quiescent satellite cells, and we will demonstrate the SMPs' *in vivo* potential by injecting cells into the cardiotoxin-injured muscle of NOD.Cg-Prkdc^{scid} Il2rg^{tm1Wjl}/SzJ (NSG) mice.

1.8 References

1. Medeiros DM, Wildman REC. 2012. Advanced Human Nutrition, 2nd ed. Jones & Bartlett Learning, Sudbury, MA.
2. Skuk D, Goulet M, Roy B, Piette V, Côté CH, Chapdelaine P, Hogrel JY, Paradis M, Bouchard JP, Sylvain M, Lachance JG, Tremblay JP. 2007. First test of a "high-density injection" protocol for myogenic cell transplantation throughout large volumes of muscles in a Duchenne muscular dystrophy patient: eighteen months follow-up. Neuromuscul Disord 17:38–46.
3. DiMario JX, Stockdale FE. 1995. Differences in the developmental fate of cultured and noncultured myoblasts when transplanted into embryonic limbs. Exp Cell Res 216:431–42.
4. Cooper RN, Thiesson D, Furling D, Di Santo JP, Butler-Browne GS, Mouly V. 2003. Extended amplification in vitro and replicative senescence: key factors implicated in the success of human myoblast transplantation. Hum Gene Ther 14:1169–79.
5. Barberi T, Willis LM, Socci ND, Studer L. 2005. Derivation of multipotent mesenchymal precursors from human embryonic stem cells. PLoS Med 2:0554–0560.
6. Barberi T, Bradbury M, Dincer Z, Panagiotakos G, Socci ND, Studer L. 2007. Derivation of engraftable skeletal myoblasts from human embryonic stem cells. Nat Med 13:642–648.
7. Ryan T, Liu J, Chu A, Wang L, Blais A, Skerjanc IS. 2012. Retinoic Acid Enhances Skeletal Myogenesis in Human Embryonic Stem Cells by Expanding the Premyogenic Progenitor Population. Stem Cell Rev Reports 8:482–493.
8. Charville GW, Cheung TH, Yoo B, Santos PJ, Lee GK, Shrager JB, Rando TA. 2015. Ex vivo expansion and in vivo self-renewal of human muscle stem cells. Stem Cell Reports 5:621–632.
9. Schiaffino S, Reggiani C. 2011. Fiber Types in Mammalian Skeletal Muscles. Physiol Rev 91:1447–1531.
10. Hwang PM, Sykes BD. 2015. Targeting the sarcomere to correct muscle function. Nat Rev Drug Discov 14:313–328.

11. Smerdu V, Karsch-Mizrachi I, Campione M, Leinwand L, Schiaffino S. 1994. Type IIx myosin heavy chain transcripts are expressed in type IIb fibers of human skeletal muscle. Am J Physiol 267:C1723–C1728.

12. Seale P, Sabourin LA, Girgis-Gabardo A, Mansouri A, Gruss P, Rudnicki MA. 2000. Pax7 Is Required for the Specification of Myogenic Satellite Cells. Cell 102:777–786.

13. Kuang S, Kuroda K, Le Grand F, Rudnicki MA. 2007. Asymmetric Self-Renewal and Commitment of Satellite Stem Cells in Muscle. Cell 129:999–1010.

14. Crist CG, Montarras D, Buckingham M. 2012. Muscle satellite cells are primed for myogenesis but maintain quiescence with sequestration of Myf5 mRNA targeted by microRNA-31 in mRNP granules. Cell Stem Cell 11:118–126.

15. Hausburg MA, Doles JD, Clement SL, Cadwallader AB, Hall MN, Blackshear PJ, Lykke-Andersen J, Olwin BB. 2015. Post-transcriptional regulation of satellite cell quiescence by TTP-mediated mRNA decay. Elife 2015:1–18.

16. Troy A, Cadwallader AB, Fedorov Y, Tyner K, Tanaka KK, Olwin BB. 2012. Coordination of satellite cell activation and self-renewal by par-complex-dependent asymmetric activation of p38α/β MAPK. Cell Stem Cell 11:541–553.

17. Bustos F, de la Vega E, Cabezas F, Thompson J, Cornelison DDW, Olwin BB, Yates JR, Olguín HC. 2015. NEDD4 Regulates PAX7 Levels Promoting Activation of the Differentiation Program in Skeletal Muscle Precursors. Stem Cells 33:3138–51.

18. Dick SA, Chang NC, Dumont NA, Bell RA V., Putinski C, Kawabe Y, Litchfield DW, Rudnicki MA, Megeney LA. 2015. Caspase 3 cleavage of Pax7 inhibits self-renewal of satellite cells. Proc Natl Acad Sci 112:E5246–E5252.

19. Smith CK, Janney MJ, Allen RE. 1994. Temporal expression of myogenic regulatory genes during activation, proliferation, and differentiation of rat skeletal muscle satellite cells. J Cell Physiol 159:379–385.

20. Yablonka-Reuveni Z, Rivera a J. 1994. Temporal expression of regulatory and structural muscle proteins during myogenesis of satellite cells on isolated adult rat fibers. Dev Biol 164:588–603.

21. Chargé SBP, Rudnicki MA. 2004. Cellular and molecular regulation of muscle regeneration. Physiol Rev 84:209–38.

22. Gussoni E, Soneoka Y, Strickland CD, Buzney EA, Khan MK, Flint AF, Kunkel LM, Mulligan RC. 1999. Dystrophin expression in the mdx mouse restored by stem cell transplantation. Nature 401:390–394.

23. Joe AWB, Yi L, Natarajan A, Le Grand F, So L, Wang J, Rudnicki MA, Rossi FM V. 2010. Muscle injury activates resident fibro/adipogenic progenitors that facilitate myogenesis. Nat Cell Biol 12:153–163.

24. Castiglioni A, Hettmer S, Lynes MD, Rao TN, Tchessalova D, Sinha I, Lee BT, Tseng YH, Wagers AJ. 2014. Isolation of progenitors that exhibit myogenic/osteogenic bipotency in vitro by fluorescence-activated cell sorting from human fetal muscle. Stem Cell Reports 2:92–106.

25. Mitchell KJ, Pannérec A, Cadot B, Parlakian A, Besson V, Gomes ER, Marazzi G, Sassoon DA. 2010. Identification and characterization of a non-satellite cell muscle resident progenitor during postnatal development. Nat Cell Biol 12:257–266.

26. Liu N, Garry GA, Li S, Bezprozvannaya S, Sanchez-Ortiz E, Chen B, Shelton JM, Jaichander P, Bassel-Duby R, Olson EN. 2017. A Twist2-dependent progenitor cell contributes to adult skeletal muscle. Nat Cell Biol 19:202–213.

27. Tonlorenzi R, Dellavalle A, Schnapp E, Cossu G, Sampaolesi M. 2007. Isolation and Characterization of Mesoangioblasts from Mouse, Dog, and Human Tissues. Curr Protoc Stem Cell Biol 1–29.

28. Bonfanti C, Rossi G, Tedesco FS, Giannotta M, Benedetti S, Tonlorenzi R, Antonini S, Marazzi G, Dejana E, Sassoon D, Cossu G, Messina G. 2015. PW1/Peg3 expression regulates key properties that determine mesoangioblast stem cell competence. Nat Commun 6:6364.

29. Dellavalle A, Sampaolesi M, Tonlorenzi1 R, Tagliafico E, Sacchetti B, Perani L, Innocenzi A, Galvez BG, Messina G, Morosetti R, Li S, Belicchi M, Peretti G, Chamberlain JS, Wright WE, Torrente Y, Ferrari S, Bianco P, Cossu G. 2007. Pericytes of human skeletal muscle are myogenic precursors distinct from satellite cells. Nat Cell Biol 9:255–267.

30. Chazaud B, Sonnet C, Lafuste P, Bassez G, Rimaniol AC, Poron F, Authier FJ, Dreyfus PA, Gherardi RK. 2003. Satellite cells attract monocytes and use macrophages as a support to escape apoptosis and enhance muscle growth. J Cell Biol 163:1133–1143.

31. Dumont NA, Wang YX, von Maltzahn J, Pasut A, Bentzinger CF, Brun CE, Rudnicki MA. 2015. Dystrophin expression in muscle stem cells regulates their polarity and asymmetric division. Nat Med 21:1455–1463.

32. Conboy IM, Conboy MJ, Wagers AJ, Girma ER, Weismann IL, Rando TA. 2005. Rejuvenation of aged progenitor cells by exposure to a young systemic environment. Nature 433:760–764.

33. Lee ASJ, Anderson JE, Joya JE, Head SI, Pather N, Kee AJ, Gunning PW, Hardeman EC. 2013. Aged skeletal muscle retains the ability to fully regenerate functional architecture. Bioarchitecture 3:25–37.

34. Grounds MD. 2014. Therapies for sarcopenia and regeneration of old skeletal muscles: more a case of old tissue architecture than old stem cells. Bioarchitecture 4:81–87.

35. George T, Velloso CP, Alsharidah M, Lazarus NR, Harridge SDR. 2010. Sera from young and older humans equally sustain proliferation and differentiation of human myoblasts. Exp Gerontol 45:875–881.

36. Alsharidah M, Lazarus NR, George TE, Agley CC, Velloso CP, Harridge SDR. 2013. Primary human muscle precursor cells obtained from young and old donors produce similar proliferative, differentiation and senescent profiles in culture. Aging Cell 12:333–344.

37. Grzybowski A, Kaufman MH. 2007. Sir Charles Bell (1774-1842): contributions to neuro-ophthalmology. Acta Ophthalmol Scand 85:897–901.

38. Duchenne GBA. 1868. Recherches sur la paralysie musculaire pseudo-hypertrophique ou paralysie myo-sclérotique. P. Asselin, Paris, France.

39. Darwin C. 1872. The expression of the emotions in man and animals. John Marry, London, UK.

40. Monaco AP, Neve RL, Colletti-Feener C, Bertelson CJ, Kurnit DM, Kunkel LM. 1986. Isolation of candidate cDNAs for portions of the Duchenne muscular dystrophy gene. Nature 323:646–50.

41. Burghes AH, Logan C, Hu X, Belfall B, Worton RG, Ray PN. 1987. A cDNA clone from the Duchenne/Becker muscular dystrophy gene. Nature 328:434–7.

42. Hoffman EP, Brown RH, Kunkel LM. 1987. Dystrophin: The protein product of the duchenne muscular dystrophy locus. Cell 51:919–928.

43. Tennyson CN, Klamut HJ, Worton RG. 1995. The human dystrophin gene requires 16 hours to be transcribed and is cotranscriptionally spliced. Nat Genet 9:184–90.

44. Norwood FLM, Harling C, Chinnery PF, Eagle M, Bushby K, Straub V. 2009. Prevalence of genetic muscle disease in Northern England: in-depth analysis of a muscle clinic population. Brain 132:3175–3186.

45. Matsumura T, Saito T, Fujimura H, Shinno S, Sakoda S. 2011. A longitudinal cause-of-death analysis of patients with Duchenne muscular dystrophy. Rinsho Shinkeigaku 51:743–750.

46. Stromberg A, Darin N, Kroksmark AK, Tulinius M. 2012. What was the age and cause of death in patients with Duchenne muscular dystrophy in Sweden during 2000–2010. Neuromuscul Disord 22:880–881.

47. Ballard E, Grey N, Jungbluth H, Wraige E, Kapetanakis S, Davidson C, Hart N. 2012. Observation cohort study of cause of death in patients with Duchenne muscular dystrophy (DMD). Eur Respir J 40:7208.

48. Angelini C. 2007. The role of corticosteroids in muscular dystrophy: A critical appraisal. Muscle and Nerve 36:424–435.

49. Aliverti A, LoMauro A, D'Angelo MG. 2015. Assessment and management of respiratory function in patients with Duchenne muscular dystrophy: current and emerging options. Ther Clin Risk Manag 1475.

50. Yoshimura M, Sakamoto M, Ikemoto M, Mochizuki Y, Yuasa K, Miyagoe-Suzuki Y, Takeda S. 2004. AAV vector-mediated microdystrophin expression in a relatively small percentage of mdx myofibers improved the mdx phenotype. Mol Ther 10:821–828.

51. Le Guiner C, Servais L, Montus M, Larcher T, Fraysse B, Moullec S, Allais M, François V, Dutilleul M, Malerba A, Koo T, Thibaut JL, Matot B, Devaux M, Le Duff J, Deschamps JY, Barthelemy I, Blot S, Testault I, Wahbi K, Ederhy S, Martin S, Veron P, Georger C, Athanasopoulos T, Masurier C, Mingozzi F, Carlier P, Gjata B, Hogrel JY, Adjali O, Mavilio F, Voit T, Moullier P, Dickson G. 2017. Long-term microdystrophin gene therapy is effective in a canine model of Duchenne muscular dystrophy. Nat Commun 8.

52. Bostick B, Shin JH, Yue Y, Duan D. 2011. AAV-microdystrophin therapy improves cardiac performance in aged female mdx mice. Mol Ther 19:1826–1832.

53. Smith BK, Collins SW, Conlon TJ, Mah CS, Lawson LA, Martin AD, Fuller DD, Cleaver BD, Clément N, Phillips D, Islam S, Dobjia N, Byrne BJ. 2013. Phase I/II Trial of Adeno-Associated Virus–Mediated Alpha-Glucosidase Gene Therapy to the Diaphragm for Chronic Respiratory Failure in Pompe Disease: Initial Safety and Ventilatory Outcomes. Hum Gene Ther 24:630–640.

54. Mendell JR, Al-Zaidy S, Shell R, Arnold WD, Rodino-Klapac LR, Prior TW, Lowes L, Alfano L, Berry K, Church K, Kissel JT, Nagendran S, L'Italien J, Sproule DM, Wells C, Cardenas JA, Heitzer MD, Kaspar A, Corcoran S, Braun L, Likhite S, Miranda C, Meyer K, Foust KD, Burghes AHM, Kaspar BK. 2017. Single-Dose Gene-Replacement Therapy for Spinal Muscular Atrophy. N Engl J Med 377:1713–1722.

55. Mendell JR, Campbell K, Rodino-Klapac L, Sahenk Z, Shilling C, Lewis S, Bowles D, Gray S, Li C, Galloway G, Malik V, Coley B, Clark KR, Li J, Xiao X, Samulski J, McPhee SW, Samulski RJ, Walker CM. 2010. Dystrophin Immunity in Duchenne's Muscular Dystrophy. N Engl J Med 363:1429–1437.

56. Amirouche A, Tadesse H, Lunde JA, Bélanger G, Côté J, Jasmin BJ. 2013. Activation of p38 signaling increases utrophin A expression in skeletal muscle via the RNA-binding protein KSRP and inhibition of AU-rich element-mediated mRNA decay: Implications for novel DMD therapeutics. Hum Mol Genet 22:3093–3111.

57. Mohacsi P, Leprince P. 2014. The CARMAT total artificial heart. Eur J Cardio-thoracic Surg 46:933–934.

58. Kawabori M, Kurihara C, Miller Y, Heck KA, Bogaev RC, Civitello AB, Cohn WE, Frazier OH, Morgan JA. 2017. Total artificial heart implantation for biventricular failure due to eosinophilic myocarditis. J Artif organs 20:266–269.

59. Mehra MR, Goldstein DJ, Uriel N, Cleveland JC, Yuzefpolskaya M, Salerno C, Walsh MN, Milano CA, Patel CB, Ewald GA, Itoh A, Dean D, Krishnamoorthy A, Cotts WG, Tatooles AJ, Jorde UP, Bruckner BA, Estep JD, Jeevanandam V, Sayer G, Horstmanshof D, Long JW, Gulati S, Skipper ER, O'Connell JB, Heatley G, Sood P, Naka Y, MOMENTUM 3 Investigators. 2018. Two-Year Outcomes with a Magnetically Levitated Cardiac Pump in Heart Failure. N Engl J Med 378:1386–1395.

60. Cove ME, MacLaren G, Federspiel WJ, Kellum JA. 2012. Bench to bedside review: Extracorporeal carbon dioxide removal, past present and future. Crit Care 16:232.

61. Kovach KM, LaBarbera MA, Moyer MC, Cmolik BL, van Lunteren E, Sen Gupta A, Capadona JR, Potkay JA. 2015. In vitro evaluation and in vivo demonstration of a biomimetic, hemocompatible, microfluidic artificial lung. Lab Chip 15:1366–1375.

62. Madhani SP, Frankowski BJ, Burgreen GW, Antaki JF, Kormos R, D'Cunha J, Federspiel WJ. 2017. In vitro and in vivo evaluation of a novel integrated wearable artificial lung. J Hear Lung Transplant 36:806–811.

63. Rouse EJ, Villagaray-Carski NC, Emerson RW, Herr HM. 2015. Design and Testing of a Bionic Dancing Prosthesis. PLoS One 10:e0135148.

64. Reardon S. 2015. The Military-Bioscience Complex. Nature 522:142–144.

65. Kubota S, Abe T, Kadone H, Fujii K, Shimizu Y, Marushima A, Ueno T, Kawamoto H, Hada Y, Matsumura A, Sankai Y, Yamazaki M. 2017. Walking ability following Hybrid Assistive Limb treatment for a patient with chronic myelopathy after surgery for cervical ossification of the posterior longitudinal ligament. J Spinal Cord Med 00:1–9.

66. Shimizu Y, Kadone H, Kubota S, Suzuki K, Abe T, Ueno T, Soma Y, Sankai Y, Hada Y, Yamazaki M. 2017. Voluntary ambulation by upper limb-triggered HAL® in patients with complete quadri/paraplegia due to chronic spinal cord injury. Front Neurosci 11:1–12.

67. Miriyev A, Stack K, Lipson H. 2017. Soft Material for Soft Actuators. Nat Commun 1–8.

68. Darwin C. 1868. The variation of animals and plants under domestication. Orange Judd & Company, New York, NY.

69. Haeckel E. 1889. Natürliche Schöpfungs-Geschichte. George Reimer, Berlin, Germany.

70. Weismann A. 1892. Die Continuität des Keimplasmas als Grundlage einer Theorie der Vererbung. Gustav Fischer, Jena, Germany.

71. Ramalho-Santos M, Willenbring H. 2007. On the Origin of the Term "Stem Cell." Cell Stem Cell 1:35–38.

72. Sabin FR, Doan CA, Forkner CE. 1932. The production of osteogenic sarcomata and the effects on lymph nodes and bone marrow of intravenous injections of radium chloride and mesothorium in rabbits. J Exp Med 56:267–89.

73. Sabin FR, Miller FR, Smithburn KC, Thomas RM, Hummel LE. 1936. Changes in the Bone Marrow and Blood Cells of Developing Rabbits. J Exp Med 64:97–120.

74. Jacobson LO, Marks EK, Robson MJ, Gaston EO, Zirkle RE. 1949. Effect of spleen protection on mortality following X-irradiation. J Lab Clin Med 34:1538–1543.

75. Ford CE, Hamerton JL, Barnes DW, Loutit JF. 1956. Cytological identification of radiation-chimaeras. Nature 177:452–4.

76. Thomas ED, Lochte HL, Lu WC, Ferrebee JW. 1957. Intravenous infusion of bone marrow in patients receiving radiation and chemotherapy. N Engl J Med 257:491–6.

77. Till JE, McCulloch EA. 1961. A direct measurement of the radiation sensitivity of normal mouse bone marrow cells. Radiat Res 14:213–22.

78. Becker AJ, McCulloch EA, Till JE. 1963. Cytological demonstration of the clonal nature of spleen colonies derived from transplanted mouse marrow cells. Nature 197:452–4.

79. Mauro A. 1961. Satellite cell of skeletal muscle fibers. J Biophys Biochem Cytol 9:493–5.

80. Tedesco FS, Dellavalle A, Diaz-manera J, Messina G, Cossu G. 2010. Review series Repairing skeletal muscle : regenerative potential of skeletal muscle stem cells. J Clin Invest 120:11–19.

81. Skuk D, Goulet M, Roy B, Chapdelaine P, Bouchard J-P, Roy R, Dugré FJ, Sylvain M, Lachance J-G, Deschênes L, Senay H, Tremblay JP. 2006. Dystrophin Expression in Muscles of Duchenne Muscular Dystrophy Patients After High-Density Injections of Normal Myogenic Cells. J Neuropathol Exp Neurol 65:371–386.

82. LaBarge MA, Blau HM. 2002. Biological progression from adult bone marrow to mononucleate muscle stem cell to multinucleate muscle fiber in response to injury. Cell 111:589–601.

83. Cossu G, Previtali SC, Napolitano S, Cicalese MP, Tedesco FS, Nicastro F, Noviello M, Roostalu U, Natali Sora MG, Scarlato M, De Pellegrin M, Godi C, Giuliani S, Ciotti F, Tonlorenzi R, Lorenzetti I, Rivellini C, Benedetti S, Gatti R, Marktel S, Mazzi B, Tettamanti A, Ragazzi M, Imro MA, Marano G, Ambrosi A, Fiori R, Sormani MP, Bonini C, Venturini M, Politi LS, Torrente Y, Ciceri F. 2015. Intra-arterial transplantation of HLA-matched donor mesoangioblasts in Duchenne muscular dystrophy. EMBO Mol Med 7:1513–1528.

84. Périé S, Trollet C, Mouly V, Vanneaux V, Mamchaoui K, Bouazza B, Marolleau JP, Laforêt P, Chapon F, Eymard B, Butler-Browne G, Larghero J, St Guily JL. 2014. Autologous Myoblast Transplantation for Oculopharyngeal Muscular Dystrophy: a Phase I/Iia Clinical Study. Mol Ther 22:219–225.

85. Parker MH, Loretz C, Tyler AE, Duddy WJ, Hall JK, Olwin BB, Bernstein ID, Storb R, Tapscott SJ. 2012. Activation of notch signaling during ex vivo expansion maintains donor muscle cell engraftment. Stem Cells 30:2212–2220.

86. Quarta M, Brett JO, DiMarco R, De Morree A, Boutet SC, Chacon R, Gibbons MC, Garcia VA, Su J, Shrager JB, Heilshorn S, Rando TA. 2016. An artificial niche preserves the quiescence of muscle stem cells and enhances their therapeutic efficacy. Nat Biotechnol 34:752–759.

87. Rohwedel J, Maltsev V, Bober E, Arnold HH, Hescheler J, Wobus AM. 1994. Muscle cell differentiation of embryonic stem cells reflects myogenesis in vivo: developmentally regulated expression of myogenic determination genes and functional expression of ionic currents. Dev Biol 164:87–101.

88. Thomson JA, Itskovitz-Eldor J, Shapiro SS, Waknitz MA, Swiergiel JJ, Marshall VS, Jones JM. 1998. Embryonic stem cell lines derived from human blastocysts. Science 282:1145–7.

89. Stevens LC. 1970. The development of transplantable teratocarcinomas from intratesticular grafts of pre- and postimplantation mouse embryos. Dev Biol 21:364–382.

90. Evans MJ, Kaufman MH. 1981. Establishment in culture of pluripotential cells from mouse embryos. Nature 292:154–156.

91. Schwartz SD, Regillo CD, Lam BL, Eliott D, Rosenfeld PJ, Gregori NZ, Hubschman JP, Davis JL, Heilwell G, Spirn M, Maguire J, Gay R, Bateman J, Ostrick RM, Morris D, Vincent M, Anglade E, Del Priore L V., Lanza R. 2015. Human embryonic stem cell-derived retinal pigment epithelium in patients with age-related macular degeneration and Stargardt's macular dystrophy: Follow-up of two open-label phase 1/2 studies. Lancet 385:509–516.

92. Song WK, Park KM, Kim HJ, Lee JH, Choi J, Chong SY, Shim SH, Del Priore L V., Lanza R. 2015. Treatment of macular degeneration using embryonic stem cell-derived retinal pigment epithelium: Preliminary results in Asian patients. Stem Cell Reports 4:860–872.

93. da Cruz L, Fynes K, Georgiadis O, Kerby J, Luo YH, Ahmado A, Vernon A, Daniels JT, Nommiste B, Hasan SM, Gooljar SB, Carr A-JF, Vugler A, Ramsden CM, Bictash M, Fenster M, Steer J, Harbinson T, Wilbrey A, Tufail A, Feng G, Whitlock M, Robson AG, Holder GE, Sagoo MS, Loudon PT, Whiting P, Coffey PJ. 2018. Phase 1 clinical study of an embryonic stem cell-derived retinal pigment epithelium patch in age-related macular degeneration. Nat Biotechnol 36:328–337.

94. Menasché P, Vanneaux V, Hagège A, Bel A, Cholley B, Cacciapuoti I, Parouchev A, Benhamouda N, Tachdjian G, Tosca L, Trouvin JH, Fabreguettes JR, Bellamy V, Guillemain R, Suberbielle Boissel C, Tartour E, Desnos M, Larghero J. 2015. Human embryonic stem cell-derived cardiac progenitors for severe heart failure treatment: First clinical case report. Eur Heart J 36:2011–2017.

95. Menasché P, Vanneaux V, Hagège A, Bel A, Cholley B, Parouchev A, Cacciapuoti I, Al-Daccak R, Benhamouda N, Blons H, Agbulut O, Tosca L, Trouvin J-H, Fabreguettes J-R, Bellamy V, Charron D, Tartour E, Tachdjian G, Desnos M, Larghero J. 2018. Transplantation of Human Embryonic Stem Cell-Derived Cardiovascular Progenitors for Severe Ischemic Left Ventricular Dysfunction. J Am Coll Cardiol 71:429–438.

96. Gu Q, Wang J, Wang L, Liu ZX, Zhu WW, Tan YQ, Han WF, Wu J, Feng CJ, Fang JH, Liu L, Wang L, Li W, Zhao XY, Hu BY, Hao J, Zhou Q. 2017. Accreditation of Biosafe Clinical-Grade Human Embryonic Stem Cells According to Chinese Regulations. Stem Cell Reports 9:366–380.

97. Fernandes RAB, Stefanini FR, Falabella P, Koss MJ, Wells T, Diniz B, Ribeiro R, Schor P, Maia M, Penha FM, Hinton DR, Tai Y-C, Humayun M. 2017. Development of a new tissue injector for subretinal transplantation of human embryonic stem cell derived retinal pigmented epithelium. Int J Retin Vitr 3:41.

98. Pedraza CE, Taylor C, Pereira A, Seng M, Tham CS, Izrael M, Webb M. 2014. Induction of oligodendrocyte differentiation and in vitro myelination by inhibition of Rho-associated kinase. ASN Neuro 6:1–17.

99. Priest CA, Manley NC, Denham J, Wirth ED 3rd, Lebkowski JS. 2015. Preclinical safety of human embryonic stem cell-derived oligodendrocyte progenitors supporting clinical trials in spinal cord injury. Regen Med 10:939–958.

100. Manley NC, Priest CA, Denham J, Wirth ED, Lebkowski JS. 2017. Human Embryonic Stem Cell-Derived Oligodendrocyte Progenitor Cells: Preclinical Efficacy and Safety in Cervical Spinal Cord Injury. Stem Cells Transl Med 6:1917–1929.

101. Darabi R, Arpke RW, Irion S, Dimos JT, Grskovic M, Kyba M, Perlingeiro RCR. 2012. Human ES- and iPS-derived myogenic progenitors restore DYSTROPHIN and improve contractility upon transplantation in dystrophic mice. Cell Stem Cell 10:610–619.

102. Tabar VS, Bond AE, Dallapiazza R, Warren AL, Sperling S, Shah BB, Elias WJ. 2016. The Development of Human Embryonic Stem Cell-Derived Dopamine Neurons for Clinical Use in Parkinson Disease. Neurosurg Online 63:2016–2017.

103. Takahashi K, Yamanaka S. 2006. Induction of Pluripotent Stem Cells from Mouse Embryonic and Adult Fibroblast Cultures by Defined Factors. Cell 126:663–676.

104. Zhou Y ye, Zeng F. 2013. Integration-free Methods for Generating Induced Pluripotent Stem Cells. Genomics, Proteomics Bioinforma 11:284–287.

105. Rohani L, Fabian C, Holland H, Naaldijk Y, Dressel R, Löffler-Wirth H, Binder H, Arnold A, Stolzing A. 2016. Generation of human induced pluripotent stem cells using non-synthetic mRNA. Stem Cell Res 16:662–672.

106. Li HL, Fujimoto N, Sasakawa N, Shirai S, Ohkame T, Sakuma T, Tanaka M, Amano N, Watanabe A, Sakurai H, Yamamoto T, Yamanaka S, Hotta A. 2015. Precise correction of the dystrophin gene in duchenne muscular dystrophy patient induced pluripotent stem cells by TALEN and CRISPR-Cas9. Stem Cell Reports 4:143–154.

107. Zhang Y, Huang H, Zhang B, Lin S. 2016. TALEN- and CRISPR-enhanced DNA homologous recombination for gene editing in zebrafish. Methods Cell Biol 135:107–20.

108. Meca-Cortés O, Guerra-Rebollo M, Garrido C, Borrós S, Rubio N, Blanco J. 2017. CRISPR/Cas9-Mediated Knockin Application in Cell Therapy: A Non-viral Procedure for Bystander Treatment of Glioma in Mice. Mol Ther - Nucleic Acids 8:395–403.

109. Zhang Z, Zhang Y, Gao F, Han S, Cheah KS, Tse HF, Lian Q. 2017. CRISPR/Cas9 Genome-Editing System in Human Stem Cells: Current Status and Future Prospects. Mol Ther - Nucleic Acids 9:230–241.

110. Young CS, Hicks MR, Ermolova N V., Nakano H, Jan M, Younesi S, Karumbayaram S, Kumagai-Cresse C, Wang D, Zack JA, Kohn DB, Nakano A, Nelson SF, Miceli MC, Spencer MJ, Pyle AD. 2016. A Single CRISPR-Cas9 Deletion Strategy that Targets the Majority of DMD Patients Restores Dystrophin Function in hiPSC-Derived Muscle Cells. Cell Stem Cell 18:533–540.

111. Allegrucci C, Wu YZ, Thurston A, Denning CN, Priddle H, Mummery CL, Ward-van Oostwaard D, Andrews PW, Stojkovic M, Smith N, Parkin T, Jones ME, Warren G, Yu L, Brena RM, Plass C, Young LE. 2007. Restriction landmark genome scanning identifies culture-induced DNA methylation instability in the human embryonic stem cell epigenome. Hum Mol Genet 16:1253–1268.

112. Vaskova EA, Stekleneva AE, Medvedev SP, Zakian SM. 2013. "Epigenetic memory" phenomenon in induced pluripotent stem cells. Acta Naturae 5:15–21.

113. Garitaonandia I, Amir H, Boscolo FS, Wambua GK, Schultheisz HL, Sabatini K, Morey R, Waltz S, Wang YC, Tran H, Leonardo TR, Nazor K, Slavin I, Lynch C, Li Y, Coleman R, Romero IG, Altun G, Reynolds D, Dalton S, Parast M, Loring JF, Laurent LC. 2015. Increased risk of genetic and epigenetic instability in human embryonic stem cells associated with specific culture conditions. PLoS One 10:1–25.

114. Hill MA. 2007. Early human development. Clin Obstet Gynecol 50:2–9.

115. Rossant J, Tam PPL. 2017. New Insights into Early Human Development: Lessons for Stem Cell Derivation and Differentiation. Cell Stem Cell 20:18–28.

116. Hill MA. 2018. https://embryology.med.unsw.edu.au/embryology/index.php/Main_Page.

117. Dar S, Lazer T, Shah PS, Librach CL. 2014. Neonatal outcomes among singleton births after blastocyst versus cleavage stage embryo transfer: A systematic review and meta-analysis. Hum Reprod Update 20:439–448.

118. Chambers I, Colby D, Robertson M, Nichols J, Lee S, Tweedie S, Smith A. 2003. Functional expression cloning of Nanog, a pluripotency sustaining factor in embryonic stem cells. Cell 113:643–655.

119. Schöler HR, Ciesiolka T, Gruss P. 1991. A nexus between Oct-4 and E1A: implications for gene regulation in embryonic stem cells. Cell 66:291–304.

120. Avilion AA, Nicolis SK, Pevny LH, Perez L, Vivian N, Lovell-Badge R. 2003. Multipotent cell lineages in early mouse development on SOX2 function. Genes Dev 17:126–140.

121. Cha J, Sun X, Dey SK. 2012. Mechanisms of implantation: Strategies for successful pregnancy. Nat Med 18:1754–1767.

122. Bianchi DW, Wilkins-Haug LE, Enders AC, Hay ED. 1993. Origin of extraembryonic mesoderm in experimental animals: Relevance to chorionic mosaicism in humans. Am J Med Genet 46:542–550.

123. Bertocchini F, Stern CD. 2002. The hypoblast of the chick embryo positions the primitive streak by antagonizing nodal signaling. Dev Cell 3:735–744.

124. Perea-Gomez A, Vella FDJ, Shawlot W, Oulad-Abdelghani M, Chazaud C, Meno C, Pfister V, Chen L, Robertson E, Hamada H, Behringer RR, Ang SL. 2002. Nodal antaginists in the anterior visceral endoderm prevent the formation of multiple primitive streaks. Dev Cell 3:745–756.

125. Tam PPL, Behringer RR. 1997. Mouse gastrulation: The formation of a mammalian body plan. Mech Dev 68:3–25.

126. Liu P, Wakamiya M, Shea MJ, Albrecht U, Behringer RR, Bradley A. 1999. Requirement for Wnt3 in vertebrate axis formation. Nat Genet 22:361–365.

127. Skromne I, Stern CD. 2001. Interactions between Wnt and Vg1 signalling pathways initiate primitive streak formation in the chick embryo. Development 128:2915–2927.

128. Ciruna B, Rossant J. 2001. FGF Signaling Regulates Mesoderm Cell Fate Specification and Morphogenetic Movement at the Primitive Streak. Dev Cell 1:37–49.

129. Yang X, Dormann D, Münsterberg AE, Weijer CJ. 2002. Cell movement patterns during gastrulation in the chick are controlled by positive and negative chemotaxis mediated by FGF4 and FGF8. Dev Cell 3:425–437.

130. Kiecker C, Bates T, Bell E. 2016. Molecular specification of germ layers in vertebrate embryos. Cell Mol Life Sci 73:923–947.

131. Conlon FL, Lyons KM, Takaesu N, Barth KS, Kispert A, Herrmann B, Robertson EJ. 1994. A primary requirement for nodal in the formation and maintenance of the primitive streak in the mouse. Development 120:1919–1928.

132. Katoh M, Katoh M. 2006. CER1 is a common target of WNT and NODAL signaling pathways in human embryonic stem cells. Int J Mol Med 17:795–799.

133. Gadue P, Huber TL, Paddison PJ, Keller GM. 2006. Wnt and TGF-beta signaling are required for the induction of an in vitro model of primitive streak formation using embryonic stem cells. Proc Natl Acad Sci U S A 103:16806–16811.

134. Aulehla A, Pourquié O. 2010. Signaling gradients during paraxial mesoderm development. Cold Spring Harb Perspect Biol 2:1–17.

135. Hester SD, Belmonte JM, Gens JS, Clendenon SG, Glazier JA. 2011. A multi-cell, multi-scale model of vertebrate segmentation and somite formation. PLoS Comput Biol 7:e1002155.

136. Cui C, Yang X, Chuai M, Glazier JA, Weijer CJ. 2005. Analysis of tissue flow patterns during primitive streak formation in the chick embryo. Dev Biol 284:37–47.

137. Piccolo S, Sasai Y, Lu B, De Robertis EM. 1996. Dorsoventral patterning in Xenopus: Inhibition of ventral signals by direct binding of chordin to BMP-4. Cell 86:589–598.

138. Zimmerman LB, De Jesús-Escobar JM, Harland RM. 1996. The Spemann organizer signal noggin binds and inactivates bone morphogenetic protein 4. Cell 86:599–606.

139. Loh KMM, Chen A, Koh PWW, Deng TZZ, Sinha R, Tsai JMM, Barkal AAA, Shen KYY, Jain R, Morganti RMM, Shyh-Chang N, Fernhoff NBB, George BMM, Wernig G, Salomon REEA, Chen Z, Vogel H, Epstein JAA, Kundaje A, Talbot WSS, Beachy PAA, Ang LTT, Weissman ILL. 2016. Mapping the Pairwise Choices Leading from Pluripotency to Human Bone, Heart, and Other Mesoderm Cell Types. Cell 166:451–468.

140. Streit A, Lee KJ, Woo I, Roberts C, Jessell TM, Stern CD. 1998. Chordin regulates primitive streak development and the stability of induced neural cells, but is not sufficient for neural induction in the chick embryo. Development 125:507–519.

141. Sweetman D, Wagstaff L, Cooper O, Weijer C, Münsterberg A. 2008. The migration of paraxial and lateral plate mesoderm cells emerging from the late primitive streak is controlled by different Wnt signals. BMC Dev Biol 8:63.

142. Edgar R, Mazor Y, Rinon A, Blumenthal J, Golan Y, Buzhor E, Livnat I, Ben-Ari S, Lieder I, Shitrit A, Gilboa Y, Ben-Yehudah A, Edri O, Shraga N, Bogoch Y, Leshansky L, Aharoni S, West MD, Warshawsky D, Shtrichman R. 2013. LifeMap Discovery™: the embryonic development, stem cells, and regenerative medicine research portal. PLoS One 8:e66629.

143. Otis EM, Brent R. 1954. Equivalent ages in mouse and human embryos. Anat Rec 120:33–63.

144. Dias AS, de Almeida I, Belmonte JM, Glazier JA, Stern CD. 2014. Somites without a clock. Science 343:791–795.

145. Yusuf F, Brand-Saberi B. 2006. The eventful somite: patterning, fate determination and cell division in the somite. Anat Embryol (Berl) 211:21–30.

146. Marcelle C, Stark MR, Bronner-fraser M. 1997. Coordinate actions of BMPs , Wnts , Shh and Noggin mediate patterning of the dorsal somite. Development 3963:3955–3963.

147. Reshef R, Maroto M, Lassar AB. 1998. Regulation of dorsal somitic cell fates: BMPs and Noggin control the timing and pattern of myogenic regulator expression. Genes Dev 12:290–303.

148. Rios AC, Serralbo O, Salgado D, Marcelle C. 2011. Neural crest regulates myogenesis through the transient activation of NOTCH. Nature 473:532–535.

149. Brand-Saberi B, Ebensperger C, Wilting J, Balling R, Christ B. 1993. The ventralizing effect of the notochord on somite differentiation in chick embryos. Anat Embryol (Berl) 188:239–45.

150. Pourquié O, Fan CM, Coltey M, Hirsinger E, Watanabe Y, Bréant C, Francis-West P, Brickell P, Tessier-Lavigne M, Le Douarin NM. 1996. Lateral and axial signals involved in avian somite patterning: A role for BMP4. Cell 84:461–471.

151. Ridgeway AG, Skerjanc IS. 2001. Pax3 is Essential for Skeletal Myogenesis and the Expression of Six1 and Eya2. J Biol Chem 276:19033–19039.

152. Grifone R. 2005. Six1 and Six4 homeoproteins are required for Pax3 and Mrf expression during myogenesis in the mouse embryo. Development 132:2235–2249.

153. Cinnamon Y, Kahane N, Bachelet I, Kalcheim C. 2001. The sub-lip domain – a distinct pathway for myotome precursors that demonstrate rostral-caudal migration. Development 128:341–351.

154. Relaix F, Rocancourt D, Mansouri A, Buckingham M. 2004. Divergent functions of murine Pax3 and Pax7 in limb muscle development. Genes Dev 18:1088–1105.

155. Kahane N, Cinnamon Y, Kalcheim C. 1998. The origin and fate of pioneer myotomal cells in the avian embryo. Mech Dev 74:59–73.

156. Mekonen HK, Hikspoors JPJM, Mommen G, Köhler SE, Lamers WH. 2015. Development of the ventral body wall in the human embryo. J Anat 227:673–85.

157. Kahane N, Cinnamon Y, Kalcheim C. 1998. The cellular mechanism by which the dermomyotome contributes to the second wave of myotome development. Development 125:4259–4271.

158. Gros J, Scaal M, Marcelle C. 2004. A two-Step mechanism for myotome formation in chick. Dev Cell 6:875–882.

159. Buckingham M, Bajard L, Chang T, Daubas P, Hadchouel J, Meilhac S, Montarras D, Rocancourt D, Relaix F. 2003. The formation of skeletal muscle: From somite to limb. J Anat 202:59–68.

160. Francis-West PH, Antoni L, Anakwe K. 2003. Regulation of myogenic differentiation in the developing limb bud. J Anat 202:69–81.

161. Ohuchi H, Nakagawa T, Yamamoto A, Araga A, Ohata T, Ishimaru Y, Yoshioka H, Kuwana T, Nohno T, Yamasaki M, Itoh N, Noji S. 1997. The mesenchymal factor, FGF10, initiates and maintains the outgrowth of the chick limb bud through interaction with FGF8, an apical ectodermal factor. Development 124:2235–44.

162. Liem IK, Aoyama H. 2009. Body wall morphogenesis: Limb-genesis interferes with body wall-genesis via its influence on the abaxial somite derivatives. Mech Dev 126:198–211.

163. Pansky B. 1982. Review of Medical Embryology. Macmillan, New York, NY.

164. Jagla K, Dollé P, Mattei MG, Jagla T, Schuhbaur B, Dretzen G, Bellard F, Bellard M. 1995. Mouse Lbx1 and human LBX1 define a novel mammalian homeobox gene family related to the Drosophila lady bird genes. Mech Dev 53:345–356.

165. Epstein JA, Shapiro DN, Cheng J, Lam PY, Maas RL. 1996. Pax3 modulates expression of the c-Met receptor during limb muscle development. Proc Natl Acad Sci U S A 93:4213–8.

166. Vasyutina E, Stebler J, Brand-Saberi B, Schulz S, Raz E, Birchmeier C. 2005. CXCR4 and Gab1 cooperate to control the development of migrating muscle progenitor cells. Genes Dev 19:2187–98.

167. Ödemis V, Lamp E, Pezeshki G, Moepps B, Schilling K, Gierschik P, Littman DR, Engele J. 2005. Mice deficient in the chemokine receptor CXCR4 exhibit impaired limb innervation and myogenesis. Mol Cell Neurosci 30:494–505.

168. Lee ASJ, Harris J, Bate M, Vijayraghavan K, Fisher L, Tajbakhsh S, Duxson M. 2013. Initiation of primary myogenesis in amniote limb muscles. Dev Dyn 242:1043–1055.

169. Edom-Vovard F, Mouly V, Barbet JP, Butler-Browne GS. 1999. The four populations of myoblasts involved in human limb muscle formation are present from the onset of primary myotube formation. J Cell Sci 112:191–9.

170. Relaix F, Rocancourt D, Mansouri A, Buckingham M. 2005. A Pax3/Pax7-dependent population of skeletal muscle progenitor cells. Nature 435:948–953.

171. Hutcheson DA, Zhao J, Merrell A, Haldar M, Kardon G. 2009. Embryonic and fetal limb myogenic cells are derived from developmentally distinct progenitors and have different requirements for B-catenin. Genes Dev 23:997–1013.

172. Murphy M, Kardon G. 2011. Origin of vertebrate limb muscle: the role of progenitor and myoblast populations. Curr Top Dev Biol 96:1–32.

173. Gros J, Manceau M, Thomé V, Marcelle C. 2005. A common somitic origin for embryonic muscle progenitors and satellite cells. Nature 435:954–958.

174. Clancy B, Darlington RB, Finlay BL. 2001. Translating developmental time across mammalian species. Neuroscience 105:7–17.

175. Nichol PF, Corliss RF, Yamada S, Shiota K, Saijoh Y. 2012. Muscle Patterning in Mouse and Human Abdominal Wall Development and Omphalocele Specimens of Humans. Anat Rec 295:2129–2140.

176. Oustanina S, Hause G, Braun T. 2004. Pax7 directs postnatal renewal and propagation of myogenic satellite cells but not their specification. EMBO J 23:3430–3439.

177. Relaix F, Montarras D, Zaffran S, Gayraud-Morel B, Rocancourt D, Tajbakhsh S, Mansouri A, Cumano A, Buckingham M. 2006. Pax3 and Pax7 have distinct and overlapping functions in adult muscle progenitor cells. J Cell Biol 172:91–102.

178. Lepper C, Conway SJ, Fan C-M. 2009. Adult satellite cells and embryonic muscle progenitors have distinct genetic requirements. Nature 460:627–631.

179. Noden DM, Francis-West P. 2006. The differentiation and morphogenesis of craniofacial muscles. Dev Dyn 235:1194–1218.

180. Tzahor E. 2009. Heart and craniofacial muscle development: A new developmental theme of distinct myogenic fields. Dev Biol 327:273–279.

181. Tirosh-Finkel L, Elhanany H, Rinon A, Tzahor E. 2006. Mesoderm progenitor cells of common origin contribute to the head musculature and the cardiac outflow tract. Development 133:1943–1953.

182. Bothe I, Dietrich S. 2006. The molecular setup of the avian head mesoderm and its implication for craniofacial myogenesis. Dev Dyn 235:2845–2860.

183. Nathan E, Monovich A, Tirosh-Finkel L, Harrelson Z, Rousso T, Rinon A, Harel I, Evans SM, Tzahor E. 2008. The contribution of Islet1-expressing splanchnic mesoderm cells to distinct branchiomeric muscles reveals significant heterogeneity in head muscle development. Development 135:647–657.

184. Sambasivan R, Gayraud-Morel B, Dumas G, Cimper C, Paisant S, Kelly R, Tajbakhsh S. 2009. Distinct Regulatory Cascades Govern Extraocular and Pharyngeal Arch Muscle Progenitor Cell Fates. Dev Cell 16:810–821.

185. Goudenege S, Lebel C, Huot NB, Dufour C, Fujii I, Gekas J, Rousseau J, Tremblay JP. 2012. Myoblasts Derived From Normal hESCs and Dystrophic hiPSCs Efficiently Fuse With Existing Muscle Fibers Following Transplantation. Mol Ther 20:2153–2167.

186. Rao L, Tang W, Wei Y, Bao L, Chen J, Chen H, He L, Lu P, Ren J, Wu L, Luan Z, Cui C, Xiao L. 2012. Highly Efficient Derivation of Skeletal Myotubes from Human Embryonic Stem Cells. Stem Cell Rev Reports 8:1109–1119.

187. Albini S, Coutinho P, Malecova B, Giordani L, Savchenko A, Forcales SV, Puri PL. 2013. Epigenetic Reprogramming of Human Embryonic Stem Cells into Skeletal Muscle Cells and Generation of Contractile Myospheres. Cell Rep 3:661–670.

188. Thomas CE, Ehrhardt A, Kay MA. 2003. Progress and problems with the use of viral vectors for gene therapy. Nat Rev Genet 4:346–358.

189. Gardlík R, Pálffy R, Hodosy J, Lukács J, Turna J, Celec P. 2005. Vectors and delivery systems in gene therapy. Med Sci Monit 11:RA110-21.

190. Nayerossadat N, Ali P, Maedeh T. 2012. Viral and nonviral delivery systems for gene delivery. Adv Biomed Res 1:27.

191. Kattman SJ, Witty AD, Gagliardi M, Dubois NC, Niapour M, Hotta A, Ellis J, Keller G. 2011. Stage-specific optimization of activin/nodal and BMP signaling promotes cardiac differentiation of mouse and human pluripotent stem cell lines. Cell Stem Cell 8:228–240.

192. Thomson M, Liu SJ, Zou LN, Smith Z, Meissner A, Ramanathan S. 2011. Pluripotency factors in embryonic stem cells regulate differentiation into germ layers. Cell 145:875–889.

193. Lian X, Hsiao C, Wilson G, Zhu K, Hazeltine LBB, Azarin SMM, Raval KKK, Zhang J, Kamp TJJ, Palecek SPP. 2012. Robust cardiomyocyte differentiation from human pluripotent stem cells via temporal modulation of canonical Wnt signaling. Proc Natl Acad Sci 109:E1848–E1857.

194. Blauwkamp TA, Nigam S, Ardehali R, Weissman IL, Nusse R. 2012. Endogenous Wnt signalling in human embryonic stem cells generates an equilibrium of distinct lineage-specified progenitors. Nat Commun 3:1070.

195. Tan JY, Sriram G, Rufaihah AJ, Neoh KG, Cao T. 2013. Efficient Derivation of Lateral Plate and Paraxial Mesoderm Subtypes from Human Embryonic Stem Cells Through GSKi-Mediated Differentiation. Stem Cells Dev 22:1893–1906.

196. Lian X, Zhang J, Zhu K, Kamp TJ, Palecek SP. 2013. Insulin inhibits cardiac mesoderm, not mesendoderm, formation during cardiac differentiation of human pluripotent stem cells and modulation of canonical Wnt signaling can rescue this inhibition. Stem Cells 31:447–57.

197. Cao N, Liang H, Huang J, Wang J, Chen Y, Chen Z, Yang H-T. 2013. Highly efficient induction and long-term maintenance of multipotent cardiovascular progenitors from human pluripotent stem cells under defined conditions. Cell Res 23:1119–1132.

198. Nazareth EJP, Ostblom JEE, Lücker PB, Shukla S, Alvarez MM, Oh SKW, Yin T, Zandstra PW. 2013. High-throughput fingerprinting of human pluripotent stem cell fate responses and lineage bias. Nat Methods 10:1225–1231.

199. Kramer T, Schmidt B, Lo Monte F. 2012. Small-Molecule Inhibitors of GSK-3: Structural Insights and Their Application to Alzheimer's Disease Models. Int J Alzheimers Dis 2012:381029.

200. Clevers H. 2006. Wnt/β-Catenin Signaling in Development and Disease. Cell 127:469–480.

201. Wang J, Sinha T, Wynshaw-Boris A. 2012. Wnt signaling in mammalian development: Lessons from mouse genetics. Cold Spring Harb Perspect Biol 4:6.

202. Turner DA, Rué P, Mackenzie JP, Davies E, Martinez Arias A. 2014. Brachyury cooperates with Wnt/β-catenin signalling to elicit primitive-streak-like behaviour in differentiating mouse embryonic stem cells. BMC Biol 12:63.

203. Xu C, Tabebordbar M, Iovino S, Ciarlo C, Liu J, Castiglioni A, Price E, Liu M, Barton ER, Kahn CR, Wagers AJ, Zon LI. 2013. A zebrafish embryo culture system defines factors that promote vertebrate myogenesis across species. Cell 155:909–921.

204. Borchin B, Chen J, Barberi T. 2013. Derivation and FACS-mediated purification of PAX3+/PAX7+ skeletal muscle precursors from human pluripotent stem cells. Stem Cell Reports 1:620–631.

205. Shelton M, Metz J, Liu J, Carpenedo RL, Demers SP, Stanford WL, Skerjanc IS. 2014. Derivation and expansion of PAX7-positive muscle progenitors from human and mouse embryonic stem cells. Stem Cell Reports 3:516–529.

206. Yamaguchi TP, Takada S, Yoshikawa Y, Wu N, McMahon AP. 1999. T (Brachyury) is a direct target of Wnt3a during paraxial mesoderm specification. Genes Dev 13:3185–3190.

207. Yoon JK, Moon RT, Wold B. 2000. The bHLH Class Protein pMesogenin1 Can Specify Paraxial Mesoderm Phenotypes. Dev Biol 222:376–391.

208. Chapman DL, Agulnik I, Hancock S, Silver LM, Papaioannou VE. 1996. Tbx6, a mouse T-Box gene implicated in paraxial mesoderm formation at gastrulation. Dev Biol 180:534–542.

209. Linker C, Lesbros C, Gros J, Burrus LW, Rawls A, Marcelle C. 2005. Beta-Catenin-dependent Wnt signalling controls the epithelial organisation of somites through the activation of paraxis. Development 132:3895–905.

210. Denham M, Bye C, Leung J, Conley BJ, Thompson LH, Dottori M. 2012. Glycogen synthase kinase 3β and activin/nodal inhibition in human embryonic stem cells induces a pre-neuroepithelial state that is required for specification to a floor plate cell lineage. Stem Cells 30:2400–2411.

211. Tahamtani Y, Azarnia M, Farrokhi A, Sharifi-Zarchi A, Aghdami N, Baharvand H. 2013. Treatment of Human Embryonic Stem Cells with Different Combinations of Priming and Inducing Factors Toward Definitive Endoderm. Stem Cells Dev 22:1419–32.

212. Choi IY, Lim HT, Estrellas K, Mula J, Cohen T V., Zhang Y, Donnelly CJ, Richard JP, Kim YJ, Kim H, Kazuki Y, Oshimura M, Li HL, Hotta A, Rothstein J, Maragakis N, Wagner KR, Lee G. 2016. Concordant but Varied Phenotypes among Duchenne Muscular Dystrophy Patient-Specific Myoblasts Derived using a Human iPSC-Based Model. Cell Rep 15:2301–2312.

213. Pallafacchina G, François S, Regnault B, Czarny B, Dive V, Cumano A, Montarras D, Buckingham M. 2010. An adult tissue-specific stem cell in its niche: A gene profiling analysis of in vivo quiescent and activated muscle satellite cells. Stem Cell Res 4:77–91.

214. Liu L, Cheung TH, Charville GW, Hurgo BMC, Leavitt T, Shih J, Brunet A, Rando TA. 2013. Chromatin Modifications as Determinants of Muscle Stem Cell Quiescence and Chronological Aging. Cell Rep 4:189–204.

Chapter 2: Developing an improved *in vitro* skeletal myogenesis protocol for human and mouse embryonic stem cells (1)

2.1 Objective of this study

Conventional serum-based methods to differentiate hESCs *in vitro* would yield cultures in which fewer than 5% of total cells were of the myogenic lineage. We used small molecules and serum replacements to more efficiently direct differentiation into skeletal muscle.

2.2 Statement of author contributions

M. S. and I. S. S. were responsible for experimental design. M. S. carried out the experiments and wrote the manuscript with I. S. S. and W. L. S. providing supervision. J. M. assisted with experimental cell culture, as well as qPCR and IF image analysis. R. L. C., S-P. D., and W. L. S. provided methods for the routine culture and monolayer plating of pluripotent hESCs. J. L. cultured pluripotent hESCs.

A version of this chapter has been published in Stem Cell Reports:

(1) Shelton, M., Metz, J., Liu, J., Carpenedo, R. L., Demers, S. P., Stanford, W. L., and Skerjanc, I. S. (2014) Derivation and expansion of PAX7-positive muscle progenitors from human and mouse embryonic stem cells. *Stem Cell Reports*. **3**, 516–529

2.3 Derivation and expansion of PAX7-positive muscle progenitors from human and mouse embryonic stem cells

Michael Shelton[1], Jeff Metz[1], Jun Liu[1], Richard L. Carpenedo[2,4], Simon-Pierre Demers[2,4], William L. Stanford[1,2,3,4], and Ilona S. Skerjanc[1*]

[1]Department of Biochemistry, Microbiology, and Immunology, University of Ottawa, Ottawa, Ontario, K1H 8M5, Canada

[2]Sprott Centre for Stem Cell Research, Regenerative Medicine Program, Ottawa Hospital Research Institute, Ottawa, Ontario, K1H 8L6, Canada

[3]Department of Cellular and Molecular Medicine, University of Ottawa, Ottawa, Ontario, K1H 8L6, Canada

[4]Faculty of Graduate and Postdoctoral Studies, University of Ottawa, Ottawa, Ontario, K1N 6N5, Canada

*Corresponding author Dr. Ilona S. Skerjanc: iskerjan@uottawa.ca, Tel: 613-562-5800 Ext. 8669; Fax: 613-562-5452.

2.4 Summary

Cell therapies treating pathological muscle atrophy or damage requires an adequate quantity of skeletal muscle progenitors not currently attainable from adult donors. Here, we generate cultures of approximately 90% skeletal myogenic cells by treating human embryonic stem cells with the GSK3-inhibitor CHIR99021 followed by FGF2 and N2 supplements. Gene expression analysis identified progressive expression of mesoderm, somite, dermomyotome, and myotome markers, following patterns of embryonic myogenesis. CHIR99021 enhanced transcript levels of the pan-mesoderm gene T and paraxial-mesoderm genes MSGN1 and TBX6; immunofluorescence confirmed that 91±6% of cells expressed T immediately following treatment. By 7 weeks, 47 ± 3% of cells were $MF20^{+}$ myocytes/myotubes surrounded by a 43 ± 4% population of $PAX7^{+}$ skeletal muscle progenitors, indicating 90% of cells had achieved myogenic identity without any cell sorting. Treatment of mouse embryonic stem cells with these factors resulted in similar enhancements of myogenesis. These studies establish a foundation for serum-free and chemically-defined monolayer skeletal myogenesis of embryonic stem cells.

2.5 Introduction

Cell therapies to reverse muscle atrophy and to strengthen skeletal muscle would greatly enhance and extend the lives of patients with muscle wasting conditions due to diseases and/or aging. Embryonic stem cells (ESC) have unlimited proliferation potential, and no need for locating a suitable immunotype-matched donor as with adult-derived stem cells (2). However, a major obstacle in the development of ESC-based therapies targeting muscle has been the generation of a homogeneous myogenic population from *in vitro* differentiation, thus requiring optimization to enrich for muscle lineage cells.

Several studies have validated the potential of mouse and human ESCs (mESC and hESC, respectively) and induced pluripotent stem cells (iPSC), in skeletal muscle therapy (3–9). Cells were differentiated into paraxial mesoderm-like muscle progenitors, either by a standard serum-based embryoid body (EB) differentiation protocol (4, 7) or by transient expression of PAX3 or PAX7 (5, 6, 8). These *in vitro* derived progenitors were able to engraft into adult myofibers of mice, replenish the muscle stem cell (satellite cell) niche, and enhance muscle contractile function (4–8). Despite promising results, these protocols are not appropriate for the generation of skeletal muscle progenitor (SMP) for clinical applications due to the inefficiency of differentiation and the use of viral vectors and potential insertional mutations (10).

Previous studies from our lab have used a serum-containing EB-induced differentiation supplemented with low levels of retinoic acid (RA) to enhance myogenesis from mouse (11) and human (12) ESCs. However, serum-containing EB-differentiation of hESCs produced relatively low yields of skeletal muscle (< 5%) and is undefined (11–13). In contrast, directed differentiation uses knowledge of embryogenesis to recreate embryonic conditions *in vitro* using combinations of signaling molecules, to support the differentiation

into one lineage (Murry and Keller, 2008). Applying the serum-free directed differentiation approach should greatly improve the efficiency of hESC-derived myogenesis for molecular analysis and for future use in cell therapies.

Wnt signalling is critically important for the development of the primitive streak and paraxial mesoderm (14), marked by the T and MSGN1 or TBX6 genes, respectively, and in the formation of posterior somites and the tail bud, (15), marked by the transcription factors PAX3, MEOX1, and PAX7. In the canonical pathway (reviewed in (16)), Wnt binds to Frizzled cell surface receptors, initiating a signaling cascade that inhibits GSK3B, preventing Beta-Catenin (CTNNB1) degradation, and allowing CTNNB1 to accumulate and translocate into the nucleus. Nuclear CTNNB1 enhances transcription by interaction with T-cell factors or lymphocyte enhancer factors (16).

It has previously been shown that the GSK3 inhibitor CHIR99021 can augment mesoderm induction (17), leading to cardiomyogenesis in ESCs (18). Recombinant proteins BMP4 and ACTIVIN-A (INHBA dimer) have similarly been used to induce mesoderm and cardiac muscle from ESCs (19, 20). These studies implicate BMP4/INHBA or CHIR99021 treatment as a potential method for generating skeletal muscle. Furthermore, we have shown that overexpression of WNT3A or CTNNB1 enhances the formation of premyogenic mesoderm in P19 embryonal carcinoma cells, resulting in increased myogenesis (21). The loss of CTNNB1 function via dominant negative mutation or knock down results in the loss of SMP formation and myogenesis, supporting the use of CHIR99021 to induce myogenesis.

The PAX3/PAX7 population that is present in the central dermomyotome appears to represent an SMP pool that is maintained throughout embryogenesis and is responsible for almost all skeletal muscle (22, 23). FGF2 prevents expression of the myoblast commitment transcription factors MYF5, MYOD1, and MYOG—collectively known as the myogenic

regulatory factors (MRF)—during satellite cell activation and thus can be utilized to enhance proliferation of PAX3/PAX7 expressing SMPs *in vitro* (24, 25). Satellite cells are more efficient in reconstituting the satellite cell niche during transplantation into muscle if they do not yet upregulate the MRFs (23, 26). N2 supplement is a combination of Insulin-Transferrin-Selenite (ITS) as well as progesterone and putrescine; while traditionally used to support the growth of neurons, we have previously shown that N2 supplemented media can enhance the terminal differentiation of myoblasts and myocytes, which would ensure SMPs are capable of complete myogenesis *in vitro* (12, 13).

In this report, we describe the robust skeletal myogenesis of hESCs and mESCs using CHIR99021 to induce mesoderm, FGF2 treatment to expand the SMP population, and N2-mediated terminal differentiation. This chemically defined, serum- and transgenic-free protocol yields a nearly homogeneous myogenic population from hESCs, consisting of 43 ± 4% $PAX7^+$ SMPs and 47 ± 3% Myosin Heavy $Chain^+$ (MYH) skeletal muscle.

2.6 Results

2.6.1 GSK3 inhibition enhanced premyogenic mesoderm formation from human ESC

Our objective was to devise a robust, serum-free directed differentiation method to obtain skeletal muscle from hESC *in vitro.* We adapted a recently developed chemically defined, feeder-free culture system to both expand pluripotent cells and induce mesoderm differentiation (27). E8 maintenance media and Matrigel extracellular matrix were observed to support pluripotency based on OCT4 expression, and hESCs retained a normal karyotype after prolonged collagenase passaging (data not shown). Removal of FGF2 and TGFB1 from E8 media—referred to as E6 media—was observed to support cell expansion, but not pluripotency based on the loss of OCT4, SOX2, and NANOG gene and protein expression.

Therefore, E6 medium provided a basal medium to which myogenic-inductive signalling molecules could be added. To control seeding density during differentiation procedures, hESCs were seeded as single cells in E8 media supplemented with ROCK-inhibitor (Y27632) (28). After overnight seeding, E8 media and ROCK-inhibitor were removed and replaced with E6 media plus the putative mesoderm inductive factors described below.

Since previous studies have shown that CHIR99021 or BMP4/INHBA treatment enhanced mesoderm induction in hESCs (18, 20, 29), we initially sought to determine an optimal dose of CHIR99021 and/or BMP4/INHBA to induce premyogenic mesoderm. For optimization of CHIR99021 treatment, concentrations of 2.5 and 10 μM were chosen to encompass a range of concentrations previously used to induce cardiac tissue-fated mesoderm (18, 29). Cells were plated on matrigel-coated dishes overnight in the presence of Y-27632 before differentiation was induced (28). Factors maintaining pluripotency were removed from the media and treated with CHIR99021 or vehicle for 2, 4, and 8 days in length: time points that encompass expression of *T* and early somite markers *PAX3* and *MEOX1* in serum-EB induced skeletal myogenesis (12). Analysis by quantitative polymerase chain reaction (qPCR) showed significant upregulation of *T* and *MSGN1* after two days of treatment with 10 μM CHIR99021, leading to significant upregulation of *PAX3* on day 8 (Fig. 2.1A). While 2.5 μM CHIR99021 treatment was able to upregulate *T* and *MSGN1* expression after 2 days of treatment, it did not upregulate *PAX3* at day 8 for any treatment length. Longer application of 10 μM CHIR99021, for 4 or 8 days, did not enhance *PAX3* expression as effectively, and appeared to have toxicity towards the cells (data not shown). *MEOX1* gene expression appeared similar between both CHIR99021 concentrations. Thus, the application of 10 μM CHIR99021 for the first 2 days of differentiation was determined optimal for enhancing the formation of $PAX3^{+}$ premyogenic mesoderm.

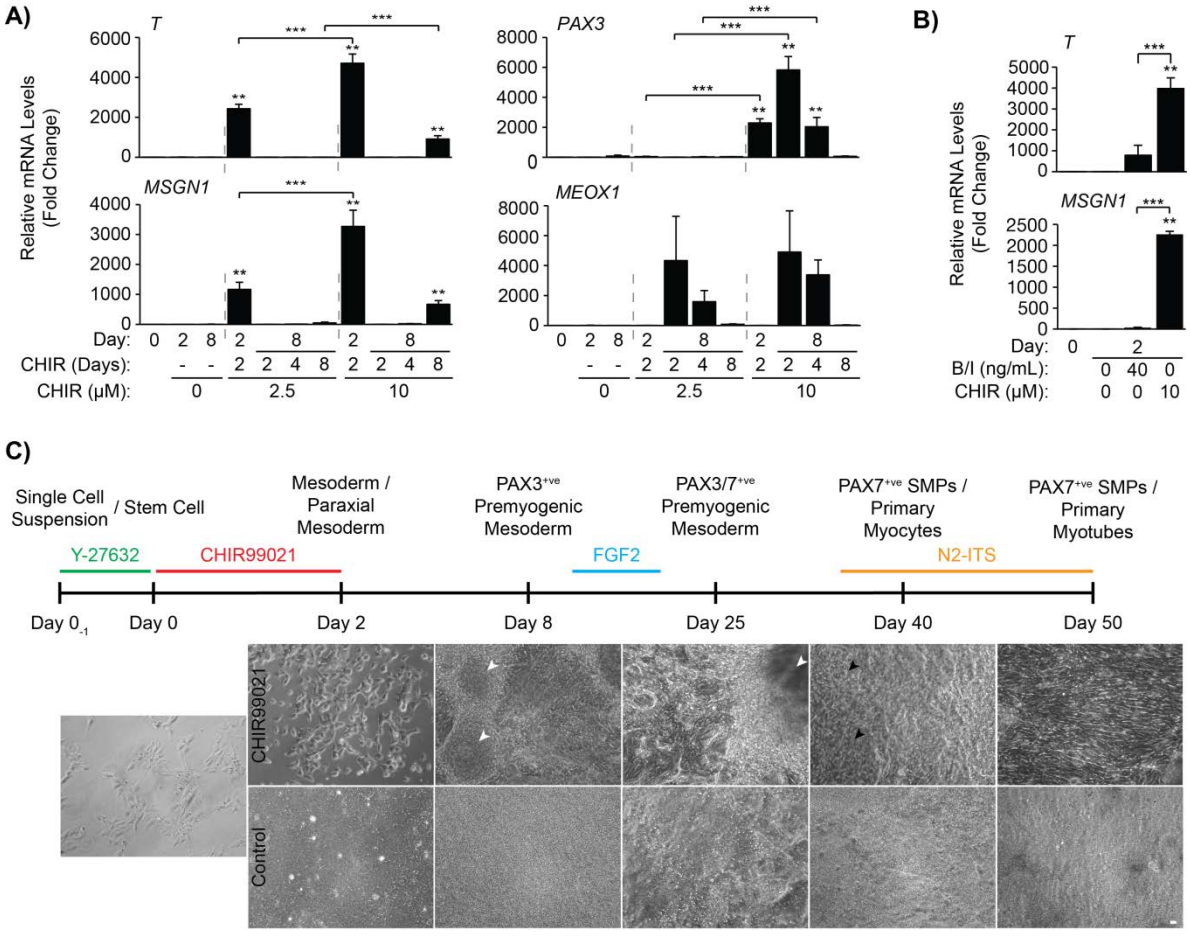
A)
T
MSGN1
PAX3
MEOX1
Relative mRNA Levels (Fold Change)
Day:
CHIR (Days):
CHIR (μM):
B)
T
MSGN1
Relative mRNA Levels (Fold Change)
Day:
B/I (ng/mL):
CHIR (μM):
C)
Single Cell Suspension / Stem Cell
Mesoderm / Paraxial Mesoderm
PAX3+ve Premyogenic Mesoderm
PAX3/7+ve Premyogenic Mesoderm
PAX7+ve SMPs / Primary Myocytes
PAX7+ve SMPs / Primary Myotubes
Y-27632
CHIR99021
FGF2
N2-ITS
Day 0-1
Day 0
Day 2
Day 8
Day 25
Day 40
Day 50
CHIR99021
Control

Figure 2.1

Figure 2.1. CHIR99021 (10 μm) applied for 2 days produces optimal levels of paraxial and premyogenic mesoderm gene expression. A) hESCs were treated in monolayer with or without 2.5 or 10 μm CHIR99021 for 2, 4, or 8 days. RNA was harvested at days 0, 2, and 8 to be analyzed by qPCR for markers of early and premyogenic mesoderm. Results are expressed as fold change over day 0, and statistics were performed with one-way ANOVA and post-hoc Tukey test (n = 3 independent experiments, *$p \leq 0.05$ vs. day 0, **$p \leq 0.05$ vs. day 0 and control, ***$p \leq 0.05$ 2.5 vs. 10 μM) **B)** CHIR99021-differentiated cells were compared to BMP4/INHBA treatment by qPCR for markers of early mesoderm. Statistics were performed with one-way ANOVA and post-hoc Tukey test (n = 3 independent experiments, *$p \leq 0.05$ vs. day 0, **$p \leq 0.05$ vs. day 0 and control, ***$p \leq 0.05$ BMP4/INHBA vs. CHIR99021). **C)** Schematic overview of the CHIR99021 directed differentiation of hESCs on a non-linear scale timeline, along with highlighting key supplemental factors applied during the differentiation, and the predicted developmental stages of skeletal myogenesis. **D)** Representative phase contrast live-cell images demonstrating the progressive changes in hESC morphology with and without CHIR99021 treatment. 3D cell clusters (white arrowheads) and the presence of skeletal myocytes (black arrowheads) are indicated at specific time points (scale bar = 20 μm).

We titrated levels of BMP4/INHBA to optimize *T* expression and found by qPCR that 40 ng/ml of BMP4/INHBA enhanced *T* transcript levels, although not as efficiently as CHIR99021-treatment (Fig. 2.1B). Furthermore, BMP4/INHBA treatment did not significantly enhance *MSGN1* expression, suggesting a lack of skeletal muscle-fated mesoderm. Thus, CHIR99021 treatment was better than BMP4/INHBA treatment to induce premyogenic mesoderm in hESCs.

2.6.2 CHIR99021 treatment resulted in up to 90% of hESCs entering the myogenic lineage

hESCs were differentiated using the two-day CHIR99021 treatment protocol devised in Fig. 2.1A, and cultured until day 50 as summarized in Fig. 2.1C, outlining the stages of myogenesis and the chief chemical and recombinant factor additions. Live-cell imaging was performed, showing the progressive morphological changes from stem cells to myotubes (Fig. 2.1D). CHIR99021-treated cells appeared morphologically distinct from control cells by day 2 of differentiation, and proliferation was reduced as judged by lower confluency compared to controls.

By day 8, CHIR99021-treated cells developed distinct three-dimensional cell clusters (Fig. 2.1D, white arrowheads) (30). FGF2 was applied from days 12 to 20, which corresponds to the timeframe that we previously detected somite or SMP markers *PAX3, MEOX1,* and *PAX7* along with *MYF5* (12). Therefore, this timeframe was an ideal target for FGF2 treatment to preferentially expand SMPs while suppressing early potential expression of the MRFs. N2 supplemented media was applied at day 35—coinciding with later detection of all MRFs previously (12)—to promote maturation of the myogenic cultures. Skeletal myocytes were observed by day 40, following five days of culture in N2 medium (Fig. 2.1D, black arrowheads). The myocytes were, for the most part, randomly arranged among other

non-bipolar cells. By day 50, cultures revealed large areas of aligned myocytes and fused myotubes, organized radially outward from the 3D-clusters (Fig. A2.1). No appreciable skeletal myogenesis was observed in control cultures that were given DMSO vehicle in place of CHIR99021 from days 0 to 2 and treated identically to CHIR99021-treated cells thereafter. Thus, CHIR99021 treatment resulted in the formation of abundant mesoderm that could be developed into easily visualized myocytes and myotubes by day 50 of differentiation.

CHIR99021 treatment resulted in detection of T protein in an average of 91 ± 6% of cells on day 2, compared to no T present in the control-treated cells (Fig. 2.2A & E). At day 8 an average of 58 ± 10% of cells expressed PAX3 after CHIR99021 treatment compared to 1 ± 1% in control cells (Fig. 2.2B & F). Skeletal myocytes were prominent by day 40 following five days of growth in N2 medium, with an average of 14 ± 3% of CHIR99021-treated hESCs expressing MYH, and were surrounded by a 37 ± 2% population of $PAX7^+$ cells (Fig. 2.2C & G). In addition to myocytes, some myotubes were present (Fig. A2.2A, white arrowheads) and skeletal muscle contractions could be observed by light microscopy (data not shown). When the cultures were left in N2 media from day 35 until day 50, 43 ± 4% of cells remained PAX7 positive while 47 ± 3% were MYH positive (Fig. 2.2D & G). A macroscopic view of the culture dishes suggests that the 3D-clusters function as myogenic foci, with high concentrations of $PAX7^+$ cells delaminating from their edges and myocytes/myotubes emanating outward (Fig. A2.2B & C). Thus, CHIR99021/FGF2/N2 treatment can induce around 90% of hESCs to enter the myogenic lineage.

We also quantified total cell number at various time points to investigate the scalability of hESC-derived myogenic cells with our protocol. The total cell number

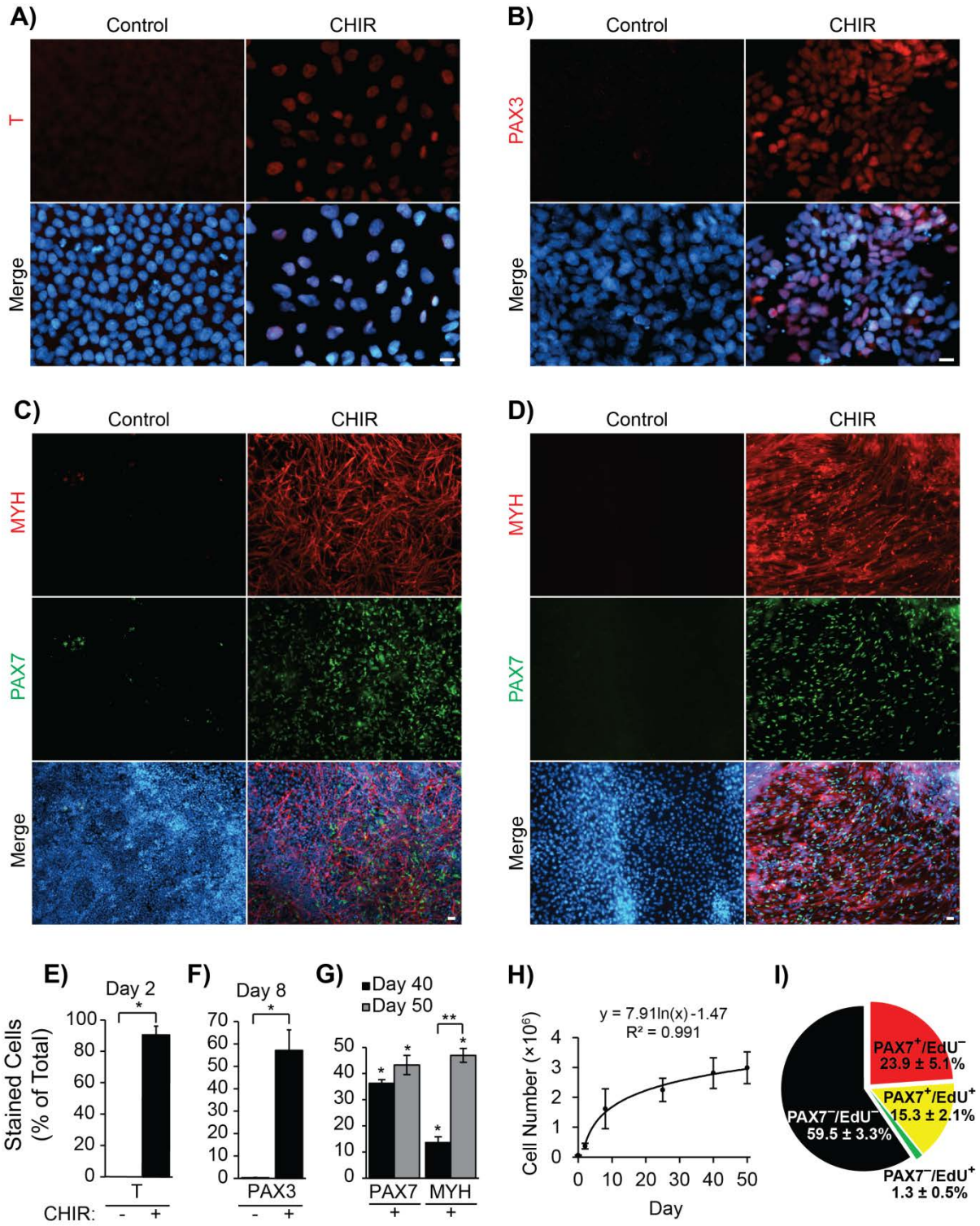
A)
Control
CHIR
T
Merge
B)
Control
CHIR
PAX3
Merge
C)
Control
CHIR
MYH
PAX7
Merge
D)
Control
CHIR
MYH
PAX7
Merge
E)
Day 2
Stained Cells (% of Total)
T
CHIR: - +
F)
Day 8
PAX3
- +
G)
Day 40
Day 50
PAX7
MYH
+ +
H)
y = 7.91ln(x) - 1.47
R² = 0.991
Cell Number (×10⁶)
Day
I)
PAX7⁺/EdU⁻ 23.9 ± 5.1%
PAX7⁺/EdU⁺ 15.3 ± 2.1%
PAX7⁻/EdU⁻ 59.5 ± 3.3%
PAX7⁻/EdU⁺ 1.3 ± 0.5%

Figure 2.2

Figure 2.2. CHIR99021 directed differentiation of hESCs induces up to a 90% myogenic population. hESCs were differentiated as described in figure 2.1. Myogenic induction was quantified by staining with antibodies against **A & E)** T at day 2, **B & F)** PAX3 at day 8, **C & G)** MYH and PAX7 at day 40, and **D & G)** MYH and PAX7 at day 50. Target populations are expressed as a percentage of total number of cells, which was quantified by Hoechst staining. Statistics were performed with one-way ANOVA and post-hoc Tukey test (n = 3 independent experiments, *$p \leq 0.05$ vs. control, **$p \leq 0.05$ day 40 vs. day 50, scale bar = 20 μm). **H)** Total number of cells was obtained by trypsinizing and counting 1-well of a 12-well culture dish at various time points of the differentiation protocol (n = 3 independent experiments). **I)** Day 50 CHIR99021-treated cells were pulsed with EdU for 4 hours and fixed and stained additionally with PAX7. EdU and PAX7 single or double positive cells were quantified and expressed as percentage of total number of cells (n = 3 independent experiments).

followed a logarithmic growth curve over the course of the differentiation protocol, resulting in roughly 20-fold more cells at day 50 compared to the initial number present at day 0 (Fig 2.2H). We also characterized the proliferation potential of our SMPs at day 50 by EdU incorporation (Fig. 2.2I & A2.2D). 42 ± 10% of $PAX7^+$ SMPs incorporated EdU during a 4 hour labeling pulse, demonstrating that our differentiation protocol yields a persistent population of actively proliferating SMPs at the final time point assayed in these studies. We examined the temporal pattern of expression of myogenic factors by qPCR during CHIR99021-directed differentiation of hESCs to confirm the immunofluorescence results. Day 2 of CHIR99021-treated hESCs showed significant upregulation of *T* transcripts, that was orders of magnitude higher than our previous results using a serum/EB method (Fig. 2.3A) (12). Significant upregulation of the paraxial mesoderm markers *MSGN1* and *TBX6* accompanied *T* at day 2, and all were downregulated by day 8, which marked peaks of the premyogenic mesoderm genes *PAX3* and *MEOX1* (Fig. 2.3B), in agreement with our previously published results (12). Two control patient-derived iPSC lines showed similar mesoderm gene elevation in response to our CHIR99021-based protocol (data not shown).

Expression of *PAX3* and *MEOX1* was downregulated by day 25, although significant levels were still detected until day 50 (data not shown). While *PAX7*, *MYF5*, *MYOD1*, and *MYOG* transcripts were notably upregulated by day 25, their expression continued to increase until significance by day 50 (Fig. 2.3C). Expression of *MYH3* transcripts also increased at days 40 and 50, suggesting an enduring SMP population coexisting with terminally differentiated skeletal myocytes/myotubes in agreement with our immunofluorescence data (Fig. 2.2D, G, I & A2.2D). Control cells showed no significant expression of *MYF5*, *MYOD1*, or *MYH3* transcripts. Overall, CHIR99021-treated cells exhibited waves of expression of mesoderm, presomitic mesoderm, muscle progenitor,

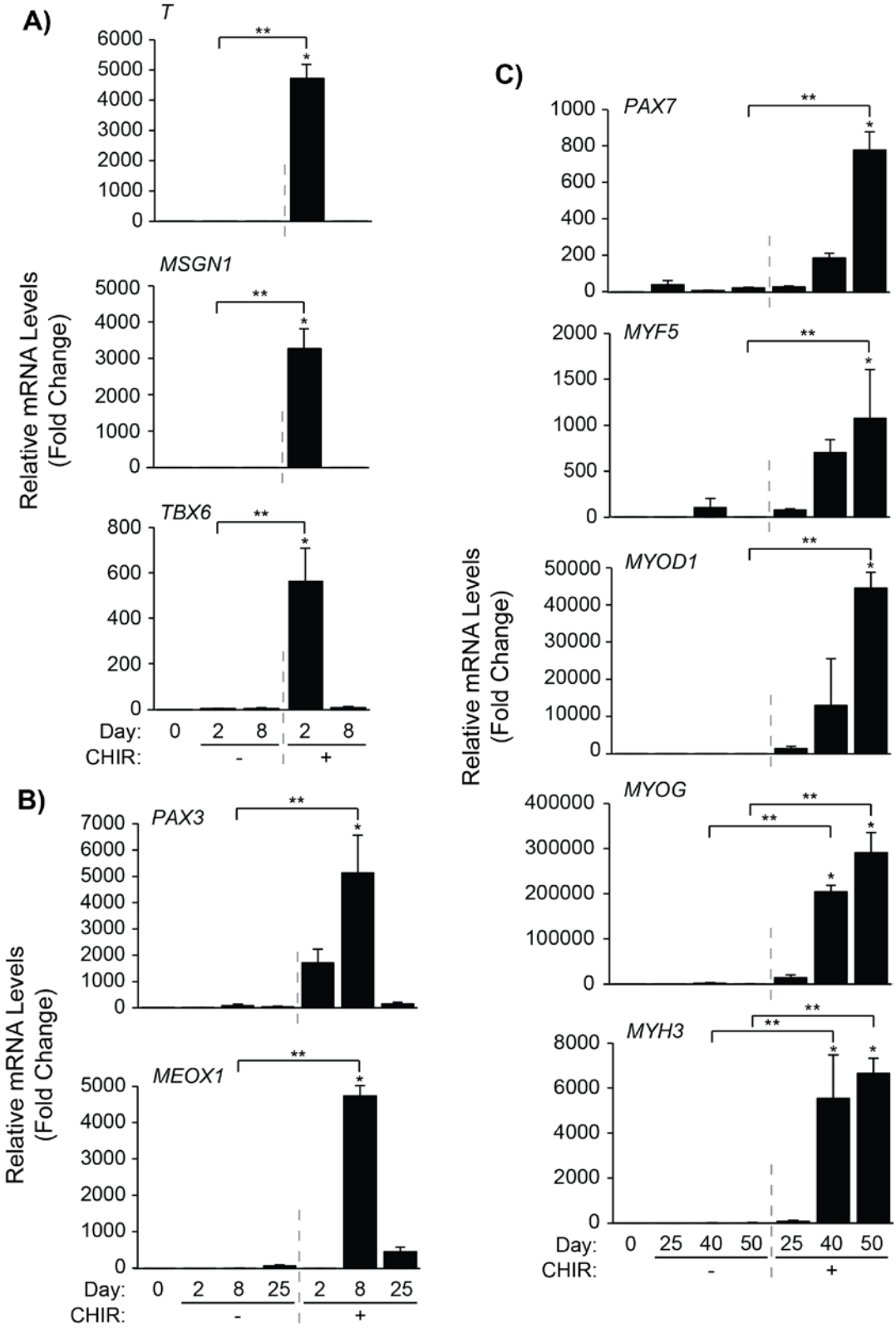
A)
T
MSGN1
TBX6
Relative mRNA Levels (Fold Change)
Day: 0 2 8 2 8
CHIR: - +
B)
PAX3
MEOX1
Relative mRNA Levels (Fold Change)
Day: 0 2 8 25 2 8 25
CHIR: - +
C)
PAX7
MYF5
MYOD1
MYOG
MYH3
Relative mRNA Levels (Fold Change)
Day: 0 25 40 50 25 40 50
CHIR: - +

Figure 2.3

Figure 2.3. qPCR profiling of CHIR99021-treated hESCs highlights a clear progression through specified mesodermal subtypes, muscle progenitor stages, and committed myogenic cultures. hESCs were differentiated as described in figure 2.1. RNA was harvested at days 0, 2, 8, 25, 40, and 50 to be analyzed by qPCR for markers several of **A)** early and paraxial mesoderm, **B)** premyogenic mesoderm, and **C)** committed or differentiated skeletal muscle. Results are expressed as fold change over day 0, and statistics were performed with one-way ANOVA and post-hoc Tukey test (n = 3 independent experiments, *$p \leq 0.05$ vs. day 0, **$p \leq 0.05$ vs. control).

myoblast, and muscle structural genes.

As Wnt signalling is important for the development of a multitude of tissues and not simply premyogenic mesoderm (16), we screened our cultures for markers of other lineages. Therefore, we assayed for other cell types that may be present in the 9% T^- cells early in differentiation, and later in the 10% of $PAX7^-/MYH^-$ cells. CHIR99021 treatment led to a significant drop in the pluripotency marker *SOX2* (Fig. 2.4A) by day 2, indicating an efficient loss of pluripotency. *SOX2* is also expressed in ectoderm lineages pertaining to the neural tube and future spinal cord (31, 32). Thus, levels of these tissues in our day 8 CHIR99021 cultures should be low for *SOX2* expression. *FOXA2*—a marker of notochord, floor plate, and future endoderm (33, 34)—was reduced in both CHIR99021-treated and control cells. Significant upregulation of *NOG* and *SOX10* was detected at day 8 of CHIR99021-mediated differentiation, which conventionally mark the roof plate and neural crest during embryonic development (35, 36). While neural crest cells may have been present early in differentiation, there was no significant upregulation in the neuronal marker *NEUROG1* at later time points (Fig. 2.4B), and immunofluorescent staining for NEFL—a neurofilament protein expressed in central and peripheral nervous system axons—was also negative (data not shown). Significant expression of the traditional cardiac muscle lineage gene *NKX2-5* and a trend toward elevated expression of the traditional cardiac myosin *MYH6* (37, 38) was detected with CHIR99021 treatment at day 50, although cells exhibiting a cardiac muscle phenotype were not readily observed in these cultures (Fig. A2.2B). As *NKX2-5* and *MYH6* have previously been detected in developing tongue skeletal muscle (39), we also assessed additional markers that are expressed exclusively in cardiomyocytes, *NPPA* and *MYL2*. No expression of these markers was detected in our day 50 differentiated cultures (Fig. 2.4C). Therefore, neither mature neuronal tissue nor cardiac muscle were present in

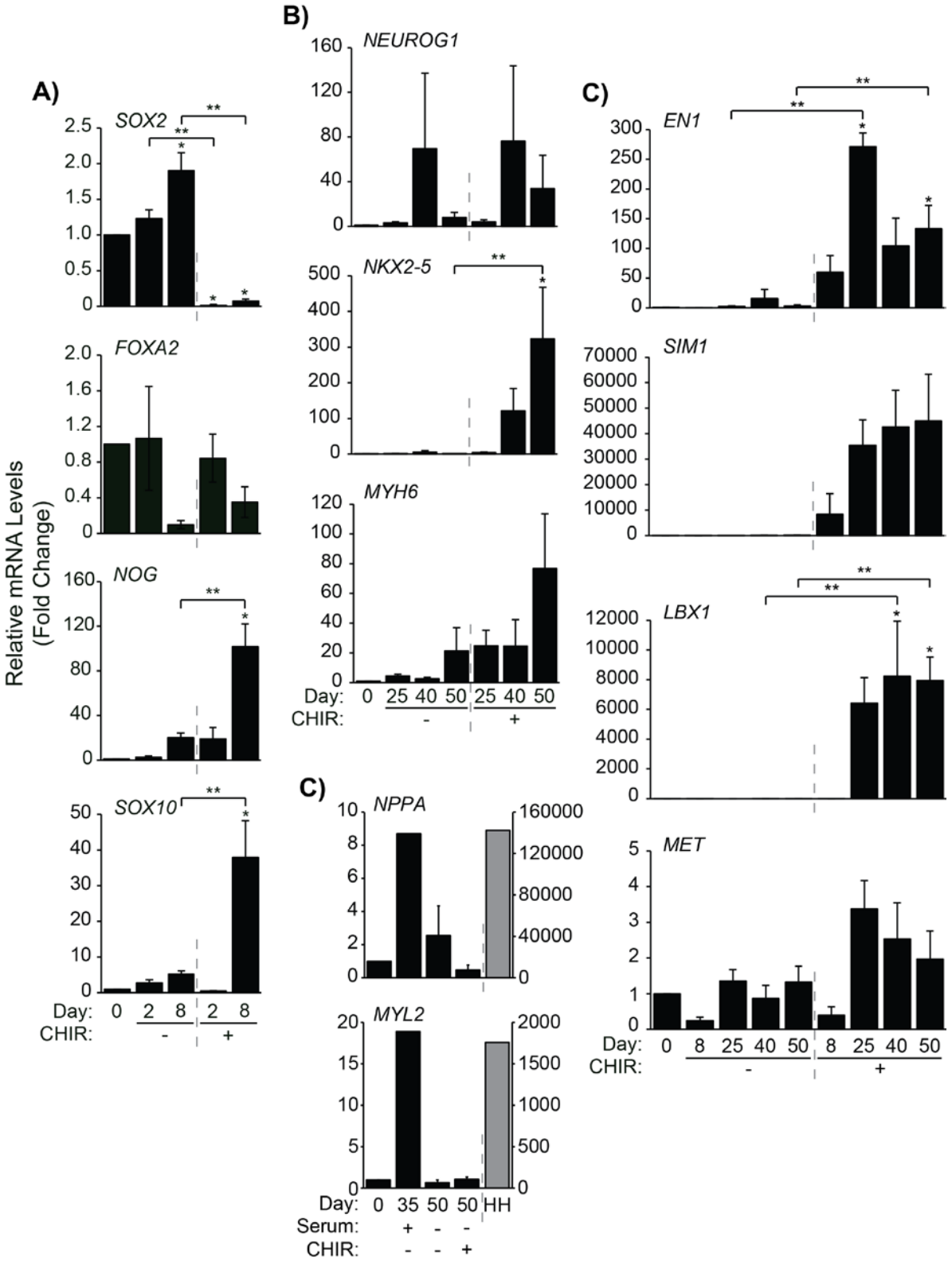
A)
B)
C)
Relative mRNA Levels
(Fold Change)
SOX2
FOXA2
NOG
SOX10
Day: 0 2 8 2 8
CHIR: - +
NEUROG1
NKX2-5
MYH6
Day: 0 25 40 50 25 40 50
CHIR: - +
NPPA
MYL2
Day: 0 35 50 50 HH
Serum: + - -
CHIR: - - +
EN1
SIM1
LBX1
MET
Day: 0 8 25 40 50 8 25 40 50
CHIR: - +

Figure 2.4

Figure 2.4. Low levels of neural crest transcripts were present in CHIR99021 treated cultures. hESCs were differentiated, harvested, and analyzed as described above for markers of **A)** pluripotency and neural ectoderm markers, **B)** differentiated neural and traditional cardiac markers, **C)** specific markers of mature cardiomyocytes, and **D)** patterned dermomyotome genes. Statistics were performed with one-way ANOVA and post-hoc Tukey test ($n = 3$ independent experiments, $*p \leq 0.05$ vs. day 0, $**p \leq 0.05$ vs. control). In **C)** RNA from serum-differentiated hESCs and human heart (HH) cardiomyocyte-positive controls were obtained ($n = 1$). All hESC fold-changes (black bars) were plotted on the primary Y-axis, and HH fold-change (grey bar) was plotted on the secondary Y-axis.

terminally differentiated cultures.

To determine the patterning of the dermomyotome, we performed qPCR for the regional dermomyotome markers *EN1*, *SIM1*, *LBX1*, and *MET* (Fig. 2.4D). The dermomyotome is patterned into the dorso-medial half—expressing *EN1* and giving rise to epaxial muscle, forming the deep back muscles—and the ventro-lateral half, expressing *SIM1* and giving rise to hypaxial muscle, forming the ventral and limb muscle (40–42). Proper migration of the hypaxial SMPs into the limb requires the expression of *LBX1* and *MET* (43). Therefore, presence of *LBX1* and *MET* expression would support the existence of SMPs similar to those found in migrating limb muscle. We found a significant increase of the two regional markers of the dermomyotome—*EN1* and *LBX1*—and a trend towards elevated SIM1 and *MET* with CHIR99021. However, *MET* was expressed at high levels throughout the differentiation, shown by low Ct values, making changes as a result of CHIR99021-treatment difficult to identify (data not shown). Thus, day 25 to 50 cultures containing muscle progenitors expressed markers of epaxial, hypaxial, and migratory dermomyotome.

2.6.3 CHIR99021 treatment enhanced skeletal myogenesis in mouse embryonic stem cells

A similar CHIR99021-based differentiation protocol was performed in mouse embryonic stem cells (mESC) and compared with BMP4/INHBA-mediated differentiation. Pax3/Pax7^{+} cells, presumably representing SMPs, were present in both BMP4/INHBA- and CHIR99021-treated mESCs at day 15, although PAX3/PAX7^{+} cells were visibly more abundant with CHIR99021 (Fig. 2.5A). Interestingly, MYH staining primarily revealed cardiomyocytes in BMP4/INHBA-treated cultures despite the presence of PAX3/PAX7^{+} cells (Fig. 2.5B). CHIR99021, conversely, promoted the differentiation of primarily skeletal

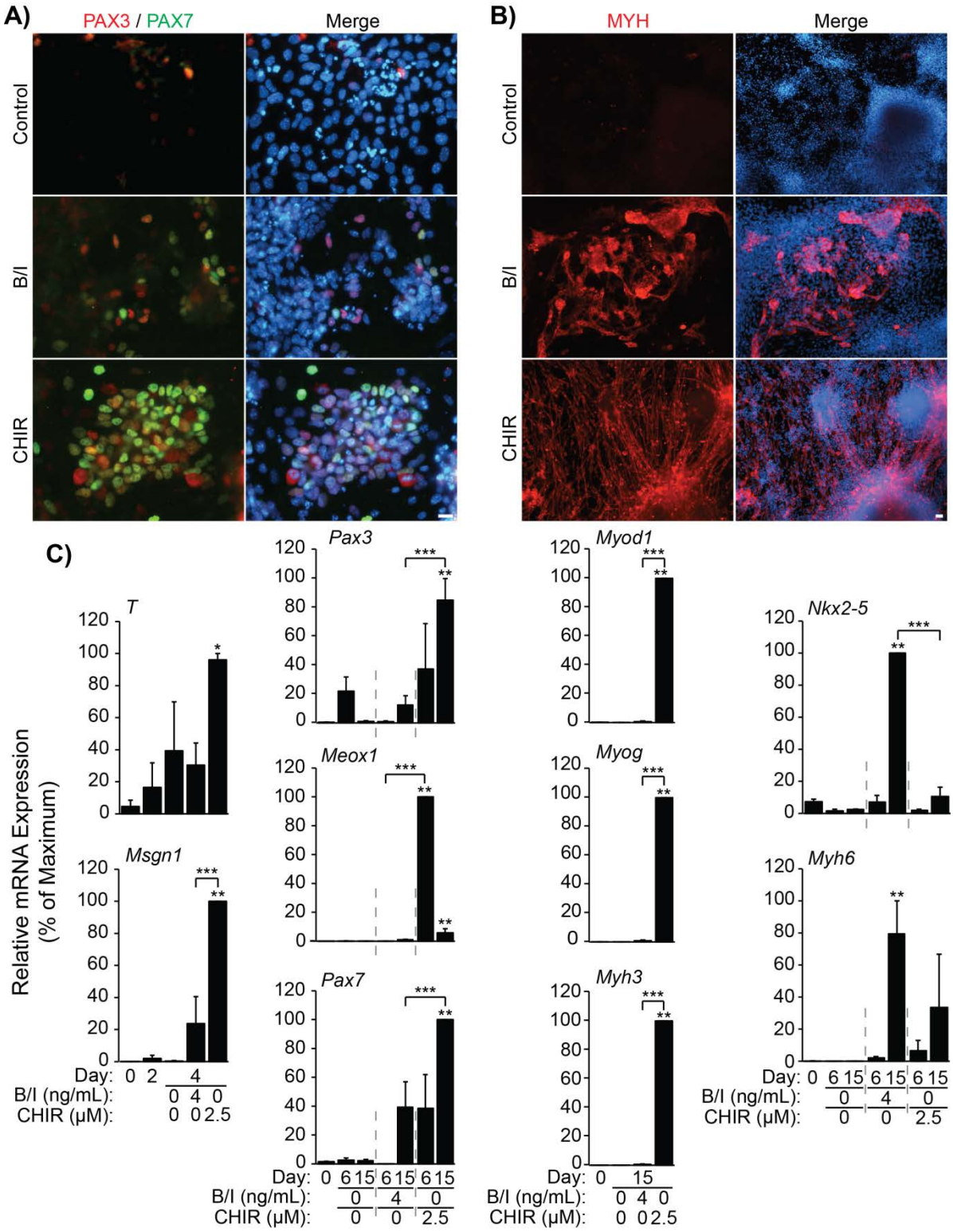
A)
PAX3 / PAX7
Merge
Control
B/I
CHIR
B)
MYH
Merge
Control
B/I
CHIR
C)
Relative mRNA Expression
(% of Maximum)
T
Msgn1
Pax3
Meox1
Pax7
Myod1
Myog
Myh3
Nkx2-5
Myh6
Day: 0 2 4
B/I (ng/mL): 0 4 0
CHIR (μM): 0 0 2.5
Day: 0 6 15 6 15 6 15
B/I (ng/mL): 0 4 0
CHIR (μM): 0 0 2.5
Day: 0 15
B/I (ng/mL): 0 4 0
CHIR (μM): 0 0 2.5
Day: 0 6 15 6 15 6 15
B/I (ng/mL): 0 4 0
CHIR (μM): 0 0 2.5

Figure 2.5

Figure 2.5. CHIR99021 enhances skeletal myogenesis in a 15-day differentiation of mESC. mESC were aggregated in differentiation medium for two days prior to treatment. CHIR99021, BMP4/INHBA, or vehicle control was applied from days 2 to 4. Immunofluorescent staining was carried out at day 15 with antibodies against **A)** PAX3 and PAX7, or **B)** MYH (scale bar = 20 μm). **C)** RNA was harvested at days 0 and 2 (prior to CHIR99021 treatment) and days 4, 6, and 15 (following treatment). Samples were analyzed by qPCR for select markers of skeletal and cardiomyogenesis. Results are expressed relative to the maximum fold change over day 0, and statistics were performed with one-way ANOVA and post-hoc Tukey test (n = 3 independent experiments, *$p \leq 0.05$ vs. day 0, **$p \leq 0.05$ vs. day 0 and control, *** $p \leq 0.05$ BMP4/INHBA vs. CHIR99021).

and not cardiac myocytes. Control cultures showed negligible or no staining with either PAX3/PAX7 or MYH antibodies. Thus, CHIR99021- treatment for 2 days upregulated PAX3/PAX7 expression, leading to enhanced skeletal myogenesis in mESCs.

Established markers of skeletal myogenesis were examined by qPCR, and demonstrated corroborating trends between CHIR99021-induced differentiation in mESCs and hESCs (Fig. 2.5C). Indeed, CHIR99021 treatment significantly enhanced the expression of key paraxial mesoderm, premyogenic mesoderm, and MRF genes, including *T*, *Msgn1*, *Pax3*, *Meox1*, *Myod1*, *Myog*, and *Myh3*. BMP4/INHBA treated cells exhibited some upregulation of the same mesodermal genes. However, BMP4/INHBA treatment did not upregulate expression of the MRFs, but did upregulate high levels of the cardiomyocyte markers *Nkx2-5* and *Myh6*. Thus, mESCs respond to CHIR99021 treatment by upregulating a similar set of muscle lineage genes as identified in hESCs, albeit in a much-reduced time frame.

2.7 Discussion

Our studies define a novel method whereby human and mouse ESCs are differentiated *in vitro* into highly enriched populations of skeletal muscle progenitor cells and myocytes/myotubes by activating Wnt signalling via the GSK3 inhibitor CHIR99021. A mere two-day exposure to the compound causes immediate changes in growth and morphology towards mesoderm, and sets in motion downstream cascades of myogenic transcription factors across weeks of culture. In due course, we achieve approximately 90% purity of skeletal muscle lineage cells from hESCs after 50 days in culture.

While forced expression of PAX3/PAX7 or MYOD in hESCs have resulted in enriched myogenic populations (8, 44–46), we sought to develop a viral- and transgenic- free

method of *in vitro* differentiation. A chemically defined protocol should be more readily adaptable to a broader number of cell lines and should allow for the examination of all of the stages of differentiation, some of which may be bypassed by transgenic overexpression (46).

Our study contrasts with previously published methods of transgene-free hESC myogenesis that were dependent upon serum, showing low overall myogenic induction and/or myogenic progenitor formation (12, 47, 48). For example, we previously obtained a 4% level of MYH^+ skeletal myocytes and 7% $PAX3^+$ SMPs with RA treatment (12). Our current CHIR99021-directed protocol improves on the serum/EB methods by directing a larger proportion of the cultures into mesoderm, leading to enriched myogenic lineage populations.

Several studies have shown that Wnt signalling modulation by CHIR99021 can maintain ESC pluripotency (49), and also can cause differentiation into tissues of all three germ layers (18, 50, 51). However, supporting factors were required immediately following CHIR99021 treatment for these approaches. Cell seeding density may also determine how GSK3 inhibition can generate skeletal muscle specific mesoderm versus other cell fates. Seeding density was critical first and foremost in determining how hESCs responded to external differentiation cues in our system (R.L.C., S-P.D., and W.L.S., unpublished data). At lower seeding densities ($< 1 \times 10^5$ cells/mL), hESC survival was reduced even in the presence of ROCK inhibitor, suggesting that cell-cell contacts are important for the initial seeding process. Additionally, sparse populations of cells responded to BMP4/INHBA treatment with increased cell death compared to higher densities. Furthermore, at higher seeding densities ($> 2 \times 10^5$ cells/mL), over-confluence was observed after 48 hours, again leading to compromised cell viability. Other monolayer approaches have used GSK3 to drive cardiomyogenesis; however, these protocols induce GSK3 inhibition once cells reach

confluence or with supplemental BMP4 inhibition (18, 29). These protocols also emphasize the critical importance of insulin depletion after GSK3 inhibition, or the need for Wnt inhibition following mesoderm induction lest cardiomyogenesis will not occur *in vitro* (20, 52). This is supported by the role of Dkk-mediated Wnt inhibition in specifying embryonic mesoderm to the primary heart field (53).

Of particular relevance to the results presented in our study was the differentiation of mesoderm from hESCs via 5 days of 5 μM CHIR99021 treatment (17). Intermediate to the desired cell types, CHIR99021 treatment caused a marked upregulation of T mRNA and protein levels, similar to our findings. Though the authors followed CHIR99021 treatment with BMP4—which typically effects lateral plate mesoderm—to develop hematopoietic and endothelial cell types and not skeletal muscle (54, 55). They also found INHBA following CHIR99021 treatment was necessary for pronounced endoderm commitment (17).

While CHIR99021 can coax differentiation of hESCs into all three germ layers, we obtained surprisingly 43 ± 4% $PAX7^+$ and 47 ± 3% MYH^+ cell populations at the experimental end point. However, trace expression of other ectoderm and mesoderm lineages can be detected early in the protocol. It is possible that other tissues, such as neural crest present early in our protocol, aid in the myogenic differentiation pathway; attempts to reach 100% T^+ cultures could demand additional signalling molecules to replace factors from these tissues (56, 57). It is likely that our current protocol can still be improved by the inclusion of additional signalling molecules at the correct time in the pathway, such as RA and Notch signalling, and/or by the use of FACS or microdissection to further enrich the SMPs.

Indeed, we attempted to improve our protocol according to a recent study published while our manuscript was in review that generated high proportions of skeletal myocytes from aggregated human iPSCs using combinatorial treatment with CHIR99021, FGF2, and

the cAMP signalling activator Forskolin (58). Hence, we included Forskolin in our culture system to determine whether activation of cAMP signalling with could improve skeletal myocyte yield in the context of our protocol (Fig. A2.3). qPCR analysis showed that, in the context of our monolayer differentiation protocol with 10 uM CHIR99021 alone, Forskolin does not provide additional benefit to myogenesis as it does with aggregate based differentiation. By day 7, however, conditions that included Forskolin were observably denser than CHIR99021 alone treated cultures, suggesting that Forskolin increases cell proliferation (data not shown). On major difference between our protocol and the published work by Zon and colleagues is that the myogenic cultures generated with Forskolin treatment appear to terminally differentiate beyond the SMP stage to over 90% $MYOG^+$ (58), whereas our system maintained a significant population of proliferating $PAX7^+$ SMPs (Fig. 2.2D, G, I, & A2.2D), suggesting that our culture system will provide replicative SMPs that could maintain homeostasis in the transplanted muscle.

During the revisions of this manuscript, two additional manuscripts were published that generated transgene-free human ESC myocytes. Barberi and colleagues utilized a lower concentration of CHIR99021 and longer treatment duration to direct skeletal myogenesis in embryonic stem cells (59). We initially determined that similar CHIR99021 conditions used by Borchin et al. induced less skeletal muscle-specific mesoderm than the optimal 10 uM for 2 days (Fig. 2.1A). Indeed, our protocol generated twice as many $PAX7^+$ SMPs at comparable timepoints (Fig. 2.2C & G). This recent publication, however, introduced a rigorous $HNK1^-/ACHR^-/CXCR4^+/MET^+$ FACS profile for isolating SMPs from bulk cultures. Therefore, future studies in embryonic-derived SMPs may benefit from implementing our differentiation protocol to generate greater numbers of starting cells, which could be enriched via the $HNK1^-/ACHR^-/CXCR4^+/MET^+$ profile.

In addition, Suzuki and colleagues present a viable alternative to monolayer directed skeletal myogenesis (60). The authors' "EZ Sphere" suspension-culture system uses high concentrations of FGF2 and EFGF to yield remarkably similar proportions of $PAX7^+$ populations at the experimental endpoint as those presented here (Fig. 2.2D, G, I & A2.2D). One caveat to the EZ Sphere method, however, is potentially upwards of 30% of cells are neural progenitors (60).

We show that CHIR99021 can mediate efficient skeletal myogenesis in mESCs using a 2-day CHIR99021 treatment similar to that used for hESCs, illustrating the effectiveness of our protocol across these species. Our current findings are consistent with our previous results showing that Wnt signalling via CTNNB1 is important for murine P19 embryonal carcinoma cell differentiation, using gain- and loss-of-function as well as a dominant negative approach (21, 61). In addition, the greater experimental variability with mouse compared to human ESC differentiation into muscle could be due to the EB-based nature of the mESC serum-free protocol. Therefore, we are adapting the more consistent monolayer approach used with our hESC method to mESCs. While hESCs are more therapeutically relevant, mESCs continue to play an integral role in our ability to study cellular differentiation, primarily due to their substantially shorter differentiation time, creating a simpler high throughput model system for detailed molecular analysis.

Overall, the results presented here have provided a method to differentiate mouse and human ESCs into highly enriched skeletal muscle lineage cultures. Most importantly, we show a stable $PAX7^+$ population of SMPs even after 7 weeks of culture. Ultimately, these studies provide the foundation for *in vitro* study of ESC skeletal myogenesis, which could contribute to future drug testing or stem cell therapies, leading to the repair of muscle in patients with muscular wasting disorders.

2.8 Experimental Procedures

2.8.1 Human cell culture

All hESC media and components are formulated in Table A2.1. H9 hESCs were maintained feeder free on BD Matrigel™ (BD Biosciences, Franklin Lakes, NJ) coated dishes in E8 media prepared in lab (27, 62, 63).

Cells were prepared for differentiation by plating 1.5×10^5 cells per well on BD Matrigel™ coated 12-well dishes in E8 supplemented with 10 μM Y-27632 (Tocris Biosciences, Bristol, UK) overnight. The medium was then replaced with E6 medium (63), supplemented with CHIR99021 (Tocris Biosciences) or BMP4 and INHBA (R&D Systems, Minneapolis, MN) for two days. DMSO was used as the vehicle control at a final concentration of 0.1%. CHIR99021 or BMP4 and INHBA were washed out at day 2, and cells were grown in un-supplemented E6 until day 12. From days 12 to 20, the medium was replaced with StemPro-34 media. Cells were returned to E6 media from days 20 to 35. The medium was then replaced with N2-ITS medium until the endpoint of the experiment. All media were changed daily. When indicated (Fig. A2.3), 20 μM Forskolin (Tocris Biosciences) and 10 ng/mL FGF2 was used from days 0 to 7 in conjunction with 0.5 μM CHIR99021, or from days 2 to 7 following 2 days of 10 μM CHIR99021 treatment.

2.8.2 Mouse cell culture

All mESC media and components are formulated in Table A2.2. R1 mESCs were maintained feeder free and passaged every other day in Maintenance Media, prepared in lab (20).

Cells were prepared for differentiation by plating 5×10^5 cells on 0.1% gelatin coated 10 cm dishes overnight in Serum Free Maintenance Media to deplete serum. The cells were

then trypsinized and aggregated into embryoid bodies at 1 x 10^5 cells/mL on petri dishes in Serum Free Differentiation Medium for two days. At day 2, EBs were trypsinized and re-aggregated at 1 × 10^5 cells/mL on petri dishes in Serum Free Differentiation Media—supplemented with 5 ng/mL VEGF (R&D Systems), and either CHIR99021 or BMP4/INHBA—from days 2 to 4 of differentiation. DMSO was used as the vehicle control at a final concentration of 0.1%. From days 4 to 10, the medium was replaced with StemPro-34 Media. EBs were plated on BD Matrigel™ coated dishes on day 6. The medium was replaced at day 10 with N2 medium until the endpoint of the experiment. All media were changed every other day.

2.8.3 Gene expression analysis

RNA was isolated from cells using either the RNeasy kit (Qiagen, Gaithersburg, MD) or Total RNA Mini Kit (FroggaBio, Toronto, ON). RNA ranging from 0.2 to 1 µg of each sample was reverse transcribed using the Quantitect Reverse Transcription kit (Qiagen). qPCR was carried out using a Mastercycler realplex and analyzed with Realplex software (Eppendorf, Mississaga, ON). For real-time detection of mRNA expression, 1/40 of the total first strand synthesis product was used as a template for PCR amplification using either GoTaq qPCR Master Mix (Promega Corporation, Madison, WI) or Kapa SYBR Fast qPCR kit (Kapa Biosystems, Woburn, MA). Primer pairs (Table A2.3) were selected from PrimerBank (64), or generated by Primer-BLAST (65), and tested for equivalent efficiency. Each reaction was carried out in duplicate, and fold changes were calculated using the comparative Ct method as described earlier (66). The resulting Ct values were normalized to either *GAPDH* in hESCs or *Actb* in mESCs. Results are shown ± S. E. of the mean of three independent experiments, unless otherwise stated.

2.8.4 Immunofluorescence

Cells were fixed for immunofluorescence with 4% formaldehyde for 15 minutes and permeabilized with PBS containing 0.5% TritonX-100 for 10 minutes. Cells were then blocked for 1 hour with PBS containing 0.1% bovine serum albumin, 0.1% TritonX-100, and 10% goat or donkey serum. Primary antibodies against T (Abcam, Cambridge, UK), PAX3 (R&D Systems), PAX7 and MF20 (Developmental Studies Hybridoma Bank, Iowa City, IA), or NEFL (Sigma-Aldrich, Oakville, ON) were incubated overnight at 4°C. Cy3-conjugated donkey anti-rabbit, goat anti-mouse IgG2a, goat anti-mouse IgG2b, Alexa488-conjugated donkey anti-goat, and DyLight488-conjugated goat anti-mouse IgG1 secondary antibodies (Jackson ImmunoResearch, Westgrove, PA) were used for detection as appropriate for 1 hour at room temperature. Cells were mounted in sPBS:glycerol containing Hoechst dye to identify cell nuclei. EdU labelling was performed using the Click-iT EdU Alexa Fluor488 Imaging Kit (Life Technologies, Eugene, OR). Cells we pulsed with EdU for 4 hours before fixing and staining as per the manufacturer's protocol.

Cells were visualized with a Leica DMI6000 B microscope (Leica Microsystems Inc., Richmond Hill, Ontario) and pictures were acquired using a Micropublisher 3.3 RTV camera (Q Imaging, Surrey, British Columbia). Staining was quantified by performing either manual or automated cell counts using the Volocity software (PerkinElmer Inc., Waltham, MA) and represented as a proportion of total nuclei. On average, 2.5×10^4 cells were quantified from each experiment. Results are shown ± S. E. of the mean of three independent experiments.

2.8.5 Statistical analysis

Statistical differences between means were calculated using one-way ANOVA and post-hoc Tukey test unless otherwise stated. P values of $p \leq 0.05$ were considered significant.

2.9 Acknowledgements

The authors would like to acknowledge Nicolas Tremblay for his assistance in the quantification of immunofluorescent images. This work was funded by an award from the Muscular Dystrophy Association to Ilona S. Skerjanc (218371), and by grants from the Natural Sciences and Engineering Research Council (RGPIN 293170-11) and Canadian Institutes of Health Research (MOP-89910) to Dr. William L. Stanford. Michael Shelton was supported in part by the Queen Elizabeth II Graduate Scholarship in Science and Technology. Richard L. Carpenedo was funded, in part, by the Government of Ontario Ministry of Economic Development and Innovation for the Ontario Research Fund supporting the International Regulome Consortium. Simon-Pierre Demers was partially supported by a Fonds de la Recherche en Santé du Québec postdoctoral fellowship. William L. Stanford was supported by the Canada Research Chair in Integrative Stem Cell Biology.

2.10 References

1. Shelton M, Metz J, Liu J, Carpenedo RL, Demers SP, Stanford WL, Skerjanc IS. 2014. Derivation and expansion of PAX7-positive muscle progenitors from human and mouse embryonic stem cells. Stem Cell Reports 3:516–529.
2. Araki R, Uda M, Hoki Y, Sunayama M, Nakamura M, Ando S, Sugiura M, Ideno H, Shimada A, Nifuji A, Abe M. 2013. Negligible immunogenicity of terminally differentiated cells derived from induced pluripotent or embryonic stem cells. Nature 494:100–104.
3. Barberi T, Bradbury M, Dincer Z, Panagiotakos G, Socci ND, Studer L. 2007. Derivation of engraftable skeletal myoblasts from human embryonic stem cells. Nat Med 13:642–648.
4. Sakurai H, Okawa Y, Inami Y, Nishio N, Isobe K. 2008. Paraxial mesodermal progenitors derived from mouse embryonic stem cells contribute to muscle regeneration via differentiation into muscle satellite cells. Stem Cells 26:1865–1873.
5. Darabi R, Gehlbach K, Bachoo RM, Kamath S, Osawa M, Kamm KE, Kyba M, Perlingeiro RCR. 2008. Functional skeletal muscle regeneration from differentiating embryonic stem cells. Nat Med 14:134–143.

6. Darabi R, Santos FNC, Filareto A, Pan W, Koene R, Rudnicki MA, Kyba M, Perlingeiro RCR. 2011. Assessment of the myogenic stem cell compartment following transplantation of Pax3/Pax7-induced embryonic stem cell-derived progenitors. Stem Cells 29:777–790.

7. Chang H, Yoshimoto M, Umeda K, Iwasa T, Mizuno Y, Fukada S, Yamamoto H, Motohashi N, Miyagoe-Suzuki Y, Takeda S, Heike T, Nakahata T. 2009. Generation of transplantable, functional satellite-like cells from mouse embryonic stem cells. FASEB J 23:1907–19.

8. Darabi R, Arpke RW, Irion S, Dimos JT, Grskovic M, Kyba M, Perlingeiro RCR. 2012. Human ES- and iPS-derived myogenic progenitors restore DYSTROPHIN and improve contractility upon transplantation in dystrophic mice. Cell Stem Cell 10:610–619.

9. Darabi R, Pan W, Bosnakovski D, Baik J, Kyba M, Perlingeiro RCR. 2011. Functional Myogenic Engraftment from Mouse iPS Cells. Stem Cell Rev Reports 7:948–957.

10. Thomas CE, Ehrhardt A, Kay MA. 2003. Progress and problems with the use of viral vectors for gene therapy. Nat Rev Genet 4:346–358.

11. Kennedy K a M, Porter T, Mehta V, Ryan SD, Price F, Peshdary V, Karamboulas C, Savage J, Drysdale T a, Li S-C, Bennett S a L, Skerjanc IS. 2009. Retinoic acid enhances skeletal muscle progenitor formation and bypasses inhibition by bone morphogenetic protein 4 but not dominant negative beta-catenin. BMC Biol 7:67.

12. Ryan T, Liu J, Chu A, Wang L, Blais A, Skerjanc IS. 2012. Retinoic Acid Enhances Skeletal Myogenesis in Human Embryonic Stem Cells by Expanding the Premyogenic Progenitor Population. Stem Cell Rev Reports 8:482–493.

13. Al Madhoun AS, Mehta V, Li G, Figeys D, Wiper-Bergeron N, Skerjanc IS. 2011. Skeletal myosin light chain kinase regulates skeletal myogenesis by phosphorylation of MEF2C. EMBO J 30:2477–2489.

14. Liu P, Wakamiya M, Shea MJ, Albrecht U, Behringer RR, Bradley A. 1999. Requirement for Wnt3 in vertebrate axis formation. Nat Genet 22:361–365.

15. Takada S, Stark KL, Shea MJ, Vassileva G, McMahon JA, McMahon AP. 1994. Wnt-3a regulates somite and tailbud formation in the mouse embryo. Genes Dev 8:174–189.

16. Clevers H. 2006. Wnt/β-Catenin Signaling in Development and Disease. Cell 127:469–480.

17. Tan JY, Sriram G, Rufaihah AJ, Neoh KG, Cao T. 2013. Efficient Derivation of Lateral Plate and Paraxial Mesoderm Subtypes from Human Embryonic Stem Cells Through GSKi-Mediated Differentiation. Stem Cells Dev 22:1893–1906.

18. Lian X, Hsiao C, Wilson G, Zhu K, Hazeltine LBB, Azarin SMM, Raval KKK, Zhang J, Kamp TJJ, Palecek SPP. 2012. Robust cardiomyocyte differentiation from human pluripotent stem cells via temporal modulation of canonical Wnt signaling. Proc Natl Acad Sci 109:E1848–E1857.

19. Murry CE, Keller G. 2008. Differentiation of Embryonic Stem Cells to Clinically Relevant Populations: Lessons from Embryonic Development. Cell 132:661–680.

20. Kattman SJ, Witty AD, Gagliardi M, Dubois NC, Niapour M, Hotta A, Ellis J, Keller G. 2011. Stage-specific optimization of activin/nodal and BMP signaling promotes cardiac differentiation of mouse and human pluripotent stem cell lines. Cell Stem Cell 8:228–240.

21. Petropoulos H, Skerjanc IS. 2002. B-catenin is essential and sufficient for skeletal myogenesis in P19 cells. J Biol Chem 277:15393–15399.

22. Buckingham M. 2007. Skeletal muscle progenitor cells and the role of Pax genes. C R Biol 330:530–3.

23. Kuang S, Kuroda K, Le Grand F, Rudnicki MA. 2007. Asymmetric Self-Renewal and Commitment of Satellite Stem Cells in Muscle. Cell 129:999–1010.

24. Hall JK, Banks GB, Chamberlain JS, Olwin BB. 2010. Prevention of muscle aging by myofiber-associated satellite cell transplantation. Sci Transl Med 2:57ra83.

25. Fedorov Y V, Jones NC, Olwin BB. 1998. Regulation of myogenesis by fibroblast growth factors requires beta-gamma subunits of pertussis toxin-sensitive G proteins. Mol Cell Biol 18:5780–7.

26. Montarras D, Morgan J, Collins C, Relaix F, Zaffran S, Cumano A, Partridge T, Buckingham M. 2005. Direct isolation of satellite cells for skeletal muscle regeneration. Science 309:2064–7.

27. Chen G, Gulbranson DR, Hou Z, Bolin JM, Ruotti V, Probasco MD, Smuga-Otto K, Howden SE, Diol NR, Propson NE, Wagner R, Lee GO, Antosiewicz-Bourget J, Teng JMC, Thomson J a, Nicole R, Propson NE, Wagner R, Lee GO, Teng JMC, Thomson J a. 2011. Chemically defined conditions for human iPS cell derivation and culture. Nat Methods 8:424–429.

28. Gauthaman K, Fong CY, Bongso A. 2010. Effect of ROCK inhibitor Y-27632 on normal and variant human embryonic stem cells (hESCs) in vitro: Its benefits in hESC expansion. Stem Cell Rev Reports 6:86–95.

29. Cao N, Liang H, Huang J, Wang J, Chen Y, Chen Z, Yang H-T. 2013. Highly efficient induction and long-term maintenance of multipotent cardiovascular progenitors from human pluripotent stem cells under defined conditions. Cell Res 23:1119–1132.

30. Rohwedel J, Maltsev V, Bober E, Arnold HH, Hescheler J, Wobus AM. 1994. Muscle cell differentiation of embryonic stem cells reflects myogenesis in vivo: developmentally regulated expression of myogenic determination genes and functional expression of ionic currents. Dev Biol 164:87–101.

31. Wood HB, Episkopou V. 1999. Comparative expression of the mouse Sox1, Sox2 and Sox3 genes from pre-gastrulation to early somite stages. Mech Dev 86:197–201.

32. D'Amour KA, Gage FH. 2003. Genetic and functional differences between multipotent neural and pluripotent embryonic stem cells. Proc Natl Acad Sci U S A 100 Suppl:11866–11872.

33. Sasaki H, Hogan BL. 1993. Differential expression of multiple fork head related genes during gastrulation and axial pattern formation in the mouse embryo. Development 118:47–59.

34. Monaghan AP, Kaestner KH, Grau E, Schutz G. 1993. Postimplantation expression patterns indicate a role for the mouse forkhead/HNF-3 alpha, beta and gamma genes in determination of the definitive endoderm, chordamesoderm and neuroectoderm. Development 119:567–578.

35. Valenzuela DM, Economides a N, Rojas E, Lamb TM, Nuñez L, Jones P, Lp NY, Espinosa R, Brannan CI, Gilbert DJ. 1995. Identification of mammalian noggin and its expression in the adult nervous system. J Neurosci 15:6077–6084.

36. Pusch C, Hustert E, Pfeifer D, Südbeck P, Kist R, Roe B, Wang Z, Balling R, Blin N, Scherer G. 1998. The SOX10/Sox10 gene from human and mouse: Sequence, expression, and transactivation by the encoded HMG domain transcription factor. Hum Genet 103:115–123.

37. Akazawa H, Komuro I. 2005. Cardiac transcription factor Csx/Nkx2-5: Its role in cardiac development and diseases. Pharmacol Ther 107:252–68.

38. Lyons GE, Schiaffino S, Sassoon D, Barton P, Buckingham M. 1990. Developmental regulation of myosin gene expression in mouse cardiac muscle. J Cell Biol 111:2427–36.

39. Diez-Roux G, Banfi S, Sultan M, Geffers L, Anand S, Rozado D, Magen A, Canidio E, Pagani M, Peluso I, Lin-Marq N, Koch M, Bilio M, Cantiello I, Verde R, De Masi C, Bianchi SA, Cicchini J, Perroud E, Mehmeti S, Dagand E, Schrinner S, Nürnberger A, Schmidt K, Metz K, Zwingmann C, Brieske N, Springer C, Hernandez AM, Herzog S, Grabbe F, Sieverding C, Fischer B, Schrader K, Brockmeyer M, Dettmer S, Helbig C, Alunni V, Battaini M-A, Mura C, Henrichsen CN, Garcia-Lopez R, Echevarria D, Puelles E, Garcia-Calero E, Kruse S, Uhr M, Kauck C, Feng G, Milyaev N, Ong CK, Kumar L, Lam M, Semple CA, Gyenesei A, Mundlos S, Radelof U, Lehrach H, Sarmientos P, Reymond A, Davidson DR, Dollé P, Antonarakis SE, Yaspo M-L, Martinez S, Baldock RA, Eichele G, Ballabio A. 2011. A high-resolution anatomical atlas of the transcriptome in the mouse embryo. PLoS Biol 9:e1000582.

40. Ordahl CP, Le Douarin NM. 1992. Two myogenic lineages within the developing somite. Development 114:339–53.

41. Cheng L, Alvares LE, Ahmed MU, El-Hanfy AS, Dietrich S. 2004. The epaxial-hypaxial subdivision of the avian somite. Dev Biol 274:348–369.

42. Pourquié O, Fan CM, Coltey M, Hirsinger E, Watanabe Y, Bréant C, Francis-West P, Brickell P, Tessier-Lavigne M, Le Douarin NM. 1996. Lateral and axial signals involved in avian somite patterning: A role for BMP4. Cell 84:461–471.

43. Vasyutina E, Birchmeier C. 2006. The development of migrating muscle precursor cells. Anat Embryol (Berl) 211:37–41.

44. Rao L, Tang W, Wei Y, Bao L, Chen J, Chen H, He L, Lu P, Ren J, Wu L, Luan Z, Cui C, Xiao L. 2012. Highly Efficient Derivation of Skeletal Myotubes from Human

Embryonic Stem Cells. Stem Cell Rev Reports 8:1109–1119.

45. Goudenege S, Lebel C, Huot NB, Dufour C, Fujii I, Gekas J, Rousseau J, Tremblay JP. 2012. Myoblasts Derived From Normal hESCs and Dystrophic hiPSCs Efficiently Fuse With Existing Muscle Fibers Following Transplantation. Mol Ther 20:2153–2167.

46. Albini S, Coutinho P, Malecova B, Giordani L, Savchenko A, Forcales SV, Puri PL. 2013. Epigenetic Reprogramming of Human Embryonic Stem Cells into Skeletal Muscle Cells and Generation of Contractile Myospheres. Cell Rep 3:661–670.

47. Hwang Y, Suk S, Lin S, Tierney M, Du B, Seo T, Mitchell A, Sacco A, Varghese S. 2013. Directed In Vitro Myogenesis of Human Embryonic Stem Cells and Their In Vivo Engraftment. PLoS One 8:e72023.

48. Awaya T, Kato T, Mizuno Y, Chang H, Niwa A, Umeda K, Nakahata T, Heike T. 2012. Selective development of myogenic mesenchymal cells from human embryonic and induced pluripotent stem cells. PLoS One 7:e51638.

49. Wu Y, Ai Z, Yao K, Cao L, Du J, Shi X, Guo Z, Zhang Y. 2013. CHIR99021 promotes self-renewal of mouse embryonic stem cells by modulation of protein-encoding gene and long intergenic non-coding RNA expression. Exp Cell Res 319:2684–2699.

50. Denham M, Bye C, Leung J, Conley BJ, Thompson LH, Dottori M. 2012. Glycogen synthase kinase 3β and activin/nodal inhibition in human embryonic stem cells induces a pre-neuroepithelial state that is required for specification to a floor plate cell lineage. Stem Cells 30:2400–2411.

51. Tahamtani Y, Azarnia M, Farrokhi A, Sharifi-Zarchi A, Aghdami N, Baharvand H. 2013. Treatment of Human Embryonic Stem Cells with Different Combinations of Priming and Inducing Factors Toward Definitive Endoderm. Stem Cells Dev 22:1419–32.

52. Lian X, Zhang J, Zhu K, Kamp TJ, Palecek SP. 2013. Insulin inhibits cardiac mesoderm, not mesendoderm, formation during cardiac differentiation of human pluripotent stem cells and modulation of canonical Wnt signaling can rescue this inhibition. Stem Cells 31:447–57.

53. Ueno S, Weidinger G, Osugi T, Kohn AD, Golob JL, Pabon L, Reinecke H, Moon RT, Murry CE. 2007. Biphasic role for Wnt/beta-catenin signaling in cardiac specification in zebrafish and embryonic stem cells. Proc Natl Acad Sci 104:9685–9690.

54. Pick M, Azzola L, Mossman A, Stanley EG, Elefanty AG. 2007. Differentiation of Human Embryonic Stem Cells in Serum-Free Medium Reveals Distinct Roles for Bone Morphogenetic Protein 4, Vascular Endothelial Growth Factor, Stem Cell Factor, and Fibroblast Growth Factor 2 in Hematopoiesis. Stem Cells 25:2206–2214.

55. Rufaihah AJ, Huang NF, Jamé S, Lee JC, Nguyen HN, Byers B, De A, Okogbaa J, Rollins M, Reijo-Pera R, Gambhir SS, Cooke JP. 2011. Endothelial cells derived from human iPSCS increase capillary density and improve perfusion in a mouse model of peripheral arterial disease. Arterioscler Thromb Vasc Biol 31:e72-9.

56. Nitzan E, Kalcheim C. 2013. Neural crest and somitic mesoderm as paradigms to investigate cell fate decisions during development. Dev Growth Differ 55:60–78.

57. Rios AC, Serralbo O, Salgado D, Marcelle C. 2011. Neural crest regulates myogenesis through the transient activation of NOTCH. Nature 473:532–535.

58. Xu C, Tabebordbar M, Iovino S, Ciarlo C, Liu J, Castiglioni A, Price E, Liu M, Barton ER, Kahn CR, Wagers AJ, Zon LI. 2013. A zebrafish embryo culture system defines factors that promote vertebrate myogenesis across species. Cell 155:909–921.

59. Borchin B, Chen J, Barberi T. 2013. Derivation and FACS-mediated purification of PAX3+/PAX7+ skeletal muscle precursors from human pluripotent stem cells. Stem Cell Reports 1:620–631.

60. Hosoyama T, McGivern J V, Van Dyke JM, Ebert AD, Suzuki M. 2014. Derivation of myogenic progenitors directly from human pluripotent stem cells using a sphere-based culture. Stem Cells Transl Med 3:564–74.

61. Wong J, Mehta V, Voronova A, Coutu J, Ryan T, Shelton M, Skerjanc IS. 2013. B-catenin Is Essential for Efficient In Vitro Premyogenic Mesoderm Formation but Can Be Partially Compensated by Retinoic Acid Signalling. PLoS One 8.

62. Chang WY, Lavoie JR, Kwon SY, Chen Z, Manias JL, Behbahani J, Ling V, Kandel RA, Stewart DJ, Stanford WL. 2013. Feeder-independent derivation of induced-pluripotent stem cells from peripheral blood endothelial progenitor cells. Stem Cell Res 10:195–202.

63. Thomson JA, Itskovitz-Eldor J, Shapiro SS, Waknitz MA, Swiergiel JJ, Marshall VS, Jones JM. 1998. Embryonic stem cell lines derived from human blastocysts. Science 282:1145–7.

64. Wang X. 2003. A PCR primer bank for quantitative gene expression analysis. Nucleic Acids Res 31:154e–154.

65. Altschul SF, Gish W, Miller W, Myers EW, Lipman DJ. 1990. Basic local alignment search tool. J Mol Biol 215:403–10.

66. Livak KJ, Schmittgen TD. 2001. Analysis of Relative Gene Expression Data Using Real-Time Quantitative PCR and the 2−ΔΔCT Method. Methods 25:402–408.

Chapter 3: Characterizing *in vitro* skeletal myogenesis of human embryonic stem cells through mRNA microarray gene expression profiling

3.1 Objective of this study

It remains unclear how closely *in vitro* skeletal myogenesis recapitulates *in vivo* muscle development. Furthermore, the type of myoblasts being generated *in vitro*—be they progenitors of early myotomal, embryonic myotubes, or fetal myotubes—would have implications for the cultures' therapeutic potential. Comprehensive gene expression profiling would help elucidate signature genes of skeletal muscle progenitors and *in vitro* myogenesis.

3.2 Statement of author contributions

M. S., I. S. S., and A. B. were responsible for experimental design. M. S. carried out the experiments and wrote the manuscript with I. S. S. and A. B. providing supervision. D. O. assisted with the microarray, from cRNA preparation through to scanning the arrays for analysis. A. B. demonstrated and instructed on the bioinformatics tools used to analyze the microarray data. J. L. cultured pluripotent hESCs.

3.3 Gene expression profiling of CHIR99021-induced skeletal myogenesis in human embryonic stem cells reveals a quiescent satellite cell-like profile for myogenic cultures

Michael Shelton[1], Jun Liu[1], Daniel O'Neil[1], Ilona S. Skerjanc[1*], Alexandre Blais[1]

[1]Department of Biochemistry, Microbiology, and Immunology, University of Ottawa, Ottawa, Ontario, K1H 8M5, Canada

*Corresponding author Dr. Ilona S. Skerjanc: iskerjan@uottawa.ca, Tel: 613-562-5800 Ext. 8669; Fax: 613-562-5452.

3.4 Summary

Embryonic-derived skeletal muscle progenitors (SMP) remain poorly characterized relative to their adult satellite cell counterparts. Here, gene expression profiling is reported in human embryonic stem cells (hESC) over a 50 day skeletal myogenesis protocol (1, 2). mRNA microarray analysis was performed to better characterize the developmental stages of the protocol, and the day 50 cultures were also compared to microarrays of other hESC-derived skeletal muscle and adult satellite cells. Expression profiling of the 50 day time course showed the majority of upregulated genes clustered into 5 groups, whereby genes involved in paraxial mesoderm induction, somitogenesis, and skeletal muscle commitment were temporally expressed in a successive fashion. Comparison to satellite cells revealed that day 50 cultures correlate closer with quiescent satellite cells, which have shown greater utility in stem cell therapy, rather than activated satellite cells. AP1-, CEBP-, and SOX-family transcription factors binding sites are significantly enriched in gene sets shared between day 50 cultures and quiescent satellite cells, building support for CEBPA/B, FOS/JUN, and SOX5/6 as key regulators in maintaining the quiescent program. Comparison with other hESC-derived skeletal muscle showed both cultures expressed genes of the sarcomere and surface proteins previously shown to mark embryonic SMPs: CXCR4, ERBB3, PDGFRA, and VCAM1. Genes CD82, ICAM1, and NGFR, however, were uniquely expressed in day 50 cultures. This study also identified ADGRA2, ADGRD1, and ADGRG6 as potential novel SMP surface markers. Overall, the gene expression profiling serves as a resource to better study the progression of *in vitro* skeletal myogenesis, and could be mined to identify novel markers of embryonic SMPs. These results also indicated that 50-day hESC-derived SMPs appear similar to therapeutically-relevant quiescent satellite cells. Future transplantation studies should proceed to address the SMPs' *in vivo* potential.

3.5 Introduction

Recent years have seen a rise in the number of studies that direct the differentiation of impressive quantities of skeletal muscle cells from human embryonic stem cells (hESC) or human induced pluripotent stem cells (hiPSC)(1–9). Previously, a directed differentiation protocol was developed capable of leading approximately 90% of cells into the skeletal muscle lineage after 50 days in culture: 43 ± 4% of cells were $PAX7^+$ skeletal muscle progenitors (SMP), surrounded by myosin heavy chain (MYH) expressing myocytes and small myotubes that comprised another 47 ± 3% of the population (Chapter 2)(1, 2).

Whereas the previous study was limited to only PAX7 and MYH immunofluorescence, and qPCR for select genes to characterize the cultures, a genome-wide analysis could be used to gain a more comprehensive understanding of how skeletal myogenesis is progressing *in vitro*. Gene expression profiling can also ascertain what characteristics 50 day $PAX7^+$ SMPs possess, be they more quiescent or activated satellite cell-like, or perhaps show that the cultures are unlike either but are more representative of an earlier $PAX7^+/PAX3^+$ dermomyotome population.

PAX7 and its paralog PAX3 are of particular interest in regards to stem cell therapy since mature fetal and adult muscle stem cells are characterized by the expression of PAX7—as well as PAX3 in some muscles or during regeneration (10, 11)—and also by the "satellite" position in which they reside adjacent to muscle fibers (12–14). Absent of muscle injury, satellite cells exist in a quiescent state expressing PAX7 and may also express one of the myogenic regulatory factors (MRF): MYF5. It is thought that $PAX7^+/MYF5^-$ quiescent satellite cells are the true adult SMP that can generate both $PAX7^+/MYF5^-$ and $PAX7^+/MYF5^+$ progeny through asymmetric cell division (15, 16). $PAX7^+/MYF5^+$ quiescent cells are capable of proliferating upon activation in response to muscle injury and

contributing to muscle repair, however, only $PAX7^{+}/MYF5^{-}$ quiescent cells are also capable of self-replenishing the satellite cell progenitor pool.

Though satellite cells can express PAX7 and PAX3, only PAX7 can maintain the satellite cell progenitor pool in adult muscle, as $PAX7^{-/-}$ mice show enhanced apoptosis and eventual loss of satellite cells regardless of PAX3 expression (17–19). Both PAX7 and PAX3 are capable of maintaining pre-natal satellite cells, however, and respectively mark the earlier secondary and primary myogenic progenitor populations (18, 20). Expression of both genes is detected in the developing somite, with PAX7 becoming more prominent in the central dermomyotomal region, and PAX3 segregating towards the dorsomedial and ventrolateral lips of the dermomyotome (18). $PAX7^{+}$ and $PAX3^{+}$ cells are capable of seeding trunk skeletal muscle, while only $PAX3^{+}$ cells can upregulate migratory genes LBX1 and MET, causing the cells to delaminate from the dermomyotome and migrate into the nascent limb buds (21–23). Transgenic expression of PAX7 driven by the PAX3 promoter is not capable of rescuing the absent limb muscle in $PAX3^{-/-}$ mice.

Therefore, although PAX7 plays an arguably greater role in satellite cell maintenance, investigating PAX3 and similarly expressed genes would be important in the context of understanding earlier SMP populations during *in vitro* embryonic myogenesis.

Knowledge gained from gene expression profiling can also help identify potential unwanted lineages during and at the end of the 50 day time course. It may also identify important signaling pathway activity that can be further manipulated with small molecules to hasten the differentiation, or to alter the final balance between $PAX7^{+}$ SMPs, MYH^{+} myocytes, and multinucleated myotubes. Targeting signaling pathways with small molecules can also help limit the expansion of unwanted lineages.

3.6 Results and Discussion

3.6.1 Expression pattern similarity identifies co-regulated developmental gene sets important for in vitro *mesoderm induction and skeletal myogenesis*

Gene expression profiling was used at various time points of the *in vitro* skeletal myogenesis protocol in order to characterize the cells' development in greater detail (1). Briefly, the differentiation of pluripotent hESCs was initiated by culturing cells in E6 media supplemented with 7.5 or 10 μM CHIR99021 for 2 days. Cells were then cultured in E6 without CHIR99021 until day 12, at which point media was changed to StemPro-34 supplemented with 5 ng/mL FGF2 until day 20. Cells were returned to E6 media from days 20 to 35, and then cultured in N2-ITS media from days 35 to 50.

Genes sharing a similar expression profile across the 50 day time course were CLICK clustered in Expander 7.0 (24), resulting in 6 groups of genes that showed increasing expression as differentiation proceeded (Fig. 3.1A), and 6 groups that showed decreasing expression (Fig. 3.1B). A full list of gene identities within each cluster can be found online (Table A3.3). ToppFun function enrichment analysis was used to identify significantly enriched Gene Ontology (GO) categories within each cluster (25), and also to identify significantly enriched Progenitor Cell Biology Consortium (PCBC) Co-expression Atlas datasets for select clusters (26). GO categories revealed that clusters 1 through 4 show a progression through mesoderm and paraxial mesoderm genes, to somitic and supportive developmental genes, to myogenic commitment and structural constituents of contractile muscle (Table 3.1).

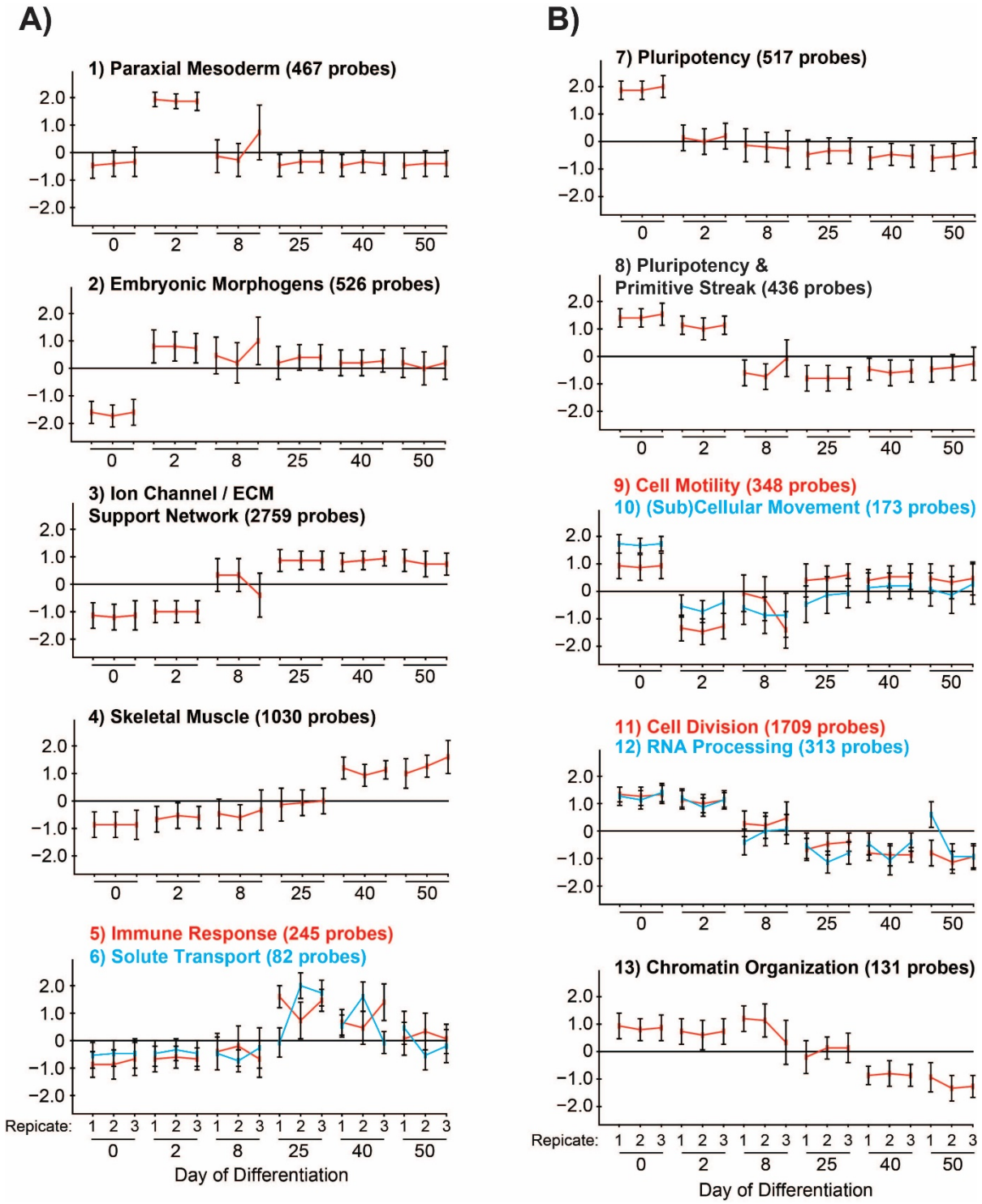
A)
1) Paraxial Mesoderm (467 probes)
2) Embryonic Morphogens (526 probes)
3) Ion Channel / ECM
Support Network (2759 probes)
4) Skeletal Muscle (1030 probes)
5) Immune Response (245 probes)
6) Solute Transport (82 probes)
Repicate:
Day of Differentiation
B)
7) Pluripotency (517 probes)
8) Pluripotency &
Primitive Streak (436 probes)
9) Cell Motility (348 probes)
10) (Sub)Cellular Movement (173 probes)
11) Cell Division (1709 probes)
12) RNA Processing (313 probes)
13) Chromatin Organization (131 probes)
Repicate:
Day of Differentiation

Figure 3.1

Figure 3.1. CLICK clustering of differentially expressed genes during in vitro skeletal myogenesis. Pluripotent H9 hESCs were differentiated for 50 days as previously described (1). mRNA samples from the indicated time points were applied to the Agilent 8x66 K-Human Genome Microarray for gene expression profiling. Microarray probe reads were $\log_2()$ transformed and quantile-normalized for analysis. Probes were filtered to exclude those with less than $\log_2() = 5$ absolute expression, and to exclude probes with less than 4-fold expression difference relative to day 0 control at any time point (n = 3). Expander 7.0 CLICK Clustering method was used—given a homogeneity value of 0.85—generating 13 clusters of similarly expressed probes across the differentiation time course. Similarly patterned clusters were manually grouped for further analysis, and clusters were divided into **A)** genes whose expression increased with differentiation, and **B)** genes whose expression decreased. A full list of gene identities within each cluster can be found online (Table A3.3).

Cluster #	GO:Biological Process		q-value	Gene / Family	Soleimani et al. (/294)	Lilja et al. (/1302)	TFBS (Z-score)
1	GO:0009952	Anterior/posterior specification	5.0 E-11	FGF8, MSGN1, WNT8A,	4 (1.36%)	24 (1.84%)	LEF1 (21.2)
	GO:0061053	Somite development	3.6 E-05	DLL3, FOXC1, LFNG	5.76 E-01	8.68 E-02	TCF7 (15.7)
	GO:0007498	Mesoderm Development	1.8 E-02	MIXL1, T, TBX6			POU5F1 (8.1)
2	GO:0048598	Embryonic morphogenesis	2.5 E-23	HOXs, PAX3, PDGFRA	13 (4.42%)	54 (4.15%)	HOXA5 (16.8)
	GO:0030509	BMP signaling pathway	8.6 E-06	BMP1/4/6/7, MSX1/2	5.73 E-03	1.64 E-07	LEF1 (16.1)
	GO:0016055	WNT signaling pathway	4.2 E-04	DKK1, RSPO3, WNT3A/5A/5B			T (6.6)
3	GO:0030198	ECM organization	2.1 E-23	COLs, LAMs, MMPs	81 (27.6%)	237 (18.2%)	SOX5/6 (20.1)
	GO:0061061	Muscle structure development	1.7 E-12	DMD, MEOX1/2, NCAM1	5.33 E-17	3.23 E-19	CEBPA (18.4)
	GO:0006811	Ion transport	9.2 E-03	CACNs, KCNs, SLCs			PRRX1/2 (17.3)
4	GO:0006936	Muscle contraction	9.7 E-27	CHRNs, MYH/Ls, TNNC/Ts	40 (13.6%)	68 (5.22%)	KLF4 (17.4)
	GO:0014706	Striated muscle development	7.6 E-24	MSTN, MRFs, PAX7	6.34 E-13	1.65 E-03	MEF2C/D (17.1)
	GO:0014902	Myotube differentiation	6.8 E-07	MEF2C, MYOD1, MYOG			MYF5/6 (12.5)
5+6	GO:0007155	Cell adhesion	1.2 E-04	CDH7, ITGA1/B2, PECAM1	7 (2.38%)	22 (1.69%)	ARID3A (23.3)
	GO:0006955	Immune response	2.6 E-04	C1Qs, FCGRs, IL6ST/7	9.66 E-02	1.43 E-01	PDX1 (21.5)
	GO:0006811	Ion transport	6.1 E-02	CCLs, CYBB, SLCs			ELF5 (5.1)

Table 3.1

Table 3.1. Gene Ontology characterization of upregulated gene clusters shows progressive development through the expected stages of skeletal myogenesis. The gene clusters generated in Figure 3.1A were passed through ToppFun functional enrichment analysis ($p < 0.05$, FDR < 0.05). Representative categories of GO:Biological Process were selected for each cluster, as well as representative genes or gene families within each GO category. Genes from each cluster were compared against a list of genes known to be differentially expressed in murine myoblasts with Pax3- or Pax7-over expression (27), and genes whose promoters are directly bound by Pax7 (28). The percentage of either lists' genes that were represented within each cluster was determined, and the hypergeometric probability of each result was calculated ($p(X) \geq n$). Clusters 2 – 4 were notably enriched for a significant number of Pax7 regulated genes. Gene clusters were also analyzed with oPOSSUM 3.0 to identify significantly enriched transcription factor binding sites (TFBS). Representative enriched motifs are listed for each cluster group; motifs whose parent transcription factor is contained within the same cluster are highlighted red.

Cluster 1 represented the transient expression of genes involved in paraxial mesoderm induction that peak at day 2 of differentiation. Examples of expected mesoderm genes in this cluster included T, TBX6, and MSGN1 (29–31), but also spermatogenesis-associated genes DAZ1, MAK, MEIG1, and SPAG11B which were not expected to follow this kinetic. The onset of NOTCH-related segmentation genes DLL3, HES7, and LFNG by day 2 of differentiation was consistent with other *in vitro* myogenesis protocols, wherein somite-related gene expression can be detected starting from 1.75 – 2.25 days (9, 32). oPOSSUM 3.0 analysis revealed a number of significantly enriched TFBSs within the genes of cluster 1, including sites for the downstream effectors of CHIR99021 and WNT signaling, LEF and TCF. The POU5F1 (OCT4) motif was also significantly enriched; while POU5F1 is an important factor for maintaining pluripotency, persistent POU5F1 protein levels are also required for proper T and mesoderm induction *in vitro* and *in vivo* (33–35).

Clusters 2 and 3 contained transcription factors and markers that may denote the differentiation of paraxial mesoderm into muscle progenitors and myoblasts, including PAX3, MEF2A, MET, and DMD (16, 36). Also seen were biological processes expected to support differentiation into contractile skeletal muscle, including extracellular matrix (ECM) collagen and laminin proteins, and numerous voltage-gated calcium and potassium channels. Of note, genes in cluster 2 peak in the early stages of the differentiation protocol but do not fall back down to baseline day 0 levels, suggesting a continued but reduced role for BMP and WNT signaling, and for PAX3 during *in vitro* embryonic myogenesis.

Cluster 4 represented genes involved in the terminal differentiation of skeletal muscle, including the myogenic regulatory transcription factors (MRF) MYF5, MYOD1, MYOG and MYF6. This cluster also contained genes of the contractile apparatus: myosin light and heavy chains, troponins, Z-disc proteins, sarcoglycans, and acetylcholine receptors

(37). Even though PAX7 is considered a marker of muscle progenitors rather than terminally differentiated muscle, its expression profile was difficult to dissect from the MRFs, likely due to the lack of resolution between the days 8 and 25 used in this study. Other studies of *in vitro* hESC myogenesis distinguish notable MYOG upregulation approximately 2 days after PAX7 (8).

Other PAX3- and PAX7-reporter studies show PAX3-reporter expression is far more robust than PAX7 at E10.5 in the embryonic somites (18). This robust somitic PAX3-reporter expression recedes by E13.5, leaving only relatively fainter expression in the trunk and limb muscle. Conversely, the PAX7-reporter does not exhibit the same degree of fluctuation in somitic expression, and only notably increases from E10.5 to E13.5 as trunk, limb, and facial muscles develop. Thus, *in vivo* PAX3- and PAX7-reporter expression patterns matched the patterns of PAX3 and PAX7 probes in the 50-day *in vitro* differentiation time course; this helps explain why CLICK clustering segregated the PAX genes into different groups.

In order to determine whether PAX3 or PAX7 may be transcriptionally active—especially in clusters 3 or 4—enrichment of the PAX3 and PAX7 TFBS was assessed in the genes of each cluster. Unfortunately, oPOSSUM 3.0 lacks data for PAX3 and PAX7 binding sites. Thus, lists of genes were used that contain experimentally determined indirect PAX3 or PAX7 targets from murine myoblasts over-expressing either transcription factor for 2 days (27), and direct PAX7 targets in murine ES-derived muscle progenitors after 3 days of induced PAX7 expression (28). Mouse specific genes with no human counterpart were excluded from each list. The greatest portion of experimentally determined PAX3 and PAX7 target genes fell under the PAX3-containing cluster 3, with 24.6% and 15.3% of the Soleimani *et al*. and Lilja *et al*. lists being represented, respectively.

Cluster 5 + 6 was a small and transient group—enriched with GO categories related to the immune system—that only appear elevated beginning at the day 25 time point before gradually falling. This may have been in response to the StemPro-34 media or supplement, which are formulated with glucocorticoids to support the culture and differentiation of hematopoietic or immune-system cells (38)

The cluster groups that showed a downward trend over time were enriched for genes and GO categories expected to drop as pluripotent cells differentiate (Table 3.2). For example, Clusters 11 – 13 appeared to represent cell cycling, DNA replication, and chromatin organization. The expected drop in expression for genes related to cell proliferation correlated with previous findings, wherein cell numbers taper off logarithmically over the 50 day differentiation, reaching half-maximal cell numbers as early as day 6 (1). Clusters 7 and 8 did not have any statistically significantly enriched GO categories, however, these genes correlated with the PCBC Coexpression Atlas dataset wherein mesoderm was induced from human embryonic stem cells; indeed, the pluripotency factors NANOG and SOX2 belong to clusters 7 ("Rapid down-regulation" cluster), and POU5F1 belonged to cluster 8 ("Delayed down-regulation" cluster). Cluster 9 + 10 was significantly enriched for numerous GO categories related to motility and cell-cell contacts.

A drop in cell-cell contact-related genes could be expected immediately following CHIR99021 treatment, as CHIR99021-treated day 2 cells appear morphologically more segregated than tightly packed pluripotent colonies (Fig. 3.2A)(1, 2). This onset of differentiation should, however, correlate with an increase in genes related to mobility, as CHIR99021 and WNT signaling are expected to cause epithelial to mesenchymal transition (EMT) in ESCs adopting a primitive streak-like fate *in vitro* (39). This discrepancy might be explained by the high levels of CHIR99021 used in the present study: it was observed that

Cluster #	GO:Biological Process		q-value	Gene / Family	Soleimani et al. (/294)	Lilja et al. (/1302)
7	No significant categories					
	Ratio Stem Cell vs. Induced-Mesoderm: Top 500 Ranked by Relative-expression PCBC_ratio_SC_vs_MESO-5_500		8.9 E-32	FGF2, NANOG, SOX2	6 (2.04%) 3.56 E-02	21 (1.61%) 5.73 E-01
8	No significant categories					
	Ratio Stem Cell vs. Induced-Mesoderm: Top 500 Ranked by Relative-expression PCBC_ratio_SC_vs_MESO-5_500		7.2 E-08	ENHO, FGF19, POU5F1	4 (1.36%) 6.66 E-01	13 (1.00%) 9.67 E-01
9+10	GO:0006928	Cell / subcellular movement	2.2 E-06	KIFs, LMNA, PODXL/2	19 (6.46%)	54 (4.15%)
	GO:0048729	Tissue morphogenesis	1.9 E-05	GLI2, KDR, PDGFA/B	8.55 E-06	3.15 E-07
	GO:0048870	Cell Motility	2.1 E-04	ARC, EPCAM, MMPs		
11+12	GO:0007049	Cell cycle	4.9 E-40	CDCs, CDKs, KIFs	11 (3.74%)	70 (5.36%)
	GO:0006260	DNA replication	5.9 E-25	BRAC1/2, MCMs, PRIM1/2	9.93 E-01	9.93 E-01
	GO:0006396	RNA processing	9.6 E-15	PRMTs, RRPs, SRSFs		
13	GO:0050000	Chromosome localization	4.4 E-07	CENPs, CEP55, KIFs	0 (0%)	5 (0.38%)
	GO:0051276	Chromosome organization	3.1 E-06	NUF2, PRMT6, REC8	0	7.52 E-01
	GO:0071103	DNA conformation change	4.1 E-02	ERN2, HIST1Hs, HIST2Hs		

Table 3.2

Table 3.2. Gene Ontology characterization of downregulated gene clusters shows progressive drop of pluripotency and cell cycling genes expected throughout differentiation. The gene clusters generated in Figure 3.1B were passed through ToppFun functional enrichment analysis ($p < 0.05$, FDR < 0.05). Representative categories of GO:Biological Process were selected for each cluster, as well as representative genes or gene families within each GO category. Where clusters 7 and 8 contained little or no significant GO categories, these clusters were significantly enriched for genes more highly expressed in pluripotent stem cells relative to induced mesoderm, according to the Progenitor Cell Biology Consortium (PCBC) expression atlas. Genes from each cluster were compared against a list of genes known to be differentially expressed in murine myoblasts with Pax3- or Pax7-over expression (27), and genes whose promoters are directly bound by Pax7 (28). The percentage of either lists' genes that were represented within each cluster was determined, and the hypergeometric probability of each result was calculated ($p(X) \geq n$). Cluster 9 + 10 was notably enriched for a significant number of Pax7 regulated genes.

higher CHIR99021 levels—while trending towards higher expression of mesoderm and paraxial mesoderm genes T, MSGN1 and TBX6 compared to lower CHIR99021 (Fig. 3.2D)(1)—also caused more visible cell stress compared to low CHIR99021 or DMSO control, as evidenced by bright irregular cell shape (Fig. 3.2A). High CHIR999021-treated cultures also contained fewer cell numbers overall (Fig. 3.2A & B). This stress could be the reason that an unexpected drop in cell mobility genes was observed, and raises interesting questions as to how high CHIR99021-induced mesoderm may develop differently than low CHIR99021 mesoderm induction.

3.6.2 CHIR99021 concentration-dependent differences in expression of T/MSGN1 and NODAL/TGFB signaling genes

Application of 3 μM or lower CHIR99021 to human pluripotent stem cells is one the more prevalent methods to induce mesoderm (32, 39–45), especially for downstream skeletal myogenesis (4, 6–8). However, the Shelton *et al*. study showed that higher levels of CHIR99021 led to greater expression of mesoderm and paraxial mesoderm genes T and MSGN1, respectively, and that only high levels of CHIR99021 induced PAX3 expression and $PAX3^+$ cells by day 8 of differentiation (1). Therefore, both high and low CHIR99021-induced day 2 mesoderm were compared with gene expression analysis to determine what differences existed between the two approaches, and how that might explain the more efficient paraxial mesoderm induction with high CHIR99021.

Confirming previous results, high (7.5 μM) CHIR99021 treatment led to more prominent T staining (Fig. 3.2A), and cell numbers remained relatively stagnant between days 0 to 2 in high CHIR99021-treated cultures relative to low (3 μM) CHIR99021 and DMSO control (Fig. 3.2B). Studies have shown that PI3K inhibition can improve mesoderm

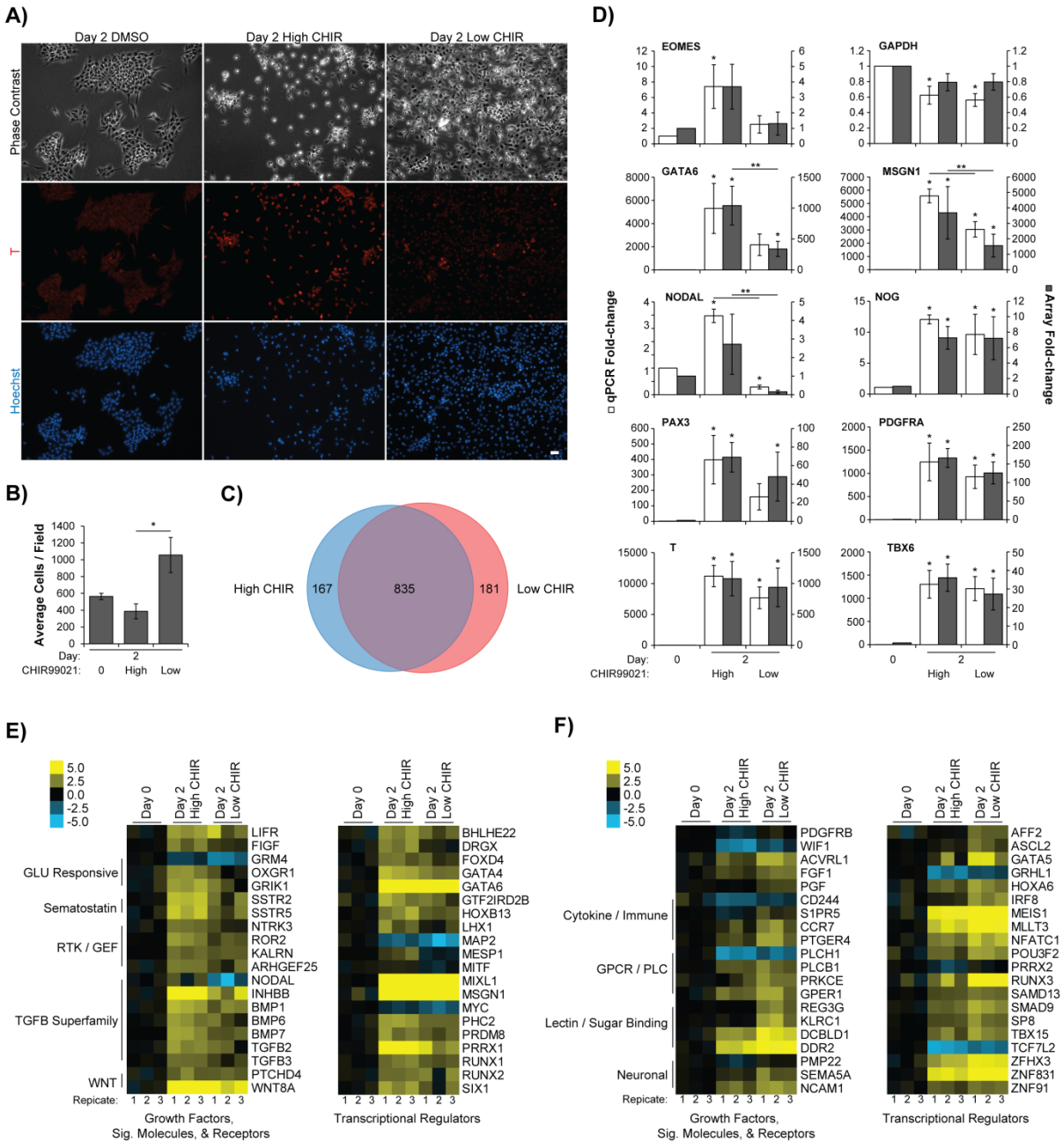
A)
Day 2 DMSO
Day 2 High CHIR
Day 2 Low CHIR
Phase Contrast
T
Hoechst
B)
Average Cells / Field
Day:
CHIR99021:
0
High
Low
C)
High CHIR
167
835
181
Low CHIR
D)
EOMES
GAPDH
GATA6
MSGN1
NODAL
NOG
PAX3
PDGFRA
T
TBX6
qPCR Fold-change
Array Fold-change
E)
Day 0
Day 2 High CHIR
Day 2 Low CHIR
GLU Responsive
Sematostatin
RTK / GEF
TGFB Superfamily
WNT
LIFR
FIGF
GRM4
OXGR1
GRIK1
SSTR2
SSTR5
NTRK3
ROR2
KALRN
ARHGEF25
NODAL
INHBB
BMP1
BMP6
BMP7
TGFB2
TGFB3
PTCHD4
WNT8A
Repicate:
Growth Factors, Sig. Molecules, & Receptors
BHLHE22
DRGX
FOXD4
GATA4
GATA6
GTF2IRD2B
HOXB13
LHX1
MAP2
MESP1
MITF
MIXL1
MSGN1
MYC
PHC2
PRDM8
PRRX1
RUNX1
RUNX2
SIX1
Transcriptional Regulators
F)
Cytokine / Immune
GPCR / PLC
Lectin / Sugar Binding
Neuronal
PDGFRB
WIF1
ACVRL1
FGF1
PGF
CD244
S1PR5
CCR7
PTGER4
PLCH1
PLCB1
PRKCE
GPER1
REG3G
KLRC1
DCBLD1
DDR2
PMP22
SEMA5A
NCAM1
AFF2
ASCL2
GATA5
GRHL1
HOXA6
IRF8
MEIS1
MLLT3
NFATC1
POU3F2
PRRX2
RUNX3
SAMD13
SMAD9
SP8
TBX15
TCF7L2
ZFHX3
ZNF831
ZNF91

Figure 3.2

Figure 3.2. Differentiating hESCs with the highest tolerable CHIR99021 concentration induces significantly more paraxial mesoderm gene expression than a lower 3 μM concentration. Pluripotent H9 hESCs were differentiated with either 7.5 μM (High) or 3 μM (Low) CHIR99021 for 2 days, and with DMSO as a vehicle control. **A)** At day 2, cells were fixed and stained with antibodies against T (Red) and Hoechst dye (Blue) to visualize cell nuclei (Scale bar = 20 μm). **B)** Volocity 6.0 software was used to count the average number of cells from 10 randomly chosen fields. High CHIR99021-treated cultures contained significantly fewer cells than low CHIR99021-treated according to one-way ANOVA with post-hoc Tukey test ($n = 3$, $p < 0.05$). **C)** Day 2 mRNA samples from high and low CHIR99021 treated cultures were applied to the Agilent 8x66 K-Human Genome Microarray for gene expression profiling, with day 0 as a control. Microarray probe reads were $\log_2()$ transformed and quantile-normalized for analysis. Probes were filtered to exclude those with less than $\log_2() = 5$ absolute expression, and to exclude probes with less than 4-fold expression difference relative to day 0 control. Expander 7.0 t-test identified 835 probes that were significantly upregulated at day 2 in both the high and low CHIR99021 conditions, relative to day 0 ($n = 3$, $p < 0.05$, FDR < 0.05). High and low CHIR99021 conditions showed 167 and 181 uniquely expressed probes, respectfully. **D)** Select genes identified in (C) were validated by qPCR. The qPCR results were expressed as a fold-change relative to day 0 on the primary Y-axis, and the microarray results on the secondary Y-axis. Several genes—including MSGN1 and NODAL—were significantly more expressed in high CHIR99021-treated cultures according to Expander 7.0 t-test of the microarray, and one-way ANOVA with post-hoc Tukey test of the qPCR ($n = 3$, $p < 0.05$). Expander 7.0 t-test was used also used to identify probes that showed significantly differential expression between high and low CHIR99021 conditions ($n = 3$, $p < 0.05$). The resulting genes—along with the 167 & 181 uniquely expressed probes from (C)—were classified using PANTHER to identify growth factors, signaling molecules, receptors, and transcriptional regulators. Heat maps were generated in TreeView 3.0 for the top 20 differentially expressed genes with **E)** high CHIR99021-treatment, and **F)** low CHIR99021-treatment. Individual replicates are shown for each condition. Replicate expression values were standardized to the average of the day 0 triplicates.

induction (9, 32, 43, 46). Given that the PI3K/AKT1/MTORC1 pathway plays a pivotal role in regulating cell proliferation, it may be that the proliferation-suppressing effect of high CHIR99021 treatment occurs through endogenous suppression of the PI3K pathway during the first 2 days of differentiation, therefore contributing to a more efficient mesoderm induction. Furthermore, beginning differentiation with relatively higher hESC densities correlates with more neuronal differentiation (47).

mRNA samples from high and low CHIR99021-treated day 2 cultures were applied to the Agilent 8x66 K-Human Genome Microarray to elucidate an underlying mechanism that might explain the differing effectiveness between both approaches. There were 835 probes significantly elevated in both approaches by at least 4-fold relative to day 0 control, with 167 and 181 probes uniquely elevated in high or low CHIR99021 treatment, respectively (Fig. 3.2C). As expected, significantly enriched GO categories shared by both protocols included paraxial mesoderm formation (GO:0048341, q = 3.31 E-02) and somitogenesis (GO:0001756, q = 1.72 E-13). Genes significantly elevated in high CHIR99021 only cells were enriched for TGFB receptor binding (GO:0005160)(Table 3.3), while genes elevated with only low CHIR99021 showed significant enrichment for the category “neuron differentiation” (GO:0030182)(Table 3.4).

A direct comparison of high and low CHIR99021-treated day 2 cultures showed the paraxial mesoderm marker MSGN1 was expressed at significantly higher levels in high CHIR99021-treated cells; qPCR for MSGN1 validated these findings (Fig. 3.2D). Others have shown that hESCs differentiated with 7.5 μM CHIR99021 for 2 days leads to notably higher expression of mesoderm markers T and PDGFRA when compared to 3 μM (44). In their study, only 3 μM CHIR99021 treaded hESCs showed expression of endoderm markers FOXA2 and SOX17. Therefore, low concentrations of CHIR99021 may be

GO Category	q-value (E-02)	Genes in Query (/139)	Example Genes
TGFB-receptor binding	0.88	5	BMP6, BMP7, GDNF, TGFB2, TGFB3
Epithelial cell differentiation	0.80	16	ABCB1, BMP6, BMP7, CES1, DMBT1, FSHR, GDNF, HOXB13, HPS1, LHX1, NKX6-1, NTRK3, OCA2, SIX1, TGFB2, WNT4
Embryonic skeletal system morphogenesis	0.97	7	BMP7, HYAL1, LHX1, RUNX2, SIX1, TGFB2, TGFB3
Cellular response to endogenous stimulus	2.08	22	BMP6, BMP7, FSHR, GDNF, IGFBP5, LHX1, NKX6-1, RUNX1, RUNX2, SSTR2, SSTR5, TGFB2, TGFB3, WNT4
Response to endogenous stimulus	3.37	26	ATP2A1, BMP6, BMP7, FSHR, GDNF, HOXB13, IGFBP5, KALRN, LHX1, NKX6-1, NTRK3, RUNX1, RUNX2, SSTR2, SSTR5, TGFB2, TGFB3, WNT4
Embryonic cranial skeleton morphogenesis	4.26	5	LHX1, RUNX2, SIX1, TGFB2, TGFB3

Table 3.3

Table 3.3. TGFB signaling Gene Ontology categories are significantly enriched among genes uniquely expressed is high CHIR99021 conditions. Probes from Figure 3.2C were passed through ToppFun functional enrichment analysis ($p < 0.05$, FDR < 0.05). A complete list of significant GO:Molecular Function and GO:Biological Process categories and select representative genes were tabulated.

GO Category	q-value (E-02)	Genes in Query (/158)	Example Genes
Neuron differentiation	2.10	26	CDH4, COL25A1, DGKG, EPB41L3, FZD1, ISPD, NIN, NRXN3, POU3F2, PTCH1, RAPH1, RNF165, RUNX3, SARM1, SATB2, SLITRK5, TCF4
Positive regulation of developmental process	2.46	25	ACVRL1, CCR7, CDH4, FGF1, GPER1, NIN, NRXN3, PLCB1, POU3F2, PTCH1, PTGER4, RAG1, SLITRK5, SMAD9, TCF4, TMEM119
Generation of neurons	3.55	27	CDH4, COL25A1, DGKG, EPB41L3, FZD1, GPER1, ISPD, NIN, NRXN3, POU3F2, PTCH1, RAPH1, RNF165, RUNX3, SARM1, SATB2, SLITRK5, TCF4
Positive regulation of lipid metabolic process	4.41	8	ACSL6, CCR7, DAB2, FGF1, IRS1, PPARA, PRKCE, SIRT4

Table 3.4

Table 3.4. Neuronal differentiation Gene Ontology categories are significantly enriched among genes uniquely expressed is low CHIR99021 conditions. Probes from Figure 3.2C were passed through ToppFun functional enrichment analysis ($p < 0.05$, FDR < 0.05). A complete list of significant GO:Molecular Function and GO:Biological Process categories and select representative genes were tabulated.

permissible for mesendoderm formation in hESCs while high concentrations restrict endoderm and lead to greater proportions of mesoderm derivatives, including MSGN1-expressing paraxial mesoderm.

Other studies have shown that 5 – 10 μM CHIR99021 concentrations upregulate T expression in hESCs as early as day 1 post-treatment: an effect not observed at 2 μM CHIR99021 (48). Expression of T at day 2 in the Tan *et al*. study was also significantly higher with 5 – 10 μM CHIR99021 relative to 2 μM CHIR99021. Mendjan *et al*. show that 8 μM CHIR99021 leads to more pronounced staining of T and a somitic mesoderm marker CDX2 compared to 3 μM CHIR99021 after 1.5 days of hESC differentiation (49).

High levels of TGFB signaling have been shown to block ectoderm specification from pluripotent cells, and to specify anterior primitive streak-like mesoderm from which the paraxial mesoderm is derived (32). In contrast, having low to moderate levels of TGFB signaling favors the specification of more posterior primitive streak-like mesoderm, which can develop into undesirable lateral plate mesoderm. The reduced expression of TGFB signaling genes with low compared to high CHIR99021-treament could therefore result in lower repression of ectoderm or neuron formation, and less desirable mesoderm specification. PAX2/PAX6 and SOX1/SOX9 are often used to detect early ectoderm formation with *in vitro* hESC differentiation, however, their expression is typically detected after 3 days of differentiation (9, 43). Of these genes, only PAX2 was upregulated at day 2 in the present study, with its expression being 1.6-fold greater in low compared high CHIR99021-differentiated cultures (data not shown).

PANTHER classification was used to identify the specific signaling pathways and transcriptional regulators that might underlie these differences. The 167 and 181 significantly expressed unique probes from Figure 3.2C were organized using PANTHER, as were

differentially expressed probes from a direct comparison of high and low CHIR99021-treated cultures; this direct comparison added 67 probes significantly more expressed in high compared to low CHIR99021-treated cultures, and 88 probes *vice versa*. The growth factors, signaling molecules, receptors, and transcriptional regulators more highly expressed with high CHIR99021 were identified (Fig. 3.2E), as were the genes with higher expression in low CHIR99021 cultures (Fig. 3.2F).

One of the starkest differences between protocols appeared to be the TGFB superfamily, and specifically NODAL signaling family members. NODAL signaling, along with WNT, are essential for *in vitro* primitive streak induction (50). Studies have shown that WNT signaling itself regulates NODAL expression during embryo patterning (51, 52). The data presented in Figure 3.2 may indicate a dose-dependent mechanism, whereby high CHIR99021 better upregulated NODAL than low CHIR99021 treatment, and thus, led to a more efficient induction of primitive streak-like cell *in vitro*. Known NODAL target genes CER1 and LHX1 were also more highly expressed with high CHIR99021 (53, 54), supporting NODAL activity.

Beyond the day 2 *in vitro* induction of mesoderm in hESCs, however, high TGFB or NODAL signaling can direct this presumptive mesoderm into the endodermal lineage, and should be inhibited to encourage the development of somite-like mesoderm (9, 32). Indeed, other groups have shown that after day 2 of hESC differentiation with 3 μM CHIR99021, A8301- or SB431542-mediated inhibition of the TGFBR1 (ALK5) receptor can improve the expression of somitic gene markers FOXC2, MEOX1, and PAX3 (7, 9). LDN193189-mediated inhibition of BMP signaling—another branch of the TGFB-superfamily—can also enhance the expression of somite markers MEOX1, PAX3, and TCF15 (6, 9). However,

BMP inhibition alone appears less effective at upregulating somitic marker expression compared to either TGFB inhibition or combinatorial BMP and TGFB inhibition (6, 9, 32).

These facts notwithstanding, the 50-day differentiation protocol yields largely myogenic cultures absent of pharmacological TGFB superfamily inhibition from day 2 of differentiation. As mentioned above, other groups show high levels of WNT signaling restrict endoderm formation (44), even though WNT signaling is capable of upregulating NODAL which subsequently drives endoderm if left uninhibited (32, 43, 51, 52). Studies also suggest that WNT pathway cross-talk may regulate TGFB-superfamily inhibitor genes CER1, CHRD, and NOG (55).

CER1 functions as a NODAL and BMP repressor by directly binding to and inhibiting these proteins' activity (56), and its expression is elevated in high CHIR99021-treated cells. In fact, gene expression analysis identified CER1 as the most similarly-expressed gene to NODAL in high CHIR99021-treated cells over the entire gene expression profiling dataset. Therefore, endogenous mechanisms to inhibit NODAL and BMP may already be active in day 2 cultures that allowed for the efficient development of somite-like mesoderm from the paraxial mesoderm *in vitro*. Future experiments could support this hypothesis by deleting or knocking down CER1, then determining if somitic markers PAX3 and MEOX1 are still appreciably detected by day 8 of the protocol. Though the differential expression did not meet the statistical significance threshold, other NODAL antagonists LEFTY1 and LEFTY2 were on average 5- and 3-fold more expressed with high versus low CHIR99021 (data not shown).

It would be interesting to determine with future experiments what benefits exogenous inhibition of TGFB, NODAL, and BMP signaling from days 2 – 4 may provide to the high CHIR99021 approach. This may improve one of the most notable differences between the

50-day directed differentiation protocol and others utilizing low CHIR99021 with exogenous TGFB-superfamily inhibitors: the duration of culture. Other protocols that inhibited TGFB or BMP post-CHIR99021 tend to show MRF expression from 2 – 2.5 weeks of differentiation (6, 7, 9, 32), while the high CHIR99021 method began to show MRF expression roughly 3 – 3.5 weeks into differentiation (1). Manipulation of the TGFB superfamily immediately following CHIR99021 treatment may lead cultures to progress at a more uniform pace through the somite- and dermomyotome-like stages *in vitro*, leading to a more uniform and rapid terminal myogenesis.

3.6.3 Day 50 hESC-derived skeletal muscle cultures share more similar gene expression with quiescent than with activated satellite cells

One goal of *in vitro* skeletal myogenesis is to generate satellite cell-like SMPs that could be used in stem cell therapy, both to repair injured muscle and replenish the resident muscle stem cell population. Given the lack of three dimensional muscle fibers with hESC culture that would normally exist *in vivo*, the physical satellite cell niche cannot be used to define *in vitro* SMPs. First and foremost, hESC-derived SMPs are expected to express PAX7. In order for SMPs to meaningfully contribute to continued muscle repair after stem cell therapy, $PAX7^+$ SMPs should not yet express MYF5 or MYOD1—similar to quiescent satellite cells—as expression of the MRFs may indicate that cells have differentiated too far to self-replenish the progenitor population in patient muscle (57).

It was previously shown that 43 ± 4% of cells stain positive for PAX7 at day 50 of differentiation (1), however, cultures could not be co-stained with MYF5 or MYOD1. Therefore, gene expression profiling was used in the present study to identify the precise similarities and differences between day 50 cultures and satellite cell populations. Gene

expression profiling has the potential to reveal other key transcriptional regulators, signaling pathways, or established surface markers that can help characterize the overall profile of hESC-derived SMPs, and to determine whether they appear more similar to quiescent or to activated satellite cells.

Two additional gene expression profiling datasets were chosen for comparison: one using *in vitro* culture-activated mouse satellite cells (Fig. 3.3A)(58), and another using *in vivo* injury-activated mouse satellite cells (Fig. 3.3B)(59). Briefly, the *in vitro* activation experiment used satellite cells isolated from $Pax3^{GFP/+}$ mice, with RNA extracted immediately after sorting or following 3 days of *in vitro* culture-induced activation. The *in vivo* activation experiment extracted RNA from isolated satellite cells of $Pax7^{CreER/+}/ROSA26^{eYFP/+}$ mice, either from uninjured muscle or muscle that was injured with barium chloride 2.5 days prior to sorting.

A total of 13 874 or 14 498 genes were paired between the hESC array and the *in vitro* or *in vivo* activation experiments, respectively. The expression values of each gene from the hESC array were plotted against their counterpart from the *in vitro* activated (Fig. 3.3A) or *in vivo* activated (Fig. 3.3B) satellite cells, where a positive correlation was seen between day 50 cultures and quiescent satellite cells. For further analysis, the expression plots were divided into four quadrants based on a 4-fold cutoff. Quadrant I—genes for which expression at day 50 is higher than day 0 and also higher in quiescent satellite cells compared to activated ones—was enriched with GO categories related to muscle structure development (GO:0061061, Fig. 3.3A q = 1.05 E-25, Fig. 3.3B q = 5.49 E-03). Key genes PAX7 and PAX3 displayed similar trends but did not meet the 4-fold cutoff of quadrant I with *in vivo* activation, showing 3.5- and 3-fold higher expression in quiescent satellite cells, espectively. Given the established importance of PAX7 and PAX3 in maintaining quiescence, however,

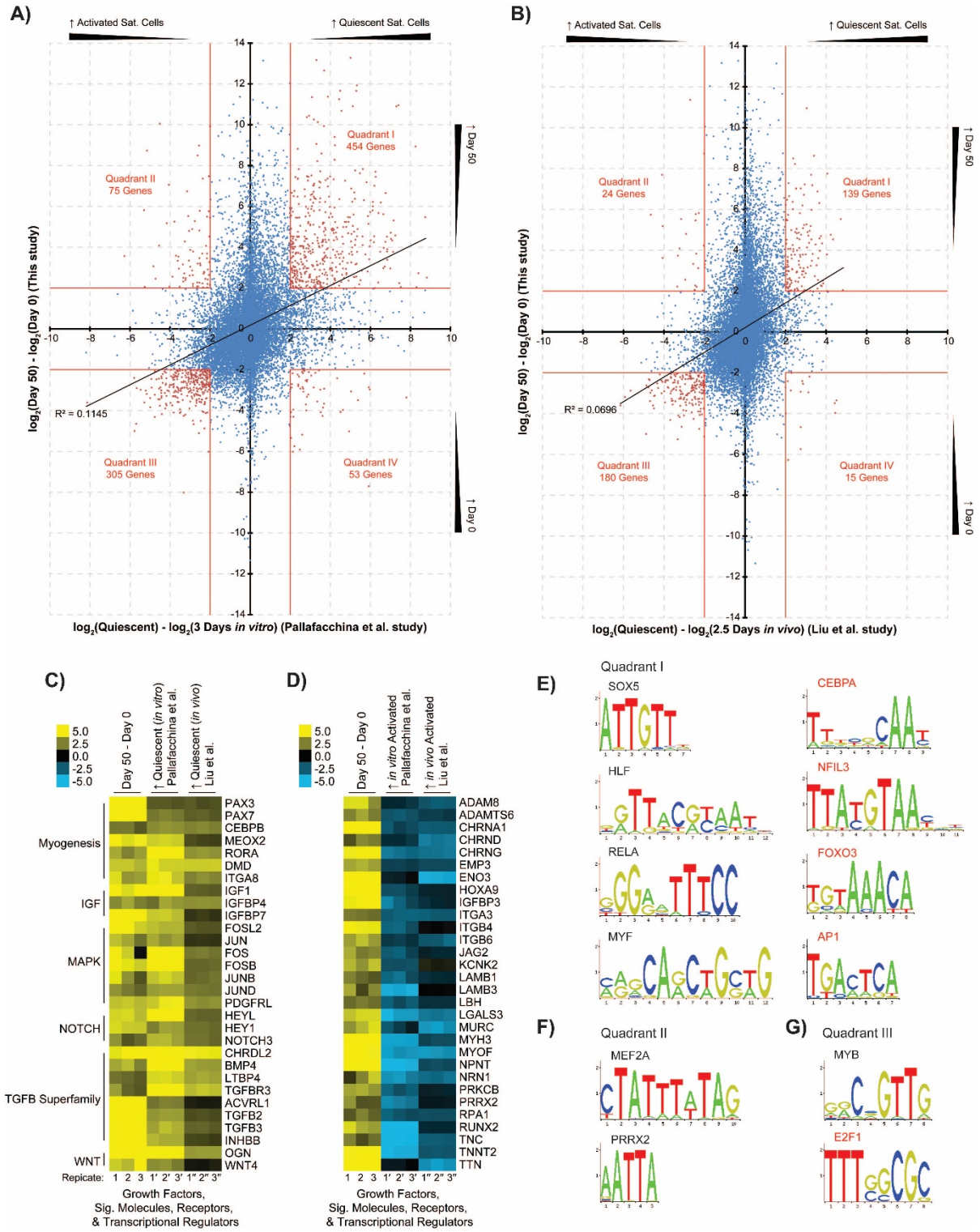
A)
↑ Activated Sat. Cells
↑ Quiescent Sat. Cells
Quadrant I
454 Genes
Quadrant II
75 Genes
Quadrant III
305 Genes
Quadrant IV
53 Genes
↑ Day 50
↑ Day 0
R² = 0.1145
log2(Day 50) - log2(Day 0) (This study)
log2(Quiescent) - log2(3 Days in vitro) (Pallafacchina et al. study)
B)
↑ Activated Sat. Cells
↑ Quiescent Sat. Cells
Quadrant I
139 Genes
Quadrant II
24 Genes
Quadrant III
180 Genes
Quadrant IV
15 Genes
↑ Day 50
↑ Day 0
R² = 0.0696
log2(Day 50) - log2(Day 0) (This study)
log2(Quiescent) - log2(2.5 Days in vivo) (Liu et al. study)
C)
5.0
2.5
0.0
-2.5
-5.0
Day 50 - Day 0
↑ Quiescent (in vitro) Pallafacchina et al.
↑ Quiescent (in vivo) Liu et al.
Myogenesis
IGF
MAPK
NOTCH
TGFB Superfamily
WNT
PAX3
PAX7
CEBPB
MEOX2
RORA
DMD
ITGA8
IGF1
IGFBP4
IGFBP7
FOSL2
JUN
FOS
FOSB
JUNB
JUND
PDGFRL
HEYL
HEY1
NOTCH3
CHRDL2
BMP4
LTBP4
TGFBR3
ACVRL1
TGFB2
TGFB3
INHBB
OGN
WNT4
Repicate: 1 2 3 1′ 2′ 3′ 1″ 2″ 3″
Growth Factors, Sig. Molecules, Receptors, & Transcriptional Regulators
D)
5.0
2.5
0.0
-2.5
-5.0
Day 50 - Day 0
↑ in vitro Activated Pallafacchina et al.
↑ in vivo Activated Liu et al.
ADAM8
ADAMTS6
CHRNA1
CHRND
CHRNG
EMP3
ENO3
HOXA9
IGFBP3
ITGA3
ITGB4
ITGB6
JAG2
KCNK2
LAMB1
LAMB3
LBH
LGALS3
MURC
MYH3
MYOF
NPNT
NRN1
PRKCB
PRRX2
RPA1
RUNX2
TNC
TNNT2
TTN
1 2 3 1′ 2′ 3′ 1″ 2″ 3″
Growth Factors, Sig. Molecules, Receptors, & Transcriptional Regulators
E)
Quadrant I
SOX5
CEBPA
HLF
NFIL3
RELA
FOXO3
MYF
AP1
F)
Quadrant II
MEF2A
PRRX2
G)
Quadrant III
MYB
E2F1

Figure 3.3

Figure 3.3. Day 50 cultures share elevated FOS/JUN, NOTCH, and TGFB-signaling with quiescent satellite cells, as well as significant CEBPA/B binding motif enrichment. The mean day 50 expression of individual genes were standardized to the mean of day 0 samples, while the mean expression of genes from **A)** *in vitro*-cultured (58) or **B)** *in vivo*-derived (59) quiescent satellite cells were standardized to the mean of their respective activated satellite cell samples (n = 3). Gene lists were generated from the four plot quadrants of (A) and (B) given an absolute 4-fold change cut-off. Genes from **C)** quadrant I, and **D)** quadrant II were classified using PANTHER to identify growth factors, signaling molecules, receptors, and transcriptional regulators. Day 50 cultures shared more genes in common with quiescent than activated satellite cells, including FOS/JUN, NOTCH, and TGFB-signaling genes, along with other notable genes BMP4, CEBPB, DES, DMD, ICAM1, and PAX7. Day 50 cultures and activated satellite cells shared more structural and ion channel genes, such as LAMB1/3, MYH3, TTN, and the Cholinergic Receptor Nicotinic (CHRN) gene gamily. Quadrant gene lists were also analyzed with oPOSSUM 3.0 to identify significantly enriched transcription factor binding sites. Only motifs whose parent transcription factor was contained within the same quadrant were considered, given a 2-fold change cut-off. Significant motifs from *in vitro*-cultured satellite cells are shown for **E)** quadrant I, **F)** quadrant II, and **G)** quadrant III; quadrant IV yielded no significant results. Motifs that are highlighted red are enriched in both *in vitro*-cultured (A) and *in vivo*-derived (B) satellite cell quadrants.

these genes were considered part of quadrant I for further analysis of the *in vivo* activation dataset.

Quadrant II—genes more highly expressed at day 50 and in activated satellite cells—resulted in extracellular matrix organization (GO:0030198, Fig. 3.3A q = 3.03 E-04, Fig 3.3B q = 1.36 E-04) or muscle contraction (GO:0006936, Fig 3.3A q = 1.49 E-01, Fig. 3.3B q = 4.22 E-06). Unsurprisingly, genes more highly expressed in activated satellite cells and day 0 pluripotent cells—quadrant III—were enriched for GO categories related to the cell cycle (GO:0007049, Fig. 3.3A q = 1.49 E-77, Fig. 3.3B q = 4.17 E-80).

Notable signaling pathways or transcription factor activity that might play key roles in regulating the gene subsets shared by day 50 cultures and quiescent satellite cells were also investigated, given that this activity may explain why the Shelton *et al.* protocol maintains a persistent $PAX7^{+}$ population and relatively few large multinucleated myotubes (1). PANTHER classification of quadrant I genes for transcription factors showed PAX7 was more highly expressed in quiescent than activated satellite cells as expected, as were important embryonic myogenesis transcription factors MEOX2 and PAX3 (Fig. 3.3C). The dystrophin gene DMD was also more prominently shared between day 50 cultures and quiescent satellite cells. Surface markers ICAM1 and VCAM1 (60, 61), known to mark embryonic-derived SMPs or adult satellite cells, were also found in quadrant I, as was ITGA8. Together with ITGB1, ITGA8 is known to interact with ECM proteins fibronectin, tenascin, and vitronectin in smooth muscle cells (62). No role has been described for ITGA8 in developing skeletal muscle or satellite cells, but the present expression profiling shows an 11-fold increase in day 50 cultures relative to pluripotent controls, and the satellite cell datasets reveal roughly 22- and 6-fold higher expression of ITGA8 in quiescent cells.

Additional PANTHER classification for growth factors and signaling molecules identified a number of genes related to NOTCH and TGFB signaling pathways, as well as several FOS/JUN-related genes downstream in MAPK signaling. Interestingly, all of the above pathways are known to maintain the satellite cell progenitor state or quiescence.

NOTCH3 specifically—whose expression elevates in response to FOXO3 (63)—is known to associate with quiescent $PAX7^{+}/MYF5^{-}$ satellite cells (15, 64), wherein NOTCH signaling is essential in maintaining quiescence (65, 66). The NOTCH downstream effector HEY1 represses expression of the CDKN1C growth arrest gene, therefore allowing progenitor cells to proliferate (67, 68). Indeed, treating murine satellite cells or embryonic forelimbs with the NOTCH inhibitor DAPT significantly reduces cell proliferation, and skews the proportion of satellite cells towards the more differentiated $PAX7^{-}/MRF^{+}$ rather than the $PAX7^{+}/MRF^{-}$ progenitor phenotype (15, 68). The FOSL2 and JUN proteins have also been implicated in repressing the differentiation of quiescent murine satellite cells, in part by binding with and inhibiting MYOD1 function (69–71). TGFB signaling has also been shown to repress satellite cell differentiation via its downstream effector, SMAD3, which binds to MYOD1 and MEF2 proteins to inhibit their functions (72, 73), while also increasing MYOD1 degradation (74), thereby maintaining the quiescent state. CEBPB—another transcription factor 50-day cultures shared with quiescent satellite cells—plays a similar role; it can repress MYOD1 function and decrease its stability in satellite cells. CEBPB over-expression also reduces myoblasts' capacity to differentiate and fuse into myotubes (75).

Relatively fewer transcription factors were identified in quadrant II: day 50 cultures were found to share only RUNX2 and PRRX2 with *in vitro* activated satellite cells (Fig. 3.3D). No shared transcription factors were identified between day 50 cultures and quadrant II of *in vivo* activated satellite cells given the 4-fold change cut-off. RUNX2 is normally

expressed in C2C12 myoblasts and activated satellite cells but it does not appear to be required for skeletal myogenesis (76, 77). However, RUNX2 along with PPARG may allow satellite cells to behave as multipotent progenitors of osteoblasts or brown fat under certain conditions (58, 77, 78). PRRX2 is expressed in limb bud development and the pharyngeal arches, and the PRRX1^{-}/PRRX2^{-} mouse display marked limb deformities (79); however, its exact role in satellite cells remains unknown. PRRX2 may bind with SOX8, which does have an established function in preventing satellite cell differentiation (80, 81). This observation could suggest that PRRX2 is responsible for lifting the SOX8-mediated suppression of satellite cell activation. Other genes of note from quadrant II were acetylcholine receptor subunits and structural muscle or ECM genes, which may indicate progression towards a more excitatory and contractile myocyte stage. Quadrant II also contained surface proteins ITGA3 in both satellite cell datasets, then ITGB4 with *in vitro* activation and ITGB6 with *in vivo* activation. ITGA3 allows for myoblast adhesion and fusion (82), while the roles of ITGB4 and ITGB6 in satellite cells are less well defined. ITGB4 marks a population of non-satellite cell vessel-associated muscle progenitors (83), and ITGB4 may be a MYOD1 target, as ITGB4 expression is notably reduced in MYOD1$^{-/-}$ myoblasts (84). ITGB6 protein rapidly accumulates in murine skeletal muscle as early as 6 hours after freeze injury but with no established function (85). These surface proteins may provide a method of isolating the more activated-like SMP populations from hESC-derived myogenic cultures, either for their more refined study, or as a negative selection to remove cells that have differentiated beyond the ideal PAX7^{+}/MRF^{-} therapeutic stage.

All quadrant gene lists were then analyzed with oPOSSUM 3.0 to help establish a functional role for the transcription factors found within each list. Considering quadrant II with *in vitro* activated satellite cells, genes were significantly enriched for the MEF2A

MADS box and PRRX2 homeodomain binding motifs (Fig. 3.3F). Due to the relatively short AATTA homeodomain consensus sequence, the oPOSSUM results for PRRX2 may also represent genes bound by other homeodomain proteins with similar binding sites, including MOEX2, PAX3, PAX7 and the PRRX2 homolog PRRX1. Although PAX3 and PAX7 were considered part of quadrant I, several genes within quadrant II have been shown to be bound by PAX7, including RUNX2 and CAVIN4 (28).

The expression levels of MEF2A were 2-fold higher with *in vitro* activated relative to quiescent cells, but this did not meet the 4-fold cut-off to be considered part of quadrant II. MEF2A is well established in muscle regeneration, and its expression is expected precisely at the 3 days post-activation time point used in the *in vitro* study (36). Interestingly, other MEF2 family members elevated in day 50 cultures were more highly expressed in quiescent satellite cells relative to their *in vitro* activated counterparts; quadrant I contained MEF2C (18-fold) and MEF2D (2-fold).

TFBS enrichment analysis of quadrant I genes showed the AP1 FOS/JUN target motif, CEBP leucine zipper, and FOXO forkhead box motifs were significantly enriched with day 50 cultures and both *in vitro* and *in vivo* quiescent satellite cells (Fig. 3.3E). As stated above, various FOS/JUN proteins and CEBPB are responsible for regulating MYOD1 activity or stability (69–71, 75). FOXO3 has been shown to maintain satellite cell quiescence, potentially through its binding to and enhanced expression of the NOTCH3 promoter (63). Beyond satellite cells, FOXO3 may also enhance mitochondrial and autophagy-related gene transcription in myotubes during low nutrient conditions (86–88).

Also of note, the binding motifs for the MRFs and SOX box transcription factors were significantly enriched with day 50 cultures and freshly isolated $Pax3^{GFP/+}$ satellite. Several SOX proteins have established roles in embryonic myogenesis and satellite cell

regulation. Results showed that SOX5 and SOX6 were shared across day 50 cultures and quiescent satellite cells. SOX6 is known to repress slow-type fiber formation during embryonic myogenesis; it may repress the expression of sarcomeric contractile genes—including CHRNG and TNNT2—and downregulate transcription factors like PROX1, MYOD1, and MYOG (89, 90). SOX5 likewise has an established role in embryonic myogenesis (91); however, the role in adult satellite cells remains unclear. Another SOX family gene that was notably expressed in day 50 cultures was SOX8, while SOX17 appeared elevated in quiescent satellite cells. These findings underscore the importance that SOX-family proteins may have in myoblast differentiation and regular satellite cell function.

Overall, the expression profiling of day 50 cultures revealed a more prominent representation of FOS/JUN, NOTCH, and TGFB signaling pathways—as well as the downstream transcriptional effectors of these pathway—that correlated more with quiescent rather than activated satellite cells.

3.6.4 Day 50 hESC-derived skeletal muscle is comparable to fetal muscle and isolated myoblasts from other studies

Next, the gene expression profile of day 50 cultures was compared to other human ES-derived skeletal muscle (GSE70955)(8). Choi *et al*. generated skeletal muscle by first inducing mesoderm with 3 μM CHIR99021 for 3 days, followed by the NOTCH inhibitor DAPT for 1 week. Myoblasts were FACS sorted for $NCAM1^{+}/HNK1^{-}$ at 30 days of differentiation, and the resulting cells were used for mRNA microarray analysis. Choi *et al*. also harvested mRNA from 18 – 19 week old fetal muscle for comparison. For clarity, the time points of the present study are referred to as days 0 and 50, and those of the Choi *et al*. study as days 0’ and 30’.

The day 50 and the Choi *et al*. day 30′ arrays were contrasted with their respective day 0 and day 0′ controls; a plot of all genes represented on both arrays revealed a positive correlation between both myogenic cultures (Fig. 3.4A). A general overview of all genes with at least 4-fold elevated expression relative to day 0 or day 0′ controls revealed 995 genes with fairly similar expression patterns in both datasets (Fig. 3.4C). A full list of the genes' identities can be found online (Table A3.4).

The two cultures shared 603 elevated genes in quadrant I, and showed significant enrichment for GO terms like striated muscle tissue development (GO:0014706, q = 4.1 E-37), muscle contraction (GO:0006936, q = 1.1 E-33), and embryo development (GO:0009790, q = 3.4 E-14). As expected, the 265 genes in quadrant III were enriched for categories related to the cell cycle (GO:0007049, q = 1.0 E-04) and stem cell population maintenance (GO:0019827, q = 1.2 E-04). Indeed, quadrant I contained genes related to striated muscle tissue development and the sarcomeric structure (Fig. 3.4B & D)(37). Expected myogenic transcription factors in quadrant I included the MRFs—with the exception of MYF5 which was only elevated in day 50 cultures—as well as MEF2A, MEF2C, PAX7, and SIX1. Also present were embryonic myogenesis genes EYA1, EYA4, and SOX6; limb bud genes MEOX2 and PRRX1; and several genes known to regulate craniofacial myogenesis ISL1, PITX2, SIM2, TBX1, and TWIST1 (92, 93). The craniofacial skeletal myosin MYH6 was also upregulated with both protocols and in fetal muscle (94). Interestingly, PAX3 fell under quadrant II, showing elevated expression in day 50 cultures but reduced expression in day 30′ cells.

Overall, the sarcomeric gene expression seen with both protocols appeared similar to fetal muscle, although day 50 cultures appeared to have more fetal-like expression of thick

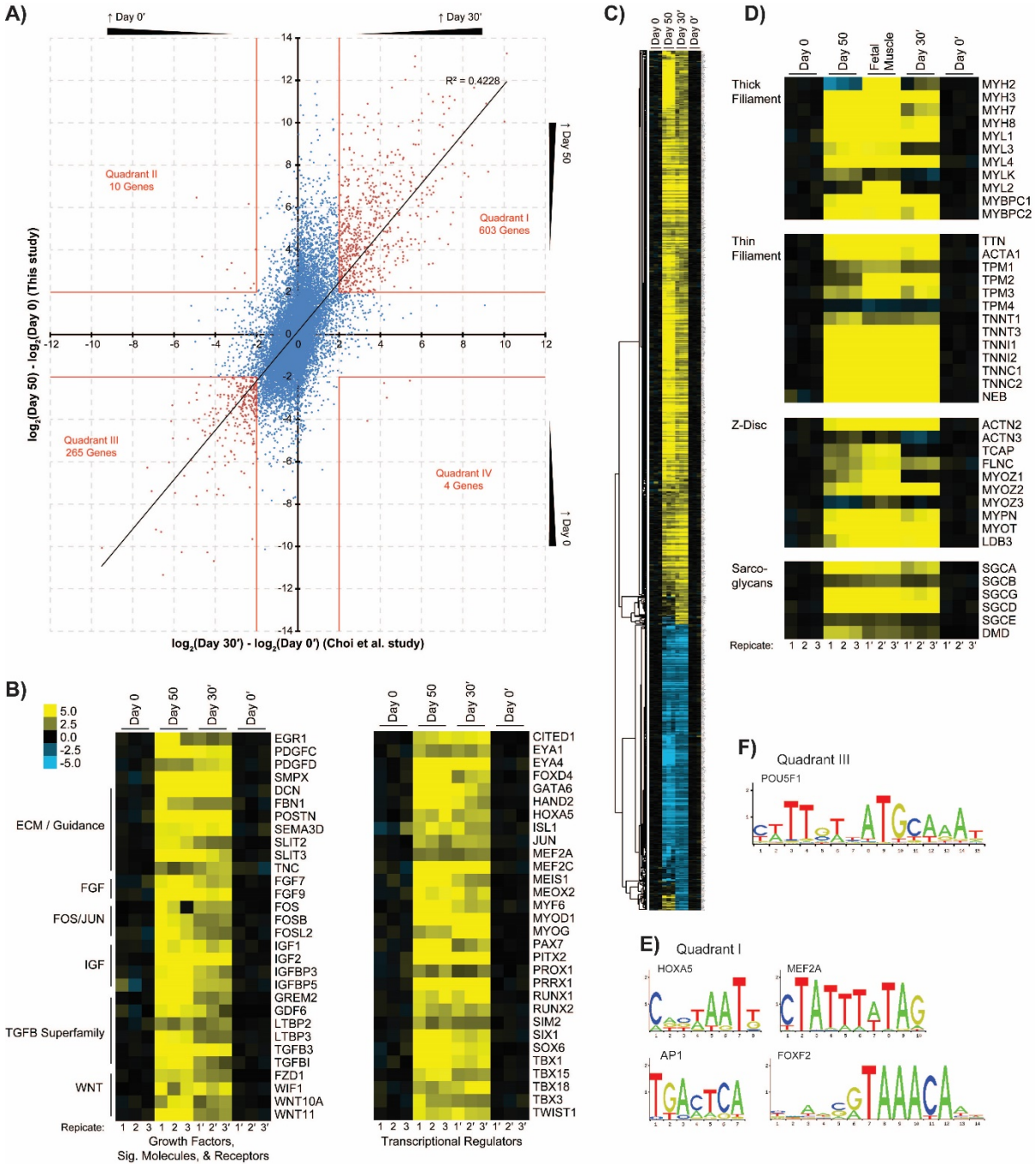
A)
↑ Day 0′
↑ Day 30′
R² = 0.4228
Quadrant II
10 Genes
Quadrant I
603 Genes
Quadrant III
265 Genes
Quadrant IV
4 Genes
↑ Day 50
↑ Day 0
log2(Day 50) - log2(Day 0) (This study)
log2(Day 30′) - log2(Day 0′) (Choi et al. study)
B)
5.0
2.5
0.0
-2.5
-5.0
Day 0
Day 50
Day 30′
Day 0′
EGR1
PDGFC
PDGFD
SMPX
DCN
FBN1
POSTN
SEMA3D
SLIT2
SLIT3
TNC
FGF7
FGF9
FOS
FOSB
FOSL2
IGF1
IGF2
IGFBP3
IGFBP5
GREM2
GDF6
LTBP2
LTBP3
TGFB3
TGFBI
FZD1
WIF1
WNT10A
WNT11
ECM / Guidance
FGF
FOS/JUN
IGF
TGFB Superfamily
WNT
Repicate:
1 2 3 1 2 3 1′ 2′ 3′ 1′ 2′ 3′
Growth Factors,
Sig. Molecules, & Receptors
CITED1
EYA1
EYA4
FOXD4
GATA6
HAND2
HOXA5
ISL1
JUN
MEF2A
MEF2C
MEIS1
MEOX2
MYF6
MYOD1
MYOG
PAX7
PITX2
PROX1
PRRX1
RUNX1
RUNX2
SIM2
SIX1
SOX6
TBX1
TBX15
TBX18
TBX3
TWIST1
Transcriptional Regulators
C)
Day 0
Day 50
Day 30′
Day 0′
D)
Day 0
Day 50
Fetal Muscle
Day 30′
Day 0′
Thick Filiament
MYH2
MYH3
MYH7
MYH8
MYL1
MYL3
MYL4
MYLK
MYL2
MYBPC1
MYBPC2
Thin Filiament
TTN
ACTA1
TPM1
TPM2
TPM3
TPM4
TNNT1
TNNT3
TNNI1
TNNI2
TNNC1
TNNC2
NEB
Z-Disc
ACTN2
ACTN3
TCAP
FLNC
MYOZ1
MYOZ2
MYOZ3
MYPN
MYOT
LDB3
Sarco-glycans
SGCA
SGCB
SGCG
SGCD
SGCE
DMD
Repicate:
1 2 3 1 2 3 1′ 2′ 3′ 1′ 2′ 3′ 1′ 2′ 3′
E)
Quadrant I
HOXA5
MEF2A
AP1
FOXF2
F)
Quadrant III
POU5F1

Figure 3.4

Figure 3.4. Day 50 and day 30′ cultures show gene expression profiles similar to quiescent satellite cells, and also share the expression of surface markers previously used to identify skeletal muscle progenitors. A) The mean expression of individual genes from (1) and (8) were standardized to the mean of their respective day 0 samples, and gene lists were generated from the four plot quadrants given an absolute 4-fold change cut-off. **B)** Genes from quadrant I were separated using PANTHER to identify growth factors, signaling molecules, receptors, and transcriptional regulators. A heat map of individual replicates for select genes were shown for each condition, generated by Java TreeView. Day 50 and day 30′ cultures share overlapping gene expression similar to that of quiescent satellite cells, including DES, IGF1, PAX7, FOS/JUN and TGFB-signaling genes. Several surface markers known to identify embryonic skeletal muscle progenitors or satellite cells—CXCR4, ERBB3, ICAM1, NCAM1, VCAM1—were also shared between both cultures while some surface markers, however, were only elevated in Day 50 cultures: CD82 and NGFR (data not shown). **C)** Genes were filtered to select only those with at least 4-fold change in expression on either array relative to their respective day 0 samples, and a heat map of individual replicates was generated by Java TreeView, showing fairly congruent expression profiles. The specific identities and expression values for each gene can be found online (Table A3.4). **D)** A list of key sarcomeric structural genes was adapted from (85). Day 50 cultures exhibited more fetal-like expression levels of MYH7, MYL3, MYLK and several Z-disc genes, while day 30′ cells appeared to express the tropomyosins TPM2/TPM3 at levels more similar to fetal muscle. **E)** Quadrant I and **F)** quadrant III gene lists were also analyzed with oPOSSUM 3.0 to identify significantly enriched transcription factor binding sites ($Z > 5$). Only motifs whose parent transcription factor was contained within the same quadrant were considered, given 2-fold change cut-off.

filament and Z-disc genes, likely due to their longer differentiation period relative to the Choi *et al*. 30 day-old cultures. Signaling pathways with a number of elevated genes included the TGFB superfamily, FOS members of MAPK signaling, and IGF proteins: a similar expression profile to more quiescent satellite cells from Figure 3.

Interestingly, quadrant I contained surface markers of murine $Lbx1^+$ embryonic muscle progenitors ITGA4 and its ligand VCAM1 (95–97), which also marks adult satellite cells or myotubes (59). Other common satellite cell markers ITGA7 and ITGB1 were highly expressed at all time points of *in vitro* differentiation and thus showed no elevated expression at day 50 or day 30′ relative to day 0 or day 0′ controls (98, 99). Quadrant I also showed markers previously used to identify adult satellite cells or embryonic SMPs, including CXCR4 (96), ERBB3 (100), NCAM1 (8, 101), and PDGRFA (102) . Other markers—CD82 (103, 104), ICAM1 (61, 64, 105), and NGFR (100)—were only elevated in day 50 but not day 30′ cultures. This may be a result of the $NCAM1^+/B3GAT1^-$ (HNK1) FACS profile used by the Choi *et al*. study; NCAM1 may mark only a subpopulation of embryonic SMPs (100). Also, over 60% of the Choi *et al.* $NCAM1^+/B3GAT1^-$ cells were already MYH^+ indicating that $PAX7^+$ SMPs make up a notably smaller fraction of their total cultures relative to the more persistent $PAX7^+$ population found in day 50 cultures (1). This would skew the day 30′ gene expression profile towards higher expression of mature muscle markers rather than markers of true progenitor populations.

Together, the shared expression of many previously identified surface proteins provides support for their utility to isolate embryonic-derived SMPs. The comparative differences also suggest more cautious investigation into precisely what myogenic populations each marker selects for, and what myogenic populations may be excluded.

Furthermore, the remaining list of shared receptors may contain other tentative SMP surface markers not yet characterized.

For example, quadrant I contained adhesion G-protein coupled receptors with potential links to muscle and its development: ADGRA2, ADGRD1, and ADGRG6. The most interesting candidate—ADGRG6—is highly expressed from E10.5 to E12.5 in the somitic mesoderm, and to a lesser extent in parts of the developing heart (106, 107). ADGRG6 expression does not appreciably overlap with myocytes in the dermomyotome, suggesting ADGRG6 may mark the pre-myocyte stage of muscle development (107). The expression pattern of ADGRG6 over the 50 day differentiation fell under Cluster 3 (Table 3.1); this placed ADGRG6 after the onset of PAX3 expression, with the expression of DMD, and prior to that of the MRFs. Also, the Pallafacchina *et al*. study showed ADGRG6 is expressed roughly 2-fold higher in quiescent relative to activated satellite cells (58).

Evidence suggests ADGRG6 may be related to the ERBB pathway. Mutant mice lacking the receptors ERBB2, ERBB3, ERBB4, or their ligand NRG1 are embryonic lethal due to defective cardiac ventricle development, while also displaying defects in Schwann cell precursors (108–110). Mice lacking ADGRG6 are likewise embryonic lethal due to failed ventricular development, and zebrafish mutant models show arrested Schwann cell precursors (107, 111), thus linking ADGRG6$^{-/-}$ defects between heart and Schwann cell development in a similar manner as ERBB deletions (108–110). ERBB1, ERBB2, and ERBB3 have been detected on murine satellite cells within 6 hours of activation, and mediate anti-apoptotic survival cues during muscle injury (112, 113). ERBB3 has recently been implicated as a marker of PAX7-positive hESC-derived SMPs (100). Like ADGRG6, ERBB3 also falls under Cluster 3 of the 50-day time course (Table 3.1). Therefore, it would

be worthwhile to determine what SMP population—if any—ADGRG6 can identify during *in vitro* skeletal myogenesis.

Transcription factor binding site enrichment between day 50 and day 30′ cultures revealed significant enrichment of FOXF2, HOXA5, and MEF2A transcription factor binding sites within quadrant I. Given the similar homeodomain binding sequence shared by many HOX factors, other HOX family proteins besides HOXA5 may be transcriptionally active in both cultures. Indeed, both cultures show elevated expression of 12 HOX genes, including HOXA10 and HOXA11 which are associated with limb development (114). The significant enrichment of MEF2A TFBSs was also expected, given that MEF2A, MEF2C, and MEF2D are notably upregulated and essential for embryonic myogenesis (36). FOXF2 has no clear role in skeletal muscle. However, its consensus sequence would likely overlap with other expressed forkhead factors like FOXO3, which does have an established role in suppressing satellite cell activation and enhancing autophagy in nutrient-starved myotubes (63, 86–88). FOXO3 expression was approximately 3- and 2-fold higher at day 50 and day 30′ relative to their respective pluripotent controls, falling short of the 4-fold cut-off to be considered part of quadrant I.

Overall, the comparison of expression profiles from variously sourced hESC-derived skeletal muscle allows for the better understanding of the muscle tissue these *in vitro* differentiation protocols generate. As may be expected for embryonic muscle development, these works showed that forkhead box, homeodomain, and MEF2 proteins are key transcriptional regulators involved at day 50 or day 30′ of *in vitro* myogenic differentiation.

It will be interesting to compare these results to expression profiles taken directly from different *in vivo* embryonic structures and stages, such as the initial myotome of the dermomyotome, the subsequent trunk muscle derived after primary myogenesis, early and

late limb muscle, and craniofacial muscle. Day 50 and day 30′ cultures both express numerous genes used to identify craniofacial muscle (92, 93); this type of muscle and its progenitors may be expected to have different therapeutic potential compared to muscle of the limb or other myogenic structures of the embryo. Cells of the medial dermomyotomal lips that go on to form the initial myotome, for example, may make poor donor cells for therapy as these cells are characteristically post-mitotic and mononuclear (115–117), whereas the later wave of cells emanating from the central domain of the dermomyotome are responsible for seeding the trunk with persistent $PAX7^+$ SMPs and contributing to myotube hypertrophy through fusion (118, 119).

Also, whole somite transplants between chick and quail embryos show that donor somites retain their HOX identity even in ectopic locations (120–122). Thoracic somites that would normally generate intercostal rib muscle continue to do so even when transplanted into the lumbar region, where abdominal trunk muscle is expected. Therefore, the innate developmental identities adopted by *in vitro*-derived SMPs may be of concern in stem cell therapy if their identify remains relatively fixed rather than adapting to the recipient muscles' composition (123). While other studies show *in vivo* transplantation of SMPs derived from the directed differentiation of hESCs or iPSCs, the possible effects of the donor cells' developmental identity with regards to the transplantation site have not been established (3, 8, 61, 124).

3.7 Conclusion

This study shows that day 50 cultures have an expression profile more reminiscent of quiescent rather than activated satellite cells, which can have several implications. This can indicate that day 50 cultures should be well suited for stem cell therapy—as satellite cells

that appear more quiescent yield more efficient *in vivo* engraftment (57, 125)—or it can indicate that day 50 cultures require additional supplementation to continue the myogenic program and generate mature myotubes. As the MYH^{+} myocytes surrounding $PAX7^{+}$ SMPs in day 50 cultures are primarily mononucleated, it would be worthwhile to establish that these cultures are capable of adequate fusion and the formation of large mature myotubes *in vitro*. This would determine whether the SMPs simply lack the appropriate stimulus to differentiate and fuse—and therefore can be cultured in an ideal state for stem cell therapy—or if they are inherently developmentally arrested and only capable of producing mononucleated myocytes with low fusion-competence. A number of recombinant proteins and small molecules exist that can help drive terminal myogenesis and fusion.

Combination treatment of pre-myogenic cultures with FGF2, HGF, and IGF1 has been used to enhance the differentiation and maturation of *in vitro* myotubes (6, 9, 126). FGF2 and HGF can be used to activate quiescent satellite cells or enhance SMP proliferation while suppressing their differentiation (127–130), which may in turn provide a more favorable myoblast density for fusion (13). Small molecule MAPK14 (p38) inhibitors like SB202190 or SB203580 have a similar effect of suppressing differentiation while allowing for the expansion of human satellite cells *in vitro* (125). IGF1 is a hypertrophic factor that can overcome the differentiation block of SB203580 and allow for the formation of myocytes from SB203580-treated myoblasts (131). IGF1 cannot, however, overcome the SB203580-mediated fusion block, but fusion can be corrected with a period of continued IGF1 treatment following the removal of SB203580 (131). Since MAPK14 is a driver of myogenic differentiation in the embryo and adult myoblasts (132–134), it may be worthwhile to also selectively activate the pathway after its inhibition using low levels of TNFA (135), or heparin (136–138) to mature the hESC-derived myogenic cells.

Myocyte fusion may be further improved by another small molecule—LDN-193189—that inhibits MSTN-signaling, leading to enhanced muscle fusion and contractility *in vitro* (139). Also, the ablated fusion of DMD patient-derived myoblasts has previously been rescued using LDN193198 and SB431542 to inhibit BMP and TGFB signaling, respectively (8). The use of LDN193198 or SB431542 may provide more fusion-ready myoblasts and myocytes in day 50 cultures, given that BMP4 and TGFB-signaling genes are notably expressed in day 50 cells, and that these two pathways are known to repress satellite cell differentiation and secondary fetal myogenesis (Fig. 3.3C)(72–74, 140, 141). Evidence suggests TGFB inhibition can, in fact, enhance myotube maturation in hESC-derived skeletal muscle (100).

One considerable limitation of this study was that mRNA microarray samples were taken from unsorted bulk cultures. This makes it impossible to definitely delineate gene expression in $PAX7^+$ SMPs from that of myoblasts or myocytes. A previous study achieved up to 96% $PAX7^+/PAX3^+$ SMP purity by FACS for $B3GAT1^-/CHRNA^-/CXCR4^+/MET^+$ in hESCs undergoing directed skeletal myogenesis (4). Recently, it was shown that $ERBB3^+/NGFR^+$ can select for hESC-derived $PAX3^+/PAX7^+$ SMPs that appear better suited for long-term engraftment *in vivo* than unsorted cultures (100). ADGRG6 was identified in the present study as a potential SMP marker that showed a similar expression pattern to ERBB3 and NGFR in these cultures.

Uncovering more novel surface proteins to mark and isolate embryonic SMPs—used individually or in conjunction with previously established surface markers—may further increase the resolution by which researchers define different SMP populations, or the purity of their sorting. Furthermore, a longer list of surface proteins to mark SMPs provides greater flexibility in choosing appropriate antibodies when staining or sorting myogenic cultures.

Ultimately, 50-day cultures contain a persistent $PAX7^+$ SMP population with an expression profile of signaling pathways and transcriptional regulators similar to quiescent satellite cells, which could prove an ideal source material for stem cell therapy. Thus the Shelton *et al.* protocol stands in contrast with other *in vitro* differentiation protocols that have low percentages of—or gradually lose—PAX7 expressing SMPs as myotubes dominate (3, 6–8). However, a delicate balance must be struck between maintaining hESC-derived SMPs in a quiescent satellite cell-like state and not repressing their differentiation too heavily to the point that they no longer respond to physiological cues to differentiate. This study confirms the expression of many previously outlined SMP surface markers in 50-day cultures, and identifies novel markers as an additional avenue to purify the persistent $PAX7^+$ SMPs for future study or attempted stem cell therapy in mice.

3.8 Experimental Procedures

3.8.1 Cell culture

Human embryonic stem cells were maintained and differentiated as in (2).

3.8.2 Cell culture analysis

Phase-contrast microscopy, cell counting, and qPCR analysis were also performed as in (1).

3.8.3 Microarray gene expression profiling

Gene expression analyses were carried out in triplicate using three biological replicates of the directed differentiation protocol. Total RNA was purified using Total RNA Mini Kit (FroggaBio). A total of 40 ng of RNA was processed and fluorescently labeled using Agilent Low Input Quick Amp Labeling Kit (Agilent Technologies, Santa Clara, CA,

USA). A total of 600 ng of Cy3-labelled cRNA was hybridized to Agilent 8x66 K-Human Genome Microarrays using Agilent Gene Expression Hybridization Kit. The microarrays were read on the Agilent DNA Microarray SureScan Scanner. The raw reads were filtered using a custom-made Perl script to retain only probes detected above background in at least 3 of the 24 samples. Probes were $\log_2()$ transformed and quartile-normalized using Expander 7.0 software (24). The data can be found online (Table A3.1).

3.8.4 Clustering and significant gene list generation

Expander 7.0 was used to perform CLICK clustering and t-test statistical analysis (24, 142). Only probes with a difference of at least 2 in their $\log_2()$ expression values, and absolute $\log_2()$ expression of at least 5, were retained and used in clustering (Table A3.2). Clustering was performed given a 0.85 homogeneity value, and the resulting clusters were manually grouped based on expression pattern similarity where deemed appropriate (Table A3.3). T-test statistical analysis were performed in Expander 7.0 using probes that changed by at least 4-fold at the time point under investigation relative to day 0, and had at least 5 $\log_2()$ expression in at least one sample. Unless otherwise stated, $p \leq 0.05$ and FDR ≤ 0.05 (by the Benjamini-Hochberg method) were used for Expander 7.0 statistical analysis. One-way ANOVA ($p < 0.05$) and post-hoc Tukey test ($p < 0.05$) were used to analyze the quantified immunofluorescence and qPCR results.

3.8.5 Gene list analysis

ToppGene Suite was used to identify significantly enriched Molecular Function and Biological Process Gene Ontology categories within a given gene set ($p \leq 0.05$, FDR ≤ 0.05 by the Bonferroni method)(25). Representative Gene Ontology categories and example genes

or gene families were manually chosen from results with $q \leq 0.05$ by Bonferroni correction. PANTHER Classification System was used to identify genes from a given set that were classified as growth factors, receptors, signaling molecules, or transcription factors (143). Genes unclassified by PANTHER were manually labeled where deemed appropriate based on published knowledge. oPOSSUM 3.0 was used to identify transcription factors with significantly over-represented binding sites within a given gene set, using a conservation cut-off = 0.60 and considering 2 000 base pairs of upstream and 2 000 base pairs downstream sequence from transcription start sites (144). Only factors with Z-score ≥ 5 were considered significantly enriched.

3.8.6 Gene expression analysis with published datasets

The mRNA microarrays used for comparison to day 50 myogenic cultures correspond to *in vitro* activated mouse satellite cells (GSE15155)(58), *in vivo* activated mouse satellite cells (GSE47177)(59), and hESC-derived and fetal skeletal muscle (GSE70955)(8).

With the Shelton *et al.* dataset, the $\log_2()$-fold changes in probe expression were calculated for each day 50 replicate by subtracting the average of triplicate undifferentiated day 0 values. Similarly, fold changes were calculated for GSE70955 skeletal muscle replicates by subtracting the average of triplicate undifferentiated cell samples. The $\log_2()$-fold changes for probes from GSE15155 and GSE47177 were calculated by subtracting the average of triplicate activated satellite cell samples from each quiescent satellite cell sample. In the event where multiple probes exist for a single gene, only the probe with the greatest absolute fold change was considered for further analysis. Genes were paired between arrays according to HUGO Gene Nomenclature Committee (HGNC) gene symbol identity.

Day 50 $\log_2()$ fold changes for each gene were plotted against those of the three comparative arrays; genes were divided into four quadrants—given a 4-fold cut off—in order to find commonly or differentially expressed genes between the datasets.

3.9 Acknowledgments

This work was funded by an award from the Muscular Dystrophy Association to Ilona S. Skerjanc (218371). Michael Shelton was supported in part by the Queen Elizabeth II Graduate Scholarship in Science and Technology. Daniel O'Neil and Alexandre Blais were funded by a grant from the Canadian Institutes of Health Research (MOP-119458).

3.10 References

1. Shelton M, Metz J, Liu J, Carpenedo RL, Demers SP, Stanford WL, Skerjanc IS. 2014. Derivation and expansion of PAX7-positive muscle progenitors from human and mouse embryonic stem cells. Stem Cell Reports 3:516–529.
2. Shelton M, Kocharyan A, Liu J, Skerjanc IS, Stanford WL. 2016. Robust generation and expansion of skeletal muscle progenitors and myocytes from human pluripotent stem cells. Methods 101:73–84.
3. Xu C, Tabebordbar M, Iovino S, Ciarlo C, Liu J, Castiglioni A, Price E, Liu M, Barton ER, Kahn CR, Wagers AJ, Zon LI. 2013. A zebrafish embryo culture system defines factors that promote vertebrate myogenesis across species. Cell 155:909–921.
4. Borchin B, Chen J, Barberi T. 2013. Derivation and FACS-mediated purification of PAX3+/PAX7+ skeletal muscle precursors from human pluripotent stem cells. Stem Cell Reports 1:620–631.
5. Hosoyama T, McGivern J V, Van Dyke JM, Ebert AD, Suzuki M. 2014. Derivation of myogenic progenitors directly from human pluripotent stem cells using a sphere-based culture. Stem Cells Transl Med 3:564–74.
6. Chal J, Oginuma M, Al Tanoury Z, Gobert B, Sumara O, Hick A, Bousson F, Zidouni Y, Mursch C, Moncuquet P, Tassy O, Vincent S, Miyanari A, Bera A, Garnier J-M, Guevara G, Hestin M, Kennedy L, Hayashi S, Drayton B, Cherrier T, Gayraud-Morel B, Gussoni E, Relaix F, Tajbakhsh S, Pourquié O. 2015. Differentiation of pluripotent stem cells to muscle fiber to model Duchenne muscular dystrophy. Nat Biotechnol 33:962–969.

7. Caron L, Kher D, Lee KL, McKernan R, Dumevska B, Hidalgo A, Li J, Yang H, Main H, Ferri G, Petek LM, Poellinger L, Miller DG, Gabellini D, Schmidt U. 2016. A Human Pluripotent Stem Cell Model of Facioscapulohumeral Muscular Dystrophy-Affected Skeletal Muscles. Stem Cells Transl Med 5:1145–1161.

8. Choi IY, Lim HT, Estrellas K, Mula J, Cohen T V., Zhang Y, Donnelly CJ, Richard JP, Kim YJ, Kim H, Kazuki Y, Oshimura M, Li HL, Hotta A, Rothstein J, Maragakis N, Wagner KR, Lee G. 2016. Concordant but Varied Phenotypes among Duchenne Muscular Dystrophy Patient-Specific Myoblasts Derived using a Human iPSC-Based Model. Cell Rep 15:2301–2312.

9. Xi H, Fujiwara W, Gonzalez K, Jan M, Liebscher S, Van Handel B, Schenke-Layland K, Pyle AD. 2017. In Vivo Human Somitogenesis Guides Somite Development from hPSCs. Cell Rep 18:1573–1585.

10. Conboy IM, Rando TA. 2002. The regulation of Notch signaling controls satellite cell activation and cell fate determination in postnatal myogenesis. Dev Cell 3:397–409.

11. Buckingham M, Bajard L, Chang T, Daubas P, Hadchouel J, Meilhac S, Montarras D, Rocancourt D, Relaix F. 2003. The formation of skeletal muscle: From somite to limb. J Anat 202:59–68.

12. Mauro A. 1961. Satellite cell of skeletal muscle fibers. J Biophys Biochem Cytol 9:493–5.

13. Chargé SBP, Rudnicki MA. 2004. Cellular and molecular regulation of muscle regeneration. Physiol Rev 84:209–38.

14. Buckingham M. 2007. Skeletal muscle progenitor cells and the role of Pax genes. C R Biol 330:530–3.

15. Kuang S, Kuroda K, Le Grand F, Rudnicki MA. 2007. Asymmetric Self-Renewal and Commitment of Satellite Stem Cells in Muscle. Cell 129:999–1010.

16. Dumont NA, Wang YX, von Maltzahn J, Pasut A, Bentzinger CF, Brun CE, Rudnicki MA. 2015. Dystrophin expression in muscle stem cells regulates their polarity and asymmetric division. Nat Med 21:1455–1463.

17. Seale P, Sabourin LA, Girgis-Gabardo A, Mansouri A, Gruss P, Rudnicki MA. 2000. Pax7 Is Required for the Specification of Myogenic Satellite Cells. Cell 102:777–786.

18. Relaix F, Rocancourt D, Mansouri A, Buckingham M. 2004. Divergent functions of murine Pax3 and Pax7 in limb muscle development. Genes Dev 18:1088–1105.

19. Oustanina S, Hause G, Braun T. 2004. Pax7 directs postnatal renewal and propagation of myogenic satellite cells but not their specification. EMBO J 23:3430–3439.

20. Hutcheson DA, Zhao J, Merrell A, Haldar M, Kardon G. 2009. Embryonic and fetal limb myogenic cells are derived from developmentally distinct progenitors and have different requirements for B-catenin. Genes Dev 23:997–1013.

21. Jagla K, Dollé P, Mattei MG, Jagla T, Schuhbaur B, Dretzen G, Bellard F, Bellard M. 1995. Mouse Lbx1 and human LBX1 define a novel mammalian homeobox gene family related to the Drosophila lady bird genes. Mech Dev 53:345–356.

22. Epstein JA, Shapiro DN, Cheng J, Lam PY, Maas RL. 1996. Pax3 modulates expression of the c-Met receptor during limb muscle development. Proc Natl Acad Sci U S A 93:4213–8.

23. Gross MK, Moran-Rivard L, Velasquez T, Nakatsu MN, Jagla K, Goulding M. 2000. Lbx1 is required for muscle precursor migration along a lateral pathway into the limb. Development 127:413–424.

24. Ulitsky I, Maron-Katz A, Shavit S, Sagir D, Linhart C, Elkon R, Tanay A, Sharan R, Shiloh Y, Shamir R. 2010. Expander: from expression microarrays to networks and functions. Nat Protoc 5:303–322.

25. Chen J, Bardes EE, Aronow BJ, Jegga AG. 2009. ToppGene Suite for gene list enrichment analysis and candidate gene prioritization. Nucleic Acids Res 37:305–311.

26. Daily K, Ho Sui SJ, Schriml LM, Dexheimer PJ, Salomonis N, Schroll R, Bush S, Keddache M, Mayhew C, Lotia S, Perumal TM, Dang K, Pantano L, Pico AR, Grassman E, Nordling Di, Hide W, Hatzopoulos AK, Malik P, Cancelas JA, Lutzko C, Aronow BJ, Omberg L. 2017. Molecular, phenotypic, and sample-associated data to describe pluripotent stem cell lines and derivatives. Sci data 4:170030.

27. Soleimani VD, Punch VG, Kawabe Y ichi, Jones AE, Palidwor GA, Porter CJ, Cross JW, Carvajal JJ, Kockx CEM, van IJcken WFJ, Perkins TJ, Rigby PWJ, Grosveld F, Rudnicki MA. 2012. Transcriptional Dominance of Pax7 in Adult Myogenesis Is Due to High-Affinity Recognition of Homeodomain Motifs. Dev Cell 22:1208–1220.

28. Lilja KC, Zhang N, Magli A, Gunduz V, Bowman CJ, Arpke RW, Darabi R, Kyba M, Perlingeiro R, Dynlacht BD. 2017. Pax7 remodels the chromatin landscape in skeletal muscle stem cells. PLoS One 12:1–24.

29. Yamaguchi TP, Takada S, Yoshikawa Y, Wu N, McMahon AP. 1999. T (Brachyury) is a direct target of Wnt3a during paraxial mesoderm specification. Genes Dev 13:3185–3190.

30. Yoon JK, Moon RT, Wold B. 2000. The bHLH Class Protein pMesogenin1 Can Specify Paraxial Mesoderm Phenotypes. Dev Biol 222:376–391.

31. Chapman DL, Agulnik I, Hancock S, Silver LM, Papaioannou VE. 1996. Tbx6, a mouse T-Box gene implicated in paraxial mesoderm formation at gastrulation. Dev Biol 180:534–542.

32. Loh KMM, Chen A, Koh PWW, Deng TZZ, Sinha R, Tsai JMM, Barkal AAA, Shen KYY, Jain R, Morganti RMM, Shyh-Chang N, Fernhoff NBB, George BMM, Wernig G, Salomon REEA, Chen Z, Vogel H, Epstein JAA, Kundaje A, Talbot WSS, Beachy PAA, Ang LTT, Weissman ILL. 2016. Mapping the Pairwise Choices Leading from Pluripotency to Human Bone, Heart, and Other Mesoderm Cell Types. Cell 166:451–468.

33. Zeineddine D, Papadimou E, Chebli K, Gineste M, Liu J, Grey C, Thurig S, Behfar A, Wallace VA, Skerjanc IS, Pucéat M. 2006. Oct-3/4 Dose Dependently Regulates Specification of Embryonic Stem Cells toward a Cardiac Lineage and Early Heart Development. Dev Cell 11:535–546.

34. Thomson M, Liu SJ, Zou LN, Smith Z, Meissner A, Ramanathan S. 2011. Pluripotency factors in embryonic stem cells regulate differentiation into germ layers. Cell 145:875–889.

35. DeVeale B, Brokhman I, Mohseni P, Babak T, Yoon C, Lin A, Onishi K, Tomilin A, Pevny L, Zandstra PW, Nagy A, van der Kooy D. 2013. Oct4 is required ~E7.5 for proliferation in the primitive streak. PLoS Genet 9:e1003957.

36. Liu N, Nelson BR, Bezprozvannaya S, Shelton JM, Richardson JA, Bassel-Duby R, Olson EN. 2014. Requirement of MEF2A, C, and D for skeletal muscle regeneration. Proc Natl Acad Sci 111:4109–4114.

37. Hwang PM, Sykes BD. 2015. Targeting the sarcomere to correct muscle function. Nat Rev Drug Discov 14:313–328.

38. Grzywacz B, Kataria N, Kataria N, Blazar BR, Miller JS, Verneris MR. 2011. Natural killer-cell differentiation by myeloid progenitors. Blood 117:3548–58.

39. Turner DA, Rué P, Mackenzie JP, Davies E, Martinez Arias A. 2014. Brachyury cooperates with Wnt/β-catenin signalling to elicit primitive-streak-like behaviour in differentiating mouse embryonic stem cells. BMC Biol 12:63.

40. Blauwkamp TA, Nigam S, Ardehali R, Weissman IL, Nusse R. 2012. Endogenous Wnt signalling in human embryonic stem cells generates an equilibrium of distinct lineage-specified progenitors. Nat Commun 3:1070.

41. Cao N, Liang H, Huang J, Wang J, Chen Y, Chen Z, Yang H-T. 2013. Highly efficient induction and long-term maintenance of multipotent cardiovascular progenitors from human pluripotent stem cells under defined conditions. Cell Res 23:1119–1132.

42. Nazareth EJP, Ostblom JEE, Lücker PB, Shukla S, Alvarez MM, Oh SKW, Yin T, Zandstra PW. 2013. High-throughput fingerprinting of human pluripotent stem cell fate responses and lineage bias. Nat Methods 10:1225–1231.

43. Loh KM, Ang LT, Zhang J, Kumar V, Ang J, Auyeong JQ, Lee KL, Choo SH, Lim CYY, Nichane M, Tan J, Noghabi MS, Azzola L, Ng ES, Durruthy-Durruthy J, Sebastiano V, Poellinger L, Elefanty AG, Stanley EG, Chen Q, Prabhakar S, Weissman IL, Lim B. 2014. Efficient endoderm induction from human pluripotent stem cells by logically directing signals controlling lineage bifurcations. Cell Stem Cell 14:237–252.

44. Naujok O, Diekmann U, Lenzen S. 2014. The generation of definitive endoderm from human embryonic stem cells is initially independent from activin A but requires canonical Wnt-signaling. Stem Cell Rev 10:480–493.

45. Hu J, Wang Y, Jiao J, Liu Z, Zhao C, Zhou Z, Zhang Z, Forde K, Wang L, Wang J, Baylink DJ, Zhang XB, Gao S, Yang B, Chen YE, Ma PX. 2015. Patient-specific cardiovascular progenitor cells derived from integration-free induced pluripotent stem cells for vascular tissue regeneration. Biomaterials 73:51–59.

46. Cheung C, Bernardo AS, Trotter MWB, Pedersen RA, Sinha S. 2012. Generation of human vascular smooth muscle subtypes provides insight into embryological origin–dependent disease susceptibility. Nat Biotechnol 30:165–173.

47. Barberi T, Bradbury M, Dincer Z, Panagiotakos G, Socci ND, Studer L. 2007. Derivation of engraftable skeletal myoblasts from human embryonic stem cells. Nat Med 13:642–648.

48. Tan JY, Sriram G, Rufaihah AJ, Neoh KG, Cao T. 2013. Efficient Derivation of Lateral Plate and Paraxial Mesoderm Subtypes from Human Embryonic Stem Cells Through GSKi-Mediated Differentiation. Stem Cells Dev 22:1893–1906.

49. Mendjan S, Mascetti VL, Ortmann D, Ortiz M, Karjosukarso DW, Ng Y, Moreau T, Pedersen RA. 2014. NANOG and CDX2 pattern distinct subtypes of human mesoderm during exit from pluripotency. Cell Stem Cell 15:310–325.

50. Gadue P, Huber TL, Paddison PJ, Keller GM. 2006. Wnt and TGF-beta signaling are required for the induction of an in vitro model of primitive streak formation using embryonic stem cells. Proc Natl Acad Sci U S A 103:16806–16811.

51. Rodríguez-Esteban C, Capdevila J, Kawakami Y, Belmonte JCI. 2001. Wnt signaling and PKA control Nodal expression and left-right determination in the chick embryo. Development 128:3189–3195.

52. Sumi T, Tsuneyoshi N, Nakatsuji N, Suemori H. 2008. Defining early lineage specification of human embryonic stem cells by the orchestrated balance of canonical Wnt/ -catenin, Activin/Nodal and BMP signaling. Development 135:2969–2979.

53. Toyama R, O'Connell ML, Wright C V, Kuehn MR, Dawid IB. 1995. Nodal induces ectopic goosecoid and lim1 expression and axis duplication in zebrafish. Development 121:383–91.

54. Katoh M, Katoh M. 2006. CER1 is a common target of WNT and NODAL signaling pathways in human embryonic stem cells. Int J Mol Med 17:795–799.

55. Guo X, Wang X-F. 2009. Signaling cross-talk between TGF-β/BMP and other pathways. Cell Res 19:71–88.

56. Belo JA, Bachiller D, Agius E, Kemp C, Borges AC, Marques S, Piccolo S, De Robertis EM. 2000. Cerberus-like is a secreted BMP and nodal antagonist not essential for mouse development. Genesis 26:265–270.

57. Montarras D, Morgan J, Collins C, Relaix F, Zaffran S, Cumano A, Partridge T, Buckingham M. 2005. Direct isolation of satellite cells for skeletal muscle regeneration. Science 309:2064–7.

58. Pallafacchina G, François S, Regnault B, Czarny B, Dive V, Cumano A, Montarras D, Buckingham M. 2010. An adult tissue-specific stem cell in its niche: A gene profiling analysis of in vivo quiescent and activated muscle satellite cells. Stem Cell Res 4:77–91.

59. Liu L, Cheung TH, Charville GW, Hurgo BMC, Leavitt T, Shih J, Brunet A, Rando TA. 2013. Chromatin Modifications as Determinants of Muscle Stem Cell Quiescence and Chronological Aging. Cell Rep 4:189–204.

60. Jesse TL, LaChance R, Iademarco MF, Dean DC. 1998. Interferon regulatory factor-2 is a transcriptional activator in muscle where It regulates expression of vascular cell adhesion molecule-1. J Cell Biol 140:1265–1276.

61. Magli A, Incitti T, Kiley J, Swanson SA, Darabi R, Rinaldi F, Selvaraj S, Yamamoto A, Tolar J, Yuan C, Stewart R, Thomson JA, Perlingeiro RCR. 2017. PAX7 Targets, CD54, Integrin α9β1, and SDC2, Allow Isolation of Human ESC/iPSC-Derived Myogenic Progenitors. Cell Rep 19:2867–2877.

62. Schnapp LM, Hatch N, Ramos DM, Klimanskaya I V., Sheppard D, Pytela R. 1995. The human integrin a8B1 functions as a receptor for tenascin, fibronectin, and vitronectin. J Biol Chem 270:23196–23202.

63. Gopinath SD, Webb AE, Brunet A, Rando TA. 2014. FOXO3 promotes quiescence in adult muscle stem cells during the process of self-renewal. Stem Cell Reports 2:414–426.

64. Fukada S, Uezumi A, Ikemoto M, Masuda S, Segawa M, Tanimura N, Yamamoto H, Miyagoe-Suzuki Y, Takeda S. 2007. Molecular Signature of Quiescent Satellite Cells in Adult Skeletal Muscle. Stem Cells 25:2448–2459.

65. Bjornson CRR, Cheung TH, Liu L, Tripathi P V., Steeper KM, Rando TA. 2012. Notch signaling is necessary to maintain quiescence in adult muscle stem cells. Stem Cells 30:232–242.

66. Philippos M, Sambasivan R, Castel D, Rocheteau P, Bizzarro V, Tajbakhsh S. 2012. A critical requirement for notch signaling in maintenance of the quiescent skeletal muscle stem cell state. Stem Cells 30:243–252.

67. Parker MH, Loretz C, Tyler AE, Duddy WJ, Hall JK, Olwin BB, Bernstein ID, Storb R, Tapscott SJ. 2012. Activation of notch signaling during ex vivo expansion maintains donor muscle cell engraftment. Stem Cells 30:2212–2220.

68. Zalc A, Hayashi S, Auradé F, Bröhl D, Chang T, Mademtzoglou D, Mourikis P, Yao Z, Cao Y, Birchmeier C, Relaix F. 2014. Antagonistic regulation of p57kip2 by Hes/Hey downstream of Notch signaling and muscle regulatory factors regulates skeletal muscle growth arrest. Development 141:2780–90.

69. Bengal E, Ransone L, Scharfmann R, Dwarki VJ, Tapscott SJ, Weintraub H, Verma IM. 1992. Functional antagonism between c-Jun and MyoD proteins: A direct physical association. Cell 68:507–519.

70. Andreucci JJ, Grant D, Cox DM, Tomc LK, Prywes R, Goldhamer DJ, Rodrigues N, Dard PAB, McDermott JC. 2002. Composition and function of AP-1 transcription complexes during muscle cell differentiation. J Biol Chem 277:16426–16432.

71. Alli NS, Yang EC, Miyake T, Aziz A, Collins-Hooper H, Patel K, McDermott JC. 2013. Signal-dependent fra-2 regulation in skeletal muscle reserve and satellite cells. Cell Death Dis 4:e692.

72. Liu D, Black BL, Derynck R. 2001. TGF-B inhibits muscle differentiation through functional repression of myogenic transcription factors by Smad3. Genes Dev 15:2950–2966.

73. Liu D, Kang JS, Derynck R. 2004. TGF-beta-activated Smad3 represses MEF2-dependent transcription in myogenic differentiation. EMBO J 23:1557–66.

74. Schabort EJ, van der Merwe M, Loos B, Moore FP, Niesler CU. 2009. TGF-B's delay skeletal muscle progenitor cell differentiation in an isoform-independent manner. Exp Cell Res 315:373–384.

75. Marchildon F, Lala N, Li G, St.-Louis C, Lamothe D, Keller C, Wiper-Bergeron N. 2012. CCAAT/enhancer binding protein beta is expressed in satellite cells and controls myogenesis. Stem Cells 30:2619–2630.

76. Lee KS, Kim HJ, Li QL, Chi XZ, Ueta C, Komori T, Wozney JM, Kim EG, Choi JY, Ryoo HM, Bae SC. 2000. Runx2 is a common target of transforming growth factor beta1 and bone morphogenetic protein 2, and cooperation between Runx2 and Smad5 induces osteoblast-specific gene expression in the pluripotent mesenchymal precursor cell line C2C12. Mol Cell Biol 20:8783–92.

77. Asakura A, Rudnicki MA, Komaki M. 2001. Muscle satellite cells are multipotential stem cells that exhibit myogenic, osteogenic, and adipogenic differentiation. Differentiation 68:245–253.

78. Gersbach CA, Byers BA, Pavlath GK, García AJ. 2004. Runx2/Cbfa1 stimulates transdifferentiation of primary skeletal myoblasts into a mineralizing osteoblastic phenotype. Exp Cell Res 300:406–417.

79. Lu M-F, Cheng H-T, Lacy AR, Kern MJ, Argao EA, Potter SS, Olson EN, Martin JF. 1999. Paired-Related Homeobox Genes Cooperate in Handplate and Hindlimb Zeugopod Morphogenesis. Dev Biol 205:145–157.

80. Wißmüller S, Kosian T, Wolf M, Finzsch M, Wegner M. 2006. The high-mobility-group domain of Sox proteins interacts with DNA-binding domains of many transcription factors. Nucleic Acids Res 34:1735–1744.

81. Schmidt K, Glaser G, Wernig A, Wegner M, Rosorius O. 2003. Sox8 is a specific marker for muscle satellite cells and inhibits myogenesis. J Biol Chem 278:29769–29775.

82. Brzóska E, Bello V, Darribère T, Moraczewski J. 2006. Integrin α3 subunit participates in myoblast adhesion and fusion in vitro. Differentiation 74:105–118.

83. Liadaki K, Casar JC, Wessen M, Luth ES, Jun S, Gussoni E, Kunkel LM. 2012. B4 Integrin Marks Interstitial Myogenic Progenitor Cells in Adult Murine Skeletal Muscle. J Histochem Cytochem 60:31–44.

84. Seale P, Ishibashi J, Holterman C, Rudnicki MA. 2004. Muscle satellite cell-specific genes identified by genetic profiling of MyoD-deficient myogenic cell. Dev Biol 275:287–300.

85. Ducceschi M, Clifton LG, Stimpson SA, Billin AN. 2014. Post-transcriptional regulation of ITGB6 protein levels in damaged skeletal muscle. J Mol Histol 45:329–336.

86. Mammucari C, Milan G, Romanello V, Masiero E, Rudolf R, Del Piccolo P, Burden SJ, Di Lisi R, Sandri C, Zhao J, Goldberg AL, Schiaffino S, Sandri M. 2007. FoxO3 Controls Autophagy in Skeletal Muscle In Vivo. Cell Metab 6:458–471.

87. Zhao J, Brault JJ, Schild A, Cao P, Sandri M, Schiaffino S, Lecker SH, Goldberg AL. 2007. FoxO3 Coordinately Activates Protein Degradation by the Autophagic/Lysosomal and Proteasomal Pathways in Atrophying Muscle Cells. Cell Metab 6:472–483.

88. Peserico A, Chiacchiera F, Grossi V, Matrone A, Latorre D, Simonatto M, Fusella A, Ryall JG, Finley LWS, Haigis MC, Villani G, Puri PL, Sartorelli V, Simone C. 2013. A novel AMPK-dependent FoxO3A-SIRT3 intramitochondrial complex sensing glucose levels. Cell Mol Life Sci 70:2015–2029.

89. Hagiwara N, Klewer SE, Samson RA, Erickson DT, Lyon MF, Brilliant MH. 2000. Sox6 is a candidate gene for p100H myopathy, heart block, and sudden neonatal death. Proc Natl Acad Sci U S A 97:4180–5.

90. An C-I, Dong Y, Hagiwara N. 2011. Genome-wide mapping of Sox6 binding sites in skeletal muscle reveals both direct and indirect regulation of muscle terminal differentiation by Sox6. BMC Dev Biol 11:59.

91. Rescan PY, Ralliere C. 2010. A Sox5 gene is expressed in the myogenic lineage during trout embryonic development. Int J Dev Biol 54:913–918.

92. Shamblott MJ, Bugg EM, Lawler AM, Gearhart JD. 2002. Craniofacial abnormalities resulting from targeted disruption of the murine Sim2 gene. Dev Dyn 224:373–380.

93. Bothe I, Dietrich S. 2006. The molecular setup of the avian head mesoderm and its implication for craniofacial myogenesis. Dev Dyn 235:2845–2860.

94. Pedrosa-Domellöf F, Eriksson PO, Butler-Browne GS, Thornell LE. 1992. Expression of alpha-cardiac myosin heavy chain in mammalian skeletal muscle. Experientia 48:491–4.

95. Cachaço AS, Pereira CS, Pardal RG, Bajanca F, Thorsteinsdóttir S. 2005. Integrin repertoire on myogenic cells changes during the course of primary myogenesis in the mouse. Dev Dyn 232:1069–1078.

96. Vasyutina E, Stebler J, Brand-Saberi B, Schulz S, Raz E, Birchmeier C. 2005. CXCR4 and Gab1 cooperate to control the development of migrating muscle progenitor cells. Genes Dev 19:2187–98.

97. Chang H, Yoshimoto M, Umeda K, Iwasa T, Mizuno Y, Fukada S, Yamamoto H, Motohashi N, Miyagoe-Suzuki Y, Takeda S, Heike T, Nakahata T. 2009. Generation of transplantable, functional satellite-like cells from mouse embryonic stem cells. FASEB J 23:1907–19.

98. Song WK, Wang WW, Foster RF, Bielser DA, Kaufman SJ. 1992. H36-alpha7 Is a Novel Integrin Alpha-Chain That Is Developmentally Regulated During Skeletal Myogenesis. J Cell Biol 117.

99. Gnocchi VF, White RB, Ono Y, Ellis JA, Zammit PS. 2009. Further characterisation of the molecular signature of quiescent and activated mouse muscle satellite cells. PLoS One 4:e5205.

100. Hicks MR, Hiserodt J, Paras K, Fujiwara W, Eskin A, Jan M, Xi H, Young CS, Evseenko D, Nelson SF, Spencer MJ, Handel B Van, Pyle AD. 2018. ERBB3 and NGFR mark a distinct skeletal muscle progenitor cell in human development and hPSCs. Nat Cell Biol 20:46–57.

101. Albini S, Coutinho P, Malecova B, Giordani L, Savchenko A, Forcales SV, Puri PL. 2013. Epigenetic Reprogramming of Human Embryonic Stem Cells into Skeletal Muscle Cells and Generation of Contractile Myospheres. Cell Rep 3:661–670.

102. Sakurai H, Okawa Y, Inami Y, Nishio N, Isobe K. 2008. Paraxial mesodermal progenitors derived from mouse embryonic stem cells contribute to muscle regeneration via differentiation into muscle satellite cells. Stem Cells 26:1865–1873.

103. Uezumi A, Nakatani M, Ikemoto-Uezumi M, Yamamoto N, Morita M, Yamaguchi A, Yamada H, Kasai T, Masuda S, Narita A, Miyagoe-Suzuki Y, Takeda S, Fukada S ichiro, Nishino I, Tsuchida K. 2016. Cell-Surface Protein Profiling Identifies Distinctive Markers of Progenitor Cells in Human Skeletal Muscle. Stem Cell Reports 7:263–278.

104. Alexander MS, Rozkalne A, Colletta A, Spinazzola JM, Johnson S, Rahimov F, Meng H, Lawlor MW, Estrella E, Kunkel LM, Gussoni E. 2016. CD82 Is a Marker for Prospective Isolation of Human Muscle Satellite Cells and Is Linked to Muscular Dystrophies. Cell Stem Cell 19:800–807.

105. Dearth CL, Goh Q, Marino JS, Cicinelli PA, Torres-Palsa MJ, Pierre P, Worth RG, Pizza FX. 2013. Skeletal muscle cells express ICAM-1 after muscle overload and ICAM-1 contributes to the ensuing hypertrophic response. PLoS One 8:e58486.

106. Moriguchi T, Haraguchi K, Ueda N, Okada M, Furuya T, Akiyama T. 2004. DREG, a developmentally regulated G protein-coupled receptor containing two conserved proteolytic cleavage sites. Genes to Cells 9:549–560.

107. Waller-Evans H, Prömel S, Langenhan T, Dixon J, Zahn D, Colledge WH, Doran J, Carlton MBL, Davies B, Aparicio SAJR, Grosse J, Russ AP. 2010. The orphan adhesion-GPCR GPR126 is required for embryonic development in the mouse. PLoS One 5:e14047.

108. Gassmann M, Casagranda F, Orioli D, Simon H, Lai C, Klein R, Lemke G. 1995. Aberrant neural and cardiac development in mice lacking the ErbB4 neuregulin receptor. Nature 378:390–4.

109. Lee KF, Simon H, Chen H, Bates B, Hung MC, Hauser C. 1995. Requirement for neuregulin receptor erbB2 in neural and cardiac development. Nature 378:394–398.

110. Meyer D, Birchmeier C. 1995. Multiple essential functions of neuregulin in development. Nature 378:386–390.

111. Monk KR, Naylor SG, Glenn TD, Mercurio S, Perlin JR, Dominguez C, Moens CB, Talbot WS. 2009. A G protein-coupled receptor is essential for Schwann cells to initiate myelination. Science 325:1402–5.

112. Andrechek ER, Hardy WR, Girgis-Gabardo AA, Perry RLS, Butler R, Graham FL, Kahn RC, Rudnicki MA, Muller WJ. 2002. ErbB2 is required for muscle spindle and myoblast cell survival. Mol Cell Biol 22:4714–22.

113. Golding JP, Calderbank E, Partridge TA, Beauchamp JR. 2007. Skeletal muscle stem cells express anti-apoptotic ErbB receptors during activation from quiescence. Exp Cell Res 313:341–356.

114. Dollé P, Izpisúa-Belmonte JC, Falkenstein H, Renucci A, Duboule D. 1989. Coordinate expression of the murine Hox-5 complex homoeobox-containing genes during limb pattern formation. Nature 342:767–72.

115. Kahane N, Cinnamon Y, Kalcheim C. 1998. The origin and fate of pioneer myotomal cells in the avian embryo. Mech Dev 74:59–73.

116. Gros J, Scaal M, Marcelle C. 2004. A two-Step mechanism for myotome formation in chick. Dev Cell 6:875–882.

117. Lee ASJ, Harris J, Bate M, Vijayraghavan K, Fisher L, Tajbakhsh S, Duxson M. 2013. Initiation of primary myogenesis in amniote limb muscles. Dev Dyn 242:1043–1055.

118. Gros J, Manceau M, Thomé V, Marcelle C. 2005. A common somitic origin for embryonic muscle progenitors and satellite cells. Nature 435:954–958.

119. Lepper C, Fan CM. 2010. Inducible lineage tracing of Pax7-descendant cells reveals embryonic origin of adult satellite cells. Genesis 48:424–436.

120. Borue X. 2004. Normal and aberrant craniofacial myogenesis by grafted trunk somitic and segmental plate mesoderm. Development 131:3967–3980.

121. Fomenou MD, Scaal M, Stockdale FE, Christ B, Huang R. 2005. Cells of all somitic compartments are determined with respect to segmental identity. Dev Dyn 233:1386–1393.

122. Dias AS, de Almeida I, Belmonte JM, Glazier JA, Stern CD. 2014. Somites without a clock. Science 343:791–795.

123. Qu Z, Huard J. 2000. Matching host muscle and donor myoblasts for myosin heavy chain improves myoblast transfer therapy. Gene Ther 7:428–37.

124. Darabi R, Arpke RW, Irion S, Dimos JT, Grskovic M, Kyba M, Perlingeiro RCR. 2012. Human ES- and iPS-derived myogenic progenitors restore DYSTROPHIN and improve contractility upon transplantation in dystrophic mice. Cell Stem Cell 10:610–619.

125. Charville GW, Cheung TH, Yoo B, Santos PJ, Lee GK, Shrager JB, Rando TA. 2015. Ex vivo expansion and in vivo self-renewal of human muscle stem cells. Stem Cell Reports 5:621–632.

126. Sakurai H, Inami Y, Tamamura Y, Yoshikai T, Sehara-Fujisawa A, Isobe KI. 2009. Bidirectional induction toward paraxial mesodermal derivatives from mouse ES cells in chemically defined medium. Stem Cell Res 3:157–169.

127. Allen RE, Sheehan SM, Taylor RG, Kendall TL, Rice GM. 1995. Hepatocyte growth factor activates quiescent skeletal muscle satellite cells in vitro. J Cell Physiol 165:307–312.

128. Tatsumi R, Anderson JE, Nevoret CJ, Halevy O, Allen RE. 1998. HGF/SF is present in normal adult skeletal muscle and is capable of activating satellite cells. Dev Biol 194:114–128.

129. Fedorov Y V, Jones NC, Olwin BB. 1998. Regulation of myogenesis by fibroblast growth factors requires beta-gamma subunits of pertussis toxin-sensitive G proteins. Mol Cell Biol 18:5780–7.

130. Hall JK, Banks GB, Chamberlain JS, Olwin BB. 2010. Prevention of muscle aging by myofiber-associated satellite cell transplantation. Sci Transl Med 2:57ra83.

131. Gardner S, Gross SM, David LL, Klimek JE, Rotwein P. 2015. Separating myoblast differentiation from muscle cell fusion using IGF-I and the p38 MAP kinase inhibitor SB202190. Am J Physiol - Cell Physiol 309:C491–C500.

132. Zetser A, Gredinger E, Bengal E. 1999. p38 mitogen-activated protein kinase pathway promotes skeletal muscle differentiation. Participation of the Mef2c transcription factor. J Biol Chem 274:5193–5200.

133. Wu Z, Woodring PJ, Bhakta KS, Tamura K, Wen F, Feramisco JR, Karin M, Wang JY, Puri PL. 2000. P38 and Extracellular Signal-Regulated Kinases Regulate the Myogenic Program At Multiple Steps. Mol Cell Biol 20:3951–64.

134. De Angelis L, Zhao J, Andreucci JJ, Olson EN, Cossu G, McDermott JC. 2005. Regulation of vertebrate myotome development by the p38 MAP kinase-MEF2 signaling pathway. Dev Biol 283:171–179.

135. Chen S-E, Jin B, Li Y-P. 2006. TNF- regulates myogenesis and muscle regeneration by activating p38 MAPK. AJP Cell Physiol 292:C1660–C1671.

136. Desgranges P, Barbaud C, Caruelle JP, Barritault D, Gautron J. 1999. A substituted dextran enhances muscle fiber survival and regeneration in ischemic and denervated rat EDL muscle. FASEB J 13:761–766.

137. Zimowska M, Szczepankowska D, Streminska W, Papy D, Tournaire MC, Gautron J, Barritault D, Moraczewski J, Martelly I. 2001. Heparan sulfate mimetics modulate calpain activity during rat Soleus muscle regeneration. J Cell Physiol 188:178–87.

138. Hashimoto T, Kihara M, Sato K, Imai N, Tanaka Y, Sakai M, Tamura K, Hirawa N, Toya Y, Kitamura H, Umemura S. 2005. Heparin recovers AT1 receptor and its intracellular signal transduction in cultured vascular smooth muscle cells. FEBS Lett 579:281–284.

139. Horbelt D, Boergermann JH, Chaikuad A, Alfano I, Williams E, Lukonin I, Timmel T, Bullock AN, Knaus P. 2015. Small molecules dorsomorphin and LDN-193189 inhibit myostatin/GDF8 signaling and promote functional myoblast differentiation. J Biol Chem 290:3390–3404.

140. Cusella-De Angelis MG, Molinari S, Le Donne A, Coletta M, Vivarelli E, Bouche M, Molinaro M, Ferrari S, Cossu G. 1994. Differential response of embryonic and fetal myoblasts to TGF beta: a possible regulatory mechanism of skeletal muscle histogenesis. Development 120:925–933.

141. Biressi S, Tagliafico E, Lamorte G, Monteverde S, Tenedini E, Roncaglia E, Ferrari S, Ferrari S, Cusella-De Angelis MG, Tajbakhsh S, Cossu G. 2007. Intrinsic phenotypic diversity of embryonic and fetal myoblasts is revealed by genome-wide gene expression analysis on purified cells. Dev Biol 304:633–651.

142. Sharan R, Shamir R. 2000. CLICK: a clustering algorithm with applications to gene expression analysis. Proc Int Conf Intell Syst Mol Biol 8:307–16.

143. Mi H, Huang X, Muruganujan A, Tang H, Mills C, Kang D, Thomas PD. 2017. PANTHER version 11: Expanded annotation data from Gene Ontology and Reactome pathways, and data analysis tool enhancements. Nucleic Acids Res 45:D183–D189.

144. Kwon AT, Arenillas DJ, Worsley Hunt R, Wasserman WW. 2012. oPOSSUM-3: advanced analysis of regulatory motif over-representation across genes or ChIP-Seq datasets. G3 (Bethesda) 2:987–1002.

Chapter 4: Assessing the *in vivo* engraftment potential of human embryonic stem cell-derived myogenic cultures in immunodeficient mouse muscle

4.1 Objective of this study

Human embryonic stem cells could be efficiently differentiated into skeletal muscle progenitors and skeletal myocytes. It remains to be seen whether or not the embryonic-derived myogenic cultures could transplant into damaged muscle and enhance repair or function. Demonstrating that the skeletal muscle progenitors could engraft in mouse models is an essential step towards supporting the cells' use in patient-oriented stem cell therapy.

4.2 Statement of author contributions

M. S., I. S. S., and A. B. were responsible for experimental design. M. S. carried out the experiments and wrote the manuscript with I. S. S. and A. B. providing supervision. A. K. developed the procedure to passage differentiating myogenic cultures. W. L. S. provided and J. L. cultured pluripotent hESCs.

4.3 Myogenic cultures derived from H9 human embryonic stem cells persist within the NOD.Cg-Prkdc^{scid} Il2rg^{tm1Wjl}/SzJ mouse tibialis anterior but contribute little to host myofibers

Michael Shelton[1], Avetik Kocharyan[1,2], Jun Liu[1], William L. Stanford[1,2,3,4], Alexandre Blais[1], Ilona S. Skerjanc[1*]

[1]Department of Biochemistry, Microbiology, and Immunology, University of Ottawa, Ottawa, Ontario, K1H 8M5, Canada

[2]The Sprott Center for Stem Cell Research, Regenerative Medicine Program, Ottawa Hospital Research Institute, Ottawa, ON K1H 8L6, Canada

[3]Department of Cellular and Molecular Medicine, University of Ottawa, Ottawa, Ontario, K1H 8L6, Canada

[4]Faculty of Graduate and Postdoctoral Studies, University of Ottawa, Ottawa, Ontario, K1N 6N5, Canada

*Corresponding author Dr. Ilona S. Skerjanc: iskerjan@uottawa.ca, Tel: 613-562-5800 Ext. 8669; Fax: 613-562-5452.

4.4 Summary

A 50-day skeletal muscle differentiation protocol was recently developed for human embryonic stem cell (hESC) capable of generating large quantities of myogenic material for study (1, 2). In order for these myogenic cultures to ultimately contribute to stem cell therapy—the treatment of injured or pathological patient muscle—their *in vivo* efficacy must first be demonstrated. Cells (1×10^6) from days 10, 35, and 50 of the differentiation time course were injected into the cardiotoxin-injured tibialis anterior (TA) muscles of immunodeficient NSG mice, and the presence of human-derived nuclei, myofibers, and satellite cells was assessed at 30 days post-injection (DPI). Too few human cells were observed to be meaningfully quantified in the TA of animals where day 10 or 35 cultures were injected. Approximately 6.2 ± 2.4% of the total cells per TA section stained human-$LMNA^+$ in muscles injected with day 50 cultures. However, the majority of human cells remained interstitial of myofibers, as determined by the cells' position outside the basal lamina; fewer than 10 human cells per section were observed encircled in laminin. Furthermore, no PAX7 expression was observed overlapping with the human cells. Passing differentiating cultures prior to *in vivo* transplantation (Appendix 1)(2), re-injury of the TA at 30 DPI with later analysis at 60 DPI, or barium chloride ($BaCl_2$) rather than cardiotoxin injury did not improve engraftment results. These results suggest that day 50 myogenic cultures may have a limited capacity to contribute to the adult muscle environment. Extended culture time or additional supplemental factors may be required *in vitro* to mature the hESC-derived myogenic cultures to a more fusion-competent developmental stage.

4.5 Introduction

Stem cell therapy—the treatment of damaged or dysfunctional tissue by transplanting progenitor cells of said tissue—is one prospective avenue to treat muscle injury and muscle wasting disorders such as Duchenne Muscular Dystrophy. Two of the greatest challenges currently faced by muscle stem cell therapy are obtaining large enough quantities of suitable donor cells, and efficiently delivering donor cells to the patients' affected muscle. Many recent works aim to address the former challenge (reviewed in (3)). An *in vitro* differentiation protocol for human embryonic stem cells (hESC) was recently developed that generated myogenic cultures wherein roughly 43% of cells were expandable $PAX7^+$ skeletal muscle progenitors (SMP) and 47% MYH^+ skeletal myocytes (Chapter 2)(1, 2).

PAX7 expression marks the population of adult muscle progenitors—known as satellite cells—that are capable of both contributing to muscle repair and self-replenishment. $PAX7^+$ satellite cells remain quiescent in uninjured muscle, and in response to damage, become activated to proliferate and differentiate. A subset of $PAX7^+$ cells will remain undifferentiated as a result of asymmetric cell division (4), where one daughter cell retains its PAX7 expression while the other will increasingly downregulate PAX7 and express the myogenic regulatory factors (MRF) MYF5, MYOD1, MYF6, and MYOG. Once this commitment occurs, the myoblast can no longer self-replenish and cannot contribute to future rounds of muscle repair (5).Thus, PAX7 expression is an essential characteristic of myogenic donor cells being considered for efficient long-term stem cell therapy, as myoblasts that have differentiated beyond the point of PAX7 expression would deplete in the host muscle.

Given the large proportion of PAX7$^{\pm}$ SMPs present in hESC-derived myogenic cultures using the Shelton *et al.* protocol, the cultures may have promising *in vivo* transplantation potential that could be examined in the injured muscle of NOD.Cg-Prkdc^{scid} Il2rg^{tm1Wjl}/SzJ (NSG) immunodeficient mice.

Xenotransplantation of human SMPs into immune deficient mice, however, appears a widespread technical challenge in the field of skeletal muscle stem cell therapy. SMPs derived from chemically directed hESC differentiations often engraft at rates too low to be meaningfully quantified *in vivo* (6–8), or the *in vivo* potential of hESC-derived SMPs is not assessed at all (9–17).

Perhaps the most robust example of hESC-derived SMP *in vivo* engraftment comes from cells differentiated via the inducible over-expression of key myogenic genes. Cells derived from hESCs by inducible MYOD1 over-expression manage appreciable engraftment resulting in 50 – 140 human spectrin-positive fibers per tibialis anterior (TA) section (18, 19). However, MYOD1 over-expression places these cells beyond the therapeutically-ideal PAX7^{+} SMP stage of development, and would limit the cells' potential to self-replenish and fill the satellite cell niche (5, 20). SMPs generated from hESCs via inducible PAX7 over-expression contribute to about 110 myofibers and 7% of all satellite cells per TA cross section in NSG-mdx^{4Cv} mice, while significantly improving absolute and specific force of the recipient muscle (21).

The *Shelton et al.* protocol aimed to generate PAX7-expressing SMPs absent of genetic alteration, however. Gene expression profiling between day 50 hESC-derived myogenic cultures and satellite cells showed that day 50 cultures displayed a more quiescent-like rather than activated profile (Chapter 3). Given that satellite cell quiescence correlates with more effective *in vivo* transplantation potential (20, 22), ultimately, the myogenic

cultures generated using this hESC differentiation protocol may have the potential to effectively contribute to muscle repair with stem cell therapy. In order for stem cell therapy to be considered effective, donor human cells should contribute $PAX7^+$ cells to the satellite cell niche, and should contribute to the host muscle fibers. Ideally, donor-derived $PAX7^+$ cells should contribute to future rounds of muscle repair and self-replenish within the satellite cell nice in response to a second injury.

4.6 Results

4.6.1 CHIR99021-differentiated hESCs—but not spontaneously differentiated controls—persistently reside in the NSG mouse TA muscle up to 30 days post injection

Other groups have shown *in vivo* engraftment with the early $PDGFRA^+$ presomitic-like mesoderm population from mouse embryonic stem cells (mESC)(23–25), and hESCs (6), undergoing *in vitro* skeletal myogenesis. Therefore, the engraftment efficiency of differentiated hESCs was explored as early as day 10: a time point of the highest overlapping expression of presomitic mesoderm markers MEOX1, PAX3, and PDGFRA (1). The *in vivo* potential was investigated at later stages of differentiation—day 35 and 50 cultures—when $PAX7^+$ SMPs and skeletal myocytes become abundant (1, 2).

Briefly, pluripotent hESCs were differentiated into a population enriched for cells expressing paraxial mesoderm associated genes—MSGN1 and TBX6—by culturing cells with 10 μM of CHIR99021 for 2 days (1, 2). CHIR99021 was removed from the media as cultures continued to differentiate for an additional 8 days before collecting the day 10 sample. Cells for the day 35 and 50 time points were grown in FGF2-supplemented StemPro-34 from days 12 – 20, then returned to E6 media from days 20 – 35, and N2-ITS media from days 35 – 50. The TA muscles of NSG mice were injured with cardiotoxin 1 day prior to

receiving 1×10^6 day 10, 35, or 50 CHIR99021-differentiated hESCs, day 10 spontaneously-differentiated control hESCs, or DPBS control. The TA muscles of mice that received day 10 CHIR99021-differentiated hESCs were then harvested at 7 and 30 days post injection (DPI), while TA muscles receiving day 35 and 50 cells were harvested at 30 DPI.

Day 10 CHIR99021-differentiated hESCs were primarily detected within the endomysium or interstitial space outside the basal lamina at 7 DPI, with few cells encircled in laminin (Fig. 4.1, white arrows). Interestingly, no day 10 control hESCs—spontaneously differentiated with DMSO in place of CHIR99021—were observed in the muscle. This suggests that CHIR99021-differentiated cells expressing MEOX1, PAX3, and PDGFRA may be more prone to retention in the host tissue, despite the relative lack of human cells contributing to host myofibers and the lack of overlap in a co-stain with antibodies against human nuclei and PAX7 (Fig. 4.2). In contrast with the numerous day 10 cells detected at 7 DPI (Fig. 4.1), fewer than 10 human cells per section were observed at 30 DPI, and only in the interstitial space (Fig. 4.3, upper panels). More human cells were observed at 30 DPI with day 35 compared to day 10 differentiated hESCs (Fig. 4.3, middle panels), and greater numbers yet with day 50 cells (Fig. 4.3, lower panels). These cells too were confined to the interstitial space and did not overlap with PAX7 expression (Data not shown).

4.6.2 Collagenase-based dissociation—compared to TrypLE—permits greater human cell retention after 30 DPI in NSG mouse TA muscle

A method to passage cultures as they differentiate was recently developed (Appendix 1)(2). This may select for cells that better tolerate dissociation, which could show greater viability *in vivo*. Collagenase IV-based dissociation of differentiating cultures also better supported continued myogenic development upon re-plating *in vitro* compared to

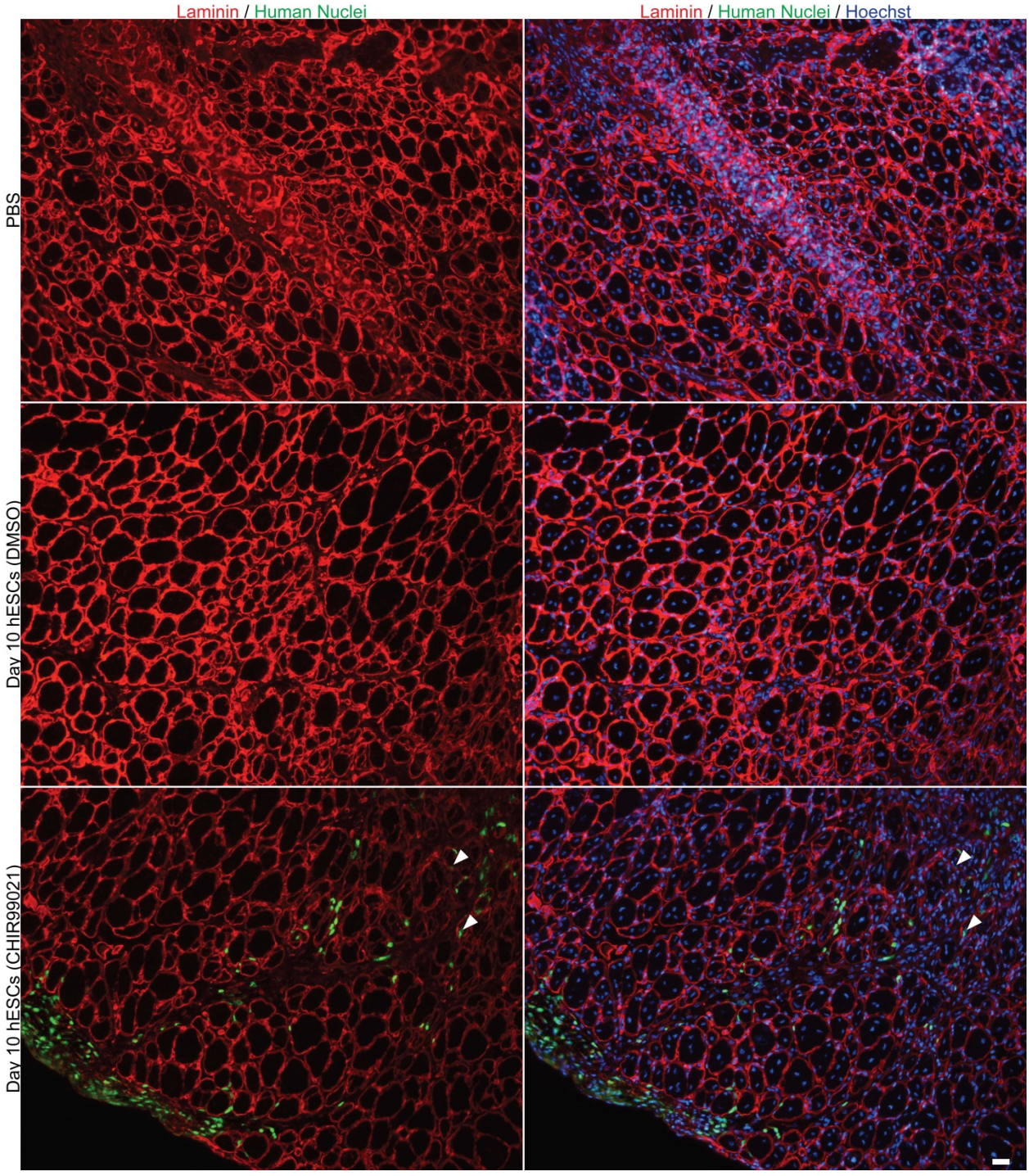
Laminin / Human Nuclei
Laminin / Human Nuclei / Hoechst
PBS
Day 10 hESCs (DMSO)
Day 10 hESCs (CHIR99021)

Figure 4.1

Figure 4.1. Day 10 CHIR99021-differentiated hESCs reside in the interstitial spaces of recipient NSG murine muscle 7 DPI. The tibialis anterior muscles of NSG mice were injured with 30 μL of 0.1 μM cardiotoxin 1 day prior to receiving H9 cell injections. Cells were differentiated as in Shelton *et al.* until day 10 (1). On the day of injection, cells were lifted in TrypLE for 10 minutes and filtered with a 70 μm screen. 1.0×10^6 cells were injected in 30 μL DPBS per animal. 1.0×10^6 DMSO-differentiated day 10 cells and DPBS were used as controls. Muscles were harvested at 7 DPI and stained with antibodies against laminin (red), human nuclei (green), and Hoechst dye (blue) to visualize all nuclei (n = 3, scale bar = 20 μm). Only CHIR99021-differentiated cells persist in the muscle, with some human cells appearing encircled in laminin rings (white arrows).

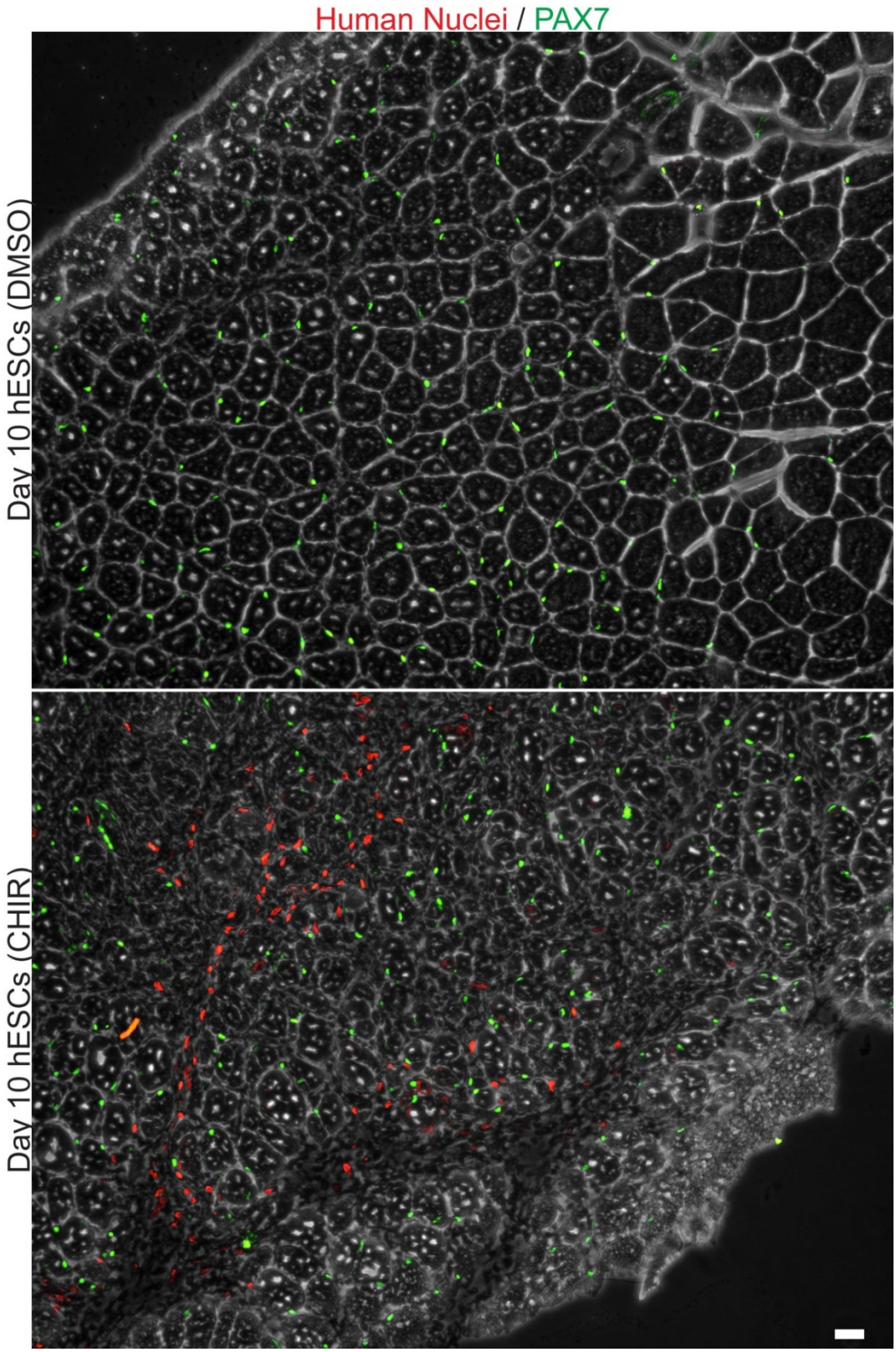

Figure 4.2

Figure 4.2 Day 10 CHIR99021-differentiated hESCs do not overlap with PAX7 expression 7 DPI. Muscle sections from Figure 4.1 were stained with antibodies against human LMNA (red), and PAX7 (green) (n = 3, scale bar = 20 μm). No overlap was detected between human nuclei and PAX7 staining.

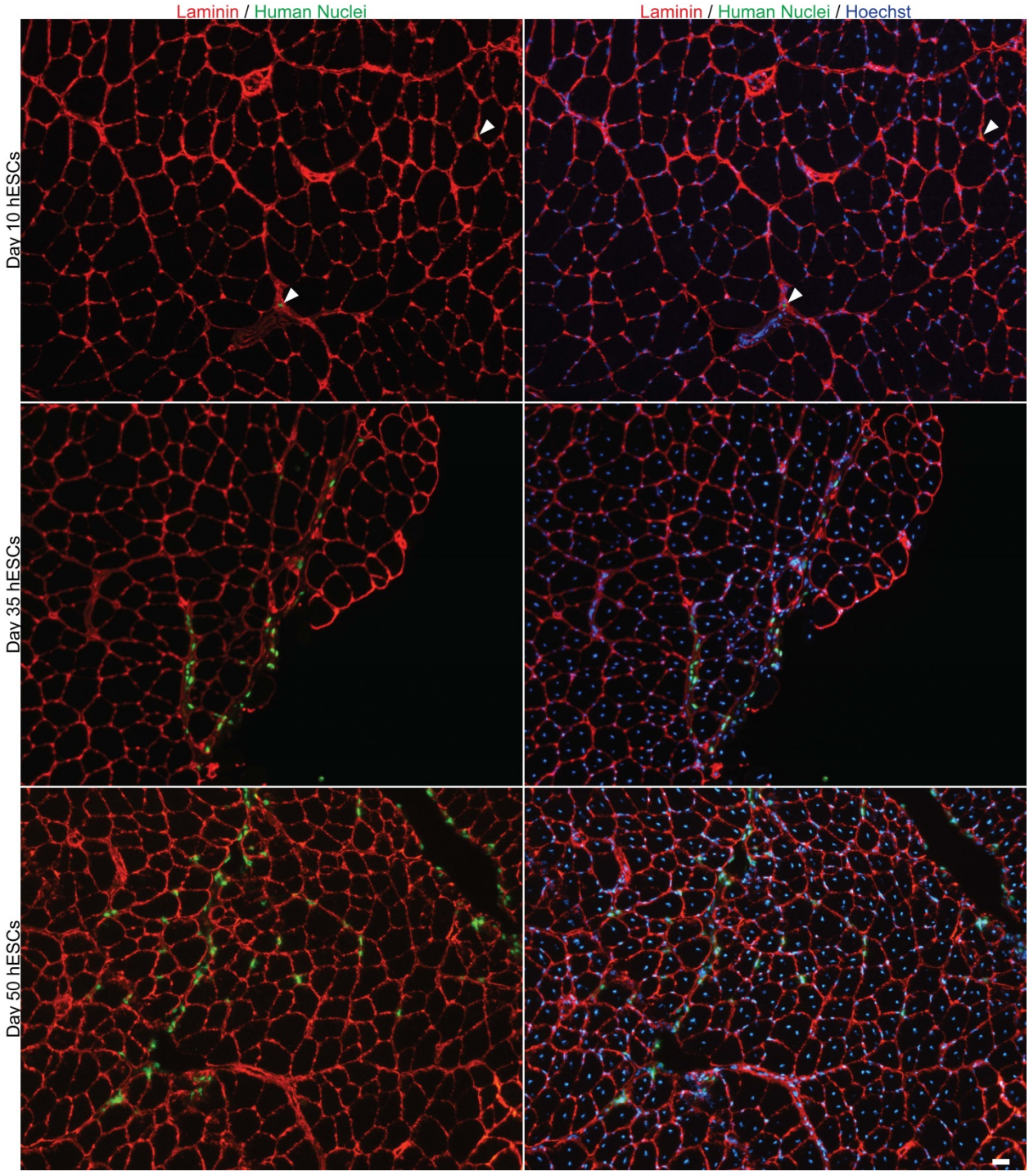
Laminin / Human Nuclei
Laminin / Human Nuclei / Hoechst
Day 10 hESCs
Day 35 hESCs
Day 50 hESCs

Figure 4.3

Figure 4.3. Longer differentiated hESCs better persist in NSG murine muscle 30 DPI. The tibialis anterior muscles of NSG mice were injured with 30 μL of 0.1 μM cardiotoxin 1 day prior to receiving H9 cell injections. Cells were differentiated as in Shelton *et al*. until day 10, 35, and 50 (1). On the days of injection, cells were lifted in TrypLE for 10 minutes and filtered with a 70 μm screen. 1.0×10^6 cells were injected in 30 μL DPBS per animal. Muscles were harvested at 30 DPI and stained with antibodies against laminin (red), human nuclei (green), and Hoechst dye (blue) to visualize all nuclei (n = 3, scale bar = 20 μm). In contrast with the numerous day 10 cells detected at 7 DPI, few day 10 human cells were detected at 30 DPI (upper panels, white arrows).

TrypLE (2). Therefore, *in vivo* transplant was attempted with passaged as well as unpassed cultures, using collagenase IV to dissociate cultures for transplant in place of TrypLE.

Day 50 hESCs—with passage at day 20 and 35, or without any passage—were injected into the cardiotoxin-preinjured TA muscles of NSG mice. The TA muscles of some animals were harvested at 30 DPI (Fig. 4.4); other animals were reinjured at 30 DPI with cardiotoxin to encourage further activation and integration of donor human cells, and the TA muscles then harvested at 60 DPI (Fig 4.5).

Contrary to the hypothesis, a greater number of human cells were observed with unpassed cultures compared to passed cultures at both 30 and 60 DPI, though the difference was not significant (Fig. 4.6). In several cases, human cells accumulate in the crural fascia between the TA and extensor digitorum longus (EDL) muscles (Fig. 4.4 & 4.5, white arrows). Other human cells that were distributed throughout the TA were primarily found in the interstitial space outside the basement membrane, as judged by their position in relation to the basal lamina (Fig. 4.4 & 4.5). In the mice receiving cells from unpassed cultures, human nuclear marker was observed in myonuclei of the TA and EDL at 60 DPI (Fig. 4.7 & 4.8, lower panels). Human cells were also seen encircled in laminin at 30 DPI in what might be small nascent human-only muscle fibers (Fig. 4.7 & 4.8, upper panels). However, the frequency of human nuclei encircled in laminin was fewer than 10 events per muscle section. Similar to previous results, no $PAX7^+$ human cells were detected (data not shown).

4.6.3 PAX7-expressing human SMPs were not observed as shortly as 1 DPI

$PAX7^+$ human cells were not observed in the previous experiments under any condition tested. Furthermore, few human cells were detected within myofibers or beneath the basal lamina as most were interstitial or intermuscular. Therefore, a series of shorter-

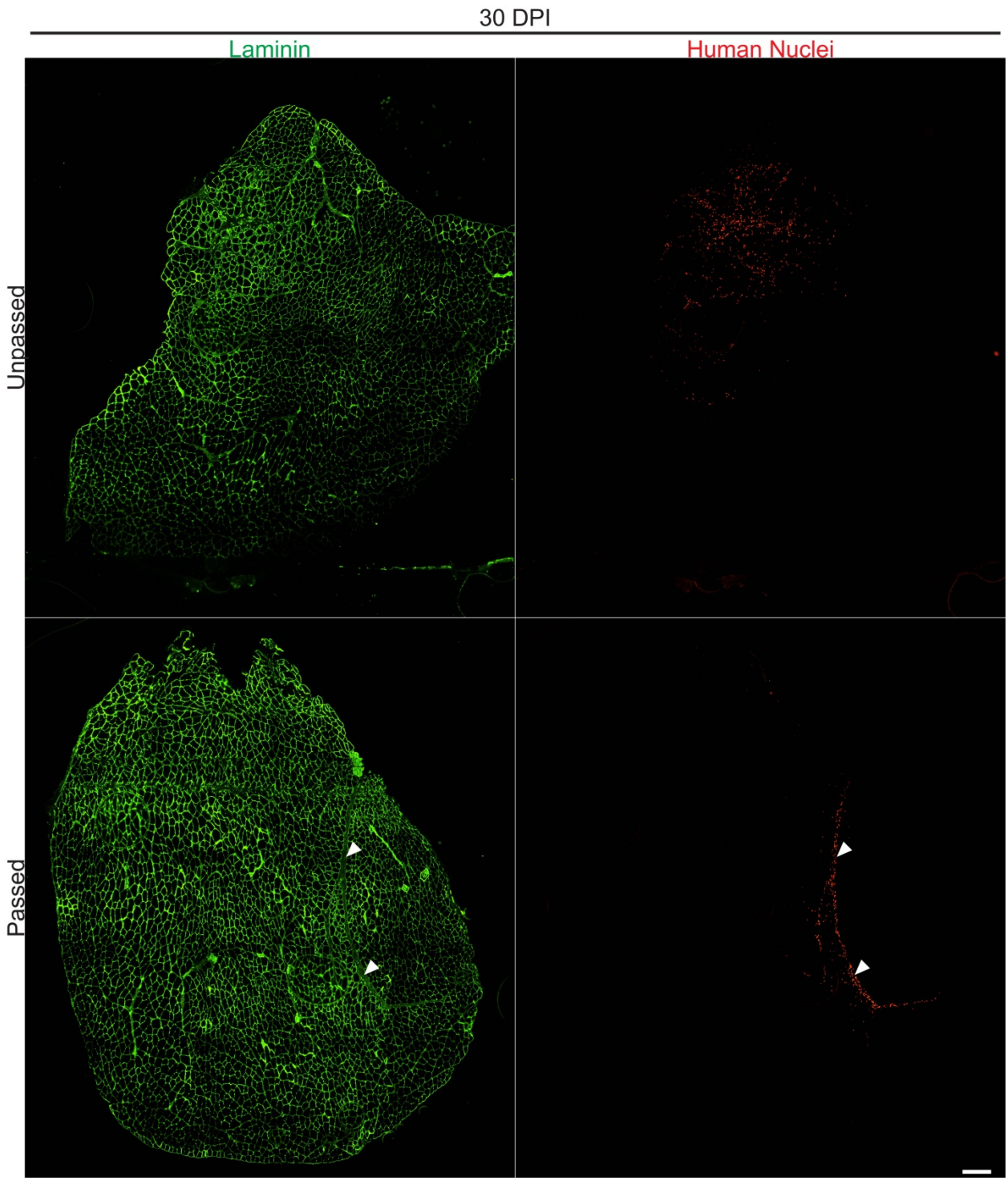

Figure 4.4

Figure 4.4. Unpassed day 50 cultures result in greater numbers of persistent donor hESCs than passed cultures in NSG murine muscle at 30 DPI. The tibialis anterior muscles of NSG mice were injured with 30 μL of 0.1 μM cardiotoxin 1 day prior to receiving H9 cell injections. Cells were differentiated as in Shelton *et al.* until day 50 (1), or until day 50 with passage on days 20 and 35 as in Shelton *et al*. (Appendix 1)(2). On the days of injection, cells were lifted in Collagenase IV for 40 minutes. 1.0×10^6 cells were injected in 30 μL DPBS per TA muscle. One set of muscles were harvested at 30 DPI. Muscle sections were stained with antibodies against laminin (green) and human LMNA (red). White arrows indicate crural fascia between the tibialis anterior and extensor digitorum longus muscle (n = 3, scale bar = 200 μm).

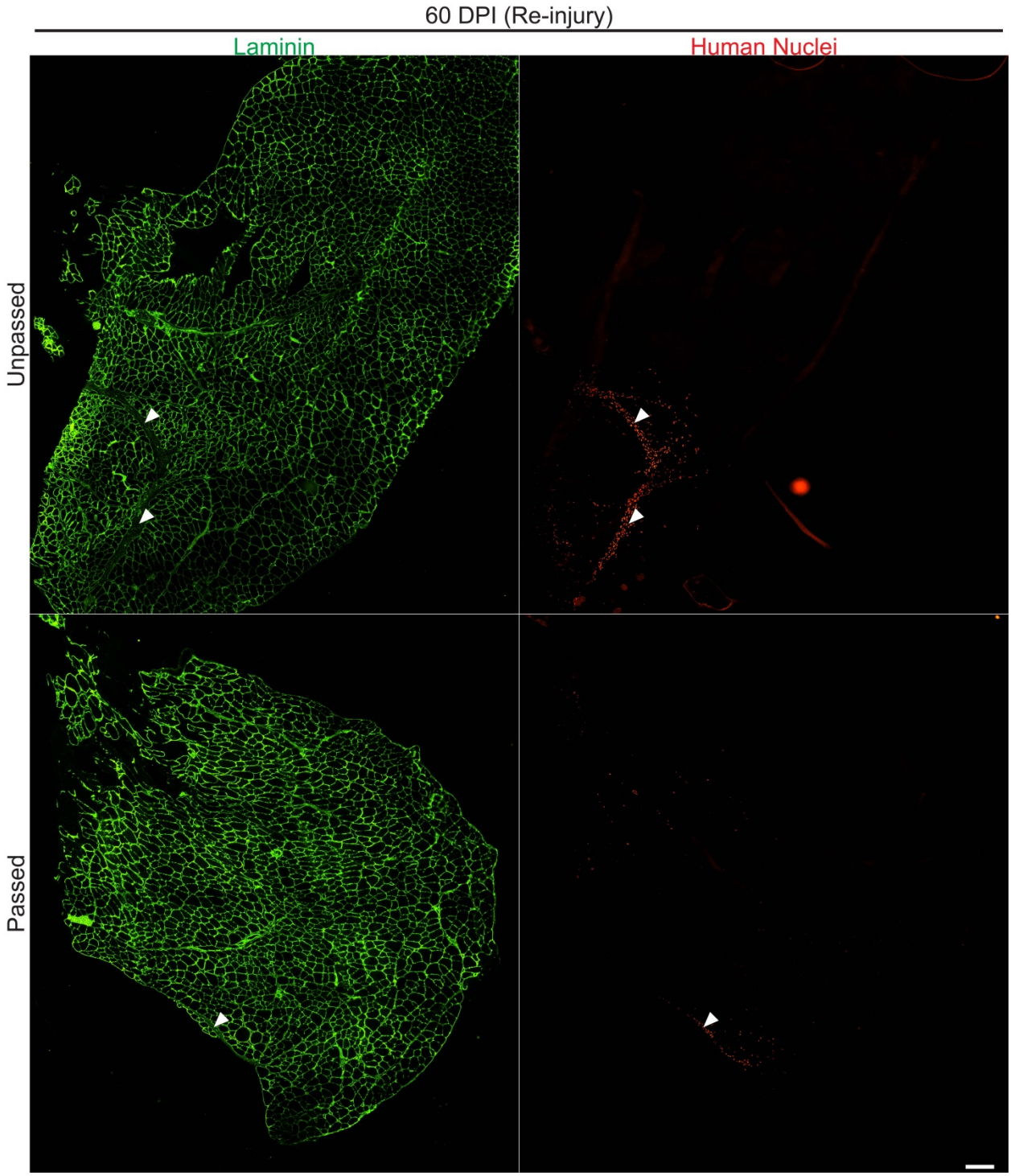

Figure 4.5

Figure 4.5. Unpassed day 50 cultures result in greater numbers of persistent donor hESCs than passed cultures in NSG murine muscle at 60 DPI. The tibialis anterior muscles of NSG mice were injured with 30 μL of 0.1 μM cardiotoxin 1 day prior to receiving H9 cell injections. Cells were differentiated as in Shelton et al. (1) until day 50, or until day 50 with passage on days 20 and 35 as in Shelton et al. (2). On the days of injection, cells were lifted in Collagenase IV for 40 minutes. 1.0×10^6 cells were injected in 30 μL DPBS per TA muscle. One set of muscles were re-injured at 30 DPI with cardiotoxin to stimulate muscle regeneration, and were harvested at 60 DPI. Muscle sections were stained with antibodies against laminin (green) and human LMNA (red). White arrows indicate crural fascia between the tibialis anterior and extensor digitorum longus muscle (n = 3, scale bar = 200 μm).

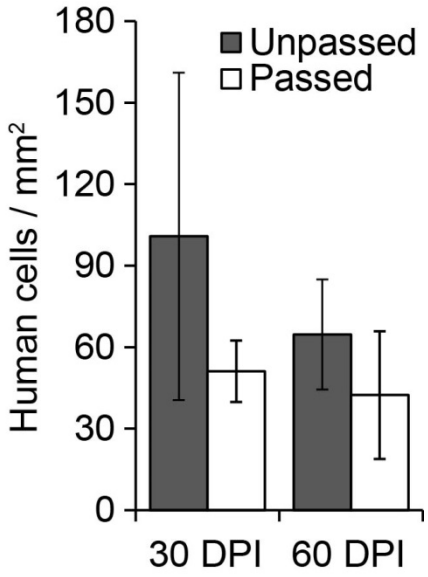
180
150
120
90
60
30
0
Human cells / mm2
Unpassed
Passed
30 DPI
60 DPI

Figure 4.6

Figure 4.6. Quantification shows unpassed compared to passed day 50 cultures trend towards greater numbers in NSG murine muscle at both 30 and 60 DPI. Human LMNA positive cells from Figure 4.4 and 4.5 were quantified and expressed relative to cross-sectional muscle area. Though a trend of more cell retention was observed with unpassed cultures, two-way ANOVA determined the difference was insignificant ($F_{(1,8)} = 1.28$, $p = 0.29$), as was the difference between 30 DPI versus re-injured 60 DPI human cell numbers ($F_{(1,8)} = 3.29$, $p = 0.11$) and the variables' interaction ($F_{(1,8)} = 0.48$, $p = 0.51$)($n = 3$).

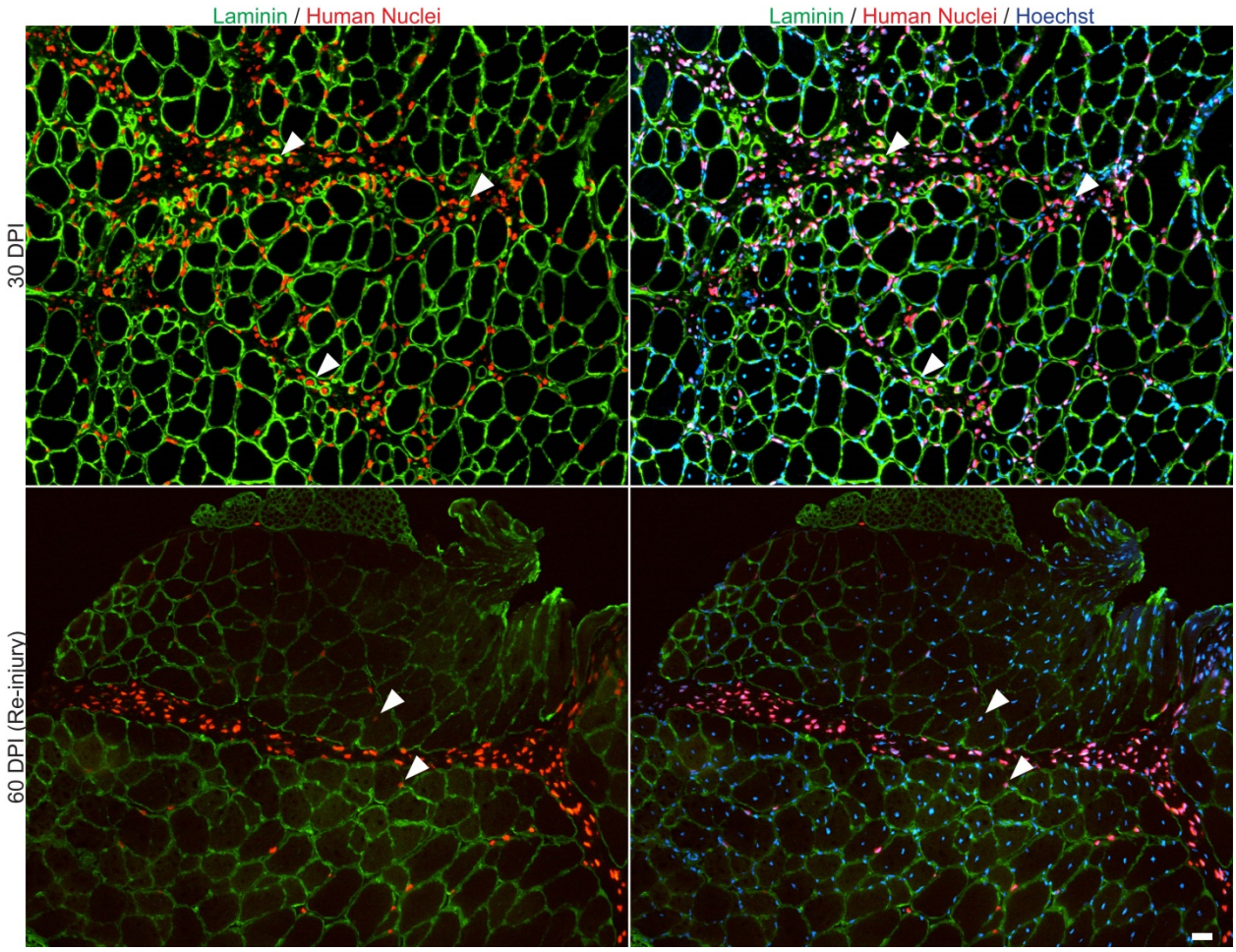
Laminin / Human Nuclei
Laminin / Human Nuclei / Hoechst
30 DPI
60 DPI (Re-injury)

Figure 4.7

Figure 4.7. Fewer than 10 hESC donor-contributed myofibers per section may be seen with day 50 cultures at 30 and 60 DPI. Muscles receiving unpassed day 50 hESCs from Figure 4.4 & 4.5 contained some sub-laminin donor cells (white arrows). Human cells were detected directly beneath the basal lamina, centralized in the myofiber, or within small myofibers (n = 3, scale bar = 200 μm).

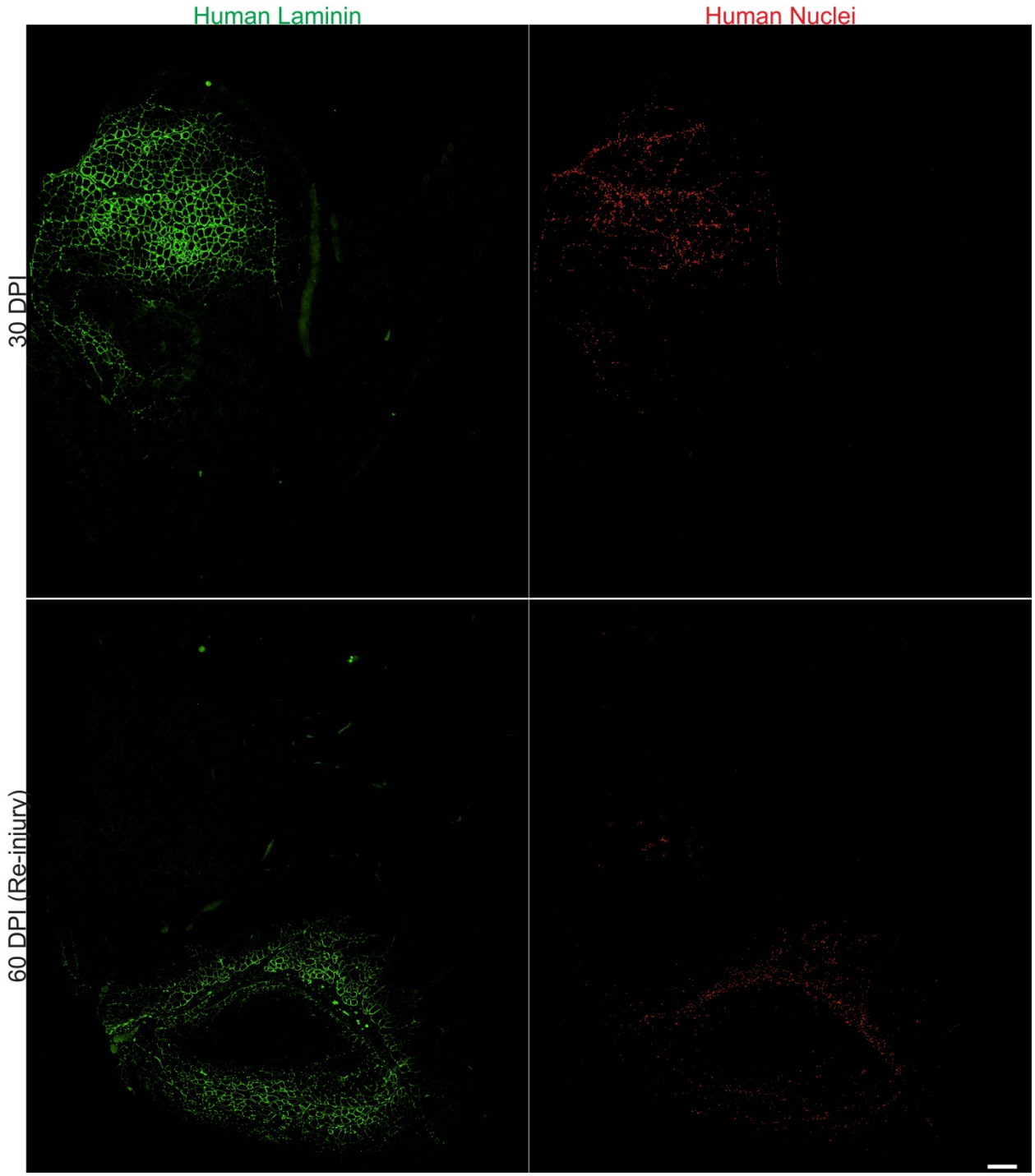

Figure 4.8

Figure 4.8. Robust human laminin staining was detected surrounding areas of interstitial human cells. Muscles receiving unpassed cultures and then harvested at 30 DPI (Fig. 4.4) and 60 DPI (Fig. 4.5) were stained with antibodies against human LAMC1 (green) and human LMNA (red). Extensive human laminin deposition was detected in the areas proximal to donor human cells (n = 3, scale bar = 200 μm).

duration *in vivo* experiments were performed in order to determine where *in vitro* $PAX7^+$ donor cells reside shortly after transplant, and when PAX7 expression or $PAX7^+$ cells may be lost. In addition to cardiotoxin injury, a set of animals was preinjured with barium chloride ($BaCl_2$) instead of cardiotoxin to determine if $BaCl_2$ damage was more supportive of donor human cell engraftment (26, 27).

Cells were differentiated to day 65 with passage every 15 days beginning at day 20, with 0.7×10^6 cells injected per TA muscle. TA muscles were harvested at 1, 4, and 7 DPI in cardiotoxin-injured animals (Fig. 4.9), and 1, 4, 7, and 30 DPI with $BaCl_2$ injury (Fig. 4.10). Consistent with previous experiments using cardiotoxin injury, human donor cells were primarily observed outside the basal lamina or within the crural fascia outside the TA muscle (Fig. 4.9). An increase in total $PAX7^+$ cells was seen during muscle regeneration at 4 and 7 DPI, however, no $PAX7^+$ human cells were detected in the cardiotoxin injured animals. Animals that received $BaCl_2$ injury presented a similar increase in total $PAX7^+$ cell number at 4 and 7 DPI, with fewer than 10 human donor cells co-staining with PAX7 at the injection site 4 DPI (Fig. 4.10, white arrows). Similar to cardiotoxin injured muscle, human donor cells persisted within the host muscle out to 30 DPI, but the human cells were observed in interstitial locations.

4.7 Discussion & Future Direction

Despite hundreds of human cells persisting within recipient NSG murine muscle (Fig. 4.4 & 4.5), and despite the promising indications towards a quiescent-like phenotype of day 50 myogenic hESC-derived cultures (Chapter 3), human cells did not meaningfully engraft into the muscle fibers nor populate the satellite cell niche. The most favorable experimental conditions—30 DPI of unpassed day 50 human cultures—resulted in 6.2% of the total nuclei

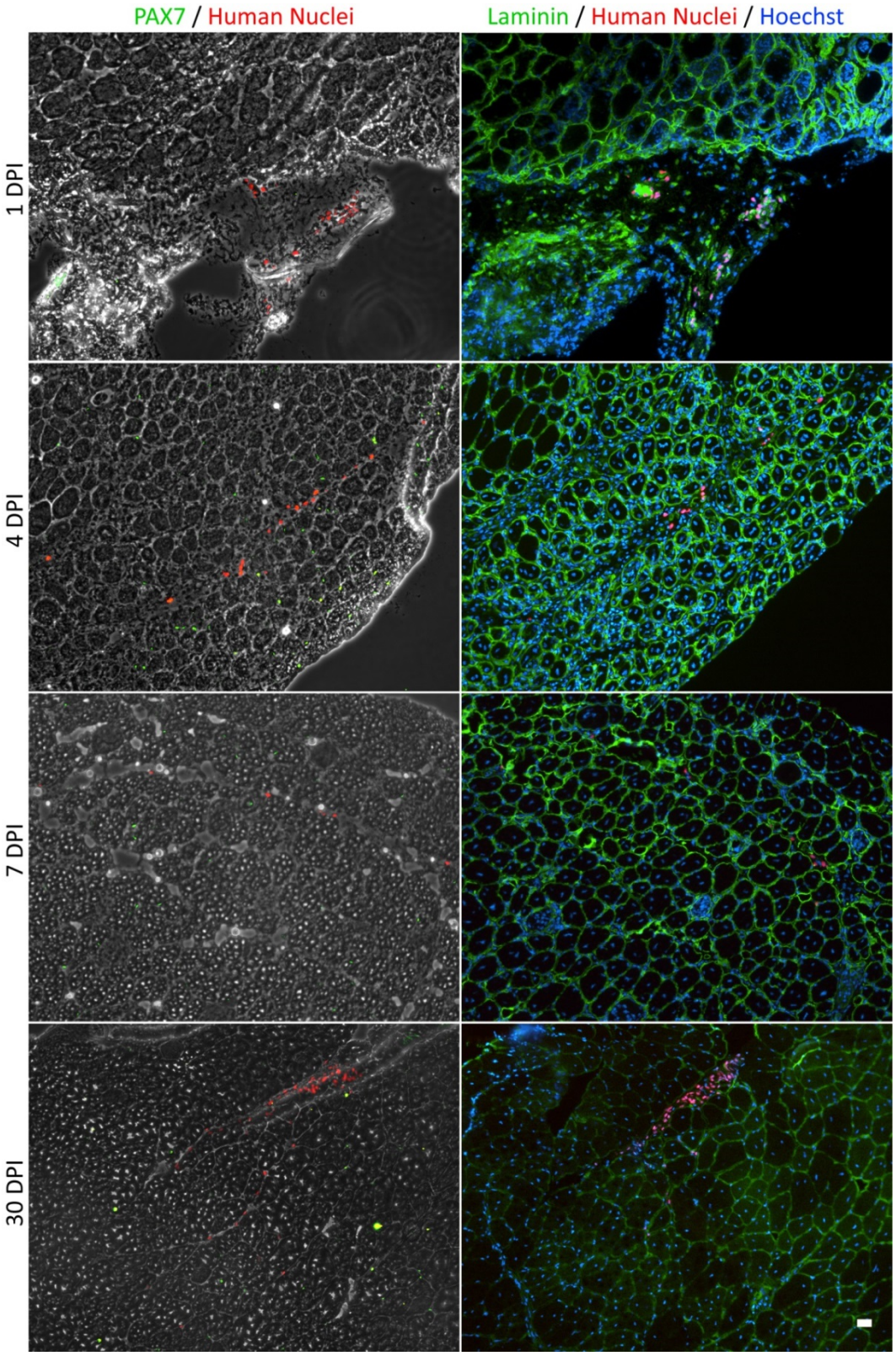
PAX7 / Human Nuclei
Laminin / Human Nuclei / Hoechst
1 DPI
4 DPI
7 DPI
30 DPI

Figure 4.9

Figure 4.9. No hESC donor cells co-stain with PAX7 and are confined to interstitial spaces of recipient NSG murine muscle regardless of cardiotoxin injury. The tibialis anterior muscle of NSG mice was injured with 30 μL of 10 μM cardiotoxin 1 day prior to receiving H9 cell injections. Cells were differentiated as in Shelton *et al.* until day 65 with passage every 15 days beginning at day 20 (2). On the day of injection, cells were lifted in collagenase IV for 40 minutes. 7.5×10^5 cells were injected in 30 μL DPBS per animal. Muscles were harvested at 1, 4, 7 DPI with cardiotoxin. Few PAX7 co-stained human cells were observed at 4 DPI with barium chloride injury (white arrows). The 30 DPI cardiotoxin images were taken from a previous experiment (n = 3, scale bar = 20 μm).

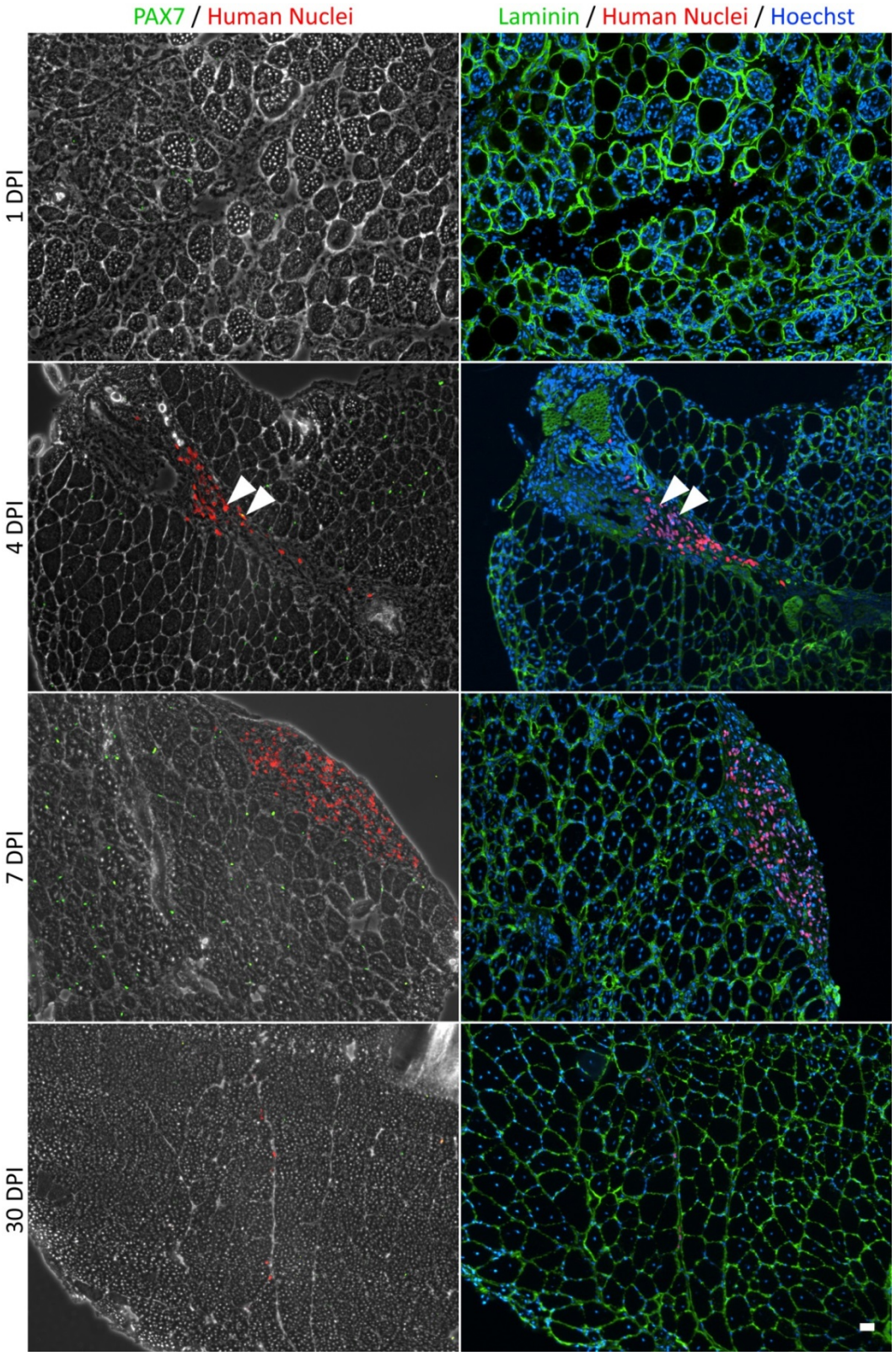
PAX7 / Human Nuclei
Laminin / Human Nuclei / Hoechst
1 DPI
4 DPI
7 DPI
30 DPI

Figure 4.10

Figure 4.10. Fewer than 10 hESC donor cells co-stain with PAX7 and are confined to interstitial spaces of recipient NSG murine muscle regardless of barium chloride injury. The tibialis anterior muscle of NSG mice was injured with 30 μL of 0.1% barium chloride 1 day prior to receiving H9 cell injections. Cells were differentiated as in Shelton *et al.* (2) until day 65 with passage every 15 days beginning at day 20. On the day of injection, cells were lifted in collagenase IV for 40 minutes. 7.5×10^5 cells were injected in 30 μL DPBS per animal. Muscles were harvested at 1, 4, 7, and 30 DPI. Few PAX7 co-stained human cells were observed at 4 DPI with barium chloride injury (white arrows)(n = 3, scale bar = 20 μm).

per TA cross section being of human origin, yet the number of human cells encircled in laminin was orders of magnitude less frequent, with fewer than 10 events per section. Future experiments could include freshly isolated adult murine or human fetal myoblasts as technical or biological positive controls. Functional tests could also be performed after transplantation, such as measures of contractile force between cell-injected versus PBS-injected control muscle, to determine if human cells confer a functional enhancement not reflected in immunofluorescent staining. It is also possible that the SMPs derived via chemically directed differentiation are too relatively immature to participate in the adult muscle environment, whereas transgenic overexpression of the key regulators PAX7 or MYOD1 expedite developmental progression, and gives the cells a more mature identity capable of functional integration *in vivo*.

Early studies of human embryonic and fetal limb muscle highlights the differences that developmental age can have regarding a myogenic population's potential for growth and fusion (28). Myoblasts taken from 7 and 18 weeks of development—then single cells cultured clonally for an additional week *in vitro*—show marked differences in their propensity to fuse into myotubes. At 7 weeks, the majority of myoblasts went on to express embryonic myosin (MYH3) and remain mononuclear; Edom-Vovard *et al*. coined these "Type I" myoblasts and are reminiscent of the first myotomal muscle. Myotubes that do form at 7 weeks were typically thin, and originated from abundant "Type II & III" myoblasts. These early myotubes contained around 10 nuclei and can express fetal myosin (MYH8) along with MYH3, and may represent primary myotubes. In contrast, the majority of myoblasts from 18 week-old fetal muscle fused into large branching secondary-like myotubes with upwards of 100 nuclei, and expressed slow myosin (MYH7) in addition to MYH3 and MYH8; these "Type IV" myoblasts share many characteristics of cultured adult

satellite cells. Interestingly, clonal expansion revealed that myoblasts destined for a specific fate—either steadfast mononuclear myocytes or large branching myotubes—were present at both time points, and merely their relative proportions are what change over time.

The day 50 hESC-derived cultures appear closer aligned to that of 7 week embryonic muscle, in that the majority of myocytes in cultures remain mononuclear or form only small myotubes (Fig. A2.2). These observations are consistent with the visual appearance of other hESC-derived myogenic cultures after similar durations of *in vitro* differentiation (8, 12–15, 17, 29), while only hESCs differentiated by induced MYOD1-over expression generate larger branching myotubes (10, 11, 18, 19). It is possible, therefore, that day 50 cultures contain a similar myogenic heterogeneity to 7 week embryonic muscle, and possess $PAX7^+$ SMPs of both low- and high-fusion competent myoblasts that could be isolated through cell sorting.

Studies in fetal muscle have shown that surface marker profiles can discriminate between SMPs with varying fusion propensities. $MCAM^+$ and especially $CD82^+/MCAM^+$ FACS-isolated SMPs from approximately 18 week-old human fetal muscle more readily fuse *in vitro* and appreciably engraft *in vivo* compared to MCAM- myogenic cells (30, 31). The $CD82^+/MCAM^+$ population exhibited twice the *in vitro* fusion of $MCAM^+$ cells and formed myotubes containing over 40 nuclei; $CD82^+/MCAM^+$ cells—when transplanted *in vivo*—formed on average 110 human donor-derived fibers per section of injected $NODRag1^{null}mdx^{5cv}$ TA (30, 31). It would be interesting to determine if the $CD82^+/MCAM^+$ profile can isolate a population of SMPs from 50-day cultures that gives rise to exclusively highly fusion-competent progeny.

A number of human cell transplantation studies exist that used adult muscle as their source material, and one recent study also highlighted the importance of sorting for

appropriately therapeutic cell populations. As few as 5 000 $ITGB1^{+}/NCAM1^{+}$ FACS-isolated donor muscle cells appreciably contributed to recipient NSG murine myofibers, whereas an equal number of unsorted cells led to no detectable engraftment (32).

Not only do Xu *et al.* owe their promising results to sorting, but they also attribute their 90% engraftment rate—in part—to the use of gamma irradiation to first ablate the host muscles' satellite cell population (26, 32); this was a procedure not implemented in the works presented here. Marg and colleagues' transplantation study with adult human donor muscle determined that gamma irradiation of the recipient mouse muscle was a prerequisite for human donor cells leaving the interstitial space—similar to the primarily interstitial human cells observed in this study (Fig. 4.3 & 4.4)—and contributing to muscle fibers and the satellite cell niche (33). Comprehensive experiments by Boldrin and colleagues demonstrate that irradiation of the host mouse muscle alone offers significantly greater donor cell engraftment potential compared to chemical injury alone (26); though statistically insignificant, following irradiation with mild chemical injury—like notexin or bupivacaine—may yield even higher engraftment rates (26, 32). These and other authors postulate that harsh chemical or physical injuries destroy too much of the muscle architecture—including the satellite cell niche, innervations, and the vasculature—and thus reduces donor cell integration and muscle repair (34). A more natural exercise-induced injury could be performed if using the NSG-mdx^{4Cv} dystrophic mouse model instead (35). However, Boldren *et al*. show that chemical injury alone does not completely ablate cell engraftment; many of the promising transgenic ES- and fetal-donor cell studies mentioned above were also performed in various mouse models without irradiation, but instead used cardiotoxin or $BaCl_2$ injury as in this study (18, 19, 21, 30, 31).

Given that non-fusing Type I and highly fusion-competent Type IV myoblasts co-exist at 7 and 18 weeks of development while maintaining their identities clonally, and given that $PAX7^+$ adult satellite cells only behave like Type IV fetal myoblasts *in vitro* (28), it stands to reason that embryonic myoblasts may already possess their terminal myogenic programs at the upstream PAX7-expressing SMP stage. However, the developmental timing and mechanism of the switch in balance between low- and high-fusion competent progeny remains unclear (reviewed in (36)), and especially so during *in vitro* myogenesis:

Are SMPs of non-fusing myoblasts acted upon by external signals to advance their developmental stage, thereby shifting their myoblast progeny from non- to high-fusion competence? Are SMPs of non-fusing myoblasts selectively culled after a certain stage of muscle development? Or do the SMPs of non-fusion competent myoblasts possess relatively limited proliferation potential, while SMPs of high-fusion competent myoblasts become the dominant population through more robust cell division? What environmental cues within the developing limb might guide these processes and how might those cues be recapitulated in culture? If a myoblast's terminal myogenic program is defined at an upstream stage, is there an even earlier point upstream of PAX7 expression at which it becomes set?

Future experiments may be undertaken to identify, isolate, and expand hESC-derived SMPs of more fusion-ready myoblasts that would more closely behave like adult satellite cells, and potentially integrate better into host muscle upon transplantation compared to the results presented in this study. For example, single-cell sequencing or clonal expansion of individual day 50 $PAX7^+$ cells may uncover that SMPs give rise to populations of myoblasts

with distinct fusion competencies and MYH expression, similar to the clonal populations identified from 7 week embryonic limb muscle (28). From clonal expansion, gene expression profiling could be used to associate surface proteins with the different populations for their purification and further study.

It may also be the case that no distinct populations are identified based on fusion criteria. Prolonged culture beyond day 50 or further media supplementation may be required *in vitro* to recapitulate the fetal muscle environment that would normally support maturation of the myogenic populations from mononuclear myocytes or primary myotubes to predominantly mature secondary myotubes (37, 38). Of course, a delicate balance must be struck between maturation and not depleting the $PAX7^+$ SMP pool through complete differentiation, as seen with other studies (14).

4.8 Experimental Procedures

4.8.1 Cell culture

Human embryonic stem cells (hESC)(H9, WA09, WiCell, Madison, WI) and induced pluripotent stem cells (iPSC)(167-1J, (39)) were maintained and differentiated as in (2) until the experimental time points specified, with or without passage as specified.

4.8.2 Cell preparation for injection

On the day of *in vivo* cell injections, *in vitro* cell culture media were first supplemented with 5 ng/mL FGF2 (Gibco by Lifetech, Grand Island, NY) and 10 μM Y-27632 (TOCRIS Bioscience, Bristol, UK) for 2 hours to suppress apoptosis (40, 41). Supplemented culture media were removed and the cells were washed with DPBS. Where indicated, cell culture were either incubated with TrypLE Express (Gibco by Lifetech, Grand

Island, NY) at 37°C for 10 minutes, or incubated with 200 U/mL Collagenase Type IV (Gibco by Lifetech, Grand Island, NY) at 37°C for 20 – 40 minutes, with gentle wide-mouth pipette agitation every 10 minutes. Dissociated cultures were collected into an equal volume of 10 μM Y-27631-supplemented KnockOut DMEM with KnockOut Serum Replacement (Gibco by Lifetech, Grand Island, NY). Where indicated, dissociated cultures were either strained through a 70 μm nylon mesh, or allowed to stand in an upright centrifugation tube for 10 – 15 seconds to allow large debris to settle out. The mesh- or gravity-strained cultures were centrifuged at 500 g for 3 minutes and washed with DPBS. Cells were resuspended in DPBS at 1×10^6 cells / 30 μL for *in vivo* injection with 1/2 cc U-100 28 1/2G 1/2" syringes, unless otherwise stated.

4.8.3 Animal preparation and cell injection

Immunodeficient NOD.Cg-Prkdc^{scid} Il2rg^{tm1Wjl}/SzJ (NSG, The Jackson Laboratory, Bar Harbor, ME) were used in all experiments. The tibialis anterior (TA) muscles of NSG mice were injured 1 day prior to receiving cell injections. Briefly, animals were anesthetized with isoflurane and given buprenorphine analgesic subcutaneously. The TA muscles were injured with 30 μL of either 10 μM cardiotoxin or 0.1% barium chloride using 1/2 cc U-100 28 1/2G 1/2" syringes. DPBS-injected or uninjured TA muscles were used as negative injury controls. On the day of cell injections, animals were anesthetized with isoflurane and given buprenorphine analgesic subcutaneously. Unless otherwise stated, 1×10^6 cells / 30 μL DPBS were injected per TA muscle. DPBS or no injection was used as negative treatment controls. Experiments were carried out in triplicate per condition, and experimental end points indicated as days post cell-injection (DPI) of the cells. All animal procedures were

approved by the University of Ottawa Animal Care Committee and were carried out according to guidelines of the Canadian Council on Animal Care.

4.8.4 Muscle sectioning and staining

After sacrificing mice, TA muscles were placed in OCT Compound (VWR, Radnor, PA) and flash frozen in melting isopentane for 2 minutes. Muscles were cryosectioned into 8 µm sections for immunofluorescent staining. All processing during staining was carried out at room temperature unless otherwise stated. Sections were fixed in 4% formadehyde-1.35% methanol-PBS for 30 minutes, quenched in 0.125 M glycine-PBS for 10 minutes, permeabilized in 0.1% Triton X-100-PBS for 10 minutes, blocked in 10% Goat serum-0.1% Triton X-100-PBS for 1 hour, stained with the appropriate primary antibodies in 10% Goat serum-0.1% Triton X-100-PBS overnight at 4°C, labeled with the appropriate secondary antibodies in 10% Goat serum-0.1% Triton X-100-PBS for 1 hour, and mounted with 1 µg/mL Hoechst dye in 50% Glyerol-PBS. Sections were visualized with a Leica DMI6000 B microscope (Leica Microsystems) and cells of whole sections were quantified using Volocity software (PerkinElemer).

4.8.5 Antibodies

Primary antibodies used in this study were against human Dystrophin (MABT827, MilliporeSigma, Burlington, MA), human Lamin-A+C (ab49721 & ab108595, Abcam, Cambridge, MA), human nuclear antigen (ab191181, Abcam, Cambridge, MA), Laminin (ab11575, Abcam, Cambridge, MA), MF20 (AB2147781, Developmental Studies Hybridoma Bank, Iowa City, IA), PAX7 (AB528428, Developmental Studies Hybridoma Bank, Iowa City, IA), and human LAMC1 (AB2134060, Developmental Studies Hybridoma

Bank, Iowa City, IA). Secondary antibodies used were AlexaFluor488 goat anti-mouse IgG1, Cy3 goat anti-mouse IgG2a, Cy3 goat anti-mouse IgG2b, AlexaFluor488 goat anti-rabbit IgG, and Cy3 goat anti-rabbit IgG (Jackson ImmunoResearch, West Grove, PA).

4.8.6 Statistical Analysis

Statistical differences between means were calculated using two-way ANOVA. P values of $p \leq 0.05$ were considered significant.

4.9 Acknowledgements

This work was funded by an award from the Muscular Dystrophy Association to Ilona S. Skerjanc (218371), and by grants from the Natural Sciences and Engineering Research Council (RGPIN 293170-11) and Canadian Institutes of Health Research (MOP-89910) to Dr. William L. Stanford. Michael Shelton was supported in part by the Queen Elizabeth II Graduate Scholarship in Science and Technology. William L. Stanford was supported by the Canada Research Chair in Integrative Stem Cell Biology. Alexandre Blais was funded by a grant from the Canadian Institutes of Health Research (MOP-119458).

4.10 References

1. Shelton M, Metz J, Liu J, Carpenedo RL, Demers SP, Stanford WL, Skerjanc IS. 2014. Derivation and expansion of PAX7-positive muscle progenitors from human and mouse embryonic stem cells. Stem Cell Reports 3:516–529.
2. Shelton M, Kocharyan A, Liu J, Skerjanc IS, Stanford WL. 2016. Robust generation and expansion of skeletal muscle progenitors and myocytes from human pluripotent stem cells. Methods 101:73–84.
3. Chal J, Pourquié O. 2017. Making muscle: skeletal myogenesis in vivo and in vitro. Development 144:2104–2122.

4. Kuang S, Kuroda K, Le Grand F, Rudnicki MA. 2007. Asymmetric Self-Renewal and Commitment of Satellite Stem Cells in Muscle. Cell 129:999–1010.

5. Chargé SBP, Rudnicki MA. 2004. Cellular and molecular regulation of muscle regeneration. Physiol Rev 84:209–38.

6. Hwang Y, Suk S, Lin S, Tierney M, Du B, Seo T, Mitchell A, Sacco A, Varghese S. 2013. Directed In Vitro Myogenesis of Human Embryonic Stem Cells and Their In Vivo Engraftment. PLoS One 8:e72023.

7. Xu C, Tabebordbar M, Iovino S, Ciarlo C, Liu J, Castiglioni A, Price E, Liu M, Barton ER, Kahn CR, Wagers AJ, Zon LI. 2013. A zebrafish embryo culture system defines factors that promote vertebrate myogenesis across species. Cell 155:909–921.

8. Choi IY, Lim HT, Estrellas K, Mula J, Cohen T V., Zhang Y, Donnelly CJ, Richard JP, Kim YJ, Kim H, Kazuki Y, Oshimura M, Li HL, Hotta A, Rothstein J, Maragakis N, Wagner KR, Lee G. 2016. Concordant but Varied Phenotypes among Duchenne Muscular Dystrophy Patient-Specific Myoblasts Derived using a Human iPSC-Based Model. Cell Rep 15:2301–2312.

9. Ryan T, Liu J, Chu A, Wang L, Blais A, Skerjanc IS. 2012. Retinoic Acid Enhances Skeletal Myogenesis in Human Embryonic Stem Cells by Expanding the Premyogenic Progenitor Population. Stem Cell Rev Reports 8:482–493.

10. Rao L, Tang W, Wei Y, Bao L, Chen J, Chen H, He L, Lu P, Ren J, Wu L, Luan Z, Cui C, Xiao L. 2012. Highly Efficient Derivation of Skeletal Myotubes from Human Embryonic Stem Cells. Stem Cell Rev Reports 8:1109–1119.

11. Albini S, Coutinho P, Malecova B, Giordani L, Savchenko A, Forcales SV, Puri PL. 2013. Epigenetic Reprogramming of Human Embryonic Stem Cells into Skeletal Muscle Cells and Generation of Contractile Myospheres. Cell Rep 3:661–670.

12. Borchin B, Chen J, Barberi T. 2013. Derivation and FACS-mediated purification of PAX3+/PAX7+ skeletal muscle precursors from human pluripotent stem cells. Stem Cell Reports 1:620–631.

13. Hosoyama T, McGivern J V, Van Dyke JM, Ebert AD, Suzuki M. 2014. Derivation of myogenic progenitors directly from human pluripotent stem cells using a sphere-based culture. Stem Cells Transl Med 3:564–74.

14. Chal J, Oginuma M, Al Tanoury Z, Gobert B, Sumara O, Hick A, Bousson F, Zidouni Y, Mursch C, Moncuquet P, Tassy O, Vincent S, Miyanari A, Bera A, Garnier J-M, Guevara G, Hestin M, Kennedy L, Hayashi S, Drayton B, Cherrier T, Gayraud-Morel B, Gussoni E, Relaix F, Tajbakhsh S, Pourquié O. 2015. Differentiation of pluripotent stem cells to muscle fiber to model Duchenne muscular dystrophy. Nat Biotechnol 33:962–969.

15. Caron L, Kher D, Lee KL, McKernan R, Dumevska B, Hidalgo A, Li J, Yang H, Main H, Ferri G, Petek LM, Poellinger L, Miller DG, Gabellini D, Schmidt U. 2016. A Human Pluripotent Stem Cell Model of Facioscapulohumeral Muscular Dystrophy-Affected Skeletal Muscles. Stem Cells Transl Med 5:1145–1161.

16. Loh KMM, Chen A, Koh PWW, Deng TZZ, Sinha R, Tsai JMM, Barkal AAA, Shen KYY, Jain R, Morganti RMM, Shyh-Chang N, Fernhoff NBB, George BMM, Wernig G, Salomon REEA, Chen Z, Vogel H, Epstein JAA, Kundaje A, Talbot WSS, Beachy PAA, Ang LTT, Weissman ILL. 2016. Mapping the Pairwise Choices Leading from Pluripotency to Human Bone, Heart, and Other Mesoderm Cell Types. Cell 166:451–468.

17. Xi H, Fujiwara W, Gonzalez K, Jan M, Liebscher S, Van Handel B, Schenke-Layland K, Pyle AD. 2017. In Vivo Human Somitogenesis Guides Somite Development from hPSCs. Cell Rep 18:1573–1585.

18. Tedesco FS, Gerli MFM, Perani L, Benedetti S, Ungaro F, Cassano M, Antonini S, Tagliafico E, Artusi V, Longa E, Tonlorenzi R, Ragazzi M, Calderazzi G, Hoshiya H, Cappellari O, Mora M, Schoser B, Schneiderat P, Oshimura M, Bottinelli R, Sampaolesi M, Torrente Y, Broccoli V, Cossu G. 2012. Transplantation of Genetically Corrected Human iPSC-Derived Progenitors in Mice with Limb-Girdle Muscular Dystrophy. Sci Transl Med 4:140ra89-140ra89.

19. Goudenege S, Lebel C, Huot NB, Dufour C, Fujii I, Gekas J, Rousseau J, Tremblay JP. 2012. Myoblasts Derived From Normal hESCs and Dystrophic hiPSCs Efficiently Fuse With Existing Muscle Fibers Following Transplantation. Mol Ther 20:2153–2167.

20. Montarras D, Morgan J, Collins C, Relaix F, Zaffran S, Cumano A, Partridge T, Buckingham M. 2005. Direct isolation of satellite cells for skeletal muscle regeneration. Science 309:2064–7.

21. Darabi R, Arpke RW, Irion S, Dimos JT, Grskovic M, Kyba M, Perlingeiro RCR. 2012. Human ES- and iPS-derived myogenic progenitors restore DYSTROPHIN and improve contractility upon transplantation in dystrophic mice. Cell Stem Cell 10:610–619.

22. Charville GW, Cheung TH, Yoo B, Santos PJ, Lee GK, Shrager JB, Rando TA. 2015. Ex vivo expansion and in vivo self-renewal of human muscle stem cells. Stem Cell Reports 5:621–632.

23. Darabi R, Gehlbach K, Bachoo RM, Kamath S, Osawa M, Kamm KE, Kyba M, Perlingeiro RCR. 2008. Functional skeletal muscle regeneration from differentiating embryonic stem cells. Nat Med 14:134–143.

24. Darabi R, Santos FNC, Filareto A, Pan W, Koene R, Rudnicki MA, Kyba M, Perlingeiro RCR. 2011. Assessment of the myogenic stem cell compartment following transplantation of Pax3/Pax7-induced embryonic stem cell-derived progenitors. Stem Cells 29:777–790.

25. Darabi R, Pan W, Bosnakovski D, Baik J, Kyba M, Perlingeiro RCR. 2011. Functional Myogenic Engraftment from Mouse iPS Cells. Stem Cell Rev Reports 7:948–957.

26. Boldrin L, Neal A, Zammit PS, Muntoni F, Morgan JE. 2012. Donor satellite cell engraftment is significantly augmented when the host niche is preserved and endogenous satellite cells are incapacitated. Stem Cells 30:1971–1984.

27. Hardy D, Besnard A, Latil M, Jouvion G, Briand D, Thépenier C, Pascal Q, Guguin A, Gayraud-Morel B, Cavaillon JM, Tajbakhsh S, Rocheteau P, Chrétien F. 2016. Comparative Study of Injury Models for Studying Muscle Regeneration in Mice. PLoS One 11:e0147198.

28. Edom-Vovard F, Mouly V, Barbet JP, Butler-Browne GS. 1999. The four populations of myoblasts involved in human limb muscle formation are present from the onset of primary myotube formation. J Cell Sci 112:191–9.

29. Magli A, Incitti T, Kiley J, Swanson SA, Darabi R, Rinaldi F, Selvaraj S, Yamamoto A, Tolar J, Yuan C, Stewart R, Thomson JA, Perlingeiro RCR. 2017. PAX7 Targets, CD54, Integrin α9β1, and SDC2, Allow Isolation of Human ESC/iPSC-Derived Myogenic Progenitors. Cell Rep 19:2867–2877.

30. Lapan AD, Rozkalne A, Gussoni E. 2012. Human fetal skeletal muscle contains a myogenic side population that expresses the melanoma cell-adhesion molecule. Hum Mol Genet 21:3668–3680.

31. Alexander MS, Rozkalne A, Colletta A, Spinazzola JM, Johnson S, Rahimov F, Meng H, Lawlor MW, Estrella E, Kunkel LM, Gussoni E. 2016. CD82 Is a Marker for Prospective Isolation of Human Muscle Satellite Cells and Is Linked to Muscular Dystrophies. Cell Stem Cell 19:800–807.

32. Xu X, Wilschut KJ, Kouklis G, Tian H, Hesse R, Garland C, Sbitany H, Hansen S, Seth R, Knott PD, Hoffman WY, Pomerantz JH. 2015. Human Satellite Cell Transplantation and Regeneration from Diverse Skeletal Muscles. Stem Cell Reports 5:419–434.

33. Marg A, Escobar H, Gloy S, Kufeld M, Zacher J, Spuler A, Birchmeier C, Izsvák Z, Spuler S. 2014. Human satellite cells have regenerative capacity and are genetically manipulatable. J Clin Invest 124:4257–4265.

34. Lee ASJ, Anderson JE, Joya JE, Head SI, Pather N, Kee AJ, Gunning PW, Hardeman EC. 2013. Aged skeletal muscle retains the ability to fully regenerate functional architecture. Bioarchitecture 3:25–37.

35. Arpke RW, Darabi R, Mader TL, Zhang Y, Toyama A, Lonetree CL, Nash N, Lowe DA, Perlingeiro RCR, Kyba M. 2013. A new immuno-, dystrophin-deficient model, the NSG-mdx4Cvmouse, provides evidence for functional improvement following allogeneic satellite cell transplantation. Stem Cells 31:1611–1620.

36. Murphy M, Kardon G. 2011. Origin of vertebrate limb muscle: the role of progenitor and myoblast populations. Curr Top Dev Biol 96:1–32.

37. Duxson MJ, Usson Y, Harris a J. 1989. The origin of secondary myotubes in mammalian skeletal muscles: ultrastructural studies. Development 107:743–750.

38. Deries M, Schweitzer R, Duxson MJ. 2010. Developmental fate of the mammalian myotome. Dev Dyn 239:2898–2910.

39. Chang WY, Lavoie JR, Kwon SY, Chen Z, Manias JL, Behbahani J, Ling V, Kandel RA, Stewart DJ, Stanford WL. 2013. Feeder-independent derivation of induced-pluripotent stem cells from peripheral blood endothelial progenitor cells. Stem Cell Res 10:195–202.

40. Hall JK, Banks GB, Chamberlain JS, Olwin BB. 2010. Prevention of muscle aging by myofiber-associated satellite cell transplantation. Sci Transl Med 2:57ra83.

41. Zhang L, Valdez JM, Zhang B, Wei L, Chang J, Xin L. 2011. ROCK inhibitor Y-27632 suppresses dissociation-induced apoptosis of murine prostate stem/progenitor cells and increases their cloning efficiency. PLoS One 6:1–9.

Chapter 5: General Discussion: The improvement and study of human embryonic stem cell *in vitro* myogenesis and remaining hurdles to muscle stem cell therapy

5.1 Summary

It was proposed in the introduction that the two major problems facing stem cell therapy were reaching the scale of donor material required for therapy, and establishing a method for efficient system-wide delivery of suitable donor cells. The works presented here make prominent strides in addressing the former problem of scale with muscle stem cell therapy: our 50 day hESC differentiation protocol generated large quantities of $PAX7^+$ SMPs (Chapter 2, Appendix 1)(1, 2). Gene expression profiling of the 50 day time course served as a resource to better understand the molecular mechanisms and transcriptional regulators involved during *in vitro* skeletal myogenesis (Chapter 3). Moreover, day 50 cultures share expression profiles closer to quiescent rather than activated satellite cells, which have better therapeutic potential *in vivo* (3, 4). However, the myogenic cultures generated in these works fall short in tackling the latter problem of limited *in vivo* delivery: few hESC-derived donor cells engraft into NSG-mouse myofibers upon intramuscular injection (Chapter 4). Thus, our transplantation method may be inadequate, or our myogenic cultures may have cell-intrinsic limitations to *in vivo* engraftment. Many of these findings have since been substantiated by other studies in the field of embryonic myogenesis (5).

5.2 Directed Skeletal Myogenic Differentiation of Human Embryonic Stem Cells

At the onset of the works presented in this thesis, the efficiency of contemporary non-transgenic hESC differentiations were limited to < 5% of total cultures becoming skeletal muscle (6–8). We have devised a 50 day *in vitro* differentiation protocol for hESCs that commits roughly 90% of cells to the skeletal muscle lineage; 47% ± 3% of the cultures are

MYH^+ myocytes or myotubes, and are surrounded by $PAX7^+$ cells comprising 43% ± 4% of total cells (1). Other groups have made tremendous strides toward improving the *in vitro* myogenesis of hESCs, both in parallel with and subsequent to the publication of our works (Table 5.1). The initial mesoderm induction from pluripotent hESCs deserves specific attention—as in our experience—subsequent efficiency can be predicted by the quality of differentiation during the first week in culture. Many approaches similarly begin with GSK3B inhibition to induce mesoderm from pluripotent hESCs. However, the concentration of GSK3B inhibitor used and the presence of other compounds mark important distinctions (Fig. 3.2).

Our approach uses the hESCs' highest tolerable concentration of the GSK3B inhibitor CHIR99021 over a two-day period. Despite *in vivo* gastrulation being a complex integration of WNT, FGF, and TGFB-superfamily signals (Fig. 1.3), brief intervention with CHIR99021 appears sufficient for the subsequent development of 91% ± 6% hESCs into T-expressing mesoderm and MSGN1-expressing paraxial mesoderm-like cells, followed by the MEOX1- and PAX3-expressing somite-like stage after 8 – 12 days in culture (1). Only two basic media formulations—FGF2-supplemented StemPro-34 and N2/ITS-supplemented DMEM:F12—carry these early cultures to 90% myogenic identity by 50 days in culture. Borchin *et al*. feature a similar level of intervention, wherein lower concentrations of CHIR99021 are used over a longer 4 day period, followed by FGF2- and N2-supplemented media (9). Our results indicate that a low CHIR99021 approach results in significantly lower MSGN1 expression; this may be reflected in the Borchin *et al*. study wherein only 18% of their cultures were $PAX3^+/PAX7^+$ by day 35 of differentiation.

Table 5.1

Primary & Principle Author	Year	Cell Type	Experimental Modulations (Compounds)	Days	+ Sort	- Sort	*in vivo*
Hicks, M. R. & Pyle, A. D.	2018	ES / iPS	Shelton et al. 2014 & Chal et al. 2015	50 – 58	ERBB3/NGFR or NCAM1	B3GAT1	+
Magli, A. & Perlingeiro, R. C. R.	2017	ES / iPS	Darabi et al. 2012 & Chal et al. 2015	30	PAX7-GFP or CD54/ITGA9/ITGB1/SDC2	-	+
Xi, H. & Pyle, A. D.	2017	ES / iPS	WNT↑ (CHIR99021), BMP↓ (LDN193189), TGFB↓ (SB431542), MAPK/ERK↑ (FGF2, HGF, IGF1)	27 – 29	-	-	-
Loh, K. M. & Weissman, I. L.	2016	ES	NODAL↑ (INHBA), WNT↑ (CHIR99021), MAPK/ERK↑ (FGF2, C59), PI3K↓ (PIK90), TGFB↓ (A83-01), BMP↓ (LDN193189), WNT↓ (C59), MAPK/ERK↓ (PD0325901), BMP↑ (BMP4), SHH↓ (Vismodegib), SHH↑ (21K), Serum (Horse)	17	-	-	-
Choi, I. Y. & Lee, G.	2016	ES / iPS	N2, WNT↑ (CHIR99021), NOTCH↓ (DAPT)	30	NCAM1	B3GAT1	+
Caron, L. & Schmidt, U.	2016	ES / iPS	WNT↑ (CHIR99021), MAPK/ERK↑ (EGF, FGF2, HGF, IGF1), Serum (Horse), TGFB↓ (RepSox, SB431542), TNF↓ (Necrosulfonamide), JAK/STAT↓ (Oncostatin)	26	-	-	-
Shelton, M. & Stanford, W. L.	2016	ES / iPS	Shelton et al. 2014	50	-	-	-
Young, C. S. & Pyle, A. D.	2016	ES / iPS	Shelton et al. 2014, Over-expression (MYOD1)	50	NCAM1	B3GAT1	+
Chal, J. & Pourquie, O.	2015	ES / iPS	WNT↑ (CHIR99021), BMP↓ (LDN193189), MAPK/ERK↑ (FGF2, HGF, IGF1)	50	-	-	-
Shelton, M. & Skerjanc, I. S.	2014	ES	WNT↑ (CHIR99021), MAPK/ERK↑ (FGF2), N2	50	-	-	-
Hwang, Y. & Varghese, S.	2014	ES	Serum (Fetal Bovine), WNT↑ (WNT3A)	30	PDGFRA	POU5F1-GFP	+
Hosoyama, T. & Suzuki, M.	2014	ES / iPS	MAPK/ERK↑ (EGF, FGF2), B27	42 – 56	-	-	-
Borchin, B. & Barberi, T.	2013	ES / iPS	WNT↑ (CHIR99021), MAPK/ERK↑ (FGF2, IGF1), N2	35 – 55	CXCR4/MET or ACHR	B3GAT1	-
Xu, C. & Zon, L. I.	2013	iPS	WNT↑ (BIO), MAPK/ERK↑ (FGF2), cAMP↑ (Forskolin), Serum (Horse)	36	-	-	+
Hwang, Y. & Varghese, S.	2013	ES	Serum (Fetal Bovine)	30	PDGFRA	POU5F1-GFP	+
Albini, S. & Puri, P. L.	2013	ES	Over-expression (BAF60, MYOD1), Serum (Fetal Bovine, Horse)	20	NCAM1	-	-
Awaya, T. & Heike, T.	2012	ES / iPS	Serum (Fetal Bovine, Horse)	49 – 63	-	-	+
Rao, L. & Xiao, L.	2012	ES	Over-expression (MYOD1), N2	8 – 10	-	-	-
Goudenege, S. & Tremblay, J. P.	2012	ES / iPS	Serum (Fetal Bovine), Over-expression (MYOD1)	10	-	-	+
Darabi, R. & Perlingeiro, R. C. R.	2012	ES / iPS	Chick Embryo Extract, Serum (Fetal Bovine, Horse), Over-expression (PAX7)	28 – 35	PAX7-GFP	-	+
Ryan, T. & Skerjanc, I. S.	2011	ES	Serum (Fetal Bovine), RA	40	-	-	-

Table 5.1. Publications of the *in vitro* myogenesis of human embryonic stem cells from the onset of the works presented in this thesis. Key experimental modulations used in each approach are listed, including signaling pathways whose activity were enhanced (↑) or inhibited (↓) during differentiation, followed by the small molecules or recombinant proteins used to alter their activity. Serum (species), transgenic overexpression (gene), and commercial media supplements are also listed where applicable. Positive or negative sorting markers used to enrich myogenic populations are indicated when used. Studies that show human cell engraftment and human myofibers with *in vivo* animal models are marked (+). Publications from the Skerjanc lab are highlighted grey.

Studies of stem cell therapy show that the origin of donor muscle—meaning the myoblasts' MYH-expression profile or fiber type (Eg. Type I-MYH7+ versus Type-IIX-MYH1), and what muscle the donor cells are extracted from (Eg. *latissimus dorsi* versus *rectus abdominis*)—can have profound effects on the rate of *in vivo* engraftment in the recipient muscle (10–12). Given these implications, it is important to characterize the type of muscle being generated with hESC-derived *in vitro* myogenesis. Moreover, findings that arise from the modeling of human myogenesis *in vitro* may not be applicable to human embryonic myogenesis as a whole if, for example, the directed differentiation only generated niche craniofacial muscles. It becomes imperative, therefore, to more precisely identify what embryonic muscle(s) may be generated and modeled with our 50-day hESC differentiation protocol.

Gene expression analysis offered insight into what types of muscle might be represented with *in vitro* culture (Fig 5.1 & 5.2). The expression of embryonic and early fetal myosins MYH3 and MYH8 (13), respectively, but lack of elevated MYH2 and MYH1 expression may indicate that day 50 cultures are on the cusp of secondary myogenesis. The appearance of small myotubes also supports the progression past mononuclear myotomal muscle and into primary myogenesis, but not yet well into secondary myogenesis where myotubes hypertrophy to much greater size (14, 15). Furthermore, day 50 cultures have significantly elevated expression of the PAX7-target gene, NFIX. The NFIX gene is known to help regulate the switch between primary and secondary myogenesis—in part—by activating MEF2A (16), which our gene expression profiling suggests is transcriptionally active (Fig. 3.3). Timewise in the human embryo, the primitive streak begins from week 2 and secondary myogenesis from week 8 (reviewed in (17, 18)): a 6 week time-frame. This roughly correlates with the ~7 week duration of our *in vitro* differentiation protocol.

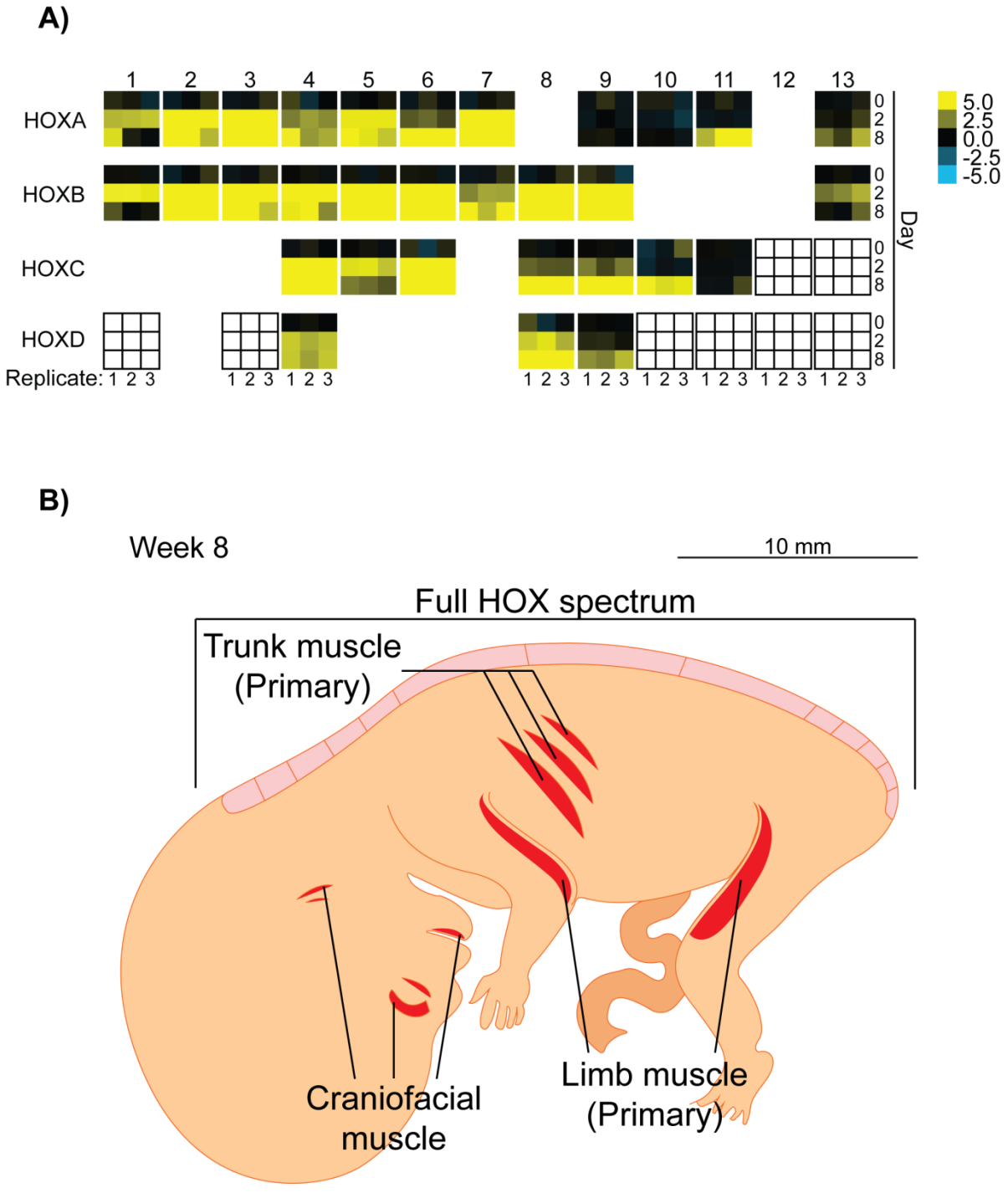
A)
1 2 3 4 5 6 7 8 9 10 11 12 13
HOXA
HOXB
HOXC
HOXD
Replicate: 1 2 3
0 2 8
Day
5.0
2.5
0.0
-2.5
-5.0
B)
Week 8
10 mm
Full HOX spectrum
Trunk muscle (Primary)
Craniofacial muscle
Limb muscle (Primary)

Figure 5.1

Figure 5.1. Gene expression profiling and qualitative assessment of *in vitro* myotube nuclei number in day 50 cultures suggests that most primary skeletal muscle of the 8 week embryo is represented. A) Gene expression profiling from Table A3.1 showed that most of the HOX genes were upregulated during *in vitro* myogenesis, suggesting a diverse representation of the embryonic anterior (HOX-1) to posterior (HOX-13) body axis in early cultures, as HOX identity remains relatively fixed from the onset of primitive streak migration (19, 20). A heatmap was generated in TreeView 3.0, and replicate expression values were standardized to the average of the day 0 triplicates. HOXC10-11, HOXD1, HOXD3, and HOXD10-13 were not represented on the array or their probes did not pass quality control filtering. **B)** Qualitative examination of Figure A2.2 revealed the presence of multinucleated myotubes in 50-day hESC-derived cultures. The number of nuclei observed per myotube is < 10 per cell, suggesting the myotubes more closely resemble those seen during embryonic primary myogenesis rather than fetal secondary myogenesis. Furthermore, qPCR in Figure 2.3 & 2.4 and expression profiling in Figure 3.4 detected significant upregulation of genetic markers used to denote the embryonic structures from which craniofacial, trunk, or limb muscle are derived; described in greater molecular detail in Figure 5.2.

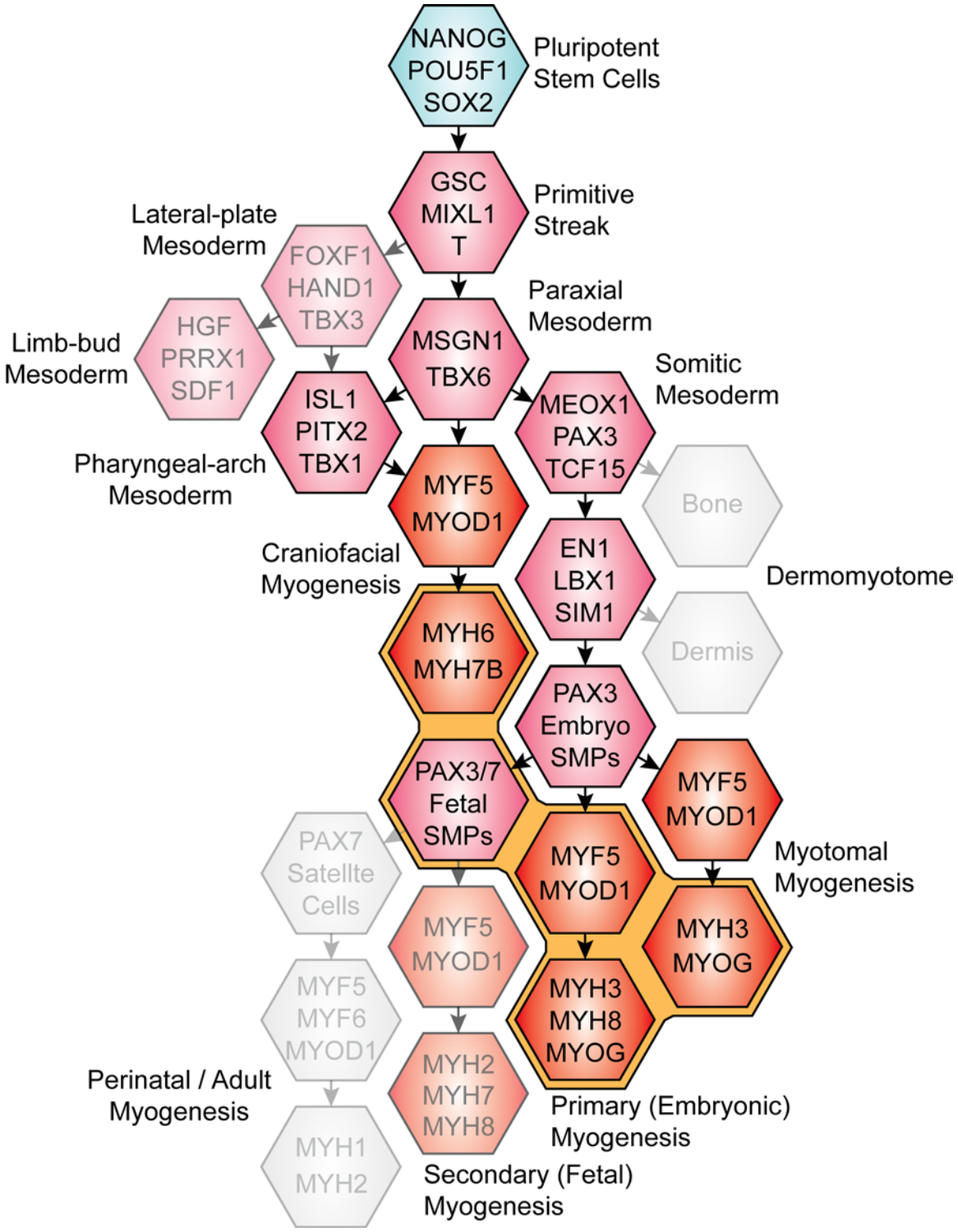
NANOG
POU5F1
SOX2
Pluripotent
Stem Cells
GSC
MIXL1
T
Primitive
Streak
Lateral-plate
Mesoderm
FOXF1
HAND1
TBX3
Paraxial
Mesoderm
HGF
PRRX1
SDF1
Limb-bud
Mesoderm
MSGN1
TBX6
Somitic
Mesoderm
ISL1
PITX2
TBX1
MEOX1
PAX3
TCF15
Pharyngeal-arch
Mesoderm
MYF5
MYOD1
Bone
Craniofacial
Myogenesis
EN1
LBX1
SIM1
Dermomyotome
MYH6
MYH7B
Dermis
PAX3
Embryo
SMPs
PAX3/7
Fetal
SMPs
MYF5
MYOD1
PAX7
Satellte
Cells
MYF5
MYOD1
Myotomal
Myogenesis
MYF5
MYOD1
MYH3
MYOG
MYF5
MYF6
MYOD1
MYH3
MYH8
MYOG
Perinatal / Adult
Myogenesis
MYH2
MYH7
MYH8
Primary (Embryonic)
Myogenesis
MYH1
MYH2
Secondary (Fetal)
Myogenesis

Figure 5.2

Figure 5.2. Proposed model of the developmental trajectory taken by hESC-derived skeletal muscle over the 50 day *in vitro* differentiation. Pluripotent hESCs undergo CHIR99021-induced differentiation by rapidly upregulating markers of pan-mesoderm, for example, GSC and T. Mild elevation of genes that denote posterior primitive streak and lateral plate mesoderm can be detected, though these tissues may also contribute to limb bud mesenchyme—which helps pattern skeletal muscle—and pharyngeal arches (21). MSGN1 and TBX6 expression are robustly elevated as early as day 2 of differentiation; paraxial mesoderm *in vivo* may contribute to pharyngeal arches, future somitic mesoderm, or remain unsegmented and contribute to craniofacial muscle directly. Moderate expression of pharyngeal arch transcription factors and craniofacial myosins MYH6 and MYH7B from day 25 suggest there is a craniofacial component to the myogenic cultures. The observation of mononuclear myocytes and small myotubes in day 50 cultures—in addition to robust MYH3, MYH8 and NFIX expression—suggests that cultures contain myotomal and primary muscle, and may be transitioning into secondary myogenesis. Hexagon color indicates genes related to pluripotency (blue), mesoderm derivatives likely present in culture (pink), terminally differentiated myogenic cells (red), and other closely related mesoderm derivatives likely not present (grey). Opacity aims to convey the extent that each stage is represented in culture. The golden outline indicates the proposed state of development with *in vitro* skeletal myogenesis as of day 50 of differentiation.

Most HOX genes present on the Agilent microarray showed elevated expression at day 2 or 8 of the differentiation protocol (Fig. 5.1A)(Table A3.1). Thus, the full anterior-posterior axis of paraxial mesoderm-like tissue could be represented with our *in vitro* differentiation. Given that the HOX identity of mesoderm appears to be fixed by the time cells have crossed the primitive streak (19, 20), we suspect that 50-day cultures represent the whole range of primary embryonic muscle: from head to "tail," or posterior limbs. However, more studies would be needed to definitely state this, and to show that *in vitro* growth does not favor the development of a specific HOX-segment of paraxial mesoderm-like cells over others between day 8 and day 50 of the protocol.

Genetic markers of the dermomyotomal hypaxial lateral lip and migratory SMPs—LBX1, MET, PAX3, and SIM1—lend evidence to limb-like muscle being present with *in vitro* culture (Fig. 2.4). Gene expression profiling also revealed elevated expression of potential limb markers HGF, PRRX1, and HOX genes implicated in limb development. Fewer quality markers exist to suggest the presence of trunk-like muscle; however, our studies identified upregulation of the dermomyotomal dorsal medial lip marker EN1. Furthermore, non-limb progeny of the SIM1 hypaxial lateral lip would contribute to the embryo's body wall musculature.

The extent of off-target non-myogenic tissue in hESC-derived myogenic cultures is unclear. Key limb development genes HGF and PRRX1, for example, are normally detected in somatic mesoderm *in vivo* (22–24). Ours and other studies suggest there may be neural crest or neuronal cells present during *in vitro* myogenesis with our 50-day protocol (Fig. 2.4)(1, 5). Elevated expression of canonical cardiac mesoderm markers—ISL1 and TBX1—and cardiac myosins—MYH6 and MYH7B—were also detected with expression profiling (Fig. 3.4). However, these canonical cardiac genes share significant overlap with craniofacial

skeletal muscle (13, 25–27). Furthermore, no concurrent elevation of other cardiac transcription factors—namely GATA4 and TBX5—were detected. We may consider an alternative hypothesis as well: that the *in vitro* differentiation of hESCs generates an abnormal skeletal-cardiac muscle lineage hybrid with no true *in vivo* counterpart. This could also underlie the engraftment deficiencies faced by day 50 cultures when injected into NSG murine muscle.

Muscle development and patterning in the embryo depends at times on external cues from surrounding tissues. The limb and trunk somatic mesoderm (28, 29), neural crest (30, 31), and sensory neurons (32, 33), are known to play pivotal roles in coordinating the skeletal myogenic program. This raises the question of whether or not a small portion of off-target cell types may actually benefit *in vitro* skeletal myogenesis. Myogenic purity would, however, be of utmost importance for potential applications in cell therapy: isolation methods such as fluorescence- (FACS) or magnetic-activated cell sorting (MACS) to exclude unwanted cells or to select for desired populations would be required. Off-target cells may also be circumvented with small molecules to suppress their development, while also using compounds to compensate for whatever signaling role the off-target tissues would normally provide during *in vivo* development.

As such, our simpler approach may not be optimal in all aspects of the directed differentiation of embryonic stem cells. Controlling the activity of additional signaling pathways should—in theory—provide finer tuned control over the developmental trajectory of pluripotent cultures. This can address a well-established difficulty with studying *in vitro* differentiation: the propensity of different hESC-lines—or even the same hESC line grown in different labs—to differentiate at widely variable rates in response to the same stimuli, or to avoid differentiation entirely (34–36). culture conditions, genomic instability, or varying

levels of endogenous signaling activity may underlie the variable outcomes observed (37–39). Therefore, protocols that are designed around the modulation of multiple signaling pathways may provide researchers with the ability to compensate and control some of this endogenous variability. Indeed, other directed myogenic protocols were developed that modulate the signaling pathways BMP, FGF, NOTCH, PI3K, or TGFB in addition to WNT during the early stages of mesoderm development (Table 5.1).

As described previously, BMP signaling is suppressed by CHRD and NOG in the anterior region of the primitive streak from which paraxial mesoderm is derived (Fig. 1.4). Thus, rather than stimulating WNT signaling alone, several groups have attempted to more efficiently differentiate paraxial mesoderm from hESCs by activating WNT while also suppressing BMP (40), or by activating WNT followed by the suppression of BMP and TGFB (21, 41). The studies by Loh *et al*. and Xi *et al*. suggest that suppressing BMP signaling after a period of WNT signaling is significantly better at inducing paraxial mesoderm gene expression than WNT alone. The approach by Loh *et al*. also modulates FGF and PI3K signaling pathways (21). Xi *et al*. suggest, however, that more complex signaling pathway modulation may not always be better; in their study, altering FGF and PI3K pathways offered no significant improvements in paraxial and somite gene expression (41). The major downsides to more multifaceted signaling manipulation are the complex optimization of each compound's concentration in conjunction with each other, and the added cost of materials. The Design of Experiments (DOE) mathematical model would invaluably aide in determining the fewest experiments required for compound optimization (42).

While the many recent protocols may vary in their complexity and efficiency, cell sorting offers a viable method to recover SMPs regardless of the differentiation approach (5,

9, 43). The surface markers that should be used to identify hESC-derived SMPs, however, are less well established than their human adult or mouse embryonic counterparts.

5.3 Not All SMPs are Created Equal

Muscle stem cell therapy has largely looked to the satellite cell—mature muscle's resident stem cell—to identify ideal characteristics for prospective *in vitro*-derived donor cells. One of these characteristics is the hallmark PAX7-expression (44). The spatiotemporal expression of PAX7, however, is profoundly heterogeneous in the developing embryonic musculature (45), and it remains unclear which of the various $PAX7^+$ pre-natal populations have more or less therapeutic potential. Furthermore, it is unfeasible to distinguish between these *in vivo* populations *in vitro* without the spatiotemporal cues of the embryo. Further complicating the characterization of hESC-derived SMPs is the fact that prospective surface markers of SMPs identified from embryonic animal models—and adult human satellite cells—do not always translate to the embryonic human system (46, 47). Thus, we broadly regard skeletal muscle progenitors as "PAX7-expressing cells with myogenic potential" at the onset of the studies presented in this thesis.

Here, we used gene expression profiling to better characterize prospective SMPs present within day 50 myogenic cultures. The day 50 myogenic cultures express several surface markers previously associated with human satellite cells and embryonic- or fetal-derived SMPs; pioneering studies on human fetal tissue from the time of secondary myogenesis identified MCAM and CD82 as SMP markers (48, 49). $PAX7^+$ hESC-derived SMPs have also been enriched with CXCR4, ICAM1, MET, or NCAM1 (9, 43, 50), all of which were elevated in our day 50 cultures. During the writing of this thesis, Hicks *et al*. demonstrated that the above-listed markers were frequently not expressed concurrently with

PAX7 in 9 week fetal muscle and *in vitro* hESC-derived myogenic cultures using our 50 day protocol (5). NCAM1—perhaps the most commonly used surface marker when isolating human myoblasts and embryonic SMPs (5, 50–52)—was shown to enrich for cells with high myogenic potential *in vitro*, but that lacked myogenic potential when transplanted *in vivo* into mice (5). Similar to unsorted day 50 cultures, $NCAM1^+$ cells would be retained in the recipient mouse muscle but fail to engraft into fibers.

Instead, Hicks and colleagues identified surface markers ERBB3 and NGFR which could isolate SMPs with high *in vitro* and *in vivo* myogenic capacity from the milieu of hESC-derived day 50 myogenic cultures. They detect these markers as early as day 27 when PAX7 expression begins to elevate. It is unclear if Hicks *et al*. investigated populations younger than day 27 for ERBB3 and NGFR expression; however, our gene expression profiling clusters ERBB3 and NGFR together in Cluster 3 (Fig. 3.1)(Table A3.3), indicating their expression pattern follows somitic transcription factors EYA1/EYA2, MEOX1/MEOX2, and also DMD as early as day 8. The candidate surface markers identified by our gene expression profiling—ADGRA2, ADGRD1, and ADGRG6—also belong to this cluster. ADGRG6 in particular may be related to ERRB signaling (53–57), and was recently shown to bind Collagen IV which is a core component of the muscle basal lamina (58).

Interestedly, the Hicks study reveals that highly myogenic $ERBB3^+/NGFR^+$ cells are present at all embryonic and fetal muscle stages investigated, but that $ERBB3^+/NGFR^-$ myogenic cells are only present during primary myogenesis and lost by the end of secondary myogenesis around 18 weeks.

This observation may complement previous work by Edom-Vovard *et al*., wherein it was demonstrated using the single cell clonal approach that human fetal myoblasts could give rise to only one type of progeny—either single-cell myocytes or multi-nucleated

myotubes—and that both of these populations existed from the onset of primary myogenesis (14). Edom-Vovard noted that the former population was lost by about 18 weeks—when secondary myofibers had formed—as the balance tipped towards the better fusing population. Thus, it may be that $ERBB3^{+}/NGFR^{-}$ cells found earlier in muscle development are in fact myotomal or primary myoblasts that lack fusion potential relative to their $ERBB3^{+}/NGFR^{+}$ counterparts. Further investigation could determine if $ERBB3^{+}/NGFR^{-}$ cells are the more prominent myogenic population in our day 50 cultures, and may explain why our transplantation studies showed few myofibers with human contribution.

5.4 Stem Cell Therapy's Largest Hurdle Remains Translating Benchtop to Clinic

In our study, direct injection of hESC-derived day 50 cultures into the cardiotoxin-injured TA muscles of NSG mice revealed that donor human cells remain in the host tissue at 30 and 60 DPI (Fig. 4.5 & 4.5). Hundreds of donor cells could be observed per muscle section at either time point (Fig. 4.6), but were mostly localized in the interstitial or intermuscular spaces. Considerable human laminin deposition was detected on myofibers in proximity to the human cells, indicating donor contribution to the ECM (Fig. 4.8). Fewer than 10 human cells per section, however, could be detected within myofibers (Fig. 4.7). Our observations are corroborated by the Hicks *et al*. study: they show that 1×10^{6} unsorted day 50 cultures had poor *in vivo* myogenic potential, showing fewer than 10 human-contributed myofibers per TA muscle section analyzed in *mdx*-NSG mice. The effect of *in vitro* culture on lowering myoblast engraftment potential compared to freshly isolated cells has been well documented as well (5, 59, 60), suggesting that cells of *in vitro* origin may have additional hurdles to overcome in cell therapy and require supplemental "priming" factors. Sorting for the most therapeutic populations may be sufficient though. Isolated $ERBB3^{+}/NGFR^{+}$ day 50

hESC-derived SMPs would generate upwards of 150 human fibers per section (5). Work from Xu *et al*. also shows the impact that sorting can have, though using adult cell material: bulk cultured myoblasts were unable to engraft in NSG mice, but numerous human myofibers were detected in animals that received as few as 5,000 $ITGB1^{+}/NCAM1^{+}$ cells.

The recipient mice used in our studies could also undergo injury and treatment regimens more amenable to donor cell engraftment. Alternatively, the NSG-mdx^{4Cv} dystrophic mouse model could be used to induce a more natural exercise-related injury (61). While some studies do show human cell engraftment in chemically injured murine muscle (62–64), other studies were unable to do so (11); in many cases ablation of the host's satellite cells using gamma irradiation either significantly improves or is required for donor cell contribution to myofibers (65–69). The recent Hicks *et al*. study suggests that donor cells can be co-injected with compounds like the TGFB inhibitor SB-431542 to improve cell engraftment (5). As our gene expression profiling suggests day 50 cells highly express genes of pathways inhibitory towards myogenesis—namely NOTCH and TGFB signaling (Fig. 3.3)—the co-injection with SB-43152 or the NOTCH inhibitor DAPT may further enhance our *in vivo* results.

The transplantation approach itself may be in need of improvement. Rather than transplanting dissociated cells, the transplantation of more in-tact hESC-derived myofibers (69)—or co-culturing hESC-derived myogenic cultures with murine myofibers prior to the myofiber transplant (70)—may yield more promising results. Recent studies have broached the possibility of engineering large (1 cm) contractile 3D myobundles from hESCs that can be directly sutured into recipient muscle (71, 72).

5.5 Conclusion

On the biological front, both stem cell therapy and AAV-mediated gene therapy have an uphill battle in translating results from model organisms into human patients (73, 74). Especially comparing the respective paces of stem cell therapy and technological advances, we may sooner see an artificial rather than biological solution to the problem of muscle atrophy (75–79). Naturally, however, a patient may rather keep the body they have than be replaced by artificial components.

There are other promising applications for *in vitro* hESC myogenesis not otherwise possible with alternative technologies. Knowledge derived from studying *in vitro* myogenesis can help us further understand the human embryo—which is ethically difficult *in vivo* compared to model organisms—and help us discern what is normal from abnormal during development. Specific muscle pathologies, for example, can be modelled *in vitro* from patient-derived iPSCs (50, 64, 80). The large quantities of human myogenic material could also be used to create a humanized-muscle mouse, wherein mouse to human variability may be reduced when conducting *in vivo* drug testing. Other hESC-derived cell types have been used for tissue-focused drug screening *in vitro* as well (81).

Overall, the works presented in this thesis have been repeatable across other labs and the differentiation protocol has served as the foundation of further research into human embryonic skeletal myogenesis.

5.6 References

1. Shelton M, Metz J, Liu J, Carpenedo RL, Demers SP, Stanford WL, Skerjanc IS. 2014. Derivation and expansion of PAX7-positive muscle progenitors from human and mouse embryonic stem cells. Stem Cell Reports 3:516–529.

2. Shelton M, Kocharyan A, Liu J, Skerjanc IS, Stanford WL. 2016. Robust generation and expansion of skeletal muscle progenitors and myocytes from human pluripotent stem cells. Methods 101:73–84.

3. Montarras D, Morgan J, Collins C, Relaix F, Zaffran S, Cumano A, Partridge T, Buckingham M. 2005. Direct isolation of satellite cells for skeletal muscle regeneration. Science 309:2064–7.

4. Charville GW, Cheung TH, Yoo B, Santos PJ, Lee GK, Shrager JB, Rando TA. 2015. Ex vivo expansion and in vivo self-renewal of human muscle stem cells. Stem Cell Reports 5:621–632.

5. Hicks MR, Hiserodt J, Paras K, Fujiwara W, Eskin A, Jan M, Xi H, Young CS, Evseenko D, Nelson SF, Spencer MJ, Handel B Van, Pyle AD. 2018. ERBB3 and NGFR mark a distinct skeletal muscle progenitor cell in human development and hPSCs. Nat Cell Biol 20:46–57.

6. Barberi T, Bradbury M, Dincer Z, Panagiotakos G, Socci ND, Studer L. 2007. Derivation of engraftable skeletal myoblasts from human embryonic stem cells. Nat Med 13:642–648.

7. Ryan T, Liu J, Chu A, Wang L, Blais A, Skerjanc IS. 2012. Retinoic Acid Enhances Skeletal Myogenesis in Human Embryonic Stem Cells by Expanding the Premyogenic Progenitor Population. Stem Cell Rev Reports 8:482–493.

8. Awaya T, Kato T, Mizuno Y, Chang H, Niwa A, Umeda K, Nakahata T, Heike T. 2012. Selective development of myogenic mesenchymal cells from human embryonic and induced pluripotent stem cells. PLoS One 7:e51638.

9. Borchin B, Chen J, Barberi T. 2013. Derivation and FACS-mediated purification of PAX3+/PAX7+ skeletal muscle precursors from human pluripotent stem cells. Stem Cell Reports 1:620–631.

10. Qu Z, Huard J. 2000. Matching host muscle and donor myoblasts for myosin heavy chain improves myoblast transfer therapy. Gene Ther 7:428–37.

11. Xu X, Wilschut KJ, Kouklis G, Tian H, Hesse R, Garland C, Sbitany H, Hansen S, Seth R, Knott PD, Hoffman WY, Pomerantz JH. 2015. Human Satellite Cell Transplantation and Regeneration from Diverse Skeletal Muscles. Stem Cell Reports 5:419–434.

12. Talbot J, Maves L. 2016. Skeletal muscle fiber type: using insights from muscle developmental biology to dissect targets for susceptibility and resistance to muscle disease. Wiley Interdiscip Rev Dev Biol 5:518–534.

13. Schiaffino S, Rossi AC, Smerdu V, Leinwand LA, Reggiani C. 2015. Developmental myosins: expression patterns and functional significance. Skelet Muscle 5:22.

14. Edom-Vovard F, Mouly V, Barbet JP, Butler-Browne GS. 1999. The four populations of myoblasts involved in human limb muscle formation are present from the onset of primary myotube formation. J Cell Sci 112:191–9.

15. Biressi S, Tagliafico E, Lamorte G, Monteverde S, Tenedini E, Roncaglia E, Ferrari S, Ferrari S, Cusella-De Angelis MG, Tajbakhsh S, Cossu G. 2007. Intrinsic phenotypic diversity of embryonic and fetal myoblasts is revealed by genome-wide gene expression analysis on purified cells. Dev Biol 304:633–651.

16. Messina G, Biressi S, Monteverde S, Magli A, Cassano M, Perani L, Roncaglia E, Tagliafico E, Starnes L, Campbell CE, Grossi M, Goldhamer DJ, Gronostajski RM, Cossu G. 2010. Nfix Regulates Fetal-Specific Transcription in Developing Skeletal Muscle. Cell 140:554–566.

17. Hill MA. 2007. Early human development. Clin Obstet Gynecol 50:2–9.

18. Hill MA. 2018. https://embryology.med.unsw.edu.au/embryology/index.php/Main_Page.

19. Fomenou MD, Scaal M, Stockdale FE, Christ B, Huang R. 2005. Cells of all somitic compartments are determined with respect to segmental identity. Dev Dyn 233:1386–1393.

20. Dias AS, de Almeida I, Belmonte JM, Glazier JA, Stern CD. 2014. Somites without a clock. Science 343:791–795.

21. Loh KMM, Chen A, Koh PWW, Deng TZZ, Sinha R, Tsai JMM, Barkal AAA, Shen KYY, Jain R, Morganti RMM, Shyh-Chang N, Fernhoff NBB, George BMM, Wernig G, Salomon REEA, Chen Z, Vogel H, Epstein JAA, Kundaje A, Talbot WSS, Beachy PAA, Ang LTT, Weissman ILL. 2016. Mapping the Pairwise Choices Leading from Pluripotency to Human Bone, Heart, and Other Mesoderm Cell Types. Cell 166:451–468.

22. Myokai F, Washio N, Asahara Y, Yamaai T, Tanda N, Ishikawa T, Aoki S, Kurihara H, Murayama Y, Saito T. 1995. Expression of the hepatocyte growth factor gene during chick limb development. Dev Dyn 202:80–90.

23. Scaal M, Bonafede a, Dathe V, Sachs M, Cann G, Christ B, Brand-Saberi B. 1999. SF/HGF is a mediator between limb patterning and muscle development. Development 126:4885–4893.

24. Taher L, Collette NM, Murugesh D, Maxwell E, Ovcharenko I, Loots GG. 2011. Global gene expression analysis of murine limb development. PLoS One 6.

25. Tirosh-Finkel L, Elhanany H, Rinon A, Tzahor E. 2006. Mesoderm progenitor cells of common origin contribute to the head musculature and the cardiac outflow tract. Development 133:1943–1953.

26. Nathan E, Monovich A, Tirosh-Finkel L, Harrelson Z, Rousso T, Rinon A, Harel I, Evans SM, Tzahor E. 2008. The contribution of Islet1-expressing splanchnic mesoderm cells to distinct branchiomeric muscles reveals significant heterogeneity in head muscle development. Development 135:647–657.

27. Sambasivan R, Gayraud-Morel B, Dumas G, Cimper C, Paisant S, Kelly R, Tajbakhsh S. 2009. Distinct Regulatory Cascades Govern Extraocular and Pharyngeal Arch Muscle Progenitor Cell Fates. Dev Cell 16:810–821.

28. Duxson MJ, Usson Y, Harris a J. 1989. The origin of secondary myotubes in mammalian skeletal muscles: ultrastructural studies. Development 107:743–750.

29. Deries M, Schweitzer R, Duxson MJ. 2010. Developmental fate of the mammalian myotome. Dev Dyn 239:2898–2910.

30. Rios AC, Serralbo O, Salgado D, Marcelle C. 2011. Neural crest regulates myogenesis through the transient activation of NOTCH. Nature 473:532–535.

31. Nitzan E, Kalcheim C. 2013. Neural crest and somitic mesoderm as paradigms to investigate cell fate decisions during development. Dev Growth Differ 55:60–78.

32. Harris AJ. 1981. Embryonic growth and innervation of rat skeletal muscles. I. Neural regulation of muscle fibre numbers. Philos Trans R Soc Lond B Biol Sci 293:257–77.

33. Kueera J, Walro JM. 1988. Histochemist The effect of neonatal deafferentation or deefferentation on myosin heavy chain expression in intrafusal muscle fibers of the rat. Histochemistry 4:151–160.

34. Osafune K, Caron L, Borowiak M, Martinez RJ, Fitz-Gerald CS, Sato Y, Cowan CA, Chien KR, Melton DA. 2008. Marked differences in differentiation propensity among human embryonic stem cell lines. Nat Biotechnol 26:313–315.

35. Närvä E, Autio R, Rahkonen N, Kong L, Harrison N, Kitsberg D, Borghese L, Itskovitz-Eldor J, Rasool O, Dvorak P, Hovatta O, Otonkoski T, Tuuri T, Cui W, Brüstle O, Baker D, Maltby E, Moore HD, Benvenisty N, Andrews PW, Yli-Harja O, Lahesmaa R. 2010. High-resolution DNA analysis of human embryonic stem cell lines reveals culture-induced copy number changes and loss of heterozygosity. Nat Biotechnol 28:371–377.

36. Chen X-M, Kan Q-C, Wang F, Kong H-J, Zhang Y-Y, Yu W-Z, Sun Y-P. 2012. Chromosome dynamic changes in two cultured chinese human embryonic stem cell lines: Single nucleotide polymorphism, copy number variation and loss of heterozygosity. J Cell Biochem 113:3520–3527.

37. Allegrucci C, Wu YZ, Thurston A, Denning CN, Priddle H, Mummery CL, Ward-van Oostwaard D, Andrews PW, Stojkovic M, Smith N, Parkin T, Jones ME, Warren G, Yu L, Brena RM, Plass C, Young LE. 2007. Restriction landmark genome scanning identifies culture-induced DNA methylation instability in the human embryonic stem cell epigenome. Hum Mol Genet 16:1253–1268.

38. Garitaonandia I, Amir H, Boscolo FS, Wambua GK, Schultheisz HL, Sabatini K, Morey R, Waltz S, Wang YC, Tran H, Leonardo TR, Nazor K, Slavin I, Lynch C, Li Y, Coleman R, Romero IG, Altun G, Reynolds D, Dalton S, Parast M, Loring JF, Laurent LC. 2015. Increased risk of genetic and epigenetic instability in human embryonic stem cells associated with specific culture conditions. PLoS One 10:1–25.

39. Kempf H, Olmer R, Haase A, Franke A, Bolesani E, Schwanke K, Robles-Diaz D, Coffee M, Göhring G, Dräger G, Pötz O, Joos T, Martinez-Hackert E, Haverich A, Buettner FFR, Martin U, Zweigerdt R. 2016. Bulk cell density and Wnt/TGFbeta signalling regulate mesendodermal patterning of human pluripotent stem cells. Nat Commun 7:13602.

40. Chal J, Oginuma M, Al Tanoury Z, Gobert B, Sumara O, Hick A, Bousson F, Zidouni Y, Mursch C, Moncuquet P, Tassy O, Vincent S, Miyanari A, Bera A, Garnier J-M, Guevara G, Hestin M, Kennedy L, Hayashi S, Drayton B, Cherrier T, Gayraud-Morel B, Gussoni E, Relaix F, Tajbakhsh S, Pourquié O. 2015. Differentiation of pluripotent stem cells to muscle fiber to model Duchenne muscular dystrophy. Nat Biotechnol 33:962–969.

41. Xi H, Fujiwara W, Gonzalez K, Jan M, Liebscher S, Van Handel B, Schenke-Layland K, Pyle AD. 2017. In Vivo Human Somitogenesis Guides Somite Development from hPSCs. Cell Rep 18:1573–1585.

42. Marinho PA, Chailangkarn T, Muotri AR. 2015. Systematic optimization of human pluripotent stem cells media using Design of Experiments. Sci Rep 5:1–13.

43. Magli A, Incitti T, Kiley J, Swanson SA, Darabi R, Rinaldi F, Selvaraj S, Yamamoto A, Tolar J, Yuan C, Stewart R, Thomson JA, Perlingeiro RCR. 2017. PAX7 Targets, CD54, Integrin α9β1, and SDC2, Allow Isolation of Human ESC/iPSC-Derived Myogenic Progenitors. Cell Rep 19:2867–2877.

44. Seale P, Sabourin LA, Girgis-Gabardo A, Mansouri A, Gruss P, Rudnicki MA. 2000. Pax7 Is Required for the Specification of Myogenic Satellite Cells. Cell 102:777–786.

45. Relaix F, Rocancourt D, Mansouri A, Buckingham M. 2004. Divergent functions of murine Pax3 and Pax7 in limb muscle development. Genes Dev 18:1088–1105.

46. Boldrin L, Muntoni F, Morgan JE. 2010. Are Human and Mouse Satellite Cells Really the Same? J Histochem Cytochem 58:941–955.

47. Bareja A, Holt JA, Luo G, Chang C, Lin J, Hinken AC, Freudenberg JM, Kraus WE, Evans WJ, Billin AN. 2014. Human and mouse skeletal muscle stem cells: convergent and divergent mechanisms of myogenesis. PLoS One 9:e90398.

48. Lapan AD, Rozkalne A, Gussoni E. 2012. Human fetal skeletal muscle contains a myogenic side population that expresses the melanoma cell-adhesion molecule. Hum Mol Genet 21:3668–3680.

49. Alexander MS, Rozkalne A, Colletta A, Spinazzola JM, Johnson S, Rahimov F, Meng H, Lawlor MW, Estrella E, Kunkel LM, Gussoni E. 2016. CD82 Is a Marker for Prospective Isolation of Human Muscle Satellite Cells and Is Linked to Muscular Dystrophies. Cell Stem Cell 19:800–807.

50. Choi IY, Lim HT, Estrellas K, Mula J, Cohen T V., Zhang Y, Donnelly CJ, Richard JP, Kim YJ, Kim H, Kazuki Y, Oshimura M, Li HL, Hotta A, Rothstein J, Maragakis N, Wagner KR, Lee G. 2016. Concordant but Varied Phenotypes among Duchenne Muscular Dystrophy Patient-Specific Myoblasts Derived using a Human iPSC-Based Model. Cell Rep 15:2301–2312.

51. Webster C, Pavlath GK, Parks DR, Walsh FS, Blau HM. 1988. Isolation of human myoblasts with the fluorescence-activated cell sorter. Exp Cell Res 174:252–265.

52. Albini S, Coutinho P, Malecova B, Giordani L, Savchenko A, Forcales SV, Puri PL. 2013. Epigenetic Reprogramming of Human Embryonic Stem Cells into Skeletal Muscle Cells and Generation of Contractile Myospheres. Cell Rep 3:661–670.

53. Meyer D, Birchmeier C. 1995. Multiple essential functions of neuregulin in development. Nature 378:386–390.

54. Gassmann M, Casagranda F, Orioli D, Simon H, Lai C, Klein R, Lemke G. 1995. Aberrant neural and cardiac development in mice lacking the ErbB4 neuregulin receptor. Nature 378:390–4.

55. Lee KF, Simon H, Chen H, Bates B, Hung MC, Hauser C. 1995. Requirement for neuregulin receptor erbB2 in neural and cardiac development. Nature 378:394–398.

56. Monk KR, Naylor SG, Glenn TD, Mercurio S, Perlin JR, Dominguez C, Moens CB, Talbot WS. 2009. A G protein-coupled receptor is essential for Schwann cells to initiate myelination. Science 325:1402–5.

57. Waller-Evans H, Prömel S, Langenhan T, Dixon J, Zahn D, Colledge WH, Doran J, Carlton MBL, Davies B, Aparicio SAJR, Grosse J, Russ AP. 2010. The orphan adhesion-GPCR GPR126 is required for embryonic development in the mouse. PLoS One 5:e14047.

58. Paavola KJ, Sidik H, Zuchero JB, Eckart M, Talbot WS. 2014. Type IV collagen is an activating ligand for the adhesion G protein-coupled receptor GPR126. Sci Signal 7:1–10.

59. DiMario JX, Stockdale FE. 1995. Differences in the developmental fate of cultured and noncultured myoblasts when transplanted into embryonic limbs. Exp Cell Res 216:431–42.

60. Cooper RN, Thiesson D, Furling D, Di Santo JP, Butler-Browne GS, Mouly V. 2003. Extended amplification in vitro and replicative senescence: key factors implicated in the success of human myoblast transplantation. Hum Gene Ther 14:1169–79.

61. Arpke RW, Darabi R, Mader TL, Zhang Y, Toyama A, Lonetree CL, Nash N, Lowe DA, Perlingeiro RCR, Kyba M. 2013. A new immuno-, dystrophin-deficient model, the NSG-mdx4Cvmouse, provides evidence for functional improvement following allogeneic satellite cell transplantation. Stem Cells 31:1611–1620.

62. Darabi R, Arpke RW, Irion S, Dimos JT, Grskovic M, Kyba M, Perlingeiro RCR. 2012. Human ES- and iPS-derived myogenic progenitors restore DYSTROPHIN and improve contractility upon transplantation in dystrophic mice. Cell Stem Cell 10:610–619.

63. Goudenege S, Lebel C, Huot NB, Dufour C, Fujii I, Gekas J, Rousseau J, Tremblay JP. 2012. Myoblasts Derived From Normal hESCs and Dystrophic hiPSCs Efficiently Fuse With Existing Muscle Fibers Following Transplantation. Mol Ther 20:2153–2167.

64. Young CS, Hicks MR, Ermolova N V., Nakano H, Jan M, Younesi S, Karumbayaram S, Kumagai-Cresse C, Wang D, Zack JA, Kohn DB, Nakano A, Nelson SF, Miceli MC, Spencer MJ, Pyle AD. 2016. A Single CRISPR-Cas9 Deletion Strategy that Targets the Majority of DMD Patients Restores Dystrophin Function in hiPSC-Derived Muscle Cells. Cell Stem Cell 18:533–540.

65. Gross JG, Bou-Gharios G, Morgan JE. 1999. Potentiation of myoblast transplantation by host muscle irradiation is dependent on the rate of radiation delivery. Cell Tissue Res 298:371–375.

66. LaBarge MA, Blau HM. 2002. Biological progression from adult bone marrow to mononucleate muscle stem cell to multinucleate muscle fiber in response to injury. Cell 111:589–601.

67. Zheng JK, Wang Y, Karandikar A, Wang Q, Gai H, Liu AL, Peng C, Sheng HZ. 2006. Skeletal myogenesis by human embryonic stem cells. Cell Res 16:713–722.

68. Boldrin L, Neal A, Zammit PS, Muntoni F, Morgan JE. 2012. Donor satellite cell engraftment is significantly augmented when the host niche is preserved and endogenous satellite cells are incapacitated. Stem Cells 30:1971–1984.

69. Marg A, Escobar H, Gloy S, Kufeld M, Zacher J, Spuler A, Birchmeier C, Izsvák Z, Spuler S. 2014. Human satellite cells have regenerative capacity and are genetically manipulatable. J Clin Invest 124:4257–4265.

70. Hall JK, Banks GB, Chamberlain JS, Olwin BB. 2010. Prevention of muscle aging by myofiber-associated satellite cell transplantation. Sci Transl Med 2:57ra83.

71. Rao L, Qian Y, Khodabukus A, Ribar T, Bursac N. 2018. Engineering human pluripotent stem cells into a functional skeletal muscle tissue. Nat Commun 9:1–12.

72. Maffioletti SM, Sarcar S, Henderson ABH, Mannhardt I, Pinton L, Moyle LA, Steele-Stallard H, Cappellari O, Wells KE, Ferrari G, Mitchell JS, Tyzack GE, Kotiadis VN, Khedr M, Ragazzi M, Wang W, Duchen MR, Patani R, Zammit PS, Wells DJ, Eschenhagen T, Tedesco FS. 2018. Three-Dimensional Human iPSC-Derived Artificial Skeletal Muscles Model Muscular Dystrophies and Enable Multilineage Tissue Engineering. Cell Rep 23:899–908.

73. Skuk D, Goulet M, Roy B, Piette V, Côté CH, Chapdelaine P, Hogrel JY, Paradis M, Bouchard JP, Sylvain M, Lachance JG, Tremblay JP. 2007. First test of a "high-density injection" protocol for myogenic cell transplantation throughout large volumes of muscles in a Duchenne muscular dystrophy patient: eighteen months follow-up. Neuromuscul Disord 17:38–46.

74. Mendell JR, Campbell K, Rodino-Klapac L, Sahenk Z, Shilling C, Lewis S, Bowles D, Gray S, Li C, Galloway G, Malik V, Coley B, Clark KR, Li J, Xiao X, Samulski J, McPhee SW, Samulski RJ, Walker CM. 2010. Dystrophin Immunity in Duchenne's Muscular Dystrophy. N Engl J Med 363:1429–1437.

75. Cove ME, MacLaren G, Federspiel WJ, Kellum JA. 2012. Bench to bedside review: Extracorporeal carbon dioxide removal, past present and future. Crit Care 16:232.

76. Mohacsi P, Leprince P. 2014. The CARMAT total artificial heart. Eur J Cardio-thoracic Surg 46:933–934.

77. Reardon S. 2015. The Military-Bioscience Complex. Nature 522:142–144.

78. Rouse EJ, Villagaray-Carski NC, Emerson RW, Herr HM. 2015. Design and Testing of a Bionic Dancing Prosthesis. PLoS One 10:e0135148.

79. Miriyev A, Stack K, Lipson H. 2017. Soft Material for Soft Actuators. Nat Commun 1–8.

80. Li HL, Fujimoto N, Sasakawa N, Shirai S, Ohkame T, Sakuma T, Tanaka M, Amano N, Watanabe A, Sakurai H, Yamamoto T, Yamanaka S, Hotta A. 2015. Precise correction of the dystrophin gene in duchenne muscular dystrophy patient induced pluripotent stem cells by TALEN and CRISPR-Cas9. Stem Cell Reports 4:143–154.

81. Zhou T, Tan L, Cederquist GY, Fan Y, Hartley BJ, Mukherjee S, Tomishima M, Brennand KJ, Zhang Q, Schwartz RE, Evans T, Studer L, Chen S. 2017. High-Content Screening in hPSC-Neural Progenitors Identifies Drug Candidates that Inhibit Zika Virus Infection in Fetal-like Organoids and Adult Brain. Cell Stem Cell 21:274–283.

Methods 101 (2016) 73–84

Contents lists available at ScienceDirect

Methods

journal homepage: www.elsevier.com/locate/ymeth

Robust generation and expansion of skeletal muscle progenitors and myocytes from human pluripotent stem cells

Michael Shelton [a], Avetik Kocharyan [a,b], Jun Liu [a], Ilona S. Skerjanc [a,*], William L. Stanford [a,b,c,d,*]

[a] Department of Biochemistry, Microbiology and Immunology, University of Ottawa, Ottawa, ON, Canada
[b] The Sprott Center for Stem Cell Research, Regenerative Medicine Program, Ottawa Hospital Research Institute, Ottawa, ON K1H 8L6, Canada
[c] Department of Cellular and Molecular Medicine, University of Ottawa, Ottawa, ON, Canada
[d] Ottawa Institute of Systems Biology, Ottawa, ON, Canada

ARTICLE INFO

Article history:
Received 28 July 2015
Received in revised form 16 September 2015
Accepted 19 September 2015
Available online 25 September 2015

Keywords:
Embryonic stem cells
Induced pluripotent stem cells
Myogenesis
CHIR99021
Skeletal muscle
PAX7

ABSTRACT

Human pluripotent stem cells provide a developmental model to study early embryonic and tissue development, tease apart human disease processes, perform drug screens to identify potential molecular effectors of *in situ* regeneration, and provide a source for cell and tissue based transplantation. Highly efficient differentiation protocols have been established for many cell types and tissues; however, until very recently robust differentiation into skeletal muscle cells had not been possible unless driven by transgenic expression of master regulators of myogenesis. Nevertheless, several breakthrough protocols have been published in the past two years that efficiently generate cells of the skeletal muscle lineage from pluripotent stem cells. Here, we present an updated version of our recently described 50-day protocol in detail, whereby chemically defined media are used to drive and support muscle lineage development from initial CHIR99021-induced mesoderm through to PAX7-expressing skeletal muscle progenitors and mature skeletal myocytes. Furthermore, we report an optional method to passage and expand differentiating skeletal muscle progenitors approximately 3-fold every 2 weeks using Collagenase IV and continued FGF2 supplementation. Both protocols have been optimized using a variety of human pluripotent stem cell lines including patient-derived induced pluripotent stem cells. Taken together, our differentiation and expansion protocols provide sufficient quantities of skeletal muscle progenitors and myocytes that could be used for a variety of studies.

1. Introduction

Human embryonic stem cells (hESCs) and induced pluripotent stem cells (iPSCs) are versatile model systems for studying a multitude of tissues: when given the proper stimuli, hESCs and iPSCs can be differentiated into desired cell types and tissues. In addition to their use in dissecting human developmental pathways and disease, pluripotent cells possess an incredible proliferation capacity amenable to generating large quantities of transplantable material for cell-based therapies. For example, heart disease being a leading cause of death world-wide has arguably motivated the development of numerous protocols to generate cardiac muscle from hESCs [1–3]. In fact, the ability to generate pure populations of functional retinal pigmented epithelial (RPE) cells from pluripotent stem cells (PSCs) has led to several ongoing clinical trials using RPE cells derived from both ESCs and iPSCs to treat age-related macular degeneration and Stargardt disease, with early success being reported in an ESC-derived RPE clinical trial [4,5].

In contrast to cardiac muscle or RPE cells, until very recently, little success has been achieved in terms of skeletal muscle differentiation from human PSCs [6–9]. Thus, while PSC-derived cardiomyocytes have been used to dissect disease mechanisms [10] and provide proof of concept for cardiac regeneration by cardiomyocyte transplantation in non-human primate pre-clinical

Abbreviations: hESCs, human embryonic stem cells; iPSCs, induced pluripotent stem cells; PSCs, pluripotent stem cells; EBs, embryoid bodies; SMPs, skeletal muscle progenitors; TC, tissue culture; MRFs, myogenic regulatory factors; FACS, fluorescence activated cell sorting; BSA, bovine serum albumin; EGF, epidermal growth factor; FGF2, fibroblast growth factor 2; E8, Essential 8 media; RPE, retinal pigmented epithelial; EMT, epithelial to mesenchymal transition; T, Brachyury; MSGN1, Mesogenin 1; GOI, gene of interest; DOI, day of interest.

* Corresponding authors at: Department of Biochemistry, Microbiology and Immunology, Rm 4218, University of Ottawa, 451 Smyth Road, Ottawa, ON K1H 8M5, Canada (I.S. Skerjanc). Ottawa Hospital Research Institute, The Ottawa Hospital, 501 Smyth Rd, Box 511, Ottawa, ON K1H 8L6, Canada (W.L. Stanford).

E-mail addresses: iskerjan@uottawa.ca (I.S. Skerjanc), wstanford@ohri.ca (W.L. Stanford).

http://dx.doi.org/10.1016/j.ymeth.2015.09.019
1046-2023/

studies [11], the skeletal muscle field has not progressed on these fronts.

The development of robust protocols to differentiate human PSCs into a specific cell or tissue type requires a thorough understanding of the developmental networks that drive specification, differentiation and expansion of the desired cell or tissue type to identify factors that can replace the highly organized physical structures and complex signaling networks—both spatial and temporal—naturally found *in vivo* [12]. A detailed account of the embryonic origins of skeletal muscle are succinctly reviewed in [13].

The first generation of non-transgenic strategies to generate skeletal muscle from ESCs utilized cell aggregation into embryoid bodies (EB) to induce differentiation [14–17]. However, cells are exposed to varying concentrations of endogenous and exogenous factors depending on their position within the EB. Furthermore, the first generation of differentiation protocols also relied on media supplemented with undefined serum, which led to variable differentiation efficiencies from one serum lot to the next. As a result, skeletal myocytes typically represented less than 10% of the total differentiated cells [18,19].

Fortunately for the skeletal muscle field, the intensive and productive research performed on cardiac muscle differentiation provides insight into the early stages of skeletal muscle differentiation as both cardiac and skeletal muscle originate from the mesodermal germ layer, allowing well-established PSC cardiac differentiation protocols to serve as a starting point for directing skeletal myogenesis. Within the past couple of years, several remarkable protocols have been established detailing chemically directed approaches to hESC and iPSC skeletal myogenesis, reaching over 50% differentiation efficiency [6,8,9]. Three recent studies, including our own, independently developed a similar approach: stimulating Wnt signaling in monolayer cells by treating with CHIR99021 to induce mesoderm [7,8]. These protocols additionally use fibroblast growth factor 2 (FGF2) to further support mesoderm commitment into the skeletal muscle lineage, although significant differences between the protocols exist including the concentration and time of application for both factors. Additionally, Suzuki and colleagues concurrently reported an efficient protocol using an aggregate-based approach in which hESCs are treated with FGF2 and epidermal growth factor (EGF) [9].

Potentially the most important result in any of the myogenic differentiation protocols—with the purpose of cell therapy in mind—is the persistence of skeletal muscle progenitors (SMPs). This is because terminally differentiated myoblasts or myocytes cannot appreciably proliferate, and therefore, have limited repair potential following transplantation.

Adult SMPs, known as satellite cells, reside beneath the basal lamina in muscle fibers and are defined by their location and expression of the transcription factor PAX7 [20]. Satellite cells are activated to proliferate in response to injury, and these dividing cells contribute to the differentiation of new myocytes and maintenance of the progenitor pool. Satellite cells cannot be identified within *in vitro* differentiation cultures because the structures forming the satellite cell niche simply are not formed. The protocol described here, however, generates proliferative PAX7 expressing cells found interspersed among skeletal myocytes and myotubes.

2. Experimental design

2.1. hESC and iPSC cell culture

Human PSC lines were maintained using Essential 8 (E8) medium as previously described [21]. In this approach, cells are maintained in a serum-free, feeder cell-free environment and cultured in Matrigel coated 6-well tissue culture (TC) plates using E8 medium. We also find routine passage with EDTA solution provides a consistent cell proliferation rate, as well as improved survival compared to enzymatic methods [22]. Another advantage of EDTA-mediated passage is the reduction in spontaneous differentiation of pluripotent colonies. Using EDTA passaging at a split ratio of 1:6, H1 and H9 hESCs as well as a variety of iPSC lines generated in our group routinely take 3–4 days post-passage to become 70–80% confluent with no alterations in karyotype for at least 20 passages: a time point in which maintenance of the cell line is terminated to prevent population drift and a new aliquot of cells is thawed. In contrast to EDTA passaging, collagenase-based passaging is also performed at a split ratio of 1:6 but every 5–7 days depending on cell loss due to spontaneous differentiation. If spontaneous differentiation occurs, we "clean" our cultures under a dissecting microscope by scraping off differentiated colonies marked by irregular, undefined borders (Fig. 1A, 5 DPP) using a pipette tip.

2.2. Differentiation into the myogenic lineage

Prior to differentiation, it is essential to ensure 80–90% of cells are undifferentiated and cultures are 70–80% confluent (Fig. 1A, 3 DPP).

The first step in our differentiation protocol, and a major hurdle of producing an efficient and reproducible protocol, is the dissociation of colonies into single cells while still maintaining their pluripotency and viability. Dissociating colonies into single cells ensures that the small molecules used to induce differentiation act evenly across all cells, and that plating densities can be better controlled for consistent amounts of crucial cell-to-cell contact between experiments.

Prior to dissociation, the pluripotent cells are treated with 10 μM ROCK inhibitor (Y-27632) to reduce dissociation-induced apoptosis [23]. We then utilize TrypLE—a mild form of trypsin—to dissociate the colonies into single cell suspension. Exposure to TrypLE for up to 5 min is sufficient for generating a single cell suspension, and has minimal effect on cell viability.

For the H9 ESC line, re-plating in E8 media supplemented with 10 μM Y-27632 at a density of 1.5×10^5 cells per well of a 12-well tissue culture plate was found to be optimal for cell survival and subsequent mesoderm induction [6]. Optimal re-plating density may vary, however, depending on the cell lines used in the protocol. We have found that optimal seeding of some cell lines—such as the 167-1J Hutchinson–Gilford Progeria Syndrome patient-derived iPSCs (unpublished)—requires up to 3×10^5 cells per well of a 12-well tissue culture plate. Cells are ready for differentiation roughly 24 h later (Fig. 1B).

Cells are then treated with 10 μM CHIR99021 supplemented E6 media—E8 media lacking the pluripotency factors FGF2 and TGF-β1—to simulate Wnt signaling during gastrulation. CHIR99021, a potent GSK3 inhibitor, has been extensively used to drive mesoderm specification in cardiac and other mesoderm-lineage differentiation protocols [1,3,24]. There is a notably high level of cell death—approximately 25% of total cells—24 h after the initial CHIR99021 treatment (Fig. 1B), which we observe to correlate with more efficient mesoderm induction. By 2 days following CHIR99021 treatment, however, the remaining cells appear to recover and their morphology is dramatically altered indicative of epithelial to mesenchymal transition (EMT) (Figs. 1B and 2A). At this point, peak levels of Brachyury (T) and Mesogenin 1 (MSGN1) can be used to confirm the presence of uncommitted and paraxial mesoderm, respectively (Fig. 1C and D). MSGN1 and TBX6, specifically, are key transcription factors which we use as markers of the early stages of skeletal muscle differentiation, as they mark the earliest mesodermal cells that possess skeletal myogenic potential [25,26], rather than cardiac or smooth muscle.

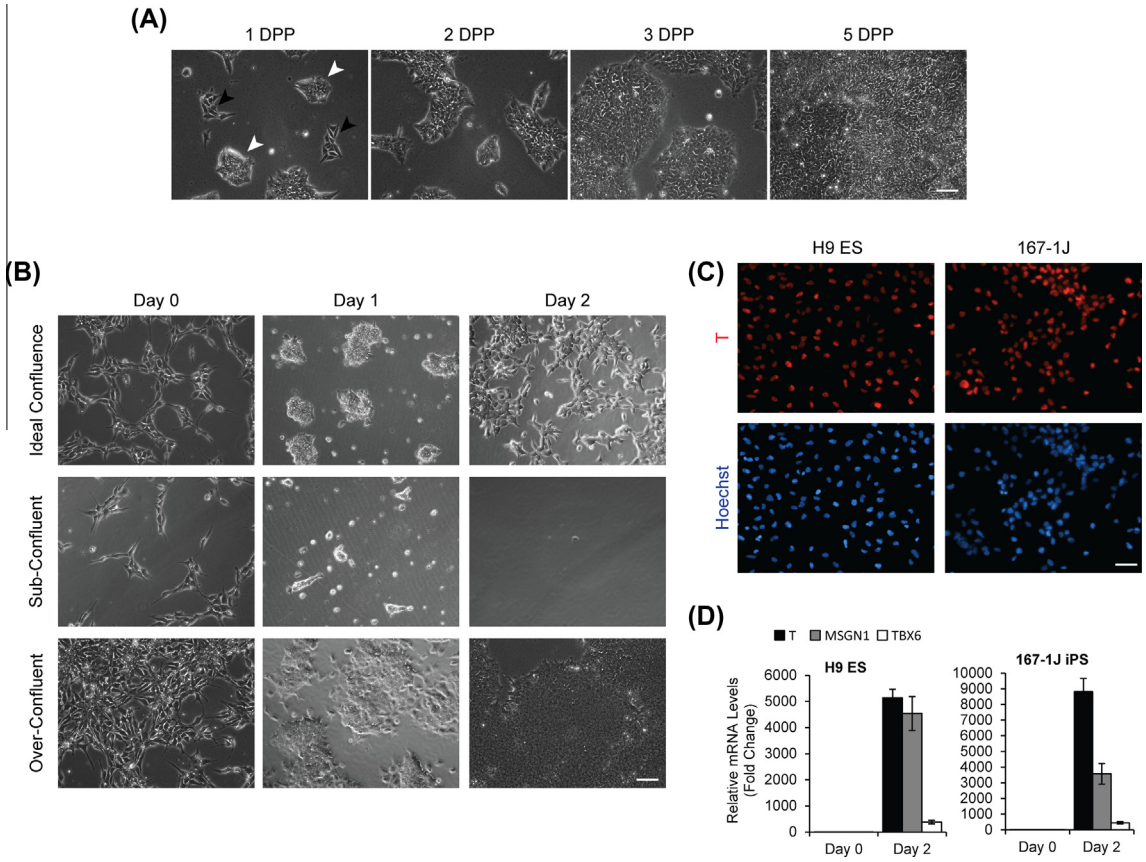

Fig. 1. Appearance of pluripotent stem cells during propagation and differentiation. (A) Pluripotent H9 cultures are shown from 1 to 5 days post passage (DPP). Prematurely differentiated cells may appear darker with distinct borders visible between cells (black arrows). Ideal pluripotent colonies appear lighter, and resolving individual cells becomes difficult (white arrows). The cells are ready for passage when cultures reach 70–80% confluence, while colonies remain distinct monolayers (as shown at 3 DPP). Cultures that no longer contain distinct colonies or show three-dimensional (3D) overgrowth—seen at 5 DPP—are not ideal (scale bar = 20 μm). (B) Differentiation: at Day 0, PSCs should ideally appear in primary clusters of approximately a dozen cells, with some interconnections between clusters (top row). Some cell stress and death is expected by Day 1, after the initiation of CHIR99021 treatment. Cells recover by Day 2—at the cessation of CHIR99021 treatment—and appear cobblestone-like with distinct cell borders. PSCs that have not formed large enough clusters, nor the appropriate cell–cell contacts between them before initiating differentiation, will likely not survive CHIR99021 (middle row). Over-confluent ESCs will likely not differentiate in response to CHIR99021 and continue to look like pluripotent colonies (bottom row) (scale bar = 20 μm). (C) Day 2 H9 ES and 167-1J iPS cells were stained with antibodies against T (red) and Hoechst dye (blue). The vast majority of cells should show nuclear T staining to indicate efficient mesoderm induction (scale bar = 20 μm). (D) Day 2 mRNA levels were analyzed by qPCR for T, MSGN1, and TBX6; results are expressed as fold change over Day 0. The ideal relative expression of T and MSGN1 ranges from mid- to high-thousands fold over Day 0, while TBX6 should appear in the mid-hundreds (n = 3).

Subsequently, cells are cultured in E6 medium without CHIR99021 until Day 12. During this period, cells undergo enhanced proliferation and reach confluence by approximately Day 4 of differentiation. Broad expression of somite markers PAX3 and MEOX1 can be detected from Days 6–12, and distinct 3D clusters should be apparent throughout the well (Fig. 2A).

Beginning on Day 12, StemPro-34 complete medium supplemented with 5 ng/mL FGF2 is used until Day 20 to support the commitment of cultures to the myogenic lineage. FGF2 is used to suppress potential early expression of myogenic regulatory factors (MRFs) [19] and promote progenitor cell proliferation [27]; thus, FGF2 supplementation during this time period supports preferential expansion of SMPs while limiting their premature differentiation.

By Day 20, there is a sizable population of actively proliferating cells that express the SMP transcription factor PAX7. By Day 20 in the differentiation protocol, the expression of the MRFs (MYF5, MYOD1, and MYOG) is observed; however, skeletal myocytes are not typically present at this stage. Therefore, we suggest examining expression of PAX7, the MRFs, and the structural muscle gene MYH3 on Day 20 to confirm that differentiation is proceeding to the early dermomyotome-like stage as expected: relative mRNA levels for *MYF5* and *MYH3* should be 3- to 10-fold more than *PAX7* [6].

From Days 20–35, the cultures are grown in E6 media (Fig. 2B), which supports both the proliferation of and differentiation of SMPs. The first differentiated myocytes start to appear in culture by Day 35, although this may occur earlier depending upon the pluripotent stem cell line.

To promote terminal differentiation and maturation of the myogenic cultures, E6 medium is changed to N2–ITS medium on Day 35 and cultured until Day 50. Expression of terminal muscle specific genes—the MRFs and muscle structural protein MYH3—peaks during this time. Day 50 is our chosen endpoint of differentiation as the vast majority of cells have committed to the skeletal muscle lineage by this time point. In our hands, approximately 50% of the cells are myocytes or myotubes and 40% are PAX7-expressing SMPs (Fig. 3). Importantly, the PAX7-expressing population is not depleted but continues to expand as many of these SMPs actively incorporate EdU [6]. This finding suggests that the cells could be expanded by passaging.

2.3. Passaging differentiating cultures

We have found that there is a large enough population of PAX7-expressing cells by Day 20 to allow for splitting and seeding the cells at roughly a 1:3 ratio (Fig. 2C). This step enables a greater

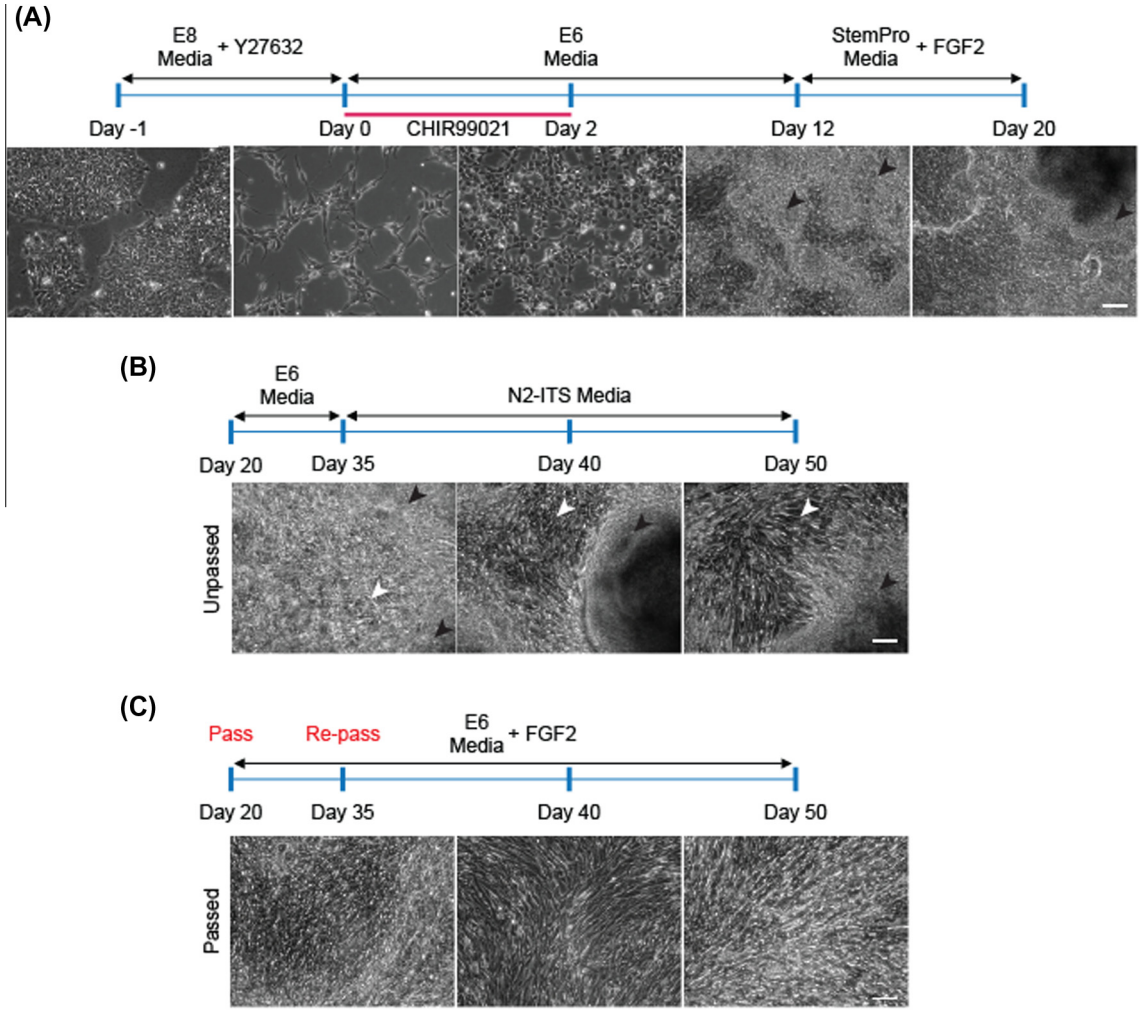

Fig. 2. Schematic timeline of the 50 Day *in vitro* differentiation. (A) Pluripotent H9 stem cell colonies—shown at Day-1—are trypsinized and plated in the presence of Y27632. Approximately 24 h later, CHIR99021 is applied to initiate differentiation, deemed Day 0. CHIR99021 is removed at Day 2, when cells express mesoderm and paraxial mesoderm markers T, MSGN1, and TBX6. Cultures eventually transition from monolayers to form 3D structures (black arrows). (B) Cultures may be left unpassed, and skeletal myocytes will become visible between Days 40 and 50 (white arrows). (C) If the 3D structures are impeding visual analysis, or SMP expansion is desired, the cells can be passed at Day 20 and again at Day 35 (scale bar = 20 μm).

expansion of the myogenic cultures, and aids visual analysis by dispersing the densely packed 3D overgrowth into a more uniform monolayer (Figs. 2 and 3). Passaging the cultures can be carried out at later stages of differentiation if the application calls for it. We find a first passage at Day 20 followed by a second passage at Day 35 permits serially-passaged cultures to expand about 9-fold by Day 50 compared to unpassaged cells.

Prior to passaging, cells must be treated with 10 μM Y-27632. As stated above, this greatly enhances cell viability by preventing anoikis. We find Collagenase IV to be more supportive of continued myogenic development than TrypLE or EDTA when it comes to dissociating differentiating cells, in contrast to pluripotent cultures.

Cultures are Collagenase IV treated for 20 min and then repeatedly triturated to achieve detachment from the plate and dissociation of the cell aggregates. It is imperative not to expose cells to collagenase for more than 40 min, or to pipette too aggressively, as this will dramatically decrease cell viability post-plating. Therefore, it is important to achieve a healthy balance between time and vigor spent mechanically dissociating the cells, and leaving cell material in too large of clumps that would make re-plating at the desired culture density more difficult and cause an excessive number of cells to be lost during any filtration steps. We recommend pipetting a single well of cells for no more than 1 min, and then letting the cell suspension settle for 10 s in a 15 mL centrifuge tube so that cell clumps over roughly 30 cells—large enough to be visible by eye—or extracellular protein aggregates settle to the bottom of the tube. This brief gravity separation step allows for a relatively more uniform distribution of cells upon re-plating.

Although a single cell suspension may not be reached, a rough cell count can obtained using an automated counter or hemocytometer. Alternatively, cells can be filtered through a 70 μm cell strainer if exact cell numbers are needed for more precise re-plating densities, or for other applications such as fluorescence activated cell sorting (FACS).

Passaged cells should be re-plated at approximate densities of 3×10^5 cells per well of a 12-well plate; this often corresponds to roughly a 1:3 passage. Passaged cells are cultured in E6 medium supplemented with FGF2 to encourage PAX7-expressing SMPs to expand (Fig. 4). Cells can be re-passaged when judged 80% confluent; as mentioned above, we suggest passage after approximately 2 weeks. Otherwise, harvest or prepare cultures for endpoint analysis.

2.4. Endpoint analysis

The experimental "endpoint" will of course depend on experimental design, and which cell population is desired. As stated

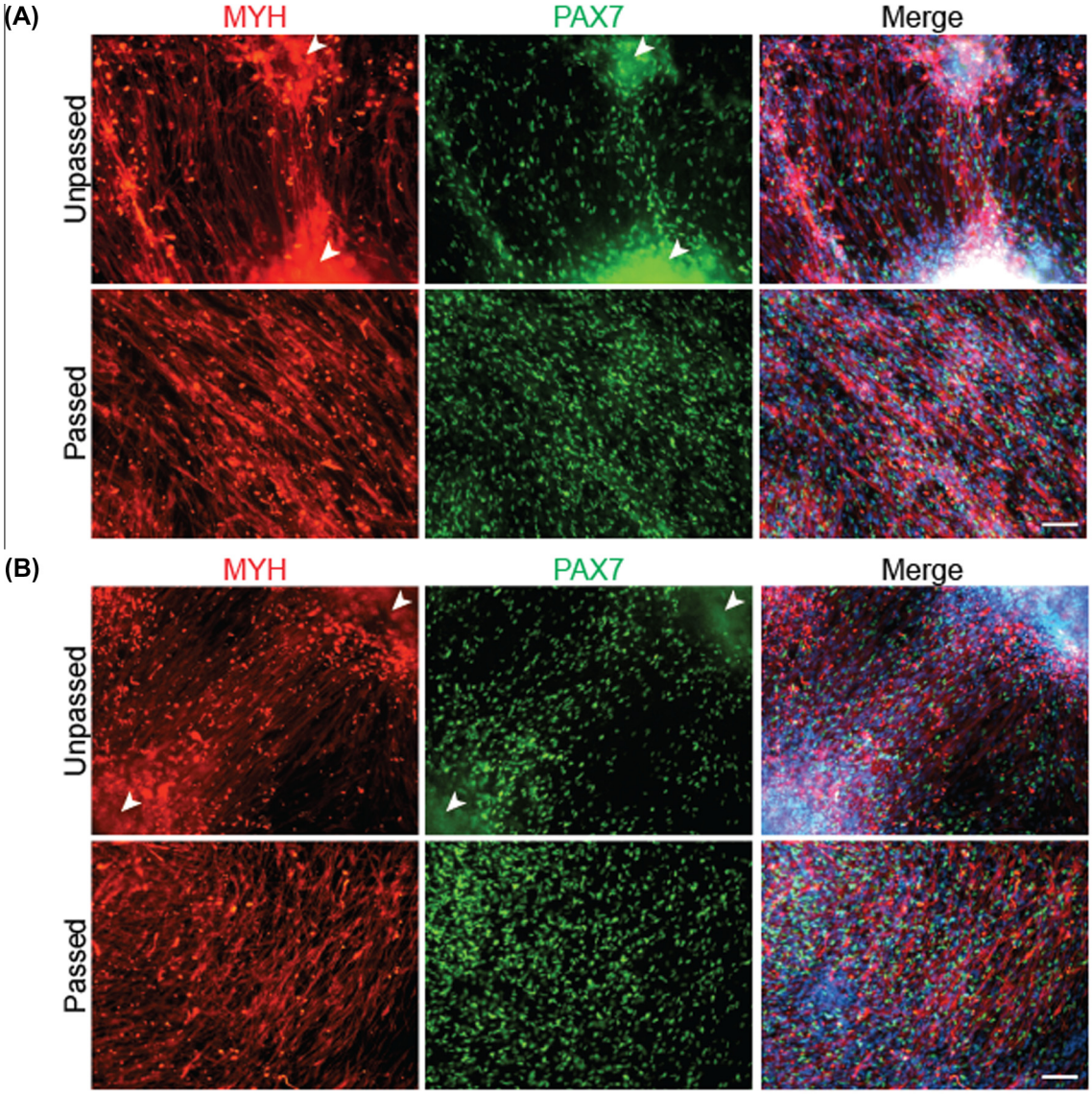

Fig. 3. Immunofluorescence comparison of both passed and unpassed myogenic cultures at Day 50. (A) H9 ES and (B) 167-1J iPS cells were differentiated as described in Fig. 2, and stained with antibodies against myosin heavy chain (MYH) (red), PAX7 (green), and Hoechst dye (blue). Levels of skeletal myogenesis appear similar in either condition, though unpassed cultures retain more difficult to image 3D structures (white arrows) (scale bar = 20 μm).

above, we provide suggested markers to monitor differentiation at particular time points that may correspond to *in vivo* developmental milestones. To our knowledge, myogenic hESC and iPSC populations can be cultured for upwards of 100 days.

During the course of this protocol, the efficiency of differentiation is primarily assayed through immunofluorescence (IF) staining. All antibody labeling is performed directly in-dish. Removable glass coverslips may be coated with Matrigel and used as well. However, glass coverslips should be harvested within roughly 2 weeks of plating cells on them. We find that cells cultured on coverslips for longer periods may lose their affinity to the glass and detach from the coverslip entirely as one intact "sheet" of cells when processing them for staining.

There is no reason why protein expression cannot be analyzed by flow cytometry; however, we have focused on IF or high content imaging because it allows us to assess the percentage of cells expressing nuclear as opposed to cytoplasmic protein, which we have noticed for T under certain conditions.

Reverse transcriptase qPCR can be used in parallel with IF staining, and may be particularly useful if quality antibodies aren't available for genes of interest.

3. Materials

3.1. Cells

Human embryonic stem cells: H9 cells, WA09 (WiCell, Madison, WI).

A variety of control and patient-derived human iPSC lines (including 167-1J, which is shown in Figs. 1 and 3) reprogrammed in the Stanford laboratory including those previously described [28,29].

3.2. Reagents

BSA (Jackson ImmunoResearch Laboratories, West Grove, PA, Catalog #001-000-161)
CHIR99021 (TOCRIS Bioscience, Bristol, UK, Catalog #4423)
Citric acid (Fisher, Waltham, MA, Catalog #A940-500)
Collagenase Type IV (Gibco by Lifetech, Grand Island, NY, Catalog #17104-019)
DMEM/F12 1:1 (Gibco by Lifetech, Grand Island, NY, Catalog #11330-032)

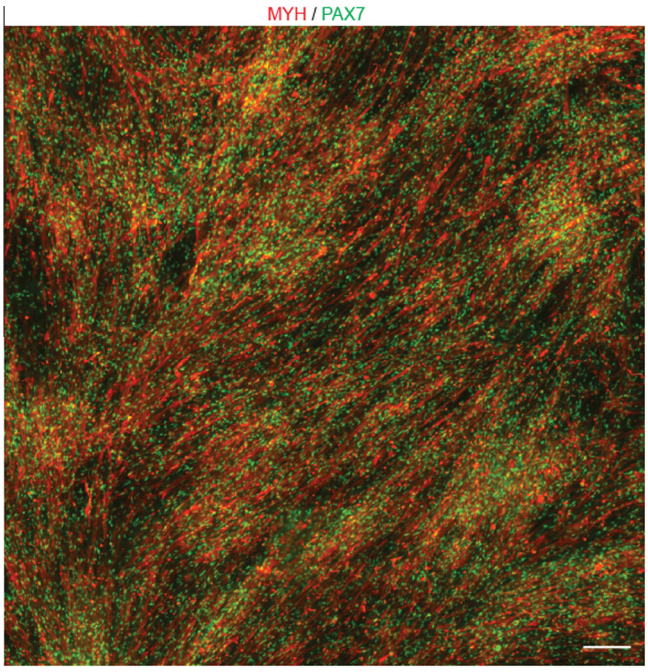

Fig. 4. Large-scale imaging of passed myogenic cultures at Day 50. H9 cells were differentiated and passed as described, followed by IF analysis for MYH (red) and PAX7 (green). Cultures contain a fairly even distribution of PAX7 positive SMPs interspersed among terminally differentiated myocytes or myotubes (scale bar = 200 μm).

DMSO (Sigma–Aldrich, St. Louis, MO, Catalog #D2650)
Donkey Serum (Jackson ImmunoResearch Laboratories, West Grove, PA, Catalog #017-000-121)
DPBS (Gibco by Lifetech, Grand Island, NY, Catalog #14190-144)
EDTA (Bio-Rad, Hercules, CA, Catalog #161-0729)
Formaldehyde (Sigma–Aldrich, St. Louis, MO, Catalog #F1635)
Gentamicin (Gibco by Lifetech, Grand Island, NY, Catalog #15750-060)
Glycerol (Fisher Scientific, Waltham, MA, Catalog #G33-1)
Goat Serum (Jackson ImmunoResearch Laboratories, West Grove, PA, Catalog #005-000-121)
Hoechst dye 33258 (Sigma–Aldrich, St. Louis, MO, Catalog #B-2883)
Human Holo-Transferrin (Sigma–Aldrich, St. Louis, MO, Catalog #T0665)
Insulin (Wisent, Saint-Jean-Baptiste, QC, Catalog #511-016-CM)
Insulin–transferrin–selenium (ITS; Gibco by Lifetech, Grand Island, NY, Catalog #41400-045)
KAPA SYBR FAST Universal qPCR Kit (KAPA Biosystems, Wilmington, MA, Catalog #KK4618)
KCl (EMD Millipore, Billerica, MA, Catalog #1049380050)
KH_2PO_4 (Fisher Chemicals, Waltham, MA, Catalog #P288-100)
KnockOut DMEM (Gibco by Lifetech, Grand Island, NY, Catalog #10829-018)
KnockOut Serum Replacement (KOSR; Gibco by Lifetech, Grand Island, NY, Catalog #10828028)
L-Ascorbic Acid 2-Phosphate Sesquimagnesium Salt Hydrate (Sigma–Aldrich, St. Louis, MO, Catalog #A8960-5G)
L-Glutamine 200 mM (Gibco by Lifetech, Grand Island, NY, Catalog #25030-149)
Matrigel (Corning, Corning, NY, Catalog #3542341)
Monothioglycerol (MTG; Sigma–Aldrich, St. Louis, MO, Catalog #M6145)
NaCl (Fisher Chemicals, Waltham, MA, Catalog #S27110)
NaH_2PO_4 (Fisher Chemicals, Waltham, MA, Catalog #S369)
Na_2HPO_4 (Fisher Chemicals, Waltham, MA, Catalog #SS373500)
$NaHCO_3$ (Sigma–Aldrich, St. Louis, MO, Catalog #S6297)
N-2 supplement (Gibco by Lifetech, Grand Island, NY, Catalog #17502-048)
QuantiTect Reverse Transcription kit (Qiagen, Hilden, Germany, Catalog #205314)
Recombinant Human FGF2 (Gibco by Lifetech, Grand Island, NY, Catalog #PHG0263)
Recombinant Human Transforming Growth Factor (TGF-β; Gibco by Lifetech, Grand Island, NY, Catalog #PHG9211)
Sodium Selenite (Sigma–Aldrich, St. Louis, MO, Catalog #214485)
StemPro-34 SFM (Gibco by Lifetech, Grand Island, NY, Catalog #10640-019)
StemPro-34 supplement (Gibco by Lifetech, Grand Island, NY, Catalog #10641-025)
E.Z.N.A. Total RNA kit I (OMEGA Bio-Tek, Norcross, GA, Catalog #R6834-02)
Triton X-100 (Bio-Rad, Hercules, CA, Catalog #161-0407)
TrypLE Express (Gibco by Lifetech, Grand Island, NY, Catalog #12604-013)
Y-27632 Dihydrochloride (TOCRIS Bioscience, Bristol, UK, Catalog #1254)

3.3. Antibodies

Brachyury T (T; Abcam, Toronto, ON, Catalog #AB20680)
MF20 (Developmental Studies Hybridoma Bank, Iowa City, IA, Catalog #AB2147781)
PAX7 (Developmental Studies Hybridoma Bank, Iowa City, IA, Catalog #AB528428)
AlexaFluor488 goat anti-mouse IgG1 (Jackson ImmunoResearch, West Grove, PA, Catalog #115-545-205)
Cy3 goat anti-mouse IgG2b (Jackson ImmunoResearch, West Grove, PA, Catalog #115-165-207)
Cy3 goat anti-rabbit IgG (Jackson ImmunoResearch, West Grove, PA, Catalog #111-165-003)

3.4. Equipment and disposables

Biosafety Cabinet
Camera: Micropublisher 3.3 RTV (Q Imaging)
Cell Lifters (Fisher Scientific, Waltham, MA, Catalog #08-100-240)
Cell strainer 70 μm Nylon (Corning, Corning, NY, Catalog # 431751)
Centrifuge
Centrifuge tubes, 15 mL (Corning, Corning, NY, Catalog #430053)
Centrifuge tubes, 50 mL (Corning, Corning, NY, Catalog #430291)
CO_2 incubator
Cytometer: Z Series Coulter Counter (Beckman Coulter)
Fluorescent microscope: Leica DMI6000 B (Leica Microsystems)
Imaging Software: Volocity (PerkinElmer)
Light Microscope
Masterclear real-time PCR Film (Eppendorf Canada, Mississauga, ON, Catalog #0030132947)
Spectrophotometer: NanoDrop ND-1000 (ThermoScientific)
Osmometer
pH Meter
Pipette, 10 μL
Pipette, 20 μL
Pipette, 200 μL
Pipette, 1000 μL
Pipette tips, 0.1–10 μL (Fisher Scientific, Waltham, MA, Catalog #02-707-147)

Pipette tips, 1–200 μL (Corning, Corning, NY, Catalog #4866)
Pipette tips, 100–1000 μL (Corning, Corning, NY, Catalog #4868)
Pipette tips, 100–1000 μL wide mouth (Axygen, Union City, CA, Catalog #TF-1005-WB-L-R-S)
qPCR Thermocycler: Mastercycler ep Realplex (Eppendorf)
Vacuum filter/bottle storage system (Corning, Corning, NY, Catalog #430758)
1 mL TB syringe (BD, Franklin Lakes, NJ, Catalog #309625)
5 mL surgical pipette (Fisherbrand, Waltham, MA, Catalog #13-678-11D)
10 mL surgical pipette (Fisherbrand, Waltham, MA, Catalog #13-678-11E)
25 mL surgical pipette (Fisherbrand, Waltham, MA, Catalog #13-678-11)
6-well tissue culture plates (Corning, Corning, NY, Catalog #3506)
12-well tissue culture plates (Corning, Corning, NY, Catalog #3512)
96-well PCR plates (Eppendorf Canada, Mississauga, ON, Catalog #E951020401)

3.5. Reagent setup

3.5.1. CHIR99021 (CHIR)
Reconstitute the powder (10 mg) with 2.149 mL of DMSO to prepare a 10 mM stock of the reagent. Aliquot and store at −20 °C.

3.5.2. Citric acid (10 mM)
Dissolve 192.12 mg of crystals in 100 mL of sterile double-distilled water to make 10 mM stock solution. Store the solution at room temperature for up to 3 months.

3.5.3. Collagenase IV
Dissolve 138 mg of Collagenase IV into 200 mL of DMEM/F12. Sterile filter the solution. Prepare aliquots and store at −20 °C.

3.5.4. EDTA passaging solution
Prepare a 0.5 M EDTA solution by dissolving 18.61 g of solid EDTA into 80 mL of sterile double-distilled water. Adjust the pH to 8. Top the volume up to 100 mL with sterile double-distilled water. Pipette 500 μL of 0.5 M EDTA into 500 mL of DPBS. Add 0.9 g of NaCl and adjust the osmolarity to 340 mOsm. Sterile filter, prepare aliquots, and store at 4 °C for up to 6 months.

3.5.5. Matrigel
Thaw the Matrigel on ice. Dilute 1:1 with cold DMEM/F12 and aliquot into pre-chilled 15 mL falcon tubes (1 mL/tube). Store the aliquots at −20 °C.

3.5.6. Matrigel coated plates
To the 1 mL of prepared 1:1 Matrigel/DMEM/F12 aliquot, add 14 mL of cold DMEM/F12. Wait for the frozen pellet to lift off from the bottom of the tube and float. Triturate using a 10 mL surgical pipette to mix the solution, avoiding the introduction of bubbles. Coat the plates by pipetting 450 μL/well for 12-well TC plates, or 1 mL/well for 6 well TC plates. Leave plates at room temperature for 1 h prior to use. Collect the Matrigel and coat a second plate. The plates with the primary coat are ready for use. Matrigel coated plates can be stored at 4 °C for a maximum of 2 week.

3.5.7. Monothioglycerol (MTG)
Add 65 μL of MTG into 5 mL of sterile double-distilled water. Aliquot and store at −20 °C.

3.5.8. Neutralizing medium
Add 1 mL of KnockOut Serum Replacement (KOSR) to 5.6 mL of KnockOut DMEM. Store the medium at 4 °C for up to 2 weeks.

3.5.9. Y-27632 (ROCK inhibitor)
Reconstitute the powder (10 mg) with 3.122 mL of sterile double-distilled water to prepare a 10 mM stock of the reagent. Aliquot and store at −20 °C. Note: ROCK inhibitor is light sensitive; minimize exposure to light while handling the product.

3.6. E8 and E6 media component stock preparation

3.6.1. Holo-Transferrin
Dissolve 50 mg of powder in 25 mL of sterile double-distilled water to make a 2 mg/mL stock solution. Prepare aliquots and store at −20 °C.

3.6.2. FGF2
Dissolve 1 mg of the powder in 25 mL of sterile double-distilled water to make a 40 μg/mL stock solution. Alternatively, a sterile solution of PBS supplemented with 0.1% BSA can be used. Prepare aliquots and store at −80 °C.

3.6.3. Insulin
Dissolve 500 mg of powder in 25 mL of sterile double-distilled water to make a 20 mg/mL stock solution. Note: concentrated HCl must be used to facilitate dissolution of insulin; HCl is added drop-wise to the solution until it is clear. Prepare aliquots and store the product at −20 °C.

3.6.4. L-Ascorbic Acid
Dissolve 5 g of powder in 120 mL of sterile double-distilled water to make a 41.67 mg/mL stock solution. Prepare aliquots and store at −20 °C.

3.6.5. $NaHCO_3$
Dissolve the appropriate amount of powder in DMEM/F12 to make a 54.3 mg/mL stock solution. Prepare 5 mL aliquots and store at −20 °C.

3.6.6. Sodium Selenite
Dissolve 5 g of powder in 10 mL of sterile double-distilled water to make a 0.5 g/mL stock solution. Perform serial dilution of 10× followed by 1000× using sterile double-distilled water to achieve a working concentration of 50 μg/mL stock solution. Divide the solutions into aliquots and store at −20 °C. Caution: at high concentrations, this substance is toxic. Proper precautions must be taken during the preparation of this solution.

3.6.7. TGF-β
Add 1 mL of 10 mM citric acid to 100 μg of the TGF-β powder. Adjust the volume to 5 mL using sterile PBS supplemented with 0.1% BSA to make a stock solution of 20 μg/mL. Prepare aliquots and store at −20 °C.

3.7. Media preparation

3.7.1. E8 medium
To a 500 mL bottle of DMEM/F12 add 768 μL of L-Ascorbic Acid stock solution (for a final concentration of 64 μg/mL in the medium), 5 mL of $NaHCO_3$ stock (final concentration of 543 μg/mL), 485 μL of insulin stock solution (final concentration of 19.4 μg/mL), 2.675 mL of transferrin stock solution (final concentration of 10.7 μg/mL), 50 μL of gentamicin (final concentration of 5 μg/mL), 140 μL of Sodium Selenite stock solution (final concentration of 14 ng/mL), 1.25 mL of FGF2 stock solution (final concentration of

100 ng/mL) and 50 μL of TGF-β stock solution (final concentration of 2 ng/mL). After the addition of all the factors, filter the medium using the vacuum filter/bottle storage system, and store at 4 °C for a maximum of 2 weeks.

3.7.2. E6 medium

Refer to the preparation, concentrations, and storage of E8 medium; E6 medium contains the same factors as E8 except for TGF-β and FGF2.

3.7.3. StemPro-34 medium

To 50 mL of StemPro-34 SFM add 1.3 mL of StemPro-34 supplement. Note: the medium and the supplement must be warmed to 37 °C before combining to achieve uniform mixing. Add 150 μL of MTG stock solution (for a final concentration of 0.45 mM in the medium), 5 μL of gentamicin (final concentration of 5 μg/mL), 500 μL of L-Glutamine (final concentration of 2 mM) and 267.5 μL of transferrin stock solution (final concentration of 10.7 μg/mL). Store the medium at 4 °C for up to 2 weeks.

3.7.4. N2–ITS medium

To 50 mL of DMEM/F12 add 500 μL of insulin–transferrin–selenium, 500 μL of N-2 supplement and 5 μL of gentamicin. Store the medium at 4 °C for up to 2 weeks.

3.8. Preparation of immunofluorescence staining materials and reagents

3.8.1. Blocking solution

To 17.58 mL of PBS, add 20 μL of Triton X-100, 2 mL of reconstituted Goat Serum, and 400 μL of 5% BSA solution. Make aliquots and store at −20 °C.

3.8.2. Cell membrane permeabilizing agent (PBS with Triton X-100)

Dissolve 1 mL of Triton X-100 in 200 mL of PBS 1× to make a solution of 0.5% Triton X-100 in PBS. Avoid vortexing, as this introduces bubbles in the solution. Sterile filter the solution and store at room temperature for up to 3 months.

3.8.3. Goat Serum

Reconstitute Goat Serum with 10 mL of sterile double-distilled water. Divide the solution into 1 mL aliquots and store at −20 °C.

3.8.4. Hoechst dye 33258

Dissolve 25 mg of the reagent in 25 mL of double-distilled water to make a 1 mg/mL stock solution. Prepare aliquots and store at 4 °C.

3.8.5. Mounting medium

Add 20 mL of filtered sPBS to 20 mL of autoclaved glycerol to prepare 40 mL 1:1 sPBS/glycerol solution. Store at room temperature for up to 6 months.

3.8.6. PBS, 10× (1 L)

Dissolve 80 g of NaCl, 2 g of KCl, 27.2 g of Na_2HPO_4-$7H_2O$ and 2.4 g of KH_2PO_4 into 800 mL of double-distilled water. Adjust the pH to 7.4 using HCl. Adjust the volume to 1 L with double-distilled water. For working concentration, dilute to 1×, using double-distilled water and autoclave to sterilize the solution. PBS can be stored at room temperature for up to 6 months.

3.8.7. sPBS, 1× (4 L)

Dissolve 32.0 g of NaCl, 0.8 g of KCl, 8.69 g of Na_2HPO_4-$7H_2O$ and 1.04 g of NaH_2PO_4-H_2O in 3.5 L of double-distilled water. Adjust the pH to 7.2 using HCl. Adjust the volume to 4 L using double-distilled water. Store the solution at room temperature for up to 6 months.

Table 1
A list of human-compatible qPCR primers to assess skeletal myogenesis.

Gene	Forward primer (5′–3′)	Reverse primer (5′–3′)
GAPDH	TGGTGCTGAGTATGTCGTGGAGT	AGTCTTCTGAGTGGCAGTGATGG
MEOX1	GCAGGGGGTTCCAAGGAAAT	GTCAGGTAGTTATGATGGGCAAA
MSGN1	AACCTGCGCGAGACTTTCC	ACAGCTGGACAGGGAGAAGA
MYF5	AATTTGGGGACGAGTTTGTG	CATGGTGGTGGACTTCCTCT
MYH3	TTGATGCCAAGACGTATTGCT	GGGGGTTCATGGCGTACAC
MYOD1	TGCACGTCGAGCAATCCAAA	CCGCTGTAGTCCATCATGCC
MYOG	GCTGTATGAGACATCCCCCTA	CGACTTCCTCTTACACACCTTAC
PAX3	CTCACCTCAGGTAATGGGACT	CGTGGTGGTAGGTTCCAGAC
PAX7	CCCCCGCACGGGATT	TATCTTGTGGCGGATGTGGTTA
T	TTCATAGCGGTGACTGCTTATCA	CACCCCCATTGGGAGTACC
TBX6	CATCCACGAGAATTGTACCCG	AGCAATCCAGTTTAGGGGTGT

3.8.8. 4% Formaldehyde in PBS

Dilute the 37% formaldehyde stock solution with PBS 1×. Prepare the required amount fresh at the time of use.

3.8.9. 5% (weight/volume) BSA in PBS solution

Dissolve 1 g of BSA in 20 mL of PBS 1×. Divide the solution into aliquots and store at −20 °C.

3.9. qPCR primers

See Table 1 for the list of human-compatible qPCR primers.

4. Procedure

*4.1. Pluripotent cell culture * TIMING: 3–5 days*

(1) Pluripotent cells are maintained in 6-well (35 mm) Matrigel coated plates. Passage is required when the plates become 70–80% confluent with healthy pluripotent colonies (Fig. 1A, 3 DPP).
(2) Prepare a new plate to pass cells into: add 2 mL of pre-warmed E8 medium per well in a 6-well Matrigel coated plate. Up to 6 new wells can be made when passing 1 well.
(3) Aspirate and discard the medium from the well to be passed. Wash the well twice with DPBS.
(4) Gently add EDTA passaging solution to the well. Leave the cells for 4 min at room temperature.

Critical step: The EDTA solution should not be added directly onto the colonies as this will prematurely lift them off the plate. Rather, gently add the solution to the side of the well. Avoid moving the plate during the 4 min incubation, as cells can start detaching when agitated.

(5) Carefully aspirate and discard the EDTA passaging solution, then add 1 mL of E8 medium to the well.
(6) Scrape the cells using a cell lifter. Pipette 160 μL of cells into the new well containing 2 mL E8 medium.

Critical step: Avoid breaking the colony pieces into very small clumps (<20–30 cells). Wide mouth pipette tips should be used to ensure the cell clumps remain over 30 cells in size.

(7) Rock the plate to evenly distribute the cells and incubate at 37 °C, 5% CO_2. Cells must be monitored daily, and spontaneously differentiated colonies scraped off under a microscope as needed. Change media daily until cell cultures reach 70–80% confluence for passage or differentiation setup.

*4.2. Differentiation setup (Day-1) * TIMING: 24 h*

(8) Cells are differentiated in 12-well Matrigel coated plates. Up to 12 wells of a 12-well plate can be prepared when starting from 1 well of pluripotent cells in a 6-well plate, prepared above. Ensure colonies appear healthy and spontaneous differentiated colonies have been removed by scraping.

Troubleshooting: In the event that the culture plate sizes used do not suit cell requirements, PSC culture and differentiation does not necessarily require 6- and 12-well plates, respectively. We find the 12-well differentiation format to be the most suitable for endpoint analysis; however, differentiation can easily be scaled to larger or smaller dishes by maintaining 4×10^4 cells/cm^2 of growth area, and using 1 mL medium/1.5×10^5 cells.

(9) Aspirate and discard the old E8 medium from pluripotent cell cultures prepared above and wash the cells once with DPBS.
(10) Add 1 mL of fresh E8 medium per well supplemented with 10 μM Y-27632. Incubate the cells for 1 h in a 37 °C, 5% CO_2 incubator.
(11) Aspirate and discard the 1 mL of E8 supplemented with Y-27632 and wash the cells once with DPBS.
(12) Add 1 mL of pre-warmed TrypLE per well. Incubate the cells for 5 min in a 37 °C, 5% CO_2 incubator.
(13) Triturate using a 1000 μL pipette in order to lift the attached colonies from the plate, and to dissociate the cells.

Critical step: It is essential to be as quick as possible during this step. Leaving the cells in TrypLE for more than 10 min will negatively affect their survival.

(14) Add 1 mL of Neutralizing Medium per well supplemented with 10 μM Y-27632 to stop the TrypLE. Triturate again using P1000 and collect the 2 mL of cell homogenate into a 15 mL falcon tube.
(15) Centrifuge the cells at 500*g* for 3 min.
(16) Aspirate and discard the supernatant. Resuspend the cell pellet using 1 mL of E8 medium supplemented with 10 μM Y-27632.

Troubleshooting: In the case of clumps of PSCs following trituration, clumps can be eliminated by letting them settle in the conical tube, or passed through a cell strainer.

(17) Take 10 μL from the 1 mL of cells to count the total number collected with an automated cell counter or a hemocytometer.
(18) Prepare a cell stock at a concentration of 1.5×10^5 cells/mL for re-plating: pipette the appropriate number of cells into the desired volume of pre-warmed E8 medium (1 mL/well of a 12-well plate) supplemented with 10 μM Y-27632.

Critical step: The optimal cell plating density can vary depending on PSC line. The 1.5×10^5 cells/mL density has been optimized for the H9 hESC cell line in our lab, while other cell lines have different ideal plating densities determined empirically. Between 0.75×10^5 and 5×10^5 cells/mL may be used when determining optimal plating density.

Troubleshooting: Empirically, we have found that cell clusters of 6–12 cells following 24 h of culture (i.e., from Day-1 to Day 0) respond best to CHIR99021 induction of paraxial mesoderm (Fig. 1B). Due to inherent variability between PSC lines or between research labs, plating densities may need to be adjusted.

(19) Pipette 1 mL of cell stock per well of a Matrigel coated 12-well plate. Place the plate in a 37 °C incubator for 24 h.

*4.3. Differentiation (Day 0–50) * TIMING: 50 days*

(20) Assess the culture density. Cells will form small clusters; clusters ranging from 6 to 12 cells on average are an ideal starting point for differentiation (Fig. 1B).

Critical step: Sufficient cell to cell contact is required for the proper response to CHIR99021 treatment. Under-confluent cultures will become too stressed, while over-confluent cultures will not efficiently differentiate into the skeletal muscle lineage.

Troubleshooting: While some cell death is to be expected when passaging cells, if massive cell death is observed, it is likely due to prolonged TrypLE exposure or over-pipetting in Steps 13 and 14. Undifferentiated pluripotent colonies are resistant to dissociation. Care must be taken to strike a balance between efficiency of cell harvesting and cell viability. Y-27632 and Matrigel are particularly tied to cell health upon differentiation setup: for this reason we recommend testing several Matrigel lots initially to determine one optimal for the cell lines used.

(21) Aspirate and discard the old media. Gently wash the cells with DPBS. Add 1 mL of E6 medium supplemented with 10 μM CHIR99021 per well. Gently replace the medium after 24 h.

Critical step: Cells become visibly stressed by CHIR99021 and gentle care should be taken when changing media at Day 1 of differentiation. Optimal CHIR99021 concentration will depend on the cell line: the 10 μM concentration has been optimized for H9 hESC lines.

Troubleshooting: It is not uncommon for upwards of 25% of cells to die at Day 1 of differentiation (Fig. 1B). In fact, this cellular stress associates with more efficient mesoderm induction and skeletal myogenesis. However, to avoid higher rates of cell death, we strongly recommend that an initial titration be carried out ranging from 0.5 to 15 μM to determine a cell line's tolerance to CHIR99021. T, MSGN1, and TBX6 staining and/or expression at Day 2 of differentiation can serve as a readout for optimal paraxial mesoderm specification. At least 90% of cells should stain positive for T at Day 2 (Fig. 1C). The expression of T and MSGN1 should be elevated 3 orders of magnitude over Day 0 cells, while TBX6 expression should be 2 orders of magnitude higher (Fig. 1D).

(22) On Day 2, aspirate and discard the old media, and gently wash the cells with DPBS. Add 1 mL of E6 medium without additional supplementation. Culture the cells in E6 medium until Day 12 of differentiation. Change the media daily.
(23) On Day 12, aspirate and discard the old media, and wash the cells with DPBS. Add 1 mL of StemPro-34 complete medium supplemented with 5 ng/mL FGF2. Culture the cells in FGF2 supplemented StemPro34 medium until Day 20 of differentiation. Change the media daily.
(24) On Day 20, aspirate and discard the old media, and wash the cells with DPBS. Add 1 mL of E6 medium, without additional supplementation. Culture the cells in E6 medium until Day 35 of differentiation. Change the media daily.

Critical step: Cells may be split at this stage, both to expand the myogenic cultures, and to disperse accumulated 3D overgrowth into more easily resolved monolayers of PAX7-expressing SMPs and skeletal myocytes for microscopy (Figs. 2 and 3). If passing the cells, on Day 20 proceed to Step 27 and repeat again on Day 35.

(25) On Day 35, aspirate and discard the old medium, and wash the cells with DPBS. Add 1 mL/well of N2–ITS medium per well. Culture the cells in N2–ITS medium until Day 50: the endpoint of differentiation. Change the medium daily.
(26) At this point, cultures should be primarily composed of proliferative PAX7-expressing SMPs and skeletal myocytes, as evidenced by immunofluorescence staining (Fig. 3).

Troubleshooting: This protocol aims to recapitulate a finely tuned process *in vitro* using select key factors. The most essential of which, we find, is CHIR99021-mediated mesoderm specification. Differentiation will not efficiently produce SMPs or skeletal myocytes if mesoderm is not first specified efficiency. If the cultures do not undergo skeletal myogenesis, it is likely due to failure to induce mesoderm early in the culture process. We recommend troubleshooting this early stage of the protocol above all else by either altering CHIR99021 concentration, or its duration of use. The genes *MSGN1* and *TBX6* can be used to assess paraxial mesoderm development as early as Day 2, and PAX7 expression by IF should be observed by Day 20 to verify that myogenic development is properly advancing. At Day 20, PAX7 expression will be within 10- to 20-fold higher relative to Day 0 cells, and gradually approach 2 orders of magnitude higher by Day 50 when roughly 40% of cells stain positive for PAX7 [6].

4.4. Passaging differentiating cells * TIMING: 15 days

(27) Aspirate and discard the old media, and wash the cells with DPBS.
(28) Add 1 mL of fresh E6 medium per well supplemented with 10 μM Y-27632. Incubate the cells for 1 h in a 37 °C, 5% CO_2 incubator.
(29) Aspirate and discard the 1 mL of E6 supplemented with Y-27632 and wash the cells once with DPBS.
(30) Add 1 mL of pre-warmed Collagenase IV per well. Incubate the cells for 20 min in a 37 °C, 5% CO_2 incubator.
(31) Triturate using a 1000 μL pipette in order to lift the overgrown cultures from the plate, and to dissociate the cells.

Critical step: Leaving the cells in Collagenase IV for more than 40 min or aggressively pipetting will negatively affect their survival when re-plating.

(32) Collect by pipetting the cells into a 15 mL centrifugation tube and allow 10–15 s for excessively large clumps to settle to the bottom. Transfer the supernatant into a new centrifugation tube.

Critical step: Automated cell counters will under-estimate the true number of cells due to some cells remaining in small clusters, ideally less than 30 cells in size: the cell count may still be used directly as provided to determine plating density. If an accurate cell count or absolute single cell suspension is required, pipette the cells through a 70 μm cell strainer before centrifugation.

Troubleshooting: It may appear that the cultures take too long to dissociate by collagenase. By Day 20 of differentiation, the cells appear to produce a thick extracellular matrix (ECM) that will endure collagenase and TrypLE treatment. The ECM will settle out in Step 32, and therefore, cultures should not be overly pipetted in attempt to break the ECM apart; a sufficient number of cells will be released from the large clump with only modest pipetting. Collagenase treatment, like TrypLE upon differentiation setup, can be staggered if the number of wells requiring passage may extend their processing time.

(33) Add an equal volume of Neutralizing Medium supplemented with 10 μM Y-27632 to the cells.
(34) Centrifuge the cells at 500*g* for 3 min.
(35) Aspirate and discard the supernatant. Resuspend the cell pellet using 1 mL of pre-warmed E6 medium supplemented with 10 μM Y-23736 and 5 ng/mL FGF2.
(36) Take 10 μL from the cell suspension to count the number of cells collected with an automated cell counter or a hemocytometer.
(37) Pipette 3×10^5 cells per well into Matrigel coated 12-well plates. Shake the cell tube between wells to ensure small clumps remain evenly suspended in solution. Top up the volume in each well to 1 mL with pre-warmed E6 medium supplemented with 10 μM Y-23736 and 5 ng/mL FGF2.
(38) Place the plate in a 37 °C, 5% CO_2 incubator overnight.
(39) Aspirate and discard the old media. Add 1 mL of E6 medium supplemented with 5 ng/mL FGF2. Culture the cells in E6 medium supplemented with 5 ng/mL FGF2 for 2 more weeks. Change the medium daily.
(40) Cultures will contain a high percentage of PAX7 expressing SMPs and skeletal myocytes at this stage. Cells can be re-passaged again (Figs. 3 and 4).

4.5. Endpoint analysis (IF staining) * TIMING: 2 days

(41) All IF staining is performed directly in-dish with 12-well tissue culture plates. T staining can be performed around Day 2 of differentiation. T staining quantifies the percentage of cells that have entered the mesodermal lineage. Use at 1:100 dilution with 1:100 Cy3 donkey anti-rabbit secondary. PAX7 staining can be performed from approximately Day 20 onwards, and MF20 from Day 35 onward, or as soon as skeletal myocytes are visible by light microscopy. Use PAX7 antibody at 1:100 dilution and label with 1:200 AlexaFluor488 goat anti-mouse IgG1, and MF20 at 1:20 dilution and label with 1:100 Cy3 goat anti-mouse IgG2B. Cells can be co-stained with both PAX7 and MF20 concurrently in the same primary antibody solution, and both respective labels in the same secondary antibody solution.
(42) Aspirate and discard the old media, and wash the cells 3 times with DPBS. Gently add 500 μL of 4% formaldehyde per well. Fix the cells in formaldehyde for 15 min at room temperature.
(43) Aspirate and discard the formaldehyde into labeled chemical waste. Wash the cells 3 times with sPBS. Add 500 μL of cell membrane permeabilizing agent per well. Leave the cells at room temperature for 10 min.
(44) Aspirate the permeabilizing agent and wash the cells 3 times with sPBS. Add 200 μL of blocking solution per well. Set the plate to rock at room temperature for 1 h.
(45) Aspirate the blocking solution and wash the cells 3 times with sPBS. Prepare the primary antibody solution by diluting the antibody in blocking solution. Add 200 μL of primary antibody solution per well. Set the plate to rock at 4 °C overnight.
(46) Aspirate and discard the primary antibody solution. Wash the cells 3 times with sPBS. Prepare the secondary antibody solution by diluting the antibody in filtered sPBS. Add 200 μL secondary antibody per well. Cover the plate in foil and set the plate to rock at room temperature for 1 h.
(47) Aspirate and discard the secondary antibody solution. Gently wash the cells 3 times with sPBS. Add 10 μL of Hoechst solution to 1 mL of mounting medium. Use 250 μL of the mounting media per well. Cover the plate in foil and store at 4 °C.
(48) Observe the cells under a fluorescent microscope.

Critical step: Staining should be analyzed within 3 months of completion, as the intensity will gradually be lost over long-term storage.

*4.6. Endpoint analysis (qPCR) * TIMING: 6–8 h*

(49) Isolate cellular RNA, reverse transcribe cDNA from the RNA samples, and perform qPCR on the cDNA using the respective manufacturers' protocols with E.Z.N.A. Total RNA kit, Qiagen QuantiTect Reverse Transcription kit, and KAPA SYBR FAST qPCR kit.

(50) Analyze the resulting *Ct* values using the $\Delta\Delta Ct$ method—where GAPDH serves as the reference gene and undifferentiated Day 0 cells serve as the reference sample—and express the gene of interest (GOI) at the day of interest (DOI) as a fold change in expression over Day 0 (Fig. 1C).

$$\Delta\Delta Ct = (Ct_{\text{Day0,GOI}} - Ct_{\text{Day0,GAPDH}}) - (Ct_{\text{DOI,GOI}} - Ct_{\text{DOI,GAPDH}})$$

$$\text{Fold Change} = 2^{\Delta\Delta Ct}$$

5. Anticipated results and discussion

Efficient skeletal muscle differentiation from PSCs *in vitro* facilitates the study of virtually any stage of myogenesis, from pluripotent stem cell, to paraxial mesoderm-like tissue, committed skeletal muscle progenitors, and finally to fully differentiated skeletal myotubes. Thus, by manipulation of exogenous factors or genetic manipulation of endogenous factors, the molecular mechanisms underlying mesodermal or myogenic differentiation can be studied at any point in this process. Furthermore, this protocol can also be applied to patient-derived iPSCs to model the initiation and molecular etiology of skeletal muscle diseases.

Furthermore, the scalability of our protocol lends itself to high throughput small molecule or shRNAs screens for to identify drugs or drug targets that regulate SMP self-renewal, proliferation, or myocyte hypertrophy. In theory this protocol could even be scaled up to meet greater demands. As current transplantation methods are generally limited in their efficacy [30], the application of our protocol could eliminate the burden of collecting starting material so that greater focus could be placed on the optimization of novel cell transplantation methods in animal models. However, proof of principle experiments are still needed to validate this protocol's SMP function *in vivo*.

Naturally, there are a few limitations to this *in vitro* model system. As aforementioned, highly organized structures normally created *in vivo* are not recapitulated *in vitro*; embryonic somites and mature muscle fibers complete with sarcolemma and innervation cannot be observed, for example. Interestingly, progress is being made toward the bioengineering of human muscle fibers, for which this protocol could provide the cellular material [31].

Secondly, different cells lines will have variable responses to this protocol, as others have shown that different human ES cell lines will preferentially respond to specific *in vitro* tissue-generation cues more than others [32]. Initial development and optimization of the protocol was carried out in the H9 hESC line, and then validated using a variety in-house generated iPSC lines. It should also be noted that the same ESC lines propagated in different laboratories will likely demonstrate clonal drift at both the gene expression and response to differentiation stimuli [32–34]. Accumulated CNVs that associate with abnormal hESC karyotypes over prolonged culture have been linked to the misregulation of thousands of genes [34], which might explain how the same cell line can response variably to differentiation cues in different laboratories. Both the manner of, and time that pluripotent ES lines spend in culture, also lead to stably inherited changes in the methylation status of imprinted genes and hundreds of potentially significant CpG islands, even while a line appears karyotypically normal [35,36]. Thus, changes to the epigenetic landscape of a cell line cultured across separate research institutions may elicit a divergent response to developmental cues. Indeed, another skeletal muscle differentiation protocol that was published during the preparation of this manuscript shows that H9 ES cells cultured in their lab respond differently to our protocol than our H9 cultures [37], emphasizing the importance of properly optimizing conditions for each PSC line by adjusting cell plating density and titrating the concentration of CHIR99021.

Acknowledgments

This work was funded by grants from the Natural Sciences and Engineering Research Council (RGPIN 293170-11) and Canadian Institutes of Health Research (MOP-133570) to Dr. William L. Stanford, and by an award from the Muscular Dystrophy Association to Ilona S. Skerjanc (218371). Avetik Kocharyan was supported in part by an Ontario Graduate Studies scholarship. Michael Shelton was supported in part by the Queen Elizabeth II Graduate Scholarship in Science and Technology. William L. Stanford was supported by the Canada Research Chair in Integrative Stem Cell Biology.

References

[1] N. Cao, H. Liang, J. Huang, J. Wang, Y. Chen, Z. Chen, H.-T. Yang, Highly efficient induction and long-term maintenance of multipotent cardiovascular progenitors from human pluripotent stem cells under defined conditions, Cell Res. 23 (2013) 1119–1132.

[2] S.J. Kattman, A.D. Witty, M. Gagliardi, N.C. Dubois, M. Niapour, A. Hotta, J. Ellis, G. Keller, Stage-specific optimization of activin/nodal and BMP signaling promotes cardiac differentiation of mouse and human pluripotent stem cell lines, Cell Stem Cell 8 (2011) 228–240.

[3] X. Lian, C. Hsiao, G. Wilson, K. Zhu, L.B. Hazeltine, S.M. Azarin, K.K. Raval, J. Zhang, T.J. Kamp, S.P. Palecek, Robust cardiomyocyte differentiation from human pluripotent stem cells via temporal modulation of canonical Wnt signaling, Proc. Natl. Acad. Sci. U.S.A. 109 (2012). E1848-57.

[4] S.D. Schwartz, J.-P. Hubschman, G. Heilwell, V. Franco-Cardenas, C.K. Pan, R.M. Ostrick, E. Mickunas, R. Gay, I. Klimanskaya, R. Lanza, Embryonic stem cell trials for macular degeneration: a preliminary report, Lancet 379 (2012) 713–720.

[5] S.D. Schwartz, C.D. Regillo, B.L. Lam, D. Eliott, P.J. Rosenfeld, N.Z. Gregori, J.-P. Hubschman, J.L. Davis, G. Heilwell, M. Spirn, J. Maguire, R. Gay, J. Bateman, R.M. Ostrick, D. Morris, M. Vincent, E. Anglade, L.V. Del Priore, R. Lanza, Human embryonic stem cell-derived retinal pigment epithelium in patients with age-related macular degeneration and Stargardt's macular dystrophy: follow-up of two open-label phase 1/2 studies, Lancet 385 (2015) 509–516.

[6] M.L. Shelton, J. Metz, J. Liu, R.L. Carpenedo, S.-P. Demers, W.L. Stanford, I.S. Skerjanc, Derivation and expansion of PAX7-positive muscle progenitors from human and mouse embryonic stem cells, Stem Cell Rep. 3 (2014) 516–529.

[7] B. Borchin, J. Chen, T. Barberi, Derivation and FACS-mediated purification of PAX3+/PAX7+ skeletal muscle precursors from human pluripotent stem cells, Stem Cell Rep. 1 (2013) 620–631.

[8] C. Xu, M. Tabebordbar, S. Iovino, C. Ciarlo, J. Liu, A. Castiglioni, E. Price, M. Liu, E. R. Barton, C.R. Kahn, A.J. Wagers, L.I. Zon, A zebrafish embryo culture system defines factors that promote vertebrate myogenesis across species, Cell 155 (2013) 909–921.

[9] T. Hosoyama, J.V. McGivern, J.M. Van Dyke, A.D. Ebert, M. Suzuki, Derivation of myogenic progenitors directly from human pluripotent stem cells using a sphere-based culture, Stem Cells Transl. Med. 3 (2014) 564–574.

[10] C.V. Theodoris, M. Li, M.P. White, L. Liu, D. He, K.S. Pollard, B.G. Bruneau, D. Srivastava, Human disease modeling reveals integrated transcriptional and epigenetic mechanisms of NOTCH1 haploinsufficiency, Cell 160 (2015) 1072–1086.

[11] J.J.H. Chong, X. Yang, C.W. Don, E. Minami, Y.-W. Liu, J.J. Weyers, W.M. Mahoney, B. Van Biber, S.M. Cook, N.J. Palpant, J.A. Gantz, J.A. Fugate, V. Muskheli, G.M. Gough, K.W. Vogel, C.A. Astley, C.E. Hotchkiss, A. Baldessari, L. Pabon, H. Reinecke, E.A. Gill, V. Nelson, H.-P. Kiem, M.A. Laflamme, C.E. Murry, Human embryonic-stem-cell-derived cardiomyocytes regenerate non-human primate hearts, Nature 510 (2014) 273–277.

[12] C.E. Murry, G. Keller, Differentiation of embryonic stem cells to clinically relevant populations: lessons from embryonic development, Cell 132 (2008) 661–680.

[13] F. Relaix, Skeletal muscle progenitor cells: from embryo to adult, Cell. Mol. Life Sci. 63 (2006) 1221–1225.

[14] H. Sakurai, Y. Okawa, Y. Inami, N. Nishio, K. Isobe, Paraxial mesodermal progenitors derived from mouse embryonic stem cells contribute to muscle regeneration via differentiation into muscle satellite cells, Stem Cells 26 (2008) 1865–1873.
[15] H. Chang, M. Yoshimoto, K. Umeda, T. Iwasa, Y. Mizuno, S. Fukada, H. Yamamoto, N. Motohashi, Y. Miyagoe-Suzuki, S. Takeda, T. Heike, T. Nakahata, Generation of transplantable, functional satellite-like cells from mouse embryonic stem cells, FASEB J. 23 (2009) 1907–1919.
[16] T. Awaya, T. Kato, Y. Mizuno, H. Chang, A. Niwa, K. Umeda, T. Nakahata, T. Heike, Selective development of myogenic mesenchymal cells from human embryonic and induced pluripotent stem cells, PLoS One 7 (2012) e51638.
[17] Y. Hwang, S. Suk, S. Lin, M. Tierney, B. Du, T. Seo, A. Mitchell, A. Sacco, S. Varghese, Directed in vitro myogenesis of human embryonic stem cells and their in vivo engraftment, PLoS One 8 (2013) e72023.
[18] K.A.M. Kennedy, T. Porter, V. Mehta, S.D. Ryan, F. Price, V. Peshdary, C. Karamboulas, J. Savage, T.A. Drysdale, S.-C. Li, S.A.L. Bennett, I.S. Skerjanc, Retinoic acid enhances skeletal muscle progenitor formation and bypasses inhibition by bone morphogenetic protein 4 but not dominant negative beta-catenin, BMC Biol. 7 (2009) 67.
[19] T. Ryan, J. Liu, A. Chu, L. Wang, A. Blais, I.S. Skerjanc, Retinoic acid enhances skeletal myogenesis in human embryonic stem cells by expanding the premyogenic progenitor population, Stem Cell Rev. Rep. 8 (2012) 482–493.
[20] S.B.P. Chargé, M.A. Rudnicki, Cellular and molecular regulation of muscle regeneration, Physiol. Rev. 84 (2004) 209–238.
[21] G. Chen, D.R. Gulbranson, Z. Hou, J.M. Bolin, V. Ruotti, M.D. Probasco, K. Smuga-Otto, S.E. Howden, N.R. Diol, N.E. Propson, R. Wagner, G.O. Lee, J. Antosiewicz-Bourget, J.M.C. Teng, J.A. Thomson, Chemically defined conditions for human iPSC derivation and culture, Nat. Methods 8 (2011) 424–429.
[22] J. Beers, D.R. Gulbranson, N. George, L.I. Siniscalchi, J. Jones, J.A. Thomson, G. Chen, Passaging and colony expansion of human pluripotent stem cells by enzyme-free dissociation in chemically defined culture conditions, Nat. Protoc. 7 (2012) 2029–2040.
[23] K. Gauthaman, C.-Y. Fong, A. Bongso, Effect of ROCK inhibitor Y-27632 on normal and variant human embryonic stem cells (hESCs) in vitro: its benefits in hESC expansion, Stem Cell Rev. 6 (2010) 86–95.
[24] J.Y. Tan, G. Sriram, A.J. Rufaihah, K.G. Neoh, T. Cao, Efficient derivation of lateral plate and paraxial mesoderm subtypes from human embryonic stem cells through GSKi-mediated differentiation, Stem Cells Dev. 22 (2013) 1893–1906.
[25] J.K. Yoon, R.T. Moon, B. Wold, The bHLH class protein pMesogenin1 can specify paraxial mesoderm phenotypes, Dev. Biol. 222 (2000) 376–391.
[26] D.L. Chapman, I. Agulnik, S. Hancock, L.M. Silver, V.E. Papaioannou, Tbx6, a mouse T-Box gene implicated in paraxial mesoderm formation at gastrulation, Dev. Biol. 180 (1996) 534–542.
[27] J.K. Hall, G.B. Banks, J.S. Chamberlain, B.B. Olwin, Prevention of muscle aging by myofiber-associated satellite cell transplantation, Sci. Transl. Med. 2 (2010) 57ra83.
[28] W.Y. Chang, J.R. Lavoie, S.Y. Kwon, Z. Chen, J.L. Manias, J. Behbahani, V. Ling, R. A. Kandel, D.J. Stewart, W.L. Stanford, Feeder-independent derivation of induced-pluripotent stem cells from peripheral blood endothelial progenitor cells, Stem Cell Res. 10 (2013) 195–202.
[29] C. Kinnear, W.Y. Chang, S. Khattak, A. Hinek, T. Thompson, D. de Carvalho Rodrigues, K. Kennedy, N. Mahmut, P. Pasceri, W.L. Stanford, J. Ellis, S. Mital, Modeling and rescue of the vascular phenotype of Williams-Beuren syndrome in patient induced pluripotent stem cells, Stem Cells Transl. Med. 2 (2013) 2–15.
[30] D. Skuk, M. Goulet, B. Roy, P. Chapdelaine, J.-P. Bouchard, R. Roy, F.J. Dugré, M. Sylvain, J.-G. Lachance, L. Deschênes, H. Senay, J.P. Tremblay, Dystrophin expression in muscles of duchenne muscular dystrophy patients after high-density injections of normal myogenic cells, J. Neuropathol. Exp. Neurol. 65 (2006) 371–386.
[31] L. Madden, M. Juhas, W.E. Kraus, G.A. Truskey, N. Bursac, Bioengineered human myobundles mimic clinical responses of skeletal muscle to drugs, Elife 4 (2015) e04885.
[32] K. Osafune, L. Caron, M. Borowiak, R.J. Martinez, C.S. Fitz-Gerald, Y. Sato, C.A. Cowan, K.R. Chien, D.A. Melton, Marked differences in differentiation propensity among human embryonic stem cell lines, Nat. Biotechnol. 26 (2008) 313–315.
[33] X.-M. Chen, Q.-C. Kan, F. Wang, H.-J. Kong, Y.-Y. Zhang, W.-Z. Yu, Y.-P. Sun, Chromosome dynamic changes in two cultured Chinese human embryonic stem cell lines: single nucleotide polymorphism, copy number variation and loss of heterozygosity, J. Cell. Biochem. 113 (2012) 3520–3527.
[34] E. Närvä, R. Autio, N. Rahkonen, L. Kong, N. Harrison, D. Kitsberg, L. Borghese, J. Itskovitz-Eldor, O. Rasool, P. Dvorak, O. Hovatta, T. Otonkoski, T. Tuuri, W. Cui, O. Brüstle, D. Baker, E. Maltby, H.D. Moore, N. Benvenisty, P.W. Andrews, O. Yli-Harja, R. Lahesmaa, High-resolution DNA analysis of human embryonic stem cell lines reveals culture-induced copy number changes and loss of heterozygosity, Nat. Biotechnol. 28 (2010) 371–377.
[35] I. Garitaonandia, H. Amir, F.S. Boscolo, G.K. Wambua, H.L. Schultheisz, K. Sabatini, R. Morey, S. Waltz, Y.-C. Wang, H. Tran, T.R. Leonardo, K. Nazor, I. Slavin, C. Lynch, Y. Li, R. Coleman, I. Gallego Romero, G. Altun, D. Reynolds, S. Dalton, M. Parast, J.F. Loring, L.C. Laurent, Increased risk of genetic and epigenetic instability in human embryonic stem cells associated with specific culture conditions, PLoS One 10 (2015) e0118307.
[36] C. Allegrucci, Y.-Z. Wu, A. Thurston, C.N. Denning, H. Priddle, C.L. Mummery, D. Ward-van Oostwaard, P.W. Andrews, M. Stojkovic, N. Smith, T. Parkin, M.E. Jones, G. Warren, L. Yu, R.M. Brena, C. Plass, L.E. Young, Restriction landmark genome scanning identifies culture-induced DNA methylation instability in the human embryonic stem cell epigenome, Hum. Mol. Genet. 16 (2007) 1253–1268.
[37] J. Chal, M. Oginuma, Z. Al Tanoury, B. Gobert, O. Sumara, A. Hick, F. Bousson, Y. Zidouni, C. Mursch, P. Moncuquet, O. Tassy, S. Vincent, A. Miyanari, A. Bera, J.-M. Garnier, G. Guevara, M. Hestin, L. Kennedy, S. Hayashi, B. Drayton, T. Cherrier, B. Gayraud-Morel, E. Gussoni, F. Relaix, S. Tajbakhsh, O. Pourquié, Differentiation of pluripotent stem cells to muscle fiber to model Duchenne muscular dystrophy, Nat. Biotechnol. 33 (2015) 962–969.

Appendix 2: Supplemental Information, related to Chapter 2

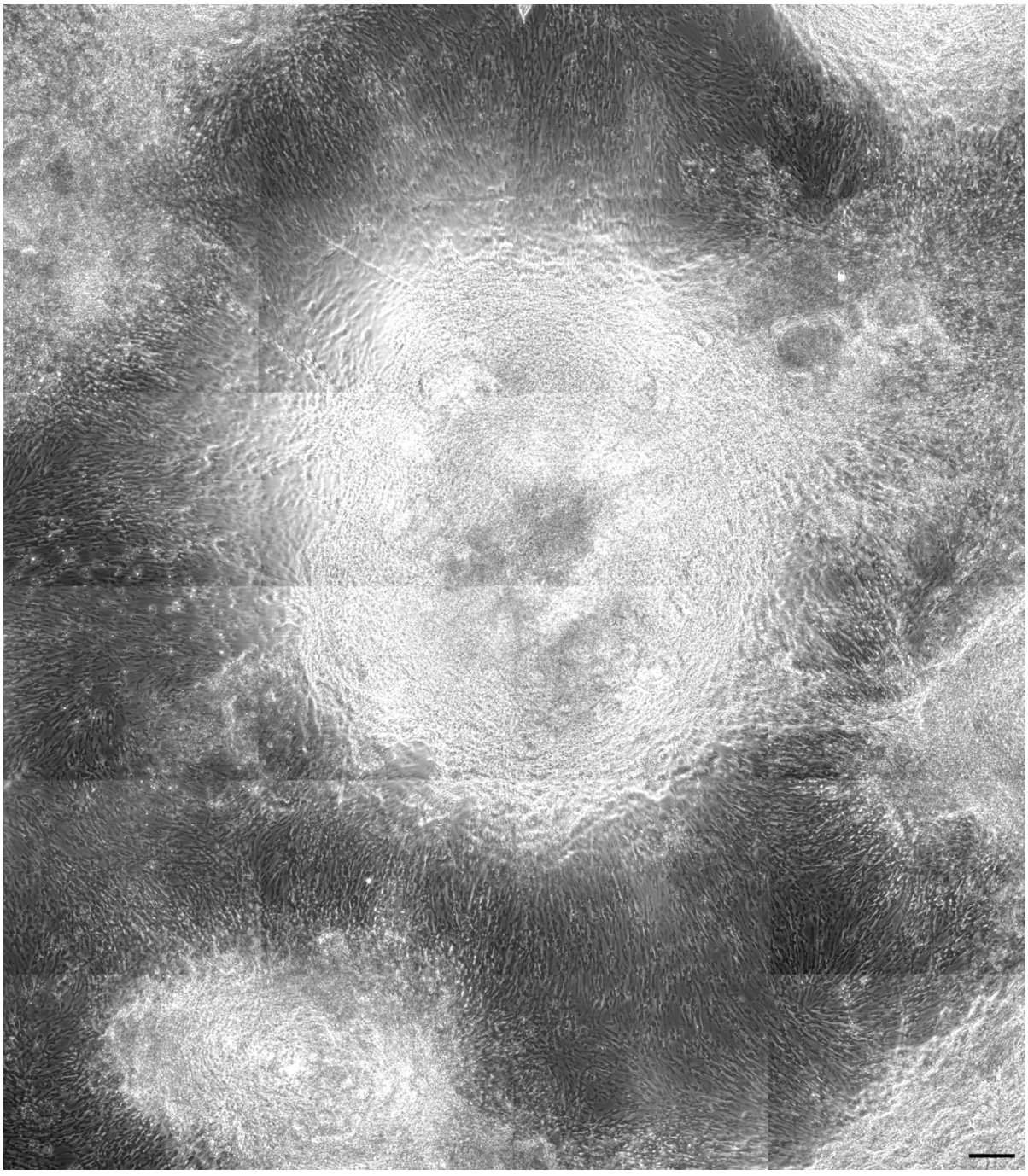

Figure A2.1

Figure A2.1. Mature CHIR99021-differentiated skeletal myocytes display orderly alignment, related to Figure 2.1. Multiple phase contrast images were captured at day 50 and tiled together using Volocity Software; depicted is an embryoid-body-like cluster of cells (center) and skeletal myocytes aligned radially around its periphery (scale bar = 200 μm).

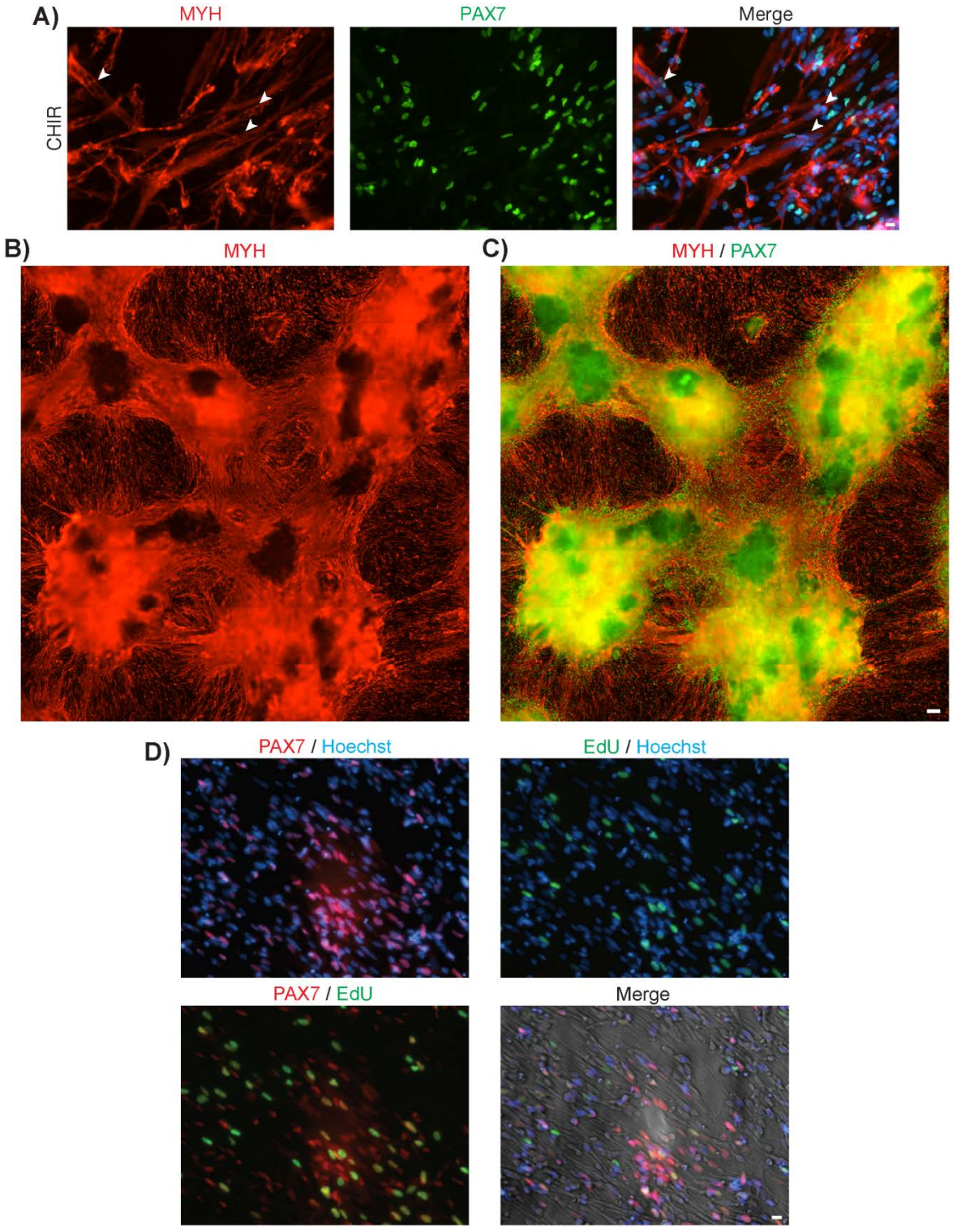
A)
MYH
PAX7
Merge
CHIR
B)
MYH
C)
MYH / PAX7
D)
PAX7 / Hoechst
EdU / Hoechst
PAX7 / EdU
Merge

Figure A2.2

Figure A2.2. Fusion competence and high resolution imaging of CHIR99021-treated cultures, related to Figure 2.2. A) Immunofluorescence staining with MF20 antibodies against striated myosin heavy chain confirms the presence of multinucleated myotubes (white arrowheads) at day 40 (scale bar = 20 μm). **B & C)** Multiple images were captured at day 50 and tiled together using Volocity Software, representing 27.06 mm^2 of culture area. Separate panels are provide for **B)** MF20, and **C)** PAX7 and MF20 merged (scale bar = 200 μm). **D)** Day 50 CHIR-treated cells were pulsed with EdU for 4 hours and stained for EdU, PAX7 and with Hoechst dye (scale bar = 20 um).

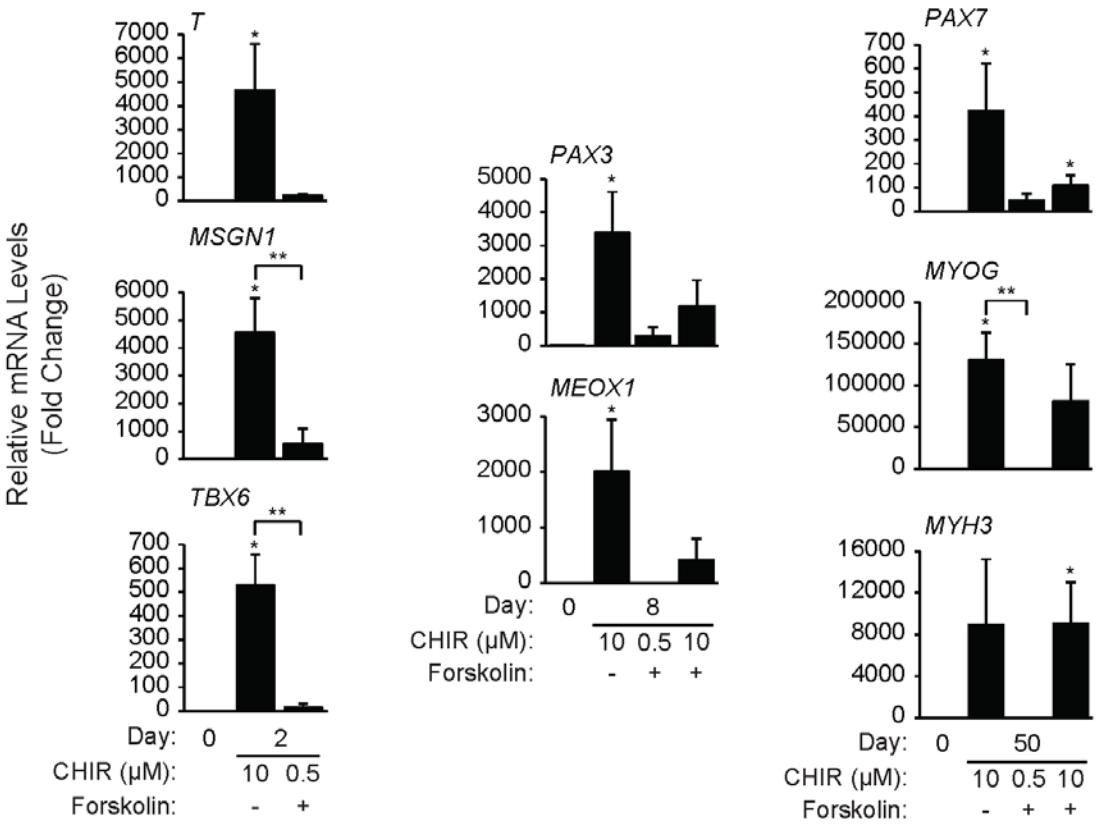
Relative mRNA Levels
(Fold Change)
T
MSGN1
TBX6
PAX3
MEOX1
PAX7
MYOG
MYH3
Day:
CHIR (μM):
Forskolin:

Figure A2.3

Figure A2.3. Forskolin did not enhance the CHIR99021-driven development of mesoderm or terminal myogenesis, related to Figure 2.3. The 0.5 μM CHIR99021, 10 ng/mL FGF2, and 20 μM Forskolin cocktail as performed by Xu *et al*. was applied for the first 7 days of our differentiation, or FGF2 and Forskolin were applied between days 2 and 7 following our 10 μM CHIR99021 treatment. Including FGF2 and Forskolin during 10 μM CHIR99021 treatment from days 0 to 2 had excessive toxicity towards the cells and was not pursued (data not shown). qPCR for early mesoderm, somite, or terminal myogenic genes showed no significant improvement with the addition of Forskolin in our protocol, according to student's t-test (n = 3 independent experiments, *$p \leq 0.05$ vs. day 0, **$p \leq 0.05$ Forskolin vs. 10 μM CHIR99021).

Table A2.1. Media and components utilized in the growth and differentiation of hESCs, related to Chapter 2 Experimental Procedures.

E8/E6 Media	
DMEM/F12	100%
Components:	
$NaHCO_3$	543 µg/mL
Ascorbic Acid	64 µg/mL
Insulin	19.4 µg/mL
Transferrin	10.7 µg/mL
Sodium Selenium	0.014 µg/mL
Gentamicin	50 µg/mL
FGF2 (E8 Only)	100 ng/mL
TGFβ1 (E8 Only)	2 ng/mL

StemPro-34 Media	
StemPro-34 SFM	100%
Components:	
L-Glutamine	2 mM
Monothioglycerol	0.45 mM
Transferrin	10.7 µg/mL
Gentamicin	5 µg/mL
FGF2	5 ng/mL

N2 Media	
DMEM/F12	100%
Components:	
Insulin / Transferrin / Selenium	1%
N2 Supplement	1%
Gentamicin	5 µg/mL

Table A2.2. Media and components utilized in the growth and differentiation of mESCs, related to Chapter 2 Experimental Procedures.

Maintenance Media	
DMEM	85%
Fetal Bovine Serum	15%
Components:	
Non-Essential Amino Acids	1%
Penicillin / Streptomycin	1%
β-Mercaptoethanol	0.1 mM
Leukemia Inhibitory Factor	1000 U/mL

Serum Free Maintenance Media	
Neurobasal	50%
DMEM/F12	50%
Components:	
B27 Supplement	1%
Penicillin / Streptomycin	1%
Bovine Serum Albumin	0.5%
N2 Supplement	0.5%
L-Glutamine	2 mM
Monothioglycerol	0.15 mM
Leukemia Inhibitory Factor	1000 U/mL
BMP4	10 ng/mL

Serum Free Differentiation Media	
IMDM	75%
F12	25%
Components:	
B27 (w/o RA) Supplement	1%
Penicillin / Streptomycin	1%
Bovine Serum Albumin	0.5%
N2 Supplement	0.5%
Monothioglycerol	0.45 mM
Ascorbic Acid	50 µg/mL

StemPro-34 Media	
StemPro-34 SFM	100%
Components:	
Penicillin / Streptomycin	1%
L-Glutamine	2 mM
FGF2	10 ng/mL

N2 Media	
DMEM/F12	100%
Components:	
N2 Supplement	1%
Penicillin / Streptomycin	1%

Table A2.3. List of qPCR primers, related to Chapter 2 Experimental Procedures.

Human Primer Name	Forward Primer (5′ - 3′)	Reverse Primer (5′ - 3′)
T	TTCATAGCGGTGACTGCTTATCA	CACCCCCATTGGGAGTACC
EN1	GAGCGCAGGGCACCAAATA	CGAGTCAGTTTTGACCACGG
FOXA2	TGTGTATTCTGGCTGCAAGG	CCTGCAACCAGACAGGGTAT
GAPDH	TGGTGCTGAGTATGTCGTGGAGT	AGTCTTCTGAGTGGCAGTGATGG
LBX1	CTCGCCAGCAAGACGTTTAAG	CGCTGCCCAAAGATGGTCATA
MEOX1	GCAGGGGGTTCCAAGGAAAT	GTCAGGTAGTTATGATGGGCAAA
MET	AGCGTCAACAGAGGGACCT	GCAGTGAACCTCCGACTGTATG
MSGN1	AACCTGCGCGAGACTTTCC	ACAGCTGGACAGGGAGAAGA
MYF5	AATTTGGGGACGAGTTTGTG	CATGGTGGTGGACTTCCTCT
MYH3	TTGATGCCAAGACGTATTGCT	GGGGGTTCATGGCGTACAC
MYH6	CAACAATCCCTACGACTACGC	ACGTCAAAGGCACTATCGGTG
MYL2	TTGGGCGAGTGAACGTGAAAA	CCGAACGTAATCAGCCTTCAG
MYOD1	TGCACGTCGAGCAATCCAAA	CCGCTGTAGTCCATCATGCC
MYOG	GCTGTATGAGACATCCCCCTA	CGACTTCCTCTTACACACCTTAC
NEUROG1	GCTCTCTGACCCCAGTAGC	GCGTTGTGTGGAGCAAGTC
NKX2-5	GCAGGACCAGACTCTGGAGC	GAGTCCCCTAGGCATGGCTT
NOG	GGCCAGCACTATCTCCACAT	ATGAAGCCTGGGTCGTAGTG
NPPA	TCCTCTGATCGATCTGCCCT	CTCTGGGCTCCAATCCTGTC
PAX3	CTCACCTCAGGTAATGGGACT	CGTGGTGGTAGGTTCCAGAC
PAX7	CCCCCGCACGGGATT	TATCTTGTGGCGGATGTGGTTA
SIM1	TCCATAATCAGACTCACGACCA	TGGGGCTACCACGAAGATGAA
SOX2	TACAGCATGTCCTACTCGCAG	GAGGAAGAGGTAACCACAGGG
SOX10	CCTCACAGATCGCCTACACC	CATATAGGAGAAGGCCGAGTAGA
TBX6	CATCCACGAGAATTGTACCCG	AGCAATCCAGTTTAGGGGTGT

Mouse Primer Name	Forward Primer (5′ - 3′)	Reverse Primer (5′ - 3′)
Actb	AAATCGTGCGTGACATCAAA	AAGGAAGGCTGGAAAAGAGC
T	CTGGACTTCGTGACGGCTG	TGACTTTGCTGAAAGACACAGG
Meox1	TGGCCTATGCAGAATCCATTCC	TGGATCTGAGCTGCGCATGTG
Msgn1	CTTCTGACACCGCTGGTCTG	GTGACTGCCGTAGCCATCG
Myh3	GCATAGCTGCACCTTTCCTC	GGCCATGTCCTCAATCTTGT
Myh6	CAACAACCCATACGACTACGC	ACATCAAAGGGCCACTATCAGTG
Myod1	CCCCGGCGGCAGAATGGCTACG	GGTCTGGGTTCCCTGTTCTGTGT
Myog	GCAATGCACTGGAGTTCG	ACGATGGACGTAAGGGAGTG
Nkx2-5	AAGCAACAGCGGTACCTGTC	GCTGTCGCTTGCACTTGTAG
Pax3	TTTCACCTCAGGTAATGGGACT	GAACGTCCAAGGCTTACTTTGT
Pax7	CTCAGTGAGTTCGATTAGCCG	AGACGGTTCCCTTTGTCGC

Appendix 3: Supplemental Information, related to Chapter 3

Table A3.1. Complete $\log_2()$ transformed and quantile-normalized gene expression dataset.

https://www.dropbox.com/s/azlsvuzqyzjop1p/Mike_rep1%2B2%2B3_gPSort.LogQuant.xlsx?dl=0

Table A3.2. Filtered dataset for probes with at least $\log_2() = 5$ expression and an absolute $\log_2() = 2$ difference in expression relative to day 0 control, related to Figure 3.1.

https://www.dropbox.com/s/82bb76aebhqky8l/Mike_rep1%2B2%2B3_gPSort.LogQuantKeep.xlsx?dl=0

Table A3.3. Clustered probes from the Table A3.2 filtered dataset, related to Figure 3.1.

https://www.dropbox.com/s/guhhdq3psd3s20j/Mike_rep1%2B2%2B3_gPSort.LogQuant_Clusters.xlsx?dl=0

Table A3.4. Filtered dataset for probes with at least $\log_2() = 5$ expression and an absolute $\log_2() = 2$ difference in expression relative to day 0 or day 0′ controls, related to Figure 3.4.

https://www.dropbox.com/s/centxjl9ibc5y33/Mike_rep1%2B2%2B3_gPSort.LogQuant_Choi_et_al.xlsx?dl=0

Appendix 4: Curriculum Vitae

MICHAEL L. SHELTON

EDUCATION AND RESEARCH EXPERIENCE

Ph.D. Biochemistry **2012 – 2018**

Supervisor: Dr. Ilona Skerjanc & Dr. Alexandre Blais University of Ottawa, Ontario

Doctoral Thesis: "Generation and characterization of human embryonic stem cell-derived muscle progenitors"

- 9.3 Cumulative GPA

Major Projects:

- Developed a protocol to generate skeletal muscle from human embryonic stem cells; the proportion of cells in culture bearing muscle identity improved from our previously published 4% to over 90% with the new protocol.
- Performed gene expression analysis on muscle generated with the new protocol, and using several bioinformatics approaches, characterized and compared embryonic stem cell-derived muscle to normal adult muscle stem cells.
- Transplanted the embryonic stem cell-derived muscle into mice to assess the cells' suitability for an eventual stem cell therapy: the treatment of human patients bearing damaged or diseased muscle with culture-derived muscle.

Relevant Courses:

- Introduction to Developmental Biology
- Physiology and Pathophysiology of Energy Metabolism and Muscle Functions
- Advanced Topics in Cell Regulation
- Neuromuscular Function and Dysfunction
- Structure and Expression of Eukaryotic and Prokaryotic Genomes

B.MSc Clinical Biochemistry, Genetics minor **2006 – 2010**

Supervisor: Dr. Gabriel E. DiMattia University of Western Ontario, Ontario

Honours Thesis: "Inhibiting Akt and mTOR signaling in epithelial ovarian cancer"

- 88.6% Grade Percentage

Major Project:

- Determined that pharmacological inhibitors of autophagy could reduce cell numbers in ovarian cancer cell lines and primary patient samples that were cultured under low nutrient conditions, modeling intraperitoneal metastasis.

AWARDS

$15 000.00 – Ontario Graduate Scholarship	**2014 – 2015**
$30 000.00 – Queen Elizabeth II – Scholarship in Science and Technology	**2012 – 2014**
$15 000.00 – Ontario Graduate Scholarship	**2011 – 2012**
$15 000.00 – University of Ottawa Excellence Scholarship	**2010 – 2014**

PROFESSIONAL EXPERIENCE

Lab Coordinator **2011 – 2017**

University of Ottawa, Ottawa, Ontario

- Managed 6 – 8 undergraduate teams during 3 – 6 hour weekly labs.
- Engaged in project planning, oral-visual presentation training, and report writing with undergraduate teams.
- Taught invaluable hands-on lab skills and techniques to students with little to no lab experience.
- Marked students' weekly and end-of-term reports in a timely and constructive manner.

Honours Undergraduate and Graduate Co-supervisor **2011 – 2018**

University of Ottawa, Ottawa, Ontario

- Mentored students in a one-on-one capacity and helped design their 4th academic year honours project.
- Taught advanced lab techniques involving living and chemical material, data and statistical analysis, and how to write a formal research article.
- Guided students through finding and interpreting published research.

VOLUNTEER EXPERIENCE

Logistics Team **2013**

uOttawa Bill Nye Organizing Committee, Ottawa, Ontario

- Helped plan the crowd flow and ticket processing for the event, and also managed the live crowd of thousands of attendees.

Orientation Week Leader **2010 – 2011**

uOttawa Science Students' Association, Ottawa, Ontario

- Welcomed university freshmen to campus through a week-long series of teambuilding and social icebreaker activities.

Tutor **2008 – 2009**

Northwest London Resource Centre, London, Ontario

- Motivated elementary school students to become self-sufficient in math and reading.

International Humanitarian Aid **2008**

LiveDifferent, Puerto Plata, Dominican Republic

- Assisted nursing students and doctors with a traveling free medical clinic, and also took part in the construction of a community center.

TECHNICAL SKILLS

Adobe Creative Suite image processing, bacterial and human cell culture, bioinformatics analysis of mRNA microarray and sequencing, fluorescent and confocal microscopy, live animal experimentation, molecular biology, WHMIS hazardous chemical training.

ORAL AND POSTER PRESENTATIONS

Poster Presentation **2014**

Keystone Symposia: Growth and Wasting in Heart and Skeletal Muscle, New Mexico, USA
Shelton M., Metz J., Liu J., Carpenedo R., Demers S. P., Stanford W. L., and Skerjanc I. S.**,** Inhibition of GSK3b enhances embryonic stem cell-derived skeletal myogenesis.

Invited Speaker / Poster Presentation **2013**

Myogenesis Gordon Research Seminar, Lucca, Italy
Shelton M., Liu J., and Skerjanc I. S., Enrichment of skeletal muscle progenitors from embryonic stem cells.

Invited Speaker **2010**

Summer Student Seminar Series, Ottawa, Ontario
Shelton M., Voronova A., and Skerjanc I. S., Regulation of Pax3 function by Mage-d1 during embryonic stem cell myogenesis.

PUBLICATIONS

***Shelton M.**, Liu J., O'Neil D., Skerjanc I. S., Blais A. Gene expression profiling of CHIR99021-induced skeletal myogenesis in human embryonic stem cells reveals a quiescent satellite cell-like profile for myogenic cultures. Manuscript in preparation.*

***Shelton M.**, Kocharyan A., Liu J., Skerjanc I. S, and Stanford W.L. Robust generation and expansion of skeletal muscle progenitors and myocytes from human pluripotent stem cells. Methods. 2016;101:73-84.*

***Shelton M.**, Metz J., Liu J., Carpenedo R. L., Demers S. P., Stanford W. L., and Skerjanc I. S. Derivation and Expansion of PAX7-Positive Muscle Progenitors from Human and Mouse Embryonic Stem Cells. Stem Cell Rep. 2014;4(3):516-29*

*Al-Madhoun A., Voronova A., Ryan T., Zakariyah A., McIntire C., Gibson L., **Shelton M.**, Ruel M., and Skerjanc I. S., Testosterone enhances cardiomyogenesis in stem cells and recruits the Androgen Receptor to the MEF2C and HCN4 genes. J Mol Cell Cardiol. 2013;60:164-71.*

*Wong, J., Mehta, V., Coutu, J., Voronova, A., Ryan, T., **Shelton, M.**, and Skerjanc, I.S., ß-catenin is essential for efficient in vitro premyogenic mesoderm formation but can be partially compensated by retinoic acid signaling, PLoS One. 2013;8(2):e57501.*

*Ryan T., **Shelton, M.**, Lambert J. P., Boisvenue S., Ruel M., Figeys D., and Skerjanc I. S., Myosin Phosphatase modulates the cardiac cell fate by regulating the subcellular localization of Nkx2.5 in a Wnt/ROCK-dependent pathway, Circulation Research, 2013;112(2):257-66.*

*Voronova, A., Al Madhoun, A., Fischer, A., **Shelton, M.**, Karamboulas, C., and Skerjanc, I.S., Gli2 and MEF2C activate each other's expression and function synergistically during cardiomyogenesis in vitro, Nucleic Acids Research, 2012;40(8):3329-3347.*